THE UNIVERSITY OF WARWICK

Library Declaration and Deposit Agreement

1. STUDENT DETAILS

Please complete the following:

Full name: ……

University ID number: ……

2. THESIS DEPOSIT

2.1 I understand that under my registration at the University, I am required to deposit my thesis with the University in BOTH hard copy and in digital format. The digital version should normally be saved as a single pdf file.

2.2 The hard copy will be housed in the University Library. The digital version will be deposited in the University's Institutional Repository (WRAP). Unless otherwise indicated (see 2.3 below) this will be made openly accessible on the Internet and will be supplied to the British Library to be made available online via its Electronic Theses Online Service (EThOS) service.
[At present, theses submitted for a Master's degree by Research (MA, MSc, LLM, MS or MMedSci) are not being deposited in WRAP and not being made available via EthOS. This may change in future.]

2.3 In exceptional circumstances, the Chair of the Board of Graduate Studies may grant permission for an embargo to be placed on public access to the hard copy thesis for a limited period. It is also possible to apply separately for an embargo on the digital version. (Further information is available in the *Guide to Examinations for Higher Degrees by Research*.)

2.4 *If you are depositing a thesis for a Master's degree by Research, please complete section (a) below. For all other research degrees, please complete both sections (a) and (b) below:*

(a) Hard Copy

I hereby deposit a hard copy of my thesis in the University Library to be made publicly available to readers (please delete as appropriate) EITHER immediately OR after an embargo period of ……..... months/years as agreed by the Chair of the Board of Graduate Studies.

I agree that my thesis may be photocopied. YES / NO (*Please delete as appropriate*)

(b) Digital Copy

I hereby deposit a digital copy of my thesis to be held in WRAP and made available via EThOS.

Please choose one of the following options:

EITHER My thesis can be made publicly available online. YES / NO (*Please delete as appropriate*)

OR My thesis can be made publicly available only after…..[date] (Please give date)
YES / NO (*Please delete as appropriate*)

OR My full thesis cannot be made publicly available online but I am submitting a separately identified additional, abridged version that can be made available online.
YES / NO (*Please delete as appropriate*)

OR My thesis cannot be made publicly available online. YES / NO (*Please delete as appropriate*)

3. GRANTING OF NON-EXCLUSIVE RIGHTS

Whether I deposit my Work personally or through an assistant or other agent, I agree to the following:

Rights granted to the University of Warwick and the British Library and the user of the thesis through this agreement are non-exclusive. I retain all rights in the thesis in its present version or future versions. I agree that the institutional repository administrators and the British Library or their agents may, without changing content, digitise and migrate the thesis to any medium or format for the purpose of future preservation and accessibility.

4. DECLARATIONS

(a) I DECLARE THAT:

- I am the author and owner of the copyright in the thesis and/or I have the authority of the authors and owners of the copyright in the thesis to make this agreement. Reproduction of any part of this thesis for teaching or in academic or other forms of publication is subject to the normal limitations on the use of copyrighted materials and to the proper and full acknowledgement of its source.

- The digital version of the thesis I am supplying is the same version as the final, hard-bound copy submitted in completion of my degree, once any minor corrections have been completed.

- I have exercised reasonable care to ensure that the thesis is original, and does not to the best of my knowledge break any UK law or other Intellectual Property Right, or contain any confidential material.

- I understand that, through the medium of the Internet, files will be available to automated agents, and may be searched and copied by, for example, text mining and plagiarism detection software.

(b) IF I HAVE AGREED (in Section 2 above) TO MAKE MY THESIS PUBLICLY AVAILABLE DIGITALLY, I ALSO DECLARE THAT:

- I grant the University of Warwick and the British Library a licence to make available on the Internet the thesis in digitised format through the Institutional Repository and through the British Library via the EThOS service.

- If my thesis does include any substantial subsidiary material owned by third-party copyright holders, I have sought and obtained permission to include it in any version of my thesis available in digital format and that this permission encompasses the rights that I have granted to the University of Warwick and to the British Library.

5. LEGAL INFRINGEMENTS

I understand that neither the University of Warwick nor the British Library have any obligation to take legal action on behalf of myself, or other rights holders, in the event of infringement of intellectual property rights, breach of contract or of any other right, in the thesis.

Please sign this agreement and return it to the Graduate School Office when you submit your thesis.

Student's signature: ..... Date: .....

CHARACTERISATION, MODELLING AND MANAGEMENT OF LITHIUM-SULPHUR BATTERIES FOR SPACECRAFT APPLICATIONS

by

Claire Elizabeth Parfitt BSc (Hons)

Thesis submitted in partial fulfilment of the requirements

for the degree of

Doctor of Philosophy in Spacecraft Engineering

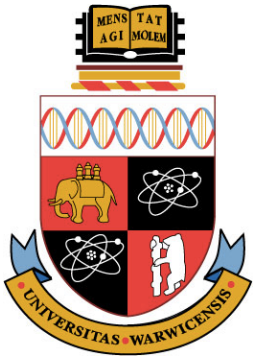

University of Warwick, School of Engineering

November 2012

“A person who never made a mistake never tried anything new.”

- Albert Einstein

“Shoot for the moon. Even if you miss, you’ll land among the stars.”

- Les Brown

“A fool thinks himself to be wise, but a wise man knows himself to be a fool.”

- William Shakespeare

"Nothing will ever be attempted if all possible objections must first be overcome."

– Samuel Johnson

TABLE OF CONTENTS

LIST OF FIGURES

LIST OF TABLES

ACKNOWLEDGEMENTS

This thesis would not have been possible without the initial encouragement and assistance I received from Professor Jon Clare, Ms. Alison Starr and Professor Phil Mawby who ignited the spark that was to set me on this course of study, and to whom I am immensely grateful.

I would like to acknowledge my sincere gratitude to the academics who have provided supervisorial support during my time at the University of Warwick, in particular to Dr. Bill Crofts and to Dr. James Covington. Both have contributed, not only a great deal of time and effort into seeing this thesis through to the end, but have been great sources of patience, advice and support.

I would also like to show my gratitude to the employees of ABSL Space Products, too numerous to name, who facilitated the practical part of my PhD. I am particularly indebted to Carl Thwaite, Dr. Rachel Buckle and Dr. Sam Roberts who, throughout my course of study, have provided invaluable technical assistance, guidance and supervision despite the chaos that usually surrounds them. I would also like to acknowledge Sion Power Corporation for providing the technology that was the inspiration for this work.

I would like to thank the many friends and colleagues who have supported me along the way and made my time at Warwick an unforgettable experience, especially the Grove Place Girls, the Old Mintonians and members of the PEATER Group, all of whom were always on hand with a pot of tea and a chocolate biscuit. I should also particularly like to thank Neil Small for his ever-patient explanations of the mysteries of MatLab, Matt Thomas for his mathematical prowess and Hannah Wade for her technical assistance with the use of LabView.

Above all, I would like to express my deep gratitude to my parents, Jane and Steve, my sister Heather and also to Carlos. Their unwavering support, understanding and encouragement, no matter the hour of day or night, has been of immeasurable help and comfort through the various trials and tribulations encountered in the undertaking of this PhD.

DECLARATION OF AUTHORSHIP

This thesis is submitted to the University of Warwick in support of my application for the degree of Doctor of Philosophy. It has been composed by myself and has not been submitted in any previous application for any degree.

The work presented in this thesis (including data generated and data analysis) was carried out by myself as the result of my own original research.

Publications

There was limited opportunity for publication of material associated with this thesis due to the proprietary nature of the data and work conducted herein. Future publication of material is intended, but is subject to clearance by the relevant parties.

C. E. Parfitt, W. E. Crofts and R. Buckle; *An Adaptable Lithium-Ion Battery Model*; ECS Trans. 2010 28(22), pp. 21-33

ABSTRACT

The lithium-sulphur couple has such a high theoretical energy density that, in principle, it could contribute significant weight and cost savings for launching a spacecraft. The principle aim of this study was to determine the suitability of lithium-sulphur cell technology for space industry applications by considering all areas of performance, modelling and electronic protection requirements.

This thesis is split into three main areas. Firstly, after examining the background material, the current state of the lithium-sulphur electrochemistry is analysed in detail. It is of great importance to have a clear understanding of the cell's electrochemical and chemical interactions as they can be used to explain the performance characteristics of the cell later in the work.

On completion of the electrochemical analysis the thesis then goes on to describe a set of electrical and thermal characterisation tests, the results of which are used to establish a novel equivalent circuit model of a Li-S battery. The equivalent circuit modelling method was chosen mainly for its ease of implementation into a full power system model and for its adaptability to future cell variations, both of which are important for the intended application. The resultant model uses electrical, thermal and "split capacity" domains to successfully predict cell performance.

Further characterisation testing results are then analysed with a view to specifying the electrical protection requirements of a Li-S battery management system suitable for different space industry applications. It was determined that the Li-S cell has safety and protection needs that exceed that of lithium-ion batteries, as well as requiring a robust housing structure, reducing the energy density of the battery pack.

The conclusion of the work is that, although the Li-S cell holds promise for the future, the current state of the cell's degradation characteristics prevents it from competing with lithium-ion cells in its current format.

NOMENCLATURE

Acronyms and Abbreviations

BCR	battery charge regulator
BDR	battery discharge regulator
BMS	battery management system
BoL	beginning of life
EMFchg	charge EMF
COTS	commercial off the shelf
CCCV	constant current constant voltage
CID	current interrupt device (s)
DoD	depth of discharge
DME	dimethoxy ethane
DOL	dioxolane
EMFdchg	discharge EMF
EMF	electromotive force (open circuit voltage)
EoC	end of charge
EoL	end of life
EMU	extravehicular mobility unit
FTS	flight termination systems

GEO	geostationary Earth orbit
ISS	International Space Station
$LiSO_2$	lithium sulphur dioxide
Li-ion	lithium-ion
Li-S	lithium-sulphur
LEO	low Earth orbit
NASA	National Aeronautics and Space Administration
NiCd	nickel-cadmium
NiH2	nickel-hydrogen
NiMH	nickel-metal-hydride
OCV	open circuit voltage
PTC	positive temperature coefficient
RTG	radioisotope thermoelectric generator
SCM	standard capacity measurement
SEI	solid electrolyte interphase
SHE	standard hydrogen electrode
SoC	state of charge
TEGDME	tetra(ethylene glycol) dimethylether
THF	tetrohydrofuran
TVC	thrust vector control

Equation Parameters

A	surface area (m^2)
A_0	hysteresis final voltage (V)
A_1	hysteresis constant 1 (V)
A_2	hysteresis constant 2 (V)
A_{age}	age coefficient ($A.h^{0.5}$)
A_{cyc}	cycling coefficient (Ah)
A_{SD}	self-discharge coefficient ($A.h^{0.5}$)
B_1	hysteresis constant 3 (V)
B_2	hysteresis constant 4 (V)
C	heat capacity (JK^{-1})
C_2	diffusion capacitance (F)
C_3	diffusion capacitance (F)
Cap	capacity transferred since current change (Ah)
C_c	irreversible capacity loss due to the cycling of the cell (Ah)
C_f	irreversible capacity fade due to the cell's age (Ah)
$C_{i,avg}$	average concentration of species ($mol\ m^{-3}$)
C_p	specific heat capacity ($Jg^{-1}K^{-1}$)
C_{sd}	reversible capacity loss due to self-discharge (Ah)

C_t	total capacity lost (Ah)
$CycNo$	number of full cycles (dimensionless)
D_1	initial discharge capacity, prior to storage (Ah)
D_2	discharge capacity after storage (Ah)
D_3	discharge capacity after storage and recharge (Ah)
$\frac{dE}{dT}$	EMF dependency on temperature factor (VK^{-1})
DF	division factor (dimensionless)
E, EMF	electromotive force (V)
E_{anode}	potential at the anode (V)
E_c	coulombic efficiency (dimensionless)
$E_{cathode}$	potential at the cathode (V)
E_H	EMF at the high plateau (V)
E_H^O	EMF at the high plateau under standard conditions (V)
E_L	EMF at the low plateau (V)
E_L^O	EMF at the low plateau under standard conditions (V)
$EMFchg$	charge EMF (V)
$EMFdchg$	discharge EMF (V)
F	Faraday's constant ($C\ mol^{-1}$)
H	SCM discharge time (hr)

I	current (A)
I_1	load current (A)
I_R	recoverable capacity equivalent current (A)
I_{SD}	self-discharge current (A)
k	thermal conductivity ($\mathrm{Wm^{-1}K^{-1}}$)
K_1	constant of integration 1 (V)
K_2	constant of integration 2 (V)
K_3	constant of integration 3 (K)
k_{cyc}	cycling time constant ($\mathrm{A^{-1}}$)
k_R	recoverable capacity constant ($\mathrm{hr^{-1}}$)
l	length (m)
m	mass (kg)
n_H	no. of electrons in the high plateau (dimensionless)
n_L	no. of electrons in the low plateau (dimensionless)
P	Peukert number (dimensionless)
p_1	cells connected in parallel before being connected in series (dimensionless)
p_2	strings connected in parallel (dimensionless)
P_{diss}	power dissipation (W)
Q	thermal energy (J)
Q_A	available capacity (Ah)

Q_{age}	capacity lost due to the age of the cell (Ah)
Q_c	thermal conductance (WK^{-1})
Q_{cyc}	rate-dependent capacity lost per cycle (Ah)
Q_D	most recent discharge capacity (Ah)
Q_e	electric charge (C)
Q_{max}	maximum recoverable capacity (Ah)
q_{other}	heat due to other effects (J)
q_p	heat due to polarization (Joule heating) (J)
Q_{rate}	available capacity at current rate I (Ah)
Q_R	recovered capacity (Ah)
Q_r	thermal radiance (WK^{-4})
q_s	heat due to entropy effects (J)
Q_{SCM}	SCM capacity (Ah)
Q_t	total cell capacity (Ah)
Q_{t1}	capacity in the first discharge region (Ah)
Q_{t2}	capacity in the second discharge region (Ah)
Q_{tC}	total cell capacity during charge (Ah)
Q_{tD}	total cell capacity during discharge (Ah)
R	total internal resistance (Ω)

R_1	Ohmic resistance (Ω)
R_2	diffusion resistance (Ω)
R_3	diffusion resistance (Ω)
R_g	ideal gas constant ($JK^{-1}mol^{-1}$)
s	cells or strings connected in series (dimensionless)
SoC	state of charge (dimensionless)
SoC_0	initial state of charge (dimensionless)
$SoCtrans$	state of charge transferred (dimensionless)
t	time (s)
T	temperature (K, ℃)
t_1	hysteresis time constant 1 (s)
T_1	cell temperature (K)
t_2	hysteresis time constant 2 (s)
T_{env}	temperature of the environment (K)
V_{1sec}	terminal voltage after 1 second of rest (V)
V_{av}	average voltage during discharge (V)
V_{Bmax}	maximum potential difference over resistor R_2 (V)
V_{Cmax}	maximum potential difference over resistor R_3 (V)
VF	view factor (dimensionless)
V_{term}	terminal voltage (V)

ΔV	potential difference (V)
ε	emissivity (dimensionless)
λ_-	negative root of 2nd order Cauer network (s^{-1})
λ_+	positive root of 2nd order Cauer network (s^{-1})
σ	Stefan-Boltzmann constant ($\mathrm{Wm^{-2}K^{-4}}$)
τ_1	hysteresis time constant 3 (dimensionless)
τ_2	hysteresis time constant 4 (dimensionless)

CHAPTER 1

INTRODUCTION

1.1 The Need for Space Travel

Since the dawn of the Space Age humankind has witnessed the evolution of an industry once limited to the imaginary world of science fiction. From the launch of the very first artificial satellite, Sputnik I, in 1957, to the present day's technological wonder, the International Space Station (ISS), the demand for satellite technology continues to increase. Space missions come in all shapes and sizes and allow us to do things that most of us take for granted. We can communicate with people on the other side of the world at any time of the day or night, we are able to know exactly where we are on the Earth's surface down to an astonishing degree of accuracy, we can organise military operations and monitor international treaties, we can find out invaluable information about the planet that we live on from weather forecasting to climate change to live monitoring of natural disasters, we can go beyond our own planet to explore other bodies in our solar system and we can even look into the depths of the Universe, to the beginning of time itself, and try to uncover the mysteries hidden there. Exploring the last frontier is still in its infancy and even though we have come a long way in the last few decades there is much more out there for space-faring crafts to achieve.

1.2 Batteries in Space

Sputnik I was powered by a small silver-zinc battery that allowed its transmitters to broadcast for the duration of the mission. This battery was a primary (non-rechargeable) battery that defined the mission length of 22 days; when the battery ran out of charge the satellite ceased to function. Modern satellites carry with them a whole host of equipment, from the housekeeping systems required to keep the satellite functioning to the experimental instruments needed to perform its mission objectives. These subsystems require a power

source to drive them for the duration of the mission. The most popular system for powering Earth-orbiting satellites is the combination of a solar array and a secondary (rechargeable) battery. In this case, the satellite's electrical power is generated by solar radiation incident on a photovoltaic cell array. A secondary battery, which is charged by the solar array during periods of sunlight, provides the required power during eclipse or if there is an extra power demand. This battery usually constitutes a significant proportion of the total mass of the spacecraft. Without rechargeable batteries it would be extremely difficult and expensive to power an Earth-orbiting satellite during periods of eclipse.

Batteries are, in fact, used across the whole spectrum of space activities. They also provide power to launch vehicle subsystems, planetary landers, rovers and other unique applications such as the Extravehicular Mobility Unit (EMU) used by astronauts during spacewalks.

1.2.1 Space battery evolution

Various rechargeable cell chemistries have been qualified for use in space. Some aspects of the most common cell chemistry's performance characteristics are compared in Table 1.1. The cycle life is given for a battery discharged by approximately 30% of its full charge before being recharged again, which is a common scheme for Earth-orbiting satellites.

Cell Chemistry	Energy Density	Cycle Life
Nickel Cadmium (NiCd)	25Wh/kg	~ 30,000
Nickel Hydrogen (NiH_2)	65-70 Wh/kg	~ 46,000
Lithium-ion	130-175 Wh/kg	>10,000

Table 1.1: A comparison of the main rechargeable batteries used in Earth-orbiting satellites

Up until the 1990's, nickel-cadmium (NiCd) and nickel-hydrogen (NiH_2) were the principal cell technologies used in satellite applications. NiCd cells have a long cycle life [1], but a low energy density of only 25Wh/kg [2]. NiCd cells also display the 'memory effect' where capacity is lost if the cells are cycled at high states of charge [3]. NiH_2 batteries were developed specifically for use in space and have a longer cycle life [4] and higher reliability [2] than NiCd batteries; they also do not use the toxic cadmium electrode, which is beneficial

to the environment. NiH_2 cells also have a higher energy density of around 65Wh/kg [1] but these cells are expensive to manufacture because they are custom-built. In the early 21st century, with the rapid advancement of lithium-ion cell technology, the use of nickel-based batteries in satellite applications began to decline. Li-ion cells are now the power source of choice for most power system designers. The Li-ion cells currently used in space are lightweight and have a high energy density ranging between 130-175 Wh/kg, which continues to improve (see Section 3.3). They also exhibit a very long cycle life of over 10,000 cycles at low depths of discharge [5,6] although they do require careful management to operate safely. The ISS uses NiH_2 batteries to provide power during eclipse [7] but there is currently an operation underway to replace these cells with Li-ion [8].

1.2.2 Space battery applications

Satellites in a low Earth orbit (LEO) orbit the Earth approximately once every 100 minutes. Of these 100 minutes about 65 minutes are spent in sunlight while the rest is spent in eclipse [9]. A battery that is required to power a satellite for 35 minutes out of every 100 undergoes around 5500 cycles per year. In contrast, satellites in a geostationary Earth orbit (GEO) experience less frequent eclipses, spending between 1 and 72 minutes in eclipse for a total of 90 days per year. The rest of the time is spent in full sunlight [9,10] and so GEO satellite batteries are therefore required to perform fewer cycles than LEO batteries. Batteries that power these types of satellite must have a very long cycle life.

A launch vehicle is essentially a rocket that carries a variety of payloads into space, but its design is not simple; it has a multitude of subsystems that are needed to operate it safely. Several different batteries are required to operate a variety of launch vehicle systems such as avionics, flight termination systems (FTS), stage separation pyrotechnics, thrust vector control (TVC) and telemetry [9]. The Ariane V launch vehicle, for example, has 17 primary and secondary batteries that are used to power these subsystems [11].

Avionics systems are found in the upper stage of a launch vehicle and control the vehicle's guidance, navigation and communication. The battery that powers this system must have a

high capacity so that it can continue to operate throughout the whole launch phase, which may last a number of hours [12]. The Ariane V launch vehicle, for example, requires 4kWh of energy over a period of 6 hours [13]. Batteries with a high energy density are therefore desirable for the avionics system. In contrast, the batteries that power the FTS and the pyrotechnics used for stage separation provide short bursts of high current during the launch phase [14]. High power batteries that can deliver large pulsed discharge currents are suitable for these systems. The SAFT VL5U cell, for example, can deliver up to 10,000W of power in 200ms pulses [15]. Some examples of these types of battery are shown in Figure 1.1.

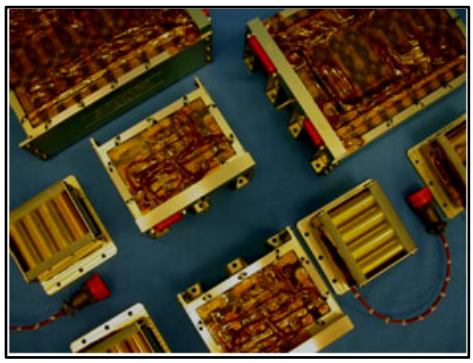

Figure 1.1: ABSL launch vehicle batteries [12]

Each stage of a launch vehicle is steered by the thrust vector control (TVC) system that manipulates the rocket engine nozzles, changing the direction of the thrust. Traditionally hydraulic, manufacturers are now moving to fully electrical systems that require high voltage batteries to power them such as the ABSL 270V TVC battery, which is shown in Figure 1.2.

Figure 1.2: A 270V ABSL thrust vector control battery [12]

This battery has over 80 cells connected in series to create the required voltage but it does not necessarily need to be of high capacity due to the short period of time it is in use.

Spacecraft that visit other bodies in the solar system generate their own power, usually via a radioisotope thermoelectric generator (RTG), as, at these distances, the Sun's rays are too weak to power a photovoltaic array. Once at its destination a battery may be required to fulfil the power demand of the mission payload, whether it is a satellite orbiting another planet, a rover travelling around an extra-terrestrial surface, or a scientific probe. The Huygens probe, for example, took seven years to reach Titan, one of Saturn's moons, on the back of the Cassini spacecraft. Once Huygens had separated from Cassini, primary lithium-sulphur dioxide ($LiSO_2$) cells were used to power the probe for the three hours spent descending to and gathering data from the surface of the moon. These cells were chosen for their ability to retain a high capacity whilst remaining inactive for a number of years [16,17].

1.2.3 Operational environment

The environmental factors that may affect the operation of a space-faring battery are reviewed here.

Launch phase

A common factor for all objects that leave Earth's atmosphere is that they must survive the initial journey. A launch vehicle and its payload have to endure extreme levels of vibration, acoustics, acceleration and shock and hence the rigours of launching an object into space dictate its entire mechanical design [18]. A typical launch of an Ariane V rocket may produce vibration frequencies of over 100Hz, a peak acceleration of 4.55g, acoustics of 140dB and shock levels of 2000g on stage separation [19]. The battery must be housed in robust casing to prevent movement of the cells during launch. The connections between individual cells and connections in the control circuitry must also be robust enough to survive the launch.

Gravity and vacuum

When something is said to be in orbit around the Earth it means that the object is freefalling vertically under the influence of gravity, but that it also has a horizontal velocity large enough so that the curvature of the Earth always falls away from it, preventing it from ever reaching

the ground. The effect is that objects in orbit around the Earth appear weightless even though gravity itself is relatively unchanged. All spacecraft also experience the extremely low density, pressure and temperature of the vacuum of space. Combined, these effects influence the thermal management of the battery. Where there is no gravitational effect or atmosphere for convection and nothing to conduct heat away from the spacecraft (although heat can be conducted through the spacecraft structure) the only natural means to keep a spacecraft cool is through radiation. The battery could also conduct heat through its connections to the spacecraft structure, though these connections can be minimal. Beyond the ideal operating range, generally between 0°C-20°C, battery performance starts to degrade.

Solar activity

Thermal radiation from the Sun incident on a spacecraft causes it to heat up considerably and, as previously discussed, there are problems with effectively dissipating this heat. In contrast, the temperature of space in a near vacuum is only 3K and so, in addition to the thermal changes associated with moving in and out of eclipse, there is a temperature variation caused by one side of the spacecraft facing the Sun whilst the other is in shade. Large thermal gradients across the spacecraft could have a significant effect on the performance of a battery [20], as cells of dissimilar temperature perform and age differently [21,22]. In most cases, however, a spacecraft battery would be thermally managed to within a few degrees of 20°C using a combination of insulation, heat sinks and heaters [10].

Individual electronic components can be disrupted by charged particles emitted by the Sun that penetrate into the core of the spacecraft causing changes that affect the way the spacecraft operates. If an incident like this affected the battery management electronics then the safety mechanisms put in place to protect the battery could be compromised, in turn compromising the mission itself. Spacecraft electronics must use redundant computer code and ideally should make use of space grade components that have been hardened against the effects of radiation damage. Even these safeguards do not guarantee that damage will not occur and care must be taken to make all systems redundant if a component does fail.

1.3 Advancing Space Battery Technology by the Increase of Specific Energy

All spacecraft batteries have one critical factor that engineers strive to optimise: specific energy. The amount of energy that a battery can deliver per unit mass is of paramount importance to an industry where the mass of the payload has a direct correlation with the cost of launching it. For LEO satellites the cost usually ranges between US$4000-6000 per kg of payload while GEO satellites can be more than 5 times that amount [23]. An increase in the specific energy of a battery means that a smaller or lighter battery may accomplish the same performance as an older battery type, whilst saving on volume or mass or both. A smaller, lighter battery requires less support, which has a knock on effect on the mass of the entire spacecraft [24]. An apparently minor saving in weight in the beginning could turn into a major cost saving down the line. In addition, it is important to realise that the battery is a key system and there would be no mission without one. Using a heavier battery could be at the expense of part of the payload; a scientific instrument might be dropped from the mission objectives if the satellite is too heavy. Therefore, any saving on the mass of a battery, or any other subsystem, may allow a payload to fly that otherwise would not have.

With the increased demand for satellite functionality comes an increase in the requirement for electrical power. The Li-ion chemistry is approaching its technological limits, so this can only translate into a larger battery. Increasing cell (or any part) numbers also increases mass and cost and reduces the reliability of the system. A new battery chemistry that is lighter whilst still delivering the same or more energy is actively sought after for this industry.

1.4 Lithium-Sulphur Technology

Advances in battery technology have given a new type of cell, never previously thought to be a viable option, the potential to outperform even the best lithium-ion batteries used today. Lithium-sulphur (Li-S) cells currently have a specific energy of around 350Wh/kg, up to two and a half times that of the lithium-ion cells used in today's satellites (See Section 3.3), and an

energy density of equal value (320Wh/l). This means that a lithium-sulphur battery weighing 1kg delivers the same energy as a 2.5kg lithium-ion battery, whilst occupying the same volume. Alternatively, a 1kg lithium-sulphur battery delivers 2.5 times the energy of a lithium-ion battery of the same mass, although it occupies a larger volume. If this increase can be exploited it would be a huge leap forward for the space industry. Satellite designers could either continue to allocate the same volume for the battery and can expect the same performance for 40% of the mass; else they could allocate the same mass as they would for a lithium-ion battery and expect a 250% increase in energy capability. It is expected that the specific energy of the cell will rise in the coming years and with a theoretical specific energy of ~2550 Wh/kg [25] there is huge room for improvement. The high specific energy of Li-S cells means that they have the potential to become the next generation of batteries in space.

1.5 Research Objectives

Theoretically Li-S has the ability to outperform lithium-ion, but in reality there are numerous obstacles, such as low cycle-life, capacity degradation and swelling, that need to be addressed. However, technological advancements in recent years and ongoing improvements to the chemical composition of the cell promise to reduce the imperfections currently seen. The potential for the lithium-sulphur chemistry to surpass lithium-ion cannot be ignored as it could make a significant impact on the future of space exploration, although this idea has not yet been addressed in the literature. In order that the cell be adopted for use by the space industry it is important that the issues associated with implementing a new technology are addressed. The objectives of this work are therefore set to:

1. **Create a Li-S battery model**: For a spacecraft power system designer it is imperative that the performance of the battery can be predicted. As such, the main objective of this work has been to fully characterise the electrical and thermal response of the Li-S cell and to incorporate these findings into a battery model suitable for use by a power system designer, something that has not yet been addressed in the literature.

2. **Determine the functionality of the battery management system (BMS)**: Space-faring batteries must be electronically protected in order to prevent a failure that could reduce, or end, the life of the mission. Characterisation tests reveal the strengths and weaknesses of the cell and can be used to define the functionality for bespoke battery management circuitry. The focus should be on the features of the Li-S cell that affect BMS design and functionality, rather than on any specific mission requirements, as these vary considerably between missions.
3. **Establish the suitability of the Li-S cell for space applications**: The results of the characterisation testing, the results of cell modelling and the requirements of the battery management system combine to allow an analysis of the suitability of the Li-S cell for the space industry.

In the remainder of this chapter the factors that contribute to each of the above objectives are reviewed.

1.6 Battery Modelling

As discussed in the previous section, a new cell technology cannot be adopted by the space industry without an accurate battery model to predict performance over a range of operating conditions. The predicted performance of a spacecraft battery needs to be known in order to determine if the battery will meet the demands of the intended mission without the opportunity for in-flight modification, replacement or repair. Predicting the response of a battery and its long-term behaviour under varying conditions can be a complex task. Each cell chemistry has a unique voltage profile and different levels of internal resistance and degradation mechanisms for example. There are also many interdependencies on which the characteristic data depends, such as temperature, age, state of charge, current rate and cell history.

A power system designer uses a battery model to determine the size of battery needed for the intended purpose and whether it can cope with the environmental and power profiles it will

be subjected to over the duration of the mission. This tool is vital in the planning of a space mission and, once operational, it requires no testing of real batteries or any knowledge of electrochemistry by the end user. The battery model may also be incorporated into a full power system model so that all of the components of the power system can be optimised. Using a model instead of a real battery saves time, cost and labour and also removes safety concerns, all of which are valuable to any business.

The battery model may continue to be used even after the spacecraft has been launched. In some applications it may be necessary to incorporate parts of a battery model into the battery management system itself so that it can judge the state of the battery and react accordingly. Additionally, the ground team may use the battery model to judge if the battery could survive a mission extension. Such a model was used to approve an extension to the Mars Express mission [26].

Determining the purpose of the battery model and the applications it is used for in the space industry defines the way the model is created. For example, a branch of modelling that deals with the electrochemical processes that occur within a cell aids manufacturers with the chemical optimisation of their cell. However, it is not in the interest of the power system designer to improve on the chemical composition of the battery and cell manufacturers do not usually make the required details of a cell's chemical composition available.

What is more suitable for the power system designer is an electrical and thermal model that can be implemented into a full power system model with standard inputs such as current, power and temperature. An equivalent circuit model, where battery characteristics are represented by standard circuit elements such as resistors, capacitors and voltage sources, would be intuitive and simple to implement for a systems engineer. Models such as these are commonly used in industry, with all major battery types catered for. A critical review of the various modelling techniques and existing models for spacecraft batteries is given in Chapter 2.

1.6.1 Modelling of lithium-sulphur batteries

Lithium-sulphur batteries have not been modelled to the same level of detail as other battery chemistries. The electrochemical processes in this cell are far more complex than for lithium-ion and are still not fully understood. There are a multitude of intermediate reduction species, the concentrations of which vary with temperature and the level of charge in the cell, which makes accurate electrochemical modelling very difficult. Kumaresn, Mikhaylik and White, of Sion Power Corporation reported an electrochemical model for Li-S in 2008 [27] of which the aim was for cell optimisation purposes only and did not deal with cell charging or temperature dependencies. Detailed knowledge of the various species concentrations, thermodynamics and kinetic properties of the electrolyte, which is usually proprietary information, are required for a full analysis.

Sion Power Corporation has published work on the modelling of the electrochemical mechanisms behind a chemical shuttle found in Li-S cells, detailed in Chapter 3 [28]. Again, the shuttle phenomenon is an electrochemical process that requires many proprietary parameters in order to be modelled accurately and even these authors, with access to all of their classified data, had to make assumptions and simplifications, such as discounting Ohmic resistances. Also, at the time this paper was written the chemical composition of the cell had not been developed to its current state and further modifications to the cell chemistry were subsequently made to limit the chemical shuttle [29] again changing the model parameters. There are no examples of equivalent circuit models implemented for the Li-S cell chemistry in the literature.

The lack of literature on the subject of lithium-sulphur modelling is likely to be due to the proprietary nature of the cells. Li-S cells are not available on the open market and so only the manufacturers have access to details of the exact chemical composition. Research institutes looking into the characteristics of lithium-sulphur, such as Stanford University [30,31] are currently concerned with the optimization of the cell chemistry and do not provide an accurate prediction of cell performance.

In work completed by another Li-S cell manufacturer, Oxis Energy, an impedance spectroscopy study was made with a view to fitting the impedance data to an equivalent circuit similar to Randle's impedance model (see Section 2.4) [32]. The aim of the work was to discover more about the movements of the lithium polysulphide species present during intermediate states of charge. Although a full equivalent circuit model was not described, the data does provide an insight into the variation of internal resistances as the cell is cycled. Dependencies such as temperature are not accounted for.

1.7 Battery Management in Space

Batteries used for any application usually require careful management if they are expected to perform correctly under the specified conditions. All batteries should be operated within a specific range of temperatures, currents and voltages, values of which vary between cell types and are provided by the manufacturer. For example, a standard ABSL 18650HC lithium-ion cell may only be operated between the voltages of 2.5V to 4.2V and at temperatures between -30°C and 60°C [33]. Outside of these ranges the performance and safety of the battery may be compromised. For spacecraft batteries, more restricted ranges may need to be implemented in order to obtain the best performance from the cell and to ensure the mission does not end prematurely due to degradation of the battery. In all instances a cell must never exceed the safety ranges provided by the manufacturer, due to the potential for severe damage a battery may cause to a spacecraft, which, once in orbit, cannot be repaired.

A battery management system (BMS) ensures that the battery stays within its specified safe operating limits. The limits of each cell, as well as the battery as a whole, are managed by the BMS. The BMS must continually monitor the state of the battery and then action must be taken when one of the predetermined limits is reached. This may mean monitoring the battery voltage and cutting off the charge current once a certain voltage is reached, or turning on a heating element if the battery gets too cold. The functionality of the BMS is determined by the type of battery being used, though the detailed design of the BMS circuitry heavily

depends on the requirements of the power system and the mission itself. Depending on the mission length, budget, cell type and operating conditions the power system designer may require different levels of protection for the battery and the cells comprising it. An overview of the features and the corresponding functionality that the BMS may provide for the battery is given in the points below:

- Protect the cells comprising the battery from exceeding safety/operational limits
    - Maximum/minimum voltage
    - Maximum charge/discharge current
    - Maximum/minimum temperature
    - Protection from abuse conditions
    - Failure protection
- Protect the battery from exceeding safety/operational limits
    - Maximum/minimum voltage
    - Maximum charge/discharge current
    - Maximum/minimum temperature
    - Protection from abuse conditions
- Monitor individual cells and/or battery
    - Voltage
    - Current
    - Temperature
- Optimise battery performance
    - Cell-balancing
    - Heater control
    - Customised charge algorithms
- State of charge determination

It is also prudent to mention that for a battery management system to be used in a spacecraft application the following design criteria must also be met [34]:

- The BMS must be as simple and reliable as possible. There should be no single point failures in the circuit design that could prevent the BMS from functioning or cause damage to the battery should a component fail.
- The BMS should be of low volume and weight so as to have minimal effect on the energy density of the battery pack.
- The BMS should not draw excess current from the battery so as to compromise the performance of the battery in its intended application.
- The BMS must not cause cell voltage imbalances or cause overdischarge from excessive current drain on the battery.
- The BMS should be adaptable to any battery topology, including possible cell and string failures within the battery.

1.7.1 BMS design

The first stage in designing a BMS is to determine the chemistry of the cells to be used in the battery. In knowing this, the safety and operational limits are known from information provided by the manufacturer. The battery topology must then be calculated, i.e. the number of cells in the battery and the series and parallel configuration in which they are arranged. The battery's topology arises from the power requirements of the spacecraft. The number of cells connected in series (a string) determines the voltage of the battery, while the number of strings connected in parallel determines the capacity and maximum current rate of the battery. The battery topology affects the design of the BMS in that a larger number of cells generally require more management than a battery comprising a lower number of cells. This is mainly due to the thermal management and cell-balancing requirements, which are described in Section 2.2.1.

The design and topology of the BMS itself also needs consideration. The different ways that a BMS can be implemented depends on the battery topology, and the level of protection required for the specific mission. The various BMS and battery topologies are discussed in detail in Section 2.3.

1.7.2 Cell and battery protection and monitoring

The level of protection the battery requires depends on the cell chemistry used. Nickel cadmium cells, for example, are tolerant to overcharge, whereas lithium-ion cells become dangerous when charged to voltages above 4.2V. Some Li-ion cells are manufactured in very large batches so their characteristics are highly similar. Consequently, monitoring series string voltages and dividing by the number of series cells is equivalent to monitoring individual cell voltages, only using less circuitry. Other Li-ion batteries cannot be so well matched and require additional monitoring and bypass circuitry.

Continually adding complex circuitry to a battery system may have advantages for battery performance and protection but equally it may have a detrimental effect. Protection circuitry requires power, provided by the battery itself. This power requirement reduces the power available to the spacecraft and increases the risk of over-discharging the battery. The BMS designer must also strive for the simplest, lightest and most reliable design possible, whilst also providing the protection essential to maintaining battery performance and safety.

1.7.3 Optimising battery performance

Optimising the performance of the battery is not vital to the safety of the battery. However, in missions of long duration, where the battery is required to perform well for up to 15 years, in the case of some LEO satellites, the power system designers seek to minimise degradation of battery performance with time. Obtaining the maximum energy from the battery for as many cycles as possible is the goal, but this is not always achievable. Novel charging algorithms, for example, may sacrifice a small amount of energy from the battery, by charging to a lower voltage for example [35], but this can reduce cell degradation and the lifetime of the battery is increased. For short duration missions the increase in lifetime may not be important and the additional complexity in the circuitry is therefore unnecessary.

Electrochemical cells of the same chemistry are not identical to each other and their characteristics may not be well matched. One cell may have a lower capacity or higher internal resistance than another cell and is said to be ‘weak’ [22]. When such cells are

connected in series the resulting string voltage and capacity is limited by the weakest cell. To prevent this from occurring circuitry may be added to keep the amount of charge in the cells balanced. This can be achieved using a number of methods, which are reviewed in Chapter 2.

An additional consideration is that of thermal gradients. A thermal gradient across a battery would cause even well matched cells to age differently and, as internal resistance is temperature dependent, cause the cells to have non-uniform internal resistances. Other temperature dependent cell characteristics, such as self-discharge, may also vary slightly between matched cells eventually creating an imbalance. This makes the thermal management of a battery crucial to maintaining the uniformity of cells.

1.7.4 Battery state of charge determination

Battery voltage, temperature and current are parameters that need to be monitored continuously. Looking at an instantaneous snapshot of these values at any given point however does not always provide the required information. One of the most important battery parameters its state of charge (SoC). The state of charge is the amount of useable charge remaining in the battery under given conditions. Unless one of the directly measurable variables, such as voltage or temperature, has a precise relationship with the state of charge then it must be calculated by other means. State of charge determination methods are reviewed in Section 2.2.2.

1.7.5 Replacing existing technologies

One of the major concerns with putting any new technology into space is its reliability. Aside from spacecraft that humans are able to visit, there is no opportunity to physically maintain a spacecraft after launch. Older technology is usually the preferred choice because it already has space heritage and is known to be reliable. The potential for Li-S cells to become more popular than the current Li-ion technology is a future possibility, but only if its reliability can be proven to match and its capabilities exceed that of lithium-ion. However, deciding to switch to a new battery type in a satellite design is not just a case of plug and play.

A full Li-S battery management system has not been described in the literature nor is one commercially available, especially not for space applications. The number of cells produced in a batch does not appear to be high. This implies that the level of cell matching will be low and cell-balancing circuitry is likely to be necessary. A safety report published in 2001 suggested that double redundancy analogue and digital electronics should be used in the protection circuitry as well as a PTC thermistor fuse [36]. It is also suggested that the Li-S cell performs best with a proprietary charging algorithm, although no details of this are given, and that the BMS will differentiate between different cell models. However, this paper is now over 10 years old and, as it makes reference to the cell's ability to accept overcharge (which is now not the case, see Chapter 3 for details), it is out of date.

More recently, in 2010, Sion Power Corporation announced that their Li-S cells had been used to power the record breaking longest duration unmanned flight of QinetiQ's Zephyr vehicle [37,38]. Due to the very low temperatures experienced on the flight (-75°C) it was necessary for the BMS to include a custom pack heating system [38]. A press release from 2007 confirms that Nexergy was commissioned to build the battery pack and management electronics for this application [39]. In this press release Nexergy imply a sophisticated charge management circuit was designed for use with solar arrays in unpredictable, varying sunlight conditions, very different to the predictable nature of spacecraft orbits. This charge management scheme is further detailed in [40]. They also imply active cell-balancing was used to maintain pack balance and safety devices were used to prevent thermal runaway, though details are not given. Further protection circuitry, developed by Nexergy, to prevent the swelling of Li-S cells is detailed in [41].

Despite the development of a Li-S battery management system for this particular application this technology has not yet been considered for use in space industry applications. A BMS dedicated to protecting these cells from the unique conditions imposed by a spacecraft and its environment, where a battery cannot be maintained or replaced, has not yet been contemplated.

1.8 Thesis Outline

Chapter 2 describes the state of the art in spacecraft and launch vehicle batteries. The current techniques used for battery modelling and battery management that are available in the public domain are reviewed.

Chapter 3 describes the electrochemistry of the Li-S cell in detail. The charge and discharge characteristics are explained as well as unconventional characteristics, specifically including swelling and the polysulphide shuttle mechanism. The Li-S cell is then compared to state of the art batteries and their advantages and disadvantages are discussed.

Chapter 4 discusses the selection of the Li-S cell used for testing. Following this, the methods and techniques used for the characterisation of the chosen cell are described and each cell level and battery level test is detailed.

Chapter 5 gives the results of the cell level characterisation tests.

Chapter 6 shows the development of an integrated Li-S cell model from design to implementation and its subsequent conversion into a full battery model. The optimised model design is verified against real test data collected under a variety of conditions.

Chapter 7 presents the results of battery level and abuse testing and describes the implications that the results have for the design of a BMS. The required functionality for a Li-S battery management system is proposed. In addition, an ideal battery topology is discussed.

Chapter 8 discusses the main objectives of the work and summarises the main findings and conclusions of the thesis. Suggestions for future work and improvements to the test methodology are described.

REFERENCES

[1] Clyde Space. (2012) Clyde Space Website. [Online]. http://www.clyde-space.com/products/spacecraft_batteries/useful_info_about_batteries/secondary_batteries

[2] R. A. Nelson, "Spacecraft battery technology," *Via Satellite*, February 1999.

[3] C.A. Hill, "Satellite Battery Technology - A Tutorial And Overview," *Aerospace and Electronic Systems Magazine*, vol. 26, no. 6, pp. 38-43, June 2011.

[4] NASA Glenn Research Center. (2000, April) Research and Technology. [Online]. http://www.grc.nasa.gov/WWW/RT/RT1999/5000/5420miller.html

[5] C.T. Martin, C.O. Kelly, H.D. Friend, C. Keen, and S.L. Wilson, "Lithium ion battery development at Eagle Pitcher," in *Battery Conference on Applications and Advances, 1999. The Fourteenth Annual*, 1999, pp. 355 - 357.

[6] NASA Glenn Research Center. (2005) Research and Technology. [Online]. http://ntrs.nasa.gov/archive/nasa/casi.ntrs.nasa.gov/20060054086_2006256314.pdf

[7] R.P. Hollandsworth, J.D. Armantrout, and G.M. Rao, "NiH2 reliability impact upon Hubble Space Telescope battery replacement," in *37th Intersociety Energy Conversion Engineering Conference*, 2002, pp. 276 - 281.

[8] NASA, "Lithium-Based Battery Performance Evaluated for NASA's Exploration Missions," in *RESEARCH & TECHNOLOGY 2007*, 2007.

[9] G. Halpert, H. Frank, and S. Surampudi, "Batteries and Fuel Cells in Space," in *The Electrochemical Society Interface*, 1999.

[10] B.W. Garino and J.D. Lanphear, "Spacecraft design, structure and operation - Chapter 22," in *Air University Space Primer.*, 2009.

[11] SAFT. Press Release N° 29-09, Saft will supply to EADS Astrium in-flight battery systems for the next 35 Ariane 5 ECA launch vehicles. [Online]. http://www.saftbatteries.com/SAFT/UploadedFiles/PressOffice/2009/CP_29-09_en.pdf

[12] ABSL Space Products. ABSL Space Products. [Online]. http://www.abslspaceproducts.com/Default.aspx?pid=3&catid=6&subcatid=8

[13] H. Barde, C. Urruty, and J. Jaumes, "Evolutions of the Ariane 5 Electrical Power System," in *Space Power, Proceedings of the Sixth European Conference*, Porto, Portugal, 2002, pp. 659-663.

[14] Quallion. Launcher batteries. [Online]. http://www.quallion.com/sub-ms-launchers.asp

[15] SAFT. (2009, October) Rechargeable lithium-ion battery: VL 5U - Ultra high power cell. [Online].http://www.saftbatteries.com/doc/Documents/defence/Cube769/VL5U_cell_data_sheet.a2c55356-164e-4fe3-b957-86bbed023422.pdf

[16] European Space Agency. (2010, February) Batteries at the heart of ESA space missions. [Online]. http://www.esa.int/esaMI/Technology/SEMNH032BZF_2.html

[17] European Space Agency. (2000, March) Huygens to test Volta's 200-year old invention at Titan. [Online]. http://sci.esa.int/science-e/www/object/index.cfm?fobjectid=13950

[18] Air Force Space Command. (2008, June) SMC Standard SMC-S-007. [Online]. http://www.everyspec.com/USAF/USAF-SMC/download.php?spec=SMC-S-007_13JUN2008.021524.PDF

[19] Ariane Space. (2011, July) Ariane Space Launch Services. [Online]. http://www.arianespace.com/launch-services-ariane5/Ariane5_users_manual_Issue5_July2011.pdf

[20] C. S. Clark, A. L. Mazarias, C. Kobayashi, and S. Nakasuka, "The Design Of A Power System For The Petsat Modular Small Spacecraft Bus," in *European Small Satellite Services Symposium*, Rhodes, 2008.

[21] M. Borne and S. Wen, "Increasing Large Li-ion battery pack energy delivery with active cell balancing," *EE Times Article*, October 2009.

[22] S. W. Moore and P. J. Schneider, "A Review of Cell Equalisation Methods for Lithium Ion and Lithium Polymer Battery Systems," *Delphi Automotive Systems* , 2001.

[23] Andrews Space & Technology. (2001) Space and Tech. [Online]. http://www.spaceandtech.com/spacedata/elvs/atlas5_specs.shtml

[24] S.C. Roberts, *PhD Thesis: An Investigation of the Feasibility of a Spacecraft Multifunctional Structure using Commercial Electrochemical Cells*, University of Southampton, 2009.

[25] Sion Power Corporation. (2008, October) Lithium Sulfur Rechargeable Battery Data. [Online]. http://sionpower.com/pdf/articles/LIS%20Spec%20Sheet%2010-3-08.pdf

[26] European Space Agency. (2009, September) What benefits does the European Battery Test Centre deliver? [Online]. http://www.esa.int/esaMI/Space_Engineering/SEMS5NV0EZF_0.html

[27] K. Kumaresan, Y. Mikhaylik, and R.E. White, "A Mathematical Model for a Lithium–Sulfur Cell," *Journal of The Electrochemical Society*, vol. 155, no. 8, pp. A576-A582, 2008.

[28] Y.V. Mikhaylik and J.R. Akridge, "Polysulfide Shuttle Study in the LiS Battery System," *Journal of the Electrochemical Society*, vol. 151, no. 11, pp. A1969-A1976, 2004.

[29] Y. Mikhaylik et al., "High energy rechargeable Li-S cells for EV applications," *ECS Transactions*, vol. 25, no. 35, pp. 23-34, 2010.

[30] Y. Yang et al., "New Nanostructured Li2S/Silicon Rechargeable Battery with High Specific Energy," *Nano Lett.*, vol. 10, pp. 1486-1491, 2010.

[31] Y. Yao et al., "Interconnected Silicon Hollow Nanospheres for Lithium-Ion Battery Anodes with Long Cycle Life," *Nano Lett.*, vol. 11, pp. 2949–2954, 2011.

[32] V.S. Kolosnitsyn, E.V. Kuzmina, E.V. Karaseva, and S.E. Mochalov, "A study of the electrochemical properties in lithium sulphur cells by impedance spectroscopy," *Journal of Power Sources*, vol. 196, pp. 1478-1482, 2011.

[33] ABSL Space Products. ABSL 18650HC Cell Data Sheet. (2008)

[34] D. Reece, "ABSL internal report," 2010.

[35] R. Spotnitz, "Simulation of capacity fade in lithium-ion batteries," *Journal of Power Sources*, vol. 113, pp. 72-80, 2003.

[36] J.R. Akridge, "Lithium Sulfur Rechargeable Battery Safety," *Battery Power Products & Technology*, October 2001.

[37] Sion Power Corporation. Sion Power Corporation. [Online]. http://sionpower.com/pdf/articles/Sion%20Power%20Zephyr%20Press%20Release%2029-07-2010.pdf

[38] Sion Power Corporation. (2007, September) Sion Power Lithium Sulfur Batteries Soar to New Heights. [Online]. http://sionpower.com/pdf/articles/SION%20Power-%20QinetiQ%20New%20Release%20Final%20Version.pdf

[39] Nexergy. (2007, March) Nexergy Develops Custom Battery Pack for Military/Aerospace Market. [Online]. http://www.iccnexergy.com/news-resources/press-releases/1209/nexergy-develops-custom-battery-pack-for-militaryaerospace-market/

[40] R. A. Ibrahim, "Multi-battery charger with individual battery bypass control," Patent 7880435, February 1, 2011.

[41] R. A. Ibrahim, "Anti-Swell Protection Circuit for Battery Cells," Patent 7830125, November 9, 2010.

CHAPTER 2

SPACE BATTERY TECHNOLOGIES AND MODELLING TECHNIQUES

In this chapter the state of the art in batteries currently used in the space industry are described. Following this, a review is made of the electronic techniques used in a battery management system to facilitate the safe and efficient operation of the battery. There is also an investigation into the methods used to model battery characteristics so that their performance can be predicted for their chosen application.

2.1 State of the Art Space Batteries

There are many manufacturers that provide the space batteries required for the applications described in Section 1.2.2. The state of the art in battery technology has almost fully moved into the Li-ion family of cell chemistries [1]. NiH_2 cells are still made by Eagle Pitcher Technologies and SAFT Batteries [2,3,4]. SAFT also produce a range of primary cells and rechargeable NiCd batteries for launch vehicle and interplanetary probe applications, but both companies also have a large range of Li-ion cell technologies in their portfolio. In fact, it is possible that Li-ion will eventually replace primary batteries, such as silver-zinc, on launch vehicles as the specific energy advantage that silver-zinc cells originally had over old nickel technologies has now been bridged. Launch vehicle batteries are only used once, and the flight battery cannot be thoroughly tested. Li-ion cells are rechargeable and so what was once an un-testable primary battery could become a testable single-use secondary battery.

Other companies that manufacture batteries used in space applications are Quallion, GS Yuasa and Lithion (Yardney). All offer Li-ion batteries for launch vehicle, satellite and space exploration applications such as the Mars Rover [5]. Their cells are usually large prismatic or cylindrical cells that are of a high capacity and can weigh anything in the region of 300g to

5kg. Currently the highest specific energy for a Li-ion large-scale cell is between 110Wh/kg and 175Wh/kg depending on whether the cell is to be used for high power applications or for high energy, long duration missions. SAFT's VES180 cell, for example, has a specific energy of 175Wh/kg, a capacity of 50Ah and can handle a discharge current rate of 100A [6]. This cell is suitable for high energy Earth-orbiting satellite applications. Their VL34P cell, on the other hand, has a capacity of 34Ah and a lower specific energy but can handle a greater continuous discharge current (up to 500A), so it is ideal for high power launch vehicle applications.

ABSL Space Products provide space batteries made of commercial off-the-shelf (COTS) cells that are much smaller than the large cells described previously. They are cylindrical '18650' cells of 18mm x 65mm dimensions and weigh only 40g [7]. ABSL provide a range of space battery solutions including high voltage and high energy cells. Their heritage cell, the 18650HC cell, has a specific energy of 130Wh/kg and a capacity of 1.5Ah. Improvements to the capacity of commercial 18650 cells have occurred over the years with some even reaching 3Ah per cell [8]. ABSL's 18650HC cell, although of lower capacity, has remained unchanged in chemistry since 1996 and has been flown in space for over a decade [9] and so its heritage is greatly valued. ABSL has recently qualified a new cell with a specific energy of 190Wh/kg [10]. The 18650NL cell will make smaller and lighter batteries than the HC cell and so, once it gains some spaceflight heritage, will be a valuable improvement.

The state of the art in spacecraft batteries does not necessarily represent that of terrestrial battery technology. The Panasonic NCR-18650A Li-ion cell has a specific energy of at least 233Wh/kg with a consistent performance over 300 cycles [11]. Li-ion cells with silicon anode technology are also under research and 700 cycles have been reported with a 56% capacity degradation [12]. Silicon anodes have a theoretical capacity of 4200mAh/g, ten times that of conventional graphite anodes and so have great potential if swelling and degradation can be minimised [13]. Nexeon have produced a silicon anode cell of 30-40% higher capacity than graphite based Li-ion cells, which is stable for over 300 cycles [14]. Prototype cells, by CEA-Liten, of a similar Si-based chemistry show a specific energy of up to 250Wh/kg [1].

2.2 Battery Management Systems

In Section 1.7 the functionality and requirements of a spacecraft battery management system were discussed. In this section the current methods used to meet these requirements are reviewed. In order to specify the functionality of a Li-S battery management system, these techniques must be analysed so as to produce the best solution for the Li-S cell technology.

2.2.1 Cell-balancing

In Section 1.7.3 the idea that unmatched cells connected in a series string could become unbalanced was introduced. Imbalance can be caused by an initial state of charge inequality, variations in total capacity and differences in internal resistance as described in detail in [15]. In addition, variations in self-discharge reactions and temperature gradients across a battery pack could also lead to imbalances. Because batteries in the space industry are built to very strict requirements it will be assumed that imbalances caused by deliberately charging the cells in a battery pack to different states of charge can be neglected. The ways in which a string of cells can be affected by imbalances are outlined in the following points:

- **Total Capacity Imbalance**: If cells of differing total capacity have an equal amount of charge removed, they will be at different states of charge, and therefore have different EMF and terminal voltage values.
- **Internal Resistance Imbalance**: Cells of equal total capacity but varying internal resistances do not have different states of charge when an equal amount of charge is removed or gained and will therefore have an equal EMF. However, they will have different terminal voltages when a current is flowing, as this is resistance dependent.
- **Self-Discharge Variations**: Cells experience parasitic reactions, which cause them to discharge, even when no load is attached. The self-discharge current is usually very small but if there is a variation in self-discharge levels between cells then this could have the same effect as a state of charge imbalance, where a different amount of charge is removed from each cell, causing differences in EMF and terminal voltage, especially during long periods of storage (on a launch pad for example).

- **Temperature Variations**: Most cell characteristics are dependent on temperature. If there is a temperature gradient across a string of cells then even cells that are completely identical in every way will experience an imbalance caused by temperature induced resistance and self-discharge changes.

The terminal voltage of a cell, V_{term}, can be described by Equation 2.1 where I is the charge or discharge current and R is the total internal resistance. I is defined as positive for a charge current and negative for a discharge current so for a cell with higher resistance than other cells in the string V_{term} will be higher during charge and lower during discharge.

$$V_{term} = EMF + I.R \quad [2.1]$$

There is no way, and no need, to electronically balance cells of differing resistances because their states of charge do not vary relative to each other and so any attempt to alter the charge entering or leaving the cell will only act to cause extra SoC imbalances.

Unfortunately, monitoring each cell voltage in a string does not indicate the cause of the imbalance. The following example illustrates this problem. A set of 5 lithium-ion cells connected in series has a total maximum voltage of 21V (assuming a maximum voltage of 4.2V per cell). In a simple BMS design, the string voltage is monitored and once 21V has been reached the charge current is discontinued. However, if the cells do not have similar properties of resistance and/or capacity, then the individual cell voltages are not identical. Three of the five cells may be at 4.2V while another is at 4V and the final cell is at 4.4V. The BMS would still read the string voltage as 21V, even though one of the cells is overcharged. One solution is to individually monitor the voltages of all of the cells in the string and cut the charge current when the first cell reaches 4.2V. However, if the other cells in the string have only reached 4V then the total string voltage will be reduced to 20.2V and the battery is not charged to its full capacity. Both of these control methods, if used exclusively, could ultimately result in a reduced performance battery that degrades faster than it should [15,16].

In the first instance, all cells in a battery pack should be well screened and have characteristics that match as closely as possible. This minimises cell imbalance, but, in cells that aren't easily matched, won't eliminate it. Nevertheless, there are electronic techniques that can be employed to aid cell balance, and hence obtain the maximum capacity from the battery, whilst maintaining the safety limits of the cell. Electronic balancing techniques fall into two main categories: passive balancing, where excess charge is dissipated and active balancing, where excess charge is redistributed.

Passive balancing: If one cell reaches its maximum charge voltage before the others in the string then the charge current entering that cell can be diverted by switching in a parallel resistor as in Figure 2.1. The value of this resistor needs to be chosen carefully so that the exact current is diverted around the cell, continuing to charge the other cells in the string. If the resistor value is chosen to be too high then not all of the charge current will be diverted around the cell, risking overcharge to that cell. If the resistance value is chosen to be too low then the cell will begin to discharge into the resistor, possibly increasing its level of imbalance further, and certainly creating a lot of heat to dissipate in the resistor. It is therefore important that the charge current is well known for this method to be used efficiently.

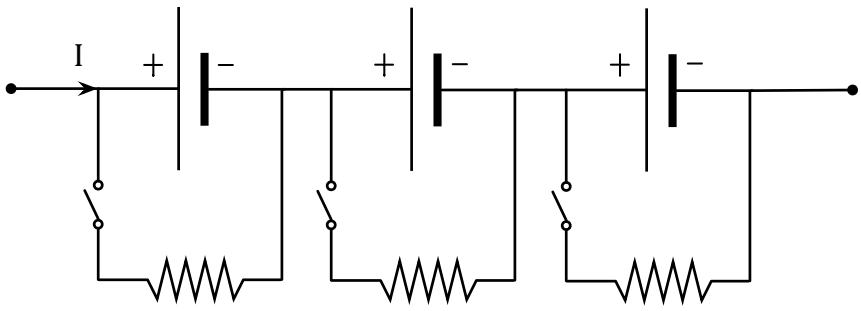

Figure 2.1: Switched resistor charge dissipation

In Li-ion cells passive balancing performs best at the end of charge or discharge when the change in voltage per mAh is at a maximum and cell resistance is at its lowest so the most accurate SoC adjustments can be made [17]. It is even more desirable to only perform this operation at the end of charge so as not to waste vital discharge capacity. Passive cell-

balancing techniques such as these are effective and simple, however, otherwise useful energy is dissipated as heat through the bypass resistors, reducing the system's efficiency.

Active balancing: In this method charge is continuously removed from cells at a higher state of charge and actively distributed to cells of lower states of charge throughout charging and discharging of the battery. There are several methods that can be used to accomplish this.

The flying capacitor method [18], shown in Figure 2.2, uses a capacitor that can be switched into parallel with a cell. The cell then charges this capacitor, losing some of its own charge. The capacitor is then switched in to the next cell in the string. If this cell is of a lower capacity (and therefore voltage) than the previous cell the capacitor will discharge into this cell, bringing it closer to the state of charge of the first cell.

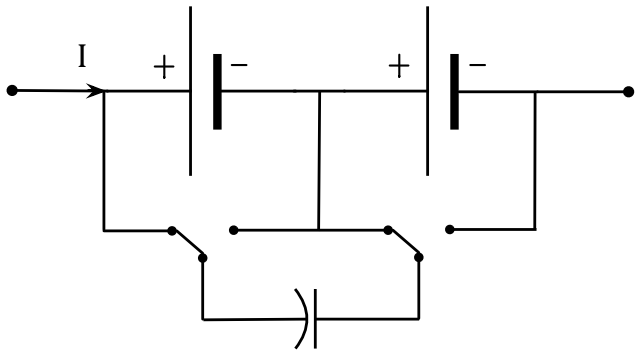

Figure 2.2: The flying capacitor charge redistribution method

This switching mechanism can follow a fixed sequence or can be programmed to selectively choose the highest and lowest cells to balance. In either case, a large number of switches and complex control circuitry are required with only a minimal amount of charge actually redistributed when dissipative heat in the switches and capacitor are accounted for. An increase in the number of capacitors can improve the efficiency of this method but, again, the additional control circuitry required lowers the reliability of the BMS. Additionally, this method can only be used for cell chemistries that did not have flat voltage profiles.

A method that would not be used in this case, but included for completeness, is active balancing of cells using a custom built transformer [19]. One method switches a single transformer into closed loop circuit around a low cell using energy from the battery pack as a

whole to bring it into balance. This is similar to the flying capacitor method and uses the same complex switching circuitry. A variation on this method is to put a tap into the secondary coil of the transformer so that each cell receives a charge current that is proportional to its voltage. Although this way can have advantages, such as fast, efficient balancing and simple circuitry, transformers have complex magnetic interactions that are not ideal for spacecraft. It is also difficult to create a flexible design once the secondary taps have been created. Nevertheless, this option is being developed by NASA as a solution to cell-balancing [20].

A combination of the active and passive methods can use the average battery voltage to determine the ideal cell voltage in a string. If an individual cell voltage is detected be higher than this ideal voltage during charge a dissipative resistor can be switched into the circuit so as to discharge the individual cell down to the required average voltage [21]. This method of cell-balancing again requires complex circuitry, which is active throughout charge and discharge. In a spacecraft BMS, where simplicity and reliability are key, the small increase in cell balance achieved by this method over passive methods would not outweigh the extra weight and complexity of the circuit required. There is also the possibility that this method could cause overdischarge if it is active at all times and could also increase cell imbalance if there was a sufficient variation in internal resistance between individual cells.

Limitations

Cell-balancing electronics cannot identify the cause of voltage imbalance. In addition, the flatness of the voltage profile determines how accurately voltage can predict the state of charge. If the balancing circuits operate at the end of charge where the steep incline in voltage gives a more accurate indication of SoC, there may not be sufficient charge time remaining for useful balancing. At large currents the internal resistance fluctuations may affect the terminal voltage more than capacity differences do, resulting in the cells of higher resistance having charge removed rather than cells of higher SoC, increasing the imbalance of the cells. Using smaller currents at the end of charge to reduce the *I.R* drop could help in this case. The *I.R* drop can be completely eliminated by stopping the current altogether and allowing the cells to relax to their EMF value, although this method is not practical on a spacecraft.

2.2.2 State of charge determination

The state of charge (SoC) is defined as the percentage of capacity left in a battery when compared to a full capacity reference point. The capacity of a battery decreases as it ages and so the reference capacity could be its initial "beginning of life" (BoL) capacity or, as is more common, the most recent capacity measurement. In this case the battery is charged at a particular charge current until a certain voltage is reached. The current may then be allowed to taper to a predetermined cut off point and at this point the battery is said to be at 100% SoC. The magnitude of the charge current and the taper cut off value used are relatively arbitrary, but provided the same process is used to get to 100% SoC each time, it can be used as a calibration point for SoC determination, irrespective of the absolute battery capacity. For a spacecraft battery, that will have undergone extensive life testing, the absolute capacity of the battery can be predicted using capacity fade models under the given power profile, in the given environmental conditions. In order to calculate the SoC, the capacity removed from or the capacity remaining in the battery must be known. This is not as simple as it first appears. There are several methods used for calculating a cell's SoC and each option is described here.

Coulomb counting: If the battery current is integrated over time the number of Amp hours (Ah) removed from or gained by the battery is known, as given by Equation 2.2, because current (I) is defined as the amount of electric charge (Q_e) that has moved through an arbitrary surface over a period of time (t):

$$Q_e = \int_{\tau_0}^{\tau_n} I(t)\, dt \qquad [2.2]$$

If the initial state of charge (SoC_0) and the total battery capacity in Ah (Q_t) is known and then current flows for a given period of time (t), the new state of charge (SoC) is a percentage given by Equation 2.3 [22]:

$$SoC = SoC_0 + \left(\frac{\int_{\tau_0}^{\tau_n} I(t)dt}{Q_t} . 100 \right) \qquad [2.3]$$

where I is defined as negative for a discharge current and positive for a charge current. The current can be 'counted' using the various sensors summarised in [23]. Current sensors have different levels of accuracy but even for the most accurate devices only the current entering or leaving the battery is counted. This method does not account for the aging of the battery (unless the capacity fade can be accurately determined and Q_t is continually updated), self-discharge current (which can vary with temperature and SoC), nor the coulombic efficiency (charge capacity vs. discharge capacity), which can also vary with age and temperature. Despite this, coulomb counting is the most common method for estimating state of charge. It can be a rough measurement if the inaccuracies are allowed to build up, especially when the current varies considerably or is low in value, but if there are regular calibration points (e.g. regularly charging the battery to 100% SoC) then these inaccuracies can be minimised [24].

Open circuit voltage (OCV) or EMF: The EMF of a battery is equal to the terminal voltage when no current is flowing and the voltage has had sufficient time to relax to its equilibrium value [25], which can extend to several hours for some battery types [24]. For many cell chemistries the EMF varies linearly with SoC and so is a good SoC indicator. However, a spacecraft battery is very rarely in the open circuit condition, especially not for long periods, so there are few opportunities for EMF measurements to be taken and no continuous SoC indication can be achieved. Even if it was convenient for the battery current to be stopped for long enough for the voltage to recover to the EMF value, the Li-ion (and at some states of charge the Li-S) EMF profile is relatively flat [26]. This means there is only a small change in EMF for each increment in SoC, providing a sizeable margin of error, depending on how accurately the EMF can be measured. This method could be used in conjunction with the coulomb counting method, using EMF measurements as a type of calibration point. An electronic device containing an EMF/SoC lookup table would need to be used to convert an EMF measurement into a SoC value.

Impedance measurements: Impedance spectroscopy is used to determine a cell's electrochemical characteristics by applying a sinusoidal voltage over a range of frequencies.

This method has been used to estimate the SoC of most battery chemistries [27,28,29] because the impedance can be directly related to SoC. However, this method is difficult to implement while the battery is in use and impedance is so highly temperature dependant that it is only of practical use in applications where the temperature is closely controlled. Impedance measurements are also quite difficult to interpret and typically need to be used with self-learning algorithms to gain accurate results.

Other indirect measurements: There may be other measureable cell parameters that vary with SoC. NiMH cells, for example, have an almost linear temperature increase during charge [30]. The SoC of a NiH_2 cell varies linearly with pressure [31]. In fact, any measureable quantity, such as internal resistance, that increases or decreases linearly during the charge or discharge of a cell could indicate state of charge. The characterisation of any new cell chemistry should always look for properties that vary linearly or predictably with SoC. Used in conjunction with coulomb counting this may lead to accurate SoC determination. Parameters of this type may not always vary linearly with state of charge until the very end of charge or discharge, such as the steep temperature increase seen at the end of the charge of a NiCd cell [30], in which case they can still be used as charge or discharge termination indicators. In [25] the EMF of a Li-ion cell was estimated using resistance models and interpolation between charge and discharge voltage curves. Indirect measurement of the EMF such as this prevents interruption of the battery current during operation. The EMF value can then be compared to a lookup table to compute the relevant SoC. In fact, all of these SoC estimation techniques require accurate look up tables to compare measured values with SoC.

Mathematical methods: There are other methods for determining state of charge that rely on mathematical techniques to solve equivalent circuit battery models (Section 2.3.1). Mathematical algorithms are used in [22,32] in order to relate the terminal voltage, which is easily measured, to the EMF, without knowing any of the other circuit element values. Complex algorithms such as Kalman filtering [33] and Observability Gramian [32] methods must be used to determine the EMF. Artificial neural networks [34] use data to 'train' an

input/output algorithm to determine one battery characteristic (namely SoC) from another (namely terminal voltage). This method can be used on any type of battery provided there is enough data to train the network. For the spacecraft application this would have to be an adaptable network that could retrain at different points in the life of the battery, meaning that another method of SoC determination would be needed to provide the training. In terms of practicality, other methods of SoC determination are more intuitive and simpler to implement.

IC chips are available that accurately gauge the capacity remaining in a battery [35]. For the spacecraft market, where the selection of components is restricted to space-grade, radiation-hardened devices, the choice is somewhat limited. Power system designers may program a custom microprocessor to do the job, although care must be taken to make the code redundant. For novel cell chemistries that don't have dedicated IC chips already programmed to suit their particular operating limits, custom-built designs are the only option.

2.3 Battery Topology

An important factor to account for when designing a battery management system is the topology, or series-parallel arrangement, of the cells in the battery. A battery of a certain voltage and capacity is required to fulfil the power requirements of the spacecraft. Single Li-ion cells, which have a maximum voltage of 4.2V, must be connected in a series string so that their voltages add up to the required operating voltage (Figure 2.3).

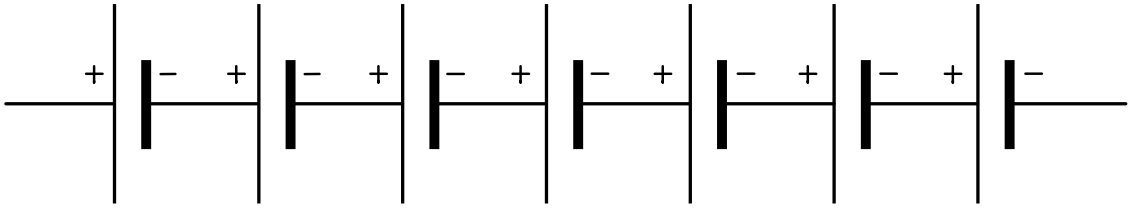

Figure 2.3: Seven Li-ion cells connected in a series string, with a maximum voltage of 29.4V

The capacity of a Li-ion cell depends on its size. The GS Yuasa LSE175 cell has a capacity of 175Ah and is the size of text book [36] while the ABSL 18650HC cell is slightly bigger than an

AA size cell and has a capacity of 1.5Ah [7]. A string of cells connected in series has the equivalent capacity of one cell and so to incrementally increase the total battery capacity this string must be connected in parallel to more strings of equal length as in Figure 2.4. This type of battery is said to be of s-p topology because cells are connected in series first and then in parallel. The battery shown in Figure 2.4 is a 7s-4p battery. If the ABSL 18650HC cell were used, this battery would have a maximum voltage of 29.4V and a capacity of 6Ah.

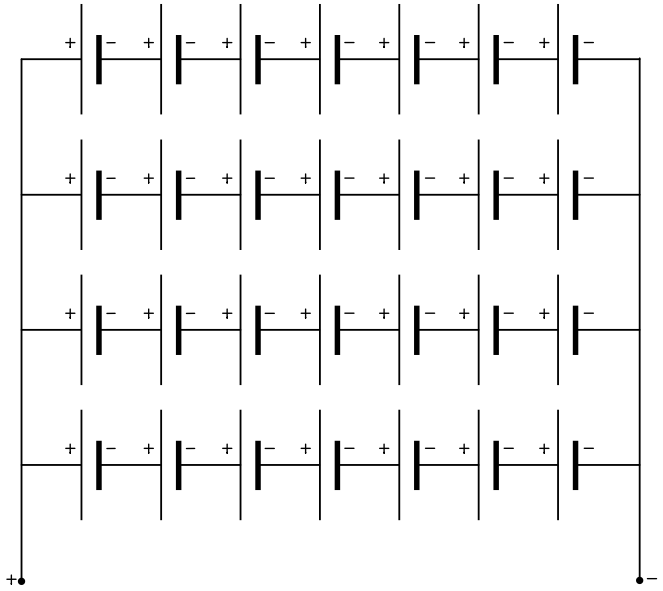

Figure 2.4: A 7s-4p battery

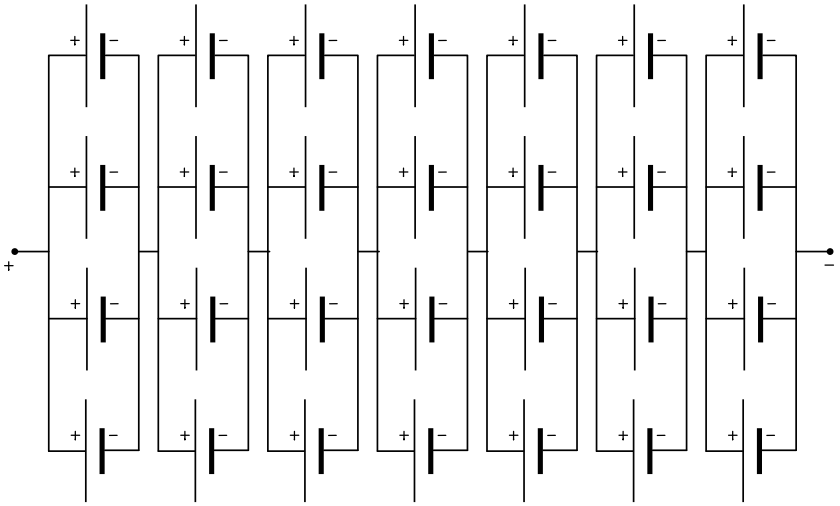

Figure 2.5: A 4p-7s battery

The same result can be achieved by first connecting the cells in parallel and then in series and is referred to as a p-s battery. A 4p-7s battery is shown in Figure 2.5, which has the same voltage and capacity as the 7s-4p battery in Figure 2.4.

If a cell were to fail open circuit in a battery of s-p topology then the whole series string would fail. This does not affect the operating voltage but reduces the capacity of the battery by one increment. If a cell were to fail short circuit then this would cause stress to the other cells in the string, which would be sharing the battery voltage between them, eventually leading to an open circuit failure of another cell and the loss of the string, again reducing battery capacity [16]. The remaining strings would then equally share the battery current between them, so any aging effects caused by the increase in current or temperature would be distributed evenly across the whole battery.

If a cell in a battery of p-s topology fails as a short circuit then the remaining cells in that parallel string are forced to the lower voltage, the whole string is in effect lost and the total battery voltage is reduced by the value of one cell voltage. If the battery continues to be charged to its original full voltage then the remaining cells will be overcharged. If a cell fails open circuit then the rest of the cells in that parallel string must share the remaining current, causing stress and eventual failure of those cells too.

Large cell battery manufactures like SAFT prefer the p-s topology for their batteries. This is because large cells do not have closely matching characteristics and require cell-balancing electronics to keep their voltages matched. Only cells connected in series require balancing and so a 4p-7s battery requires just 7 cell-balancing circuits whereas a 7s-4p battery requires balancing circuits for each of its 28 cells. Small cell battery manufacturers prefer the s-p cell topology [37] because the cells' characteristics are so closely matched and cell-balancing electronics are therefore not required. The advantage is that capacity, rather than voltage, is affected should a string fail. S-p batteries are therefore designed to have an extra, redundant string to allow for a failure. This ensures that the battery can still perform reliably to the end of its life [38] and the BMS does not have to alter its voltage limits should a string fail.

2.3.1 BMS topology

In addition to the design requirements described in the previous sections, the topology of the BMS itself needs careful consideration. There are three main methods for implementing a battery management system, centralised, master-slave and distributed [39]. A centralised BMS, depicted in Figure 2.6, consists of a single system containing all of the protection, balancing and monitoring circuits in one central place, and is powered by the total battery voltage [16]. This method is the simplest and the cheapest to implement however it is only beneficial to batteries that have a low number of cells in series. Even very small monitoring currents can add up over a long string, leading to a state of charge imbalance between cells.

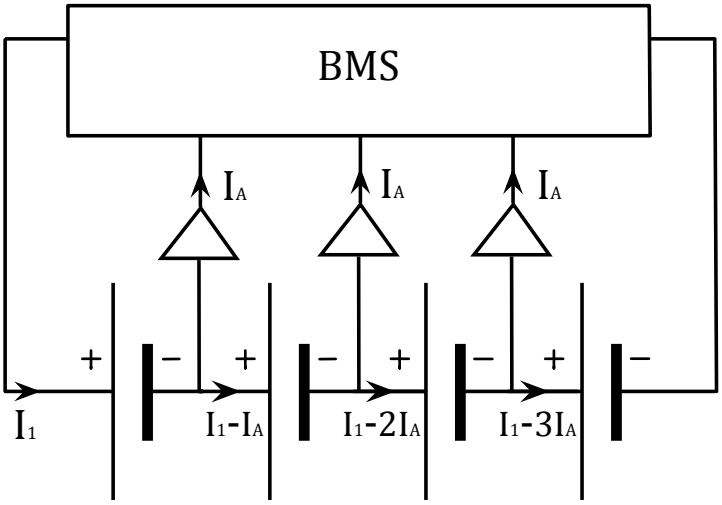

Figure 2.6: Centralised battery management topology

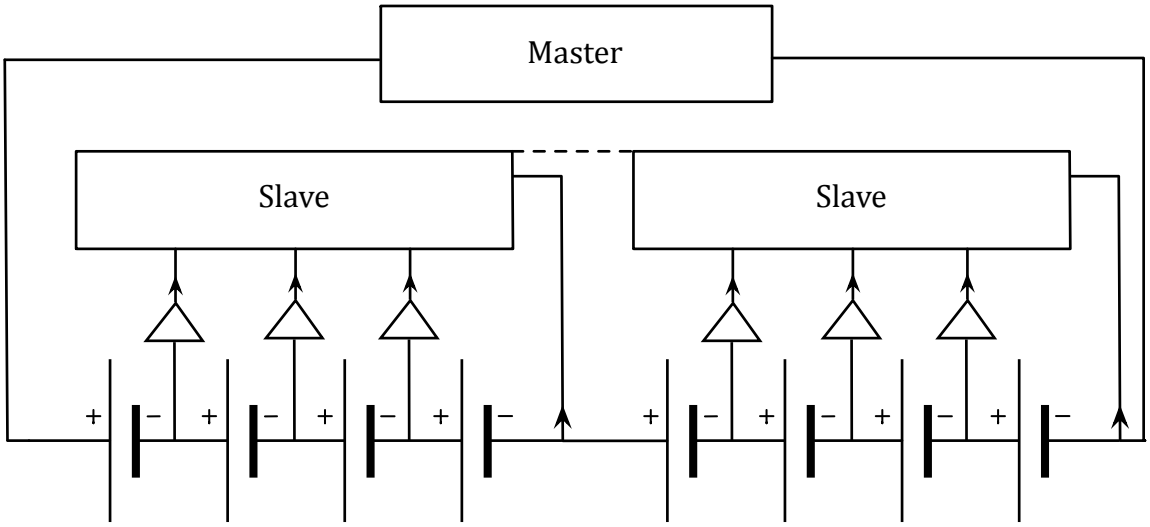

Figure 2.7: Master-slave battery management topology

In a master-slave BMS, shown in Figure 2.7, a small group of cells each has its own centralised BMS system that is local to those few cells. All of the cell level protection, balancing and monitoring is done in the slave modules. The slaves then communicate to a master controller, which contains all of the battery level protection and monitoring [16]. This topology is more complicated and expensive to implement than the centralised system but because the slaves are local to only a few cells, there is less chance of the electronics interfering with the voltage balance of the cells.

A distributed BMS uses individual management circuits that are connected to each individual cell in the battery and are controlled by a centralised BMS controller. This type of BMS is not practical for use with spacecraft batteries due to the high part count, complexity and additional weight, especially as simpler methods are available [39].

Space power system designers have a number of options when deciding how to manage their battery and there are a range of patented COTS solutions for Li-ion batteries that employ the methods described above [40]. The choice ultimately depends on the mass budget, cost, battery size, cell chemistry, the level of protection needed and the required reliability.

2.4 Battery Modelling

In this section the various approaches to modelling electrochemical cells are critically reviewed. As it is not the objective of this thesis to improve the chemical composition of the Li-S cell itself, models that predict cell behaviour will be focussed on. In Chapter 4 the choice of modelling technique used in this work is justified.

2.4.1 Battery modelling techniques

There are several approaches to designing battery models and the choice of which to adopt depends on the information already known about the battery, the required outputs of the model and how accurate the model needs to be. Models for analysing battery performance fall into three main categories: electrochemical, analytical and equivalent circuit.

Electrochemical

Electrochemical models use non-linear partial differential equations to describe the behaviour of the chemicals within a cell so that macroscopic battery parameters such as voltage and current can be accurately predicted [41]. Various electrochemical models have been described in the literature for lithium-ion [42,43,44,45], nickel-based [45,46] and lead-acid batteries [47]. It is possible to use computer programs such as Dualfoil [48] to solve these differential equations. Other mathematical techniques and computer packages are reviewed in [44]. Electrochemical modelling can achieve very good accuracy, typically 1-5%, so long as the electrochemistry is well understood, but only under well defined operating conditions. Many tens of electrochemical parameters [44,48] need to be calculated in order to solve the equations in this type of model, so this is only a viable option if these parameters are either known, or can be computed, which is normally not the case for the end user. This type of model also takes extensive periods of computational time to solve. These factors mean that this modelling technique is used mainly for cell optimisation purposes.

Analytical

Analytical models use simple mathematical formula to describe battery level behaviour, such as battery lifetime and capacity, as opposed to internal cell characteristics, such as current densities and species concentrations. Although these types of model are easier to implement than their electrochemical counterparts they can also be quite abstract, providing minimal useful information, and are relatively inaccurate with errors of anything between 5%-20% [41]. Several analytical modelling methods are reviewed in [48]. Peukert's Law, for example, approximates battery lifetime based on the discharge current rate used but is only valid for constant load profiles and is not accurate for varying or interrupted profiles, where rest periods are incorporated [49,48]. Battery runtime can also be predicted using a combination of Fick's Laws and Faraday's Laws of Electrolysis and is potentially more accurate than using only Peukert's Law, but it requires knowledge of all of the concentration and diffusion coefficients associated with each species that occurs during cell operation [49,50]. The kinetic

battery model proposed by Manwell and McGowan [51] attempts to model the recovery effects associated with interrupted current profiles. In [52] a diffusion based analytical model was proposed but this did not account for temperature and cycle aging effects. An improved model, which did account for these effects, was reported in [53] yet both models are still limited to predicting runtime and remaining capacity. Analytical methods are useful only for predicting certain aspects, such as runtime, of the battery's performance and must be used in conjunction with other methods to fully model battery behaviour.

Equivalent circuit

Equivalent circuit modelling techniques are the most intuitive method of battery modelling to an electrical engineer and can be as simple or as complicated as desired. Although generally less accurate than electrochemical models with an error in the region of 10% [48], all manner of characteristics can be modelled relatively accurately and do not take a huge amount of computational time to solve. In equivalent circuit modelling, battery characteristics are replaced with simple electric circuit elements such as voltage sources, resistors and capacitors and the terminal voltage is predicted from a combination these components. A simple equivalent circuit of battery is shown in Figure 2.8.

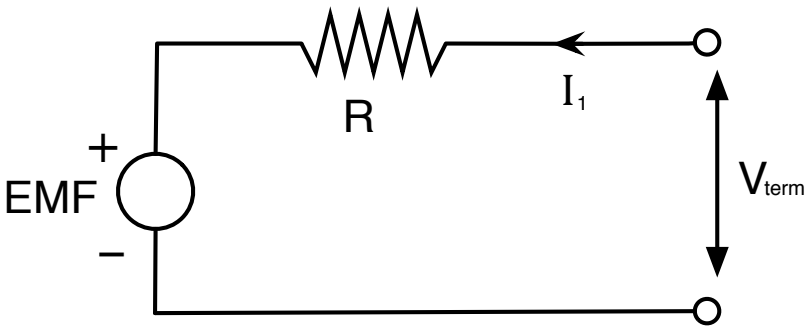

Figure 2.8: Simple battery model

The EMF gives the voltage across an ideal battery and the series resistance *R* represents the total internal resistance of the battery. *R* modifies the EMF, by an amount proportional to the load current I_1, to give the terminal voltage V_{term}. There is no concept of battery capacity or state of charge in this circuit model so an unlimited amount of capacity can be removed from the battery and the model can only be used for simple applications [54]. The state of charge

can be taken into account by summing the capacity removed from the battery and taking it as a percentage of the full capacity. Making EMF and *R* dependent on SoC improves the model's accuracy.

The Thévenin battery model depicted in Figure 2.9 improves on the simple battery model by the addition of a parallel resistor and capacitor network. This RC network mimics the diffusion process in the electrode that causes a time-dependent voltage recovery effect during periods of rest. The modelling of this transient response is thus an improvement on the first model, although it is inaccurate if constant values are used for the circuit elements [55]. More accuracy can be achieved by increasing the number of RC ladder networks, at the expense of complexity and computational time, and by varying the components' values with SoC [56].

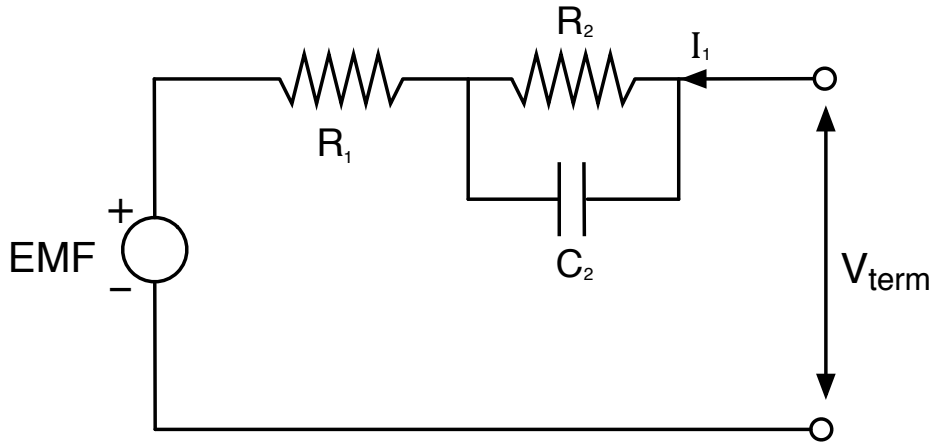

Figure 2.9: Thévenin battery model

The advanced dynamic model presented in [54] is similar to the Thévenin equivalent circuit. It is dynamic because the battery current is used to calculate the state of charge of the battery, which is then compared to values of EMF in an empirical lookup table. If the other circuit components are also known for all states of charge then the model can be continually updated using these lookup tables to provide a real-time response. The model also calculates the available capacity left in the battery by putting its dependence on current rate in another lookup table. Temperature dependencies can also be integrated in this way. The accuracy of this type of dynamic model is heavily dependent on the quality of the tabulated data [57] but it is highly adaptable to different cell chemistries if the lookup tables are replaced.

Another notable equivalent circuit model is the Zimmerman-Peterson model (Figure 2.10), a comprehensive analysis of which is given in [58]. Diodes are used as an equivalent to the RC network. The capacity is represented by a mathematical distribution, which can be modified to include temperature and current rate dependencies [50]. More complex forms of this model have voltage dependent switches on additional parallel capacitors. This improves accuracy at low states of charge where some capacitive elements have little effect [48]. This model has successfully been adapted to lithium-ion cells, but it requires lengthy statistical analysis in order to identify the necessary coefficients for the model's equations [59].

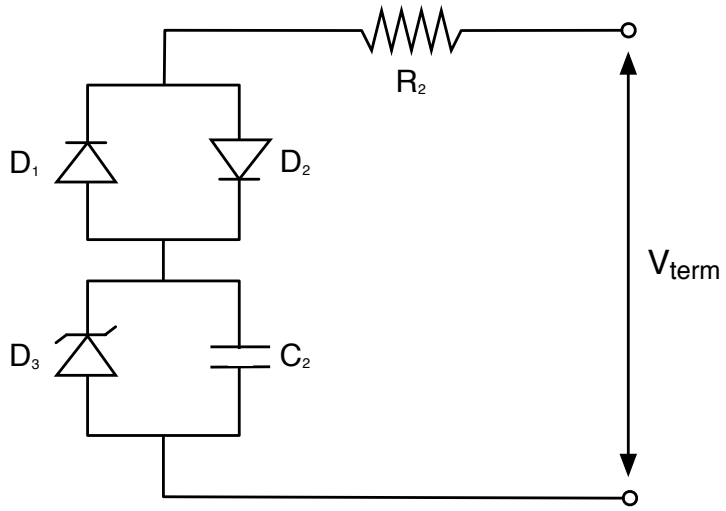

Figure 2.10: Zimmerman-Peterson model

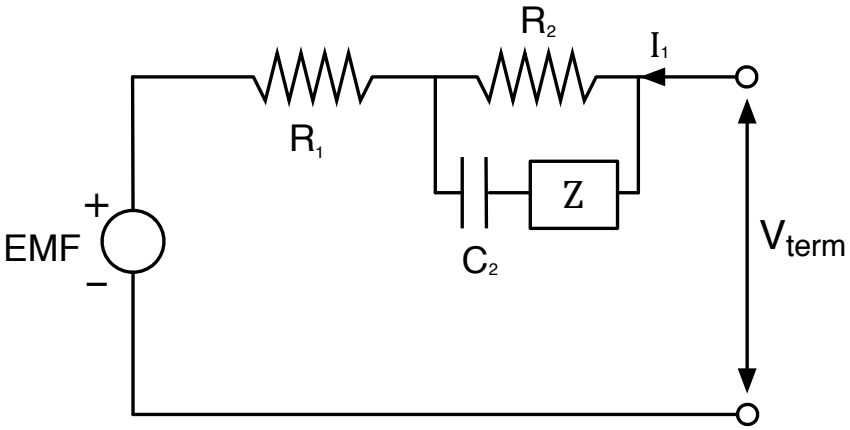

Figure 2.11: Randle's impedance model

Impedance based models [41,60,61] use electrochemical impedance spectroscopy to obtain the empirical values required for a model such as that shown in Figure 2.11. This requires an

equivalent network, Z, to be built to fit the impedance spectra to. This process is complex and counter-intuitive [41] and cannot predict battery runtime [62].

Geoff Dudley of ESA [56] developed a model of the 18650HC cell, using the concept of electrode slicing where each small slice of electrode is represented by an RC network. Although accurate, acquiring the necessary data for the equivalent circuit components requires either a reference electrode or destruction of a cell so that measurements can be made on individual electrodes, which is not generally possible or practical for the end user.

Space battery manufacturers have their own battery modelling software that they can make available to customers without having to publicly reveal proprietary data [63]. This allows customers to see how the battery they are purchasing will perform on the mission it is intended for, without having to test real cells or design models of their own. These models focus on the long-term performance of the battery, to see if it is able to complete the intended mission, rather than accurately modelling detailed transient responses to pulsed loads.

2.4.2 Lithium-sulphur model design

When designing a Li-S model with the spacecraft systems engineer in mind as an end user, certain considerations must be taken into account. The model needs to be able to:

- Be adaptable to any topology of battery.
- Be adaptable to future changes to the electrochemistry and cell design.
- Function over the desired battery operating temperature range of 0°C – 20°C.
- Provide real time feedback and/or have reasonable solve times.
- Be integrated into a full power system model.
- Have minimal input from the end user.
- Be capable of handling user defined varying power and temperature profiles.
- Predict the behaviour of the battery during all phases of the spacecraft's life and tell the power system designer whether the battery is suitable for the mission.
- Have a simple user interface.

2.5 Conclusions

This chapter was split into four parts. In the first part the space battery environment was discussed and the various cell technologies that are qualified for use in space were considered. The current state of the art in space batteries is lithium-ion cell technology with most new Earth-orbiting satellites using this chemistry as their secondary power source. The ISS is having its NiH_2 batteries replaced with Li-ion while launch vehicle batteries, which were traditionally primary silver-zinc batteries, are also being replaced with Li-ion counterparts. This change is being driven by the long cycle life, good energy density and proven reliability of lithium-ion.

Battery management system functionality was described in the second part of this chapter. Methods of cell-balancing, which is thought to be a key function of a Li-S battery management system as well as state of charge determination were looked at in more detail. The possible topologies of both battery and BMS were analysed in the third part of the chapter and laid down the foundation for deciding on appropriate topologies for a Li-S battery and its BMS in a space environment. Published work on existing Li-S battery management systems were also reviewed.

The various methods of battery modelling were described in the final part of this chapter, with emphasis being made on dynamic performance models that describe and predict battery behaviour over different states of charge and at different temperatures. A critical review of existing Li-S models reported in the literature was made in Chapter 1 and showed a gap in the area of equivalent circuit performance models. By considering the needs of the space industry, the aims of the Li-S battery model implemented in this work were specified.

REFERENCES

[1] M. Nestoridi et al., "FURTHER ADVANCED LITHIUM CELL DEVELOPMENT ," in *Proc. '9th European Space Power Conference'*, Saint Raphaël, France, 2011.

[2] G. Halpert, H. Frank, and S. Surampudi, "Batteries and Fuel Cells in Space," in *The Electrochemical Society Interface*, 1999.

[3] Eagle Picher Technologies, LLC. (2012, October) Nickel-Hydrogen Batteries and Cells. [Online]. http://www.eaglepicher.com/technologies/battery-power/nickel-hydrogen-ni-h2

[4] Saft Batteries. (2012, March) Space. [Online]. http://www.saftbatteries.com/MarketSegments/Space/tabid/152/Language/en-US/Default.aspx

[5] Yardney. (2012, March) Lithion. [Online]. http://www.yardney.com/Lithion/lithion.html

[6] Saft Batteries. (2012, March) Lithium-ion (Li-ion) : Space VES cell range. [Online]. http://www.saftbatteries.com/MarketSegments/Space/tabid/152/Language/en-US/saft/tabid/301/TypeControl/Produit/ProduitId/58/Default.aspx

[7] ABSL Space Products. ABSL 18650HC Cell Data Sheet. (2008)

[8] Samsung. (2012, March) ICR 185650-30A Li-ion Rechargeable Battery. [Online]. http://www.samsungsdi.com/battery/cylindrical-ICR185650-30A.jsp

[9] K Schrantz, C Pearson, and N. Russel, "Experiences From the Early Evolution of the Lithium-ion Space Battery Sector," in *NASA Battery Workshop*, Hunstville, Alabama, 2008.

[10] J. Neubauer, H. Alcock, N. Ahmed, and C. Pearson, "Progress on the Space Qualification of the High Energy ABSL 18650NL Cell," in *NASA Battery Workshop*, Huntsville Alabama, 2009.

[11] Panasonic. (2010, February) Panasonic Corporation Website. [Online]. http://industrial.panasonic.com/www-data/pdf2/ACA4000/ACA4000CE254.pdf

[12] Y. Yao et al., "Interconnected Silicon Hollow Nanospheres for Lithium-Ion Battery Anodes with Long Cycle Life ," *Nano Lett.*, vol. 11, pp. 2949-2954, 2011.

[13] H.K. Liu, Z.P. Guo, J.Z. Wang, and K. Konstantinov, "Si-based anode materials for lithium rechargeable batteries," *J. Mater. Chem.*, vol. 20, pp. 10055-10057, 2010.

[14] Nexeon Ltd. (2012, May) Benefits of Nexeon Technology. [Online]. http://www.nexeon.co.uk/technology/benefits-of-nexeon-technology/

[15] Y Barsukov. Texas Instruments Website. [Online]. http://focus.ti.com/download/trng/docs/seminar/Topic%202%20-%20Battery%20Cell%20Balancing%20-%20What%20to%20Balance%20and%20How.pdf

[16] D. Reece, "ABSL internal report," 2010.

[17] Y. Drori and C. Martinez. (2005) The benefits of cell balancing; intersil application note AN141.0. [Online]. http://www.neue-verpackung.de/ai/resources/a03b3cf05d5.pdf

[18] S. W. Moore and P. J. Schneider, "A Review of Cell Equalisation Methods for Lithium Ion and Lithium Polymer Battery Systems," *Delphi Automotive Systems* , 2001.

[19] T. Mazz, "Li-Ion Charge Balancing and Cell Voltage Monitoring for Performance and Safety," in *2010 Advanced Energy Conference*, 2010.

[20] NASA Johnson Space Center. (2012, March) Battery Management System. [Online]. http://www.nasa.gov/centers/johnson/techtransfer/technology/MSC-24466-1_Batt-Mgmt-Sys_prt.htm

[21] G. J. Dudley, D. Olsson, and P. Brochard, "Maintaining Cell State of Charge Balance in Lithium Ion Batteries," in *Space Power, Proceedings of the Sixth European Conference*, Porto, Portugal, 2002, p. 501.

[22] S. Pang, J. Farrell, J. Du, and M. Barth, "Battery State-Of-Charge Estimation," in *Proceedings of the American Control Conference*, Arlington, VA, 2001.

[23] mpoweruk. (2009, March) Battery state of charge determination. [Online]. www.mpoweruk.com/sco.htm

[24] S. Piller, M. Perrin, and A. Jossen, "Methods for state of charge determination and their applications," *J. Power Sources*, vol. 96, pp. 113-120, 2001.

[25] V. Pop et al., "Modeling battery behaviour for accurate state of charge indication," *Journal of The Electrochemical Society*, vol. 153, no. 11, pp. A2013-A2022, 2006.

[26] J. Christo. (2010, May) Problems with the Interim Li Ion Rechargeable Batteries Type Approval Procedure. [Online]. http://www.sarsat.noaa.gov/BMW%202010_files/Proposed%20changes%20to%20the%20Interim%20Li%20Ion%20rechargeable%20rev%201_JC.pdf

[27] F. Huet, "A review of impedance measurements for determination of the state-of-charge or state-of-health of secondary batteries; ," *Journal of Power Sources*, vol. 70, no. 1, pp. 59-69, 1998.

[28] H. Blanke et al., "Impedance measurements on lead–acid batteries for state-of-charge, state-of-health and cranking capability prognosis in electric and hybrid electric vehicles," *Journal of Power Sources*, vol. 144, pp. 418-425, 2005.

[29] S. Rodrigues, N. Munichandraiah, and A.K. Shukla, "A review of state of charge indication of batteries by means of ac impedance measurement ," *Journal of Power Sources*, vol. 87, pp. 12-20, 2000.

[30] C. Simpson. (2012, October) National Semiconductor; Battery Charging. [Online]. http://cegt201.bradley.edu/projects/proj2008/lcc/pdf/national_battery_charging.pdf

[31] J. D. Dunlop, J. N. Brill, and R. Erisman, "CHAPTER 32 NICKEL-HYDROGEN BATTERIES," in *Handbook of Batteries*.: McGraw-Hill, 2002.

[32] J. Chiasson and B. Vairamohan, "Estimating the State of Charge of a Battery," *Control Systems Technology, IEEE Trans,* vol. 13, no. 3, pp. 465-470, May 2005.

[33] S. Lee, J. Kim, J. Lee, and B.H. Cho, "State-of-charge and capacity estimation of lithium-ion battery using a new open-circuit voltage versus state-of-charge," *Journal of Power Sources*, vol. 185, pp. 1367-1373, 2008.

[34] C. Ehret, S. Piller, W. Schroer, and A. Jossen, "State-of-chargedetermination for lead-acid batteries in PV-applications," in *Proceedings of the 16th European Photovoltaic Solar Energy Conference*, Glasgow, 2000.

[35] Texas Instruments. (2012, October) Texas Instruments Power Management. [Online]. http://focus.ti.com/paramsearch/docs/parametricsearch.tsp?family=analog&familyId=412&uiTemplateId=NODE_STRY_PGE_T

[36] GS Yuasa. (2012, October) GS Yuasa Lithium Power. [Online]. http://www.gsyuasa-lp.com/gylp-products

[37] C. Pearson, A. Bennetti, and R. Spurrett, "Advances in Battery Technology Relevant For Planetary Probes," in *Fourth Annual International Planetary Probe Workshop*, Pasadena, California, 2006.

[38] C.A. Hill, "Satellite Battery Technology - A Tutorial And Overview," *Aerospace and Electronic Systems Magazine*, vol. 26, no. 6, pp. 38-43, June 2011.

[39] D. Andrea, *Battery Management Systems for Large Lithium-Ion Battery Packs.*: Artech House, 2010.

[40] Aeroflex Microelectronic Solutions. (2012, March) Battery Electronic Units (BEU). [Online]. http://www.aeroflex.com/ams/pagesproduct/prods-power-beu.cfm

[41] M Chen and G A. Rincon-Mora, "Accurate electrical battery model capable of predicting runtime and I-V performance," *IEEE TRANSACTIONS ON ENERGY CONVERSION*, vol. 21, no. 2, 2006.

[42] T.F. Fuller, M. Doyle, and J. Newman, "Simulation and optimization of the dual lithium ion insertion cell," *Journal of the Electrochemical Society*, vol. 141, no. 1, 1994.

[43] J. Newman, K.E. Thomas, H. Hafezi, and D.R. Wheeler, "Modeling of lithium-ion batteries," *Journal of Power Sources*, vol. 119–121, pp. 838–843, 2003.

[44] G.G. Botte, V.R. Subramanian, and R.E. White, "Mathematical Modeling of secondary lithium batteries;," *2000 Electrochimica Acta*, vol. 45, pp. 2595-2609, 2000.

[45] P.M. Gomadam, J.W. Weidner, R.A. Dougal, and R.E. White, "Mathematical modelling of lithium ion and nickel battery systems," *Journal of Power Sources*, vol. 110, pp. 267-284, 2002.

[46] D. Fan and R.E. White, "A Mathematical Model of a Sealed Nickel-Cadmium Battery," *J. Electrochem. Soc*, vol. 138, no. 1, 1991.

[47] E. Karden, P. Mauracher, and F. Schöpe, "Electrochemical modelling of lead/acid batteries under operating conditions of electric vehicles," *Journal of Power Sources*, vol. 64, no. 1-2, pp. 175-180, 1997.

[48] M.R. Jongerden and B.R. Haverkort, "Battery Modeling," Centre for Telematics and Information Technology , University of Twente, Enschede, Technical Report TR-CTIT-08-01, 2008.

[49] D Rakhmatov and and D. A. Wallach S. Vrudhula, "A Model for Battery Lifetime Analysis for Organizing Applications on a Pocket Computer," *IEEE TRANSACTIONS ON VERY LARGE SCALE INTEGRATION (VLSI) SYSTEMS*, vol. 11, no. 6, pp. 1019-1030, 2003.

[50] M. P. Cassagne et al., "Comparison between ELAN test results and an improved Zimmerman model 1998," in *Proceedings of the Fifth European Space Power Conference (ESPC)*, Tarragona, Spain, 1998, p. 727.

[51] J. Manwell and J. McGowan, "Lead acid battery storage model for hybrid energy systems," *Solar Energy*, vol. 50, pp. 399–405, 1993.

[52] D.N. Rakhmatov and S.B.K. Vrudhula, "An Analytical High-Level Battery Model for Use in Energy Management of Portable Electronic Systems".

[53] P Rong and M. Pedram, "An Analytical Model for Predicting the Remaining battery capacity of lithium ion batteries;," *IEEE TRANSACTIONS ON VERY LARGE SCALE INTEGRATION (VLSI) SYSTEMS*, vol. 14, no. 5, pp. 441-451, 2006.

[54] M, Durr, A. Cruden, S. Gair, and J.R. McDonald, "Dynamic model of a lead acid battery for use in a domestic fuel cell system," *Journal of Power Sources*, vol. 161, pp. 1400-1411, 2006.

[55] Z.M. Salameh, M.A. Casacca, and W.A. Lynch, "A mathematical model for lead acid batteries," *IEEE Transactions on Energy Conversion*, vol. 7, no. 1, 1992.

[56] G. J. Dudley, J. De Roche, F. Tonicello, and C. Thwaite, "Electrical/Thermal Model of a Sony 18650HC Li-ion Cell," in *Proc. 'Seventh European Space Power Conference'*, Stresa, Italy, 2005.

[57] H.J. Bergveld, W.S. Kruijt, and P.H.L. Notten, "Electronic-network modelling of rechargeable NiCd cells and its application to the design of battery management systems;," *Journal of Power Sources*, vol. 77, no. 2, pp. 143-158, 1999.

[58] H.G Zimmerman and R.G. Peterson, "An electrochemical cell equivalent circuit for storage battery / power system calculations by digital computer," in *IECEC*, 1970.

[59] A. Capel, "Mathematical model for the representation of the electrical behaviour of a lithium cell.," in *Power Electronics Specialists Conference, IEEE 32nd Annual*, vol. 4, 2001, pp. 1976 - 1981.

[60] M. Urbain, M. Hinaje, S. Rael, B. Davat, and S. Desprez, "Energetical Modeling of Lithium-Ion Batteries Including Electrode Porosity Effects," *IEEE TRANSACTIONS ON ENERGY CONVERSION*, vol. 25, no. 3, 2010.

[61] C. R. Gould, C. M. Bingham, D. A. Stone, and P. Bentley, "New Battery Model and State-of-Health Determination Through Subspace Parameter Estimation and State-Observer Techniques," *IEEE TRANSACTIONS ON VEHICULAR TECHNOLOGY*, vol. 58, no. 8, pp. 3905-3916, 2009.

[62] S. Buller, M. Thele, R.W.D. Doncker, and E. Karden, "Impedance-based simulation models of supercapacitors and Li-ion batteries for power electronic applications," *Industry Applications, IEEE Transactions on*, vol. 41, no. 3, pp. 742 - 747 , 2005.

[63] D.Z. Genc and C. Thwaite, "PROBA-1 AND MARS EXPRESS: AN ABSL LITHIUM-ION LEGACY," in *European Space Power Conference (ESPC)*, St Raphael, France., 2011.

CHAPTER 3

LITHIUM-SULPHUR CELL TECHNOLOGY

In this chapter the electrochemistry of the lithium-sulphur cell is discussed in detail. It is important to have a thorough understanding of the inner workings of the cell in order to know how best to proceed with cell characterisation, model cell characteristics, determine protection requirements of the cells and explain testing results.

The general performance and operation of the cell is reviewed initially, followed by an analysis of the electrochemical reactions that take place during charge and discharge, as well as considering parasitic side reactions and unwanted side effects. Finally, the Li-S chemistry is compared to state of the art Li-ion technology with a view to discussing the strengths and weaknesses of both cell types in relation to spacecraft applications.

3.1 The Lithium-Sulphur Cell

3.1.1 The lithium-sulphur couple

The use of negative intercalation (carbon lattice) electrodes in Li-ion cells significantly limits their practical energy density when compared to that of the pure lithium metal electrodes used in Li-S cells. A standard LiC_6 negative electrode has a maximum specific capacity of 372mAh/g, while pure lithium metal has a value ten times higher at 3860mAh/g [1]. This difference is due to the structure of the intercalation electrode. No matter how accommodating it is to lithium ions its energy density can never be as high as pure lithium because the carbon lattice always uses up space without contributing to the capacity. With a lithium metal anode, the whole electrode can theoretically contribute to the cell's capacity.

The extreme reactivity of lithium has hindered many an attempt to safely harness its power as a pure metal anode. In spite of this, lithium has always been a desirable choice as an electrode material due to its low equivalent weight, highly negative reduction potential and

high specific energy [2,3]. For these reasons, considerable research and development has been dedicated to making this a safe and viable commercial option. A key factor in allowing a lithium metal anode to be used safely is to find a suitable cathode material to complement it.

Sulphur is an attractive choice for this cathode material. It is non-toxic and therefore environmentally benign, is abundant and cheap, and has a low equivalent weight, which are all sought after electrode properties. While elemental sulphur is well known to be electrically insulating, sulphur in the liquid phase can take part in electrochemical reactions and so, despite the comparably low cell voltages it produces [4], sulphur appeals as an electrode material.

The alkali metal-sulphur combination was known to be an attractive coupling [5] because of its high theoretical energy density. In fact, the lithium-sulphur couple has one of the highest theoretical energy densities of any battery couple (see Section 3.1.3). Despite its potential, rechargeable, ambient-temperature lithium-sulphur batteries were historically never considered to be commercially viable as they were thought to be too unreliable, expensive and unsafe [4,6]. The reactions that occur in the cell mean that sulphur is reduced to an alkali metal sulphide and although this reaction has a high theoretical energy density, solid sulphur S_8 and its final discharge product Li_2S are highly insoluble electrical insulators at room temperature, having high resistivity and low electroactivity [6]. Early research focussed on molten electrode/electrolyte combinations but this required very high operating temperatures and the cells suffered from very low sulphur utilization and poor reversibility [7,8]. Although elemental sulphur can take part in electrochemical reactions in the dissolved state, this causes problems in joining a sulphur electrode to a current collector and, most importantly, an insulating film of sulphur is formed on recharge and a film of Li_2S on discharge which act to electrically isolate the cathode components [9,10].

Lithium-sulphur batteries were not considered suitable for commercial applications until the mid 1990s when a new cell design, incorporating active sulphur into a carbon composite electrode structure, gave high sulphur utilizations at ambient temperatures [11,10].

3.1.2 Modern cell design and operation

Modern lithium-sulphur cells are manufactured as pouch cells, the basic operation of which is depicted in Figure 3.1. A solid lithium metal foil is used as the negative electrode, or anode[1], while the positive electrode is an open-pore carbon composite structure that is filled with elemental sulphur. This electrode, although constructed of solid carbon and solid sulphur in its pre-discharged state, can be classed as a liquid cathode because it is only when the sulphur is dissolved that it takes part in electrochemical reactions. The open pore structure facilitates this process as the solid sulphur dissolves into the electrolyte, filling the cathode.

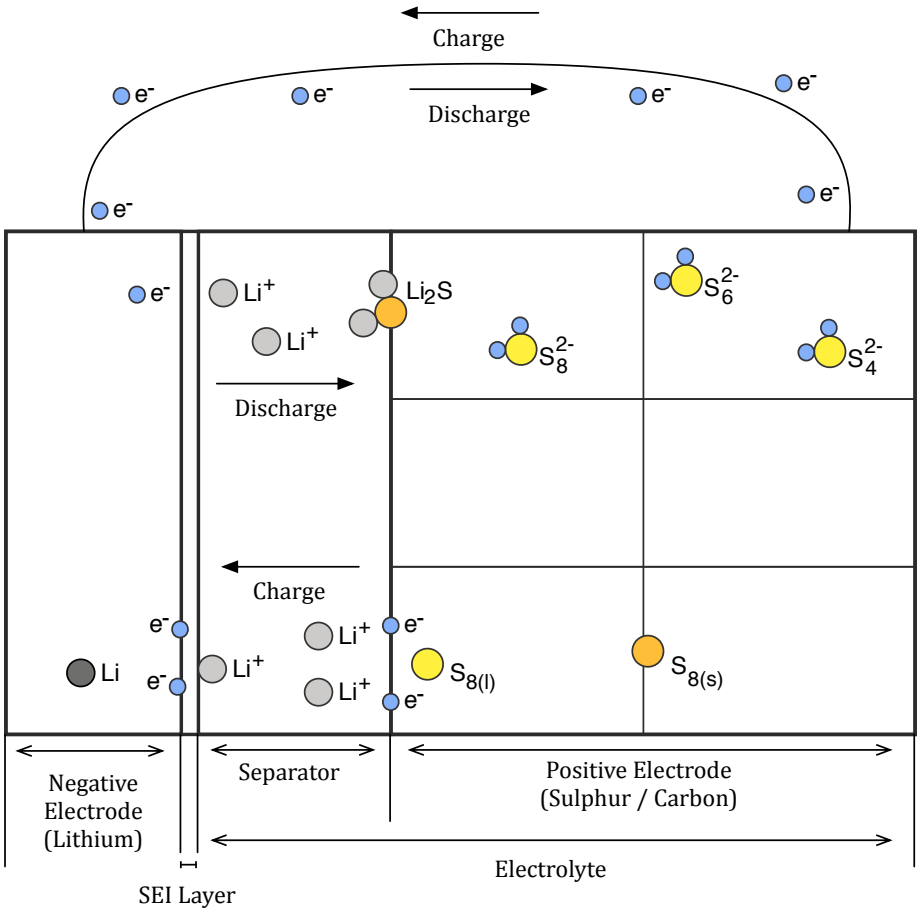

Figure 3.1: Operation of a lithium-sulphur cell

[1] The electrodes of a battery are referred to as the anode and the cathode. Strictly speaking, the anode is the electrode that loses electrons to the external circuit whereas the cathode is the electrode that receives electrons. This means that during discharge the anode is the negative electrode and the cathode is the positive electrode. During charge the electrons flow in the opposite direction so the positive electrode becomes the anode and the negative electrode becomes the cathode. It is convenient to refer to the electrodes in the discharging state so in this work, unless otherwise stated, reference to the anode signifies the negative electrode whilst reference to the cathode signifies the positive electrode.

The volume of the pores in the cathode must be at least 1.79 times larger that the initial volume of sulphur [12]. This allows adequate space for the high volume discharge products that will gather on its surface without impeding good cell operation. Cathodes without an open pore structure become easily blocked with excess discharge product and can also keep a significant part of the sulphur capacity outside of the active area of the electrode [13]. The carbon matrix is easily accessible by the electrons supplied from the external circuit, allowing them to flow between the current collector to any point in the carbon structure. This permits the transport of electrons to and from the active sulphur, which enables good sulphur utilization. The cathode also performs well at ambient temperatures, which is a key factor in manufacturing a commercially viable rechargeable lithium-sulphur cell.

The ionically conducting liquid electrolyte is entirely incorporated into the porous structure of the cathode and separator while remaining in contact with the surface of the anode. The electrolyte permeates through the pores of the cathode and so is in intimate contact with the active sulphur that is attached to it. This facilitates a flow of ions through the cathode and separator and so aids the utilization of sulphur [10,14,15]. There must be adequate means for ions to freely pass between the anode and the cathode in order to allow the use of reasonable current rates on the cell [13].

As depicted in Figure 3.1, during discharge, lithium ions that form at the anode diffuse through the electrolyte and react with sulphur ions to produce a series of soluble and insoluble lithium polysulphides of various chain lengths. During charge, these polysulphides are oxidised back to their solid elemental sulphur form while the lithium ions travel back to the anode, reacting with electrons and forming lithium metal once more. Ideally, these lithium polysulphides need to be able to flow unimpeded between the electrodes. Electrolytes that allow polysulphides to easily dissolve are desirable as they improve rate capability, sulphur utilization and allow the cathode to operate as a liquid (or soluble) cathode. The work of R. D. Rauh in the late seventies showed that lithium polysulphides were highly soluble in electrolytes containing substances such as dimethyl sulphoxide and THF

[9,16]. Further work showed that dioxolane (DOL), 1,2–Dimethoxy Ethane (DME) and glyme solvents were even better solvents for polysulphides [2,12,17,18,19]. DME has very high polysulphide solubility, which gives the cell a high discharge capacity, but it is also very reactive with lithium metal, causing severe corrosion. An unprotected anode encourages parasitic side reactions with dissolved polysulphides in the electrolyte. DOL has low polysulphide solubility when compared to DME but its properties encourage a stable protective layer, or Solid Electrolyte Interphase (SEI) (see Section 3.2.3), on the anode surface. This layer forms in the first discharge of the cell and protects the lithium from further corrosion by the polysulphides in the electrolyte. The ratio of DME to DOL is controlled to 2:1 [20] and using them together creates an electrolyte optimised for the operation of the cathode and the protection of the anode [12,21].

A highly porous separating material electrically insulates the electrodes from one another in order to prevent electrical shorts between the electrodes. Suitable separators such as plastic, glass or paper, can be used as porous membranes that resist damage caused by the electrolyte and by the electric potential between the electrodes. Each electrode is fixed to a highly conductive current collector that allows an external circuit to draw a current from the battery. Aluminium, copper and stainless steel are good choices of current collector material as they are excellent conductors, resistant to degradation and able to withstand repeated cycling [22,23]. All components are layered, wound and then enclosed in an insulated foil pouch that protects the reactive elements within the cell. Only conducting tags, which extend out of the casing, are external to the cell, allowing the cell to be attached to a separate circuit.

3.1.3 General performance characteristics

Capacity and C-rate

The total capacity of a cell is defined as the amount of charge, given in Amp hours (Ah), that a cell can deliver when discharged from 100% SoC to 0% SoC. To get the maximum amount of charge from a battery requires an extremely slow discharge so that there are minimal losses from resistance and heat dissipation in the cell. At high current the rate-dependent difference

in potential between the EMF and the terminal voltage, caused by internal resistance, means that the cell reaches its safety voltage limits before the cell's full capacity is realised. A cell can be held at this voltage limit while the current is tapered, allowing more charge to enter or leave the cell. Usually a nominal capacity is defined as the capacity obtained at a reasonable current rate, where discharge takes between 5-10 hours.

It is standard practice to use the capacity of a battery to define the current levels used on it. The lithium-sulphur cell used in this work has a nominal capacity of 2.8Ah and so it would take 1 hour to discharge the cell at 2.8A. This is known as the C-rate and charge or discharge currents are often given as fraction or multiple of this rate. For example, C/2 would be 1.4A and would discharge the cell, theoretically, in two hours. However, it is only at very low current rates that the terminal voltage closely follows the open circuit voltage (or EMF) so using higher rates, where the terminal voltage deviates from the EMF, would deplete the cell in less time than the given C rate would imply.

Theoretical Capacity

The theoretical capacity of a battery is the ideal amount of electric charge that it can deliver if every single atom of reactant were fully reduced to its final discharge product. In real batteries this does not occur and the actual capacity is always lower than the theoretical capacity due to internal losses.

The theoretical capacity of a lithium-sulphur battery is restricted by the capacity of elemental sulphur, which is 1672mAh/g [24]. The theoretical capacity of pure lithium is much higher at 3830mAh/g [24] but in this cell type it is the amount and capacity of sulphur at the cathode that determines how long the cell reactions can last for and therefore the capacity of the whole cell. The derivation of the theoretical capacity of the Li-S cell is given in Appendix A.

Cell Potential

The cell voltage for the lithium-sulphur couple is determined by comparing the standard reduction potentials for each electrode. Equation 3.1 gives the reaction at the sulphur

cathode. The standard reduction potential of this reaction relative to the standard hydrogen electrode (SHE) is -0.48V [25]. Equation 3.2 gives the reaction at the lithium anode. The standard reduction potential of this reaction when compared to the SHE is -3.05V [25].

$$S + 2e^- \leftrightarrows S^{2-} \quad [3.1]$$

$$Li \leftrightarrows Li^+ + e^- \quad [3.2]$$

It is convention to determine the total cell potential by calculating the difference between the potentials of the cathode and the anode [26]. This potential difference ΔV determines the maximum open circuit voltage of the cell so:

$$\Delta V = E_{cathode} - E_{anode} \quad [3.3]$$

The lithium-sulphur cell voltage, given by Equation 3.3, is 2.57V. In fact, as will be shown, the potential is dependent on the concentration of different species within the cell and varies as these species undergo redox reactions during cycling.

Theoretical Energy Density and Specific Energy

Energy density describes the amount of energy contained within a battery per unit volume. The theoretical energy density of the lithium-sulphur couple is 2862Wh/l [27]. Specific energy describes the amount of energy contained within a battery per unit mass. The theoretical specific energy of the lithium-sulphur couple is 2550Wh/kg [27]. These theoretical values are significant amounts and are much higher than any other presently known cell couple [24]. These values are derived in Appendix A and are valid for an ideal cell.

In reality the values are much lower due to non-ideal cell reactions and the mass of cell components that do not contribute to cell capacity. Li-S cells currently in production claim to have specific energies of around 350Wh/kg [12,27] and energy densities of around 320Wh/l [27] in a nominal 2.8Ah cell.

3.2 Electrochemical Performance Characteristics

The lithium-sulphur cell has unique electrochemical characteristics and understanding these characteristics makes it possible to determine not only how well the cell will perform under different conditions but how the cell can be modelled and protected and how suitable it is for certain applications.

3.2.1 Discharge characteristics

A typical discharge curve for a lithium-sulphur cell at ambient temperature is shown in Figure 3.2. This profile was produced from data taken during the characterisation testing that is described in Chapter 4. The discharge curve can be split into two main regions. The first discharge region corresponds to a voltage range of approximately 2.45V – 2.1 V and contains a voltage plateau at around 2.35V with a shallow knee at 2.3V. The second region corresponds to the voltage range 2.1V to 1.7V and contains a distinct voltage plateau at about 2.12V with a sharp knee at the end of discharge. The shape of the voltage profile can be investigated by looking at the complex polysulphide reduction processes.

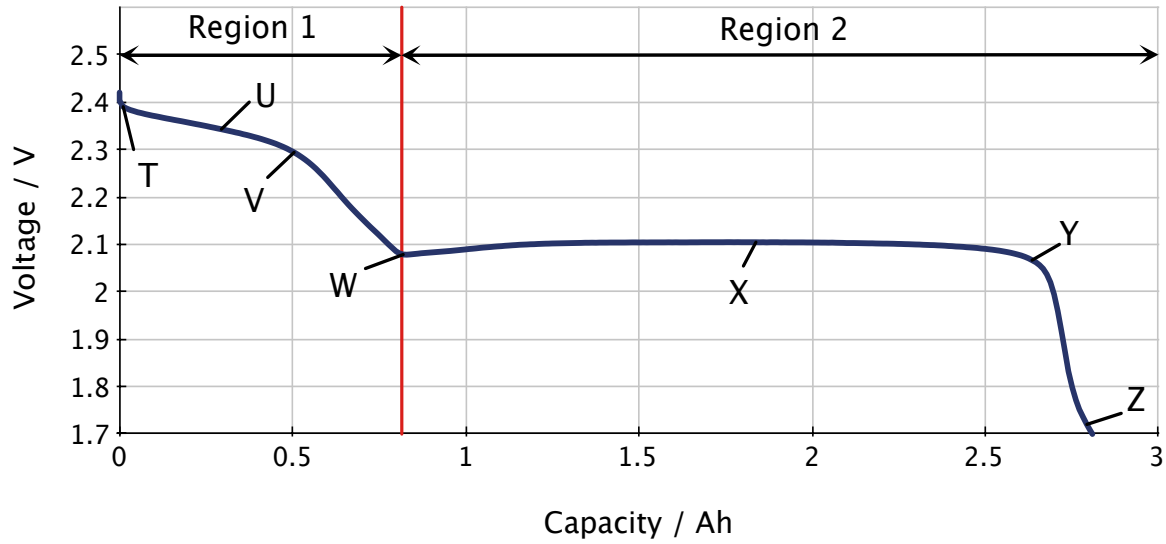

Figure 3.2: Discharge profile of a lithium-sulphur cell taken at 0.315A (~C/9)

When the cell is fully charged, the cathode predominately contains solid elemental sulphur $S_{8(s)}$. Solid elemental sulphur is able to dissolve into the electrolyte and into its liquid phase $S_{8(l)}$ even though it has relatively low solubility (19 mol/m^3) [28]. As such, the cell begins

discharge with a layer of sulphur already dissolved in the electrolyte and adsorbed to the carbon matrix [29,30]. This is given by the following relationship:

$$S_{8(l)} \leftrightarrows S_{8(s)} \qquad [3.4]$$

The phase transformation of elemental sulphur increases the porosity of the cathode structure and the separator [28]. When the cell begins to discharge (Figure 3.1, point T), by application of an external load, the lithium metal in the anode is oxidised, supplying electrons to the load and leaving lithium ions at the anode, as given by Equation 3.2. The initial state of the cell as discharge begins is depicted in Figure 3.3.

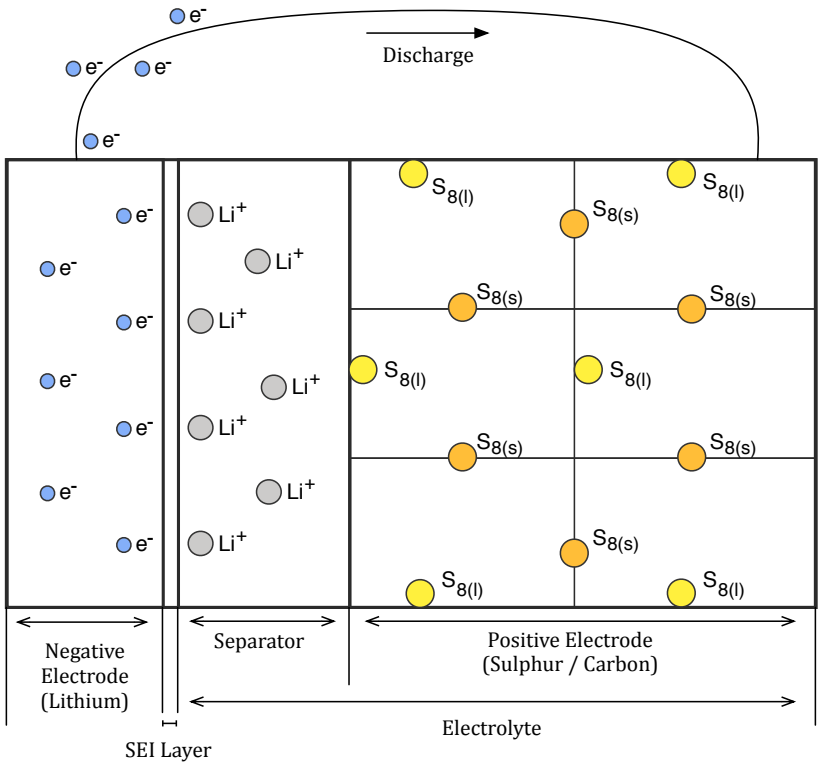

Figure 3.3: Initial state of Li-S cell as discharge begins from full capacity

Due to the newly formed concentration gradient of positively charged lithium ions at the surface of the anode, the lithium ions diffuse into the electrolyte contained within the separator and the pores of the cathode. As more electrons leave the anode the concentration of lithium ions in the electrolyte increases. Meanwhile, as depicted in Figure 3.4, the cathode receives electrons from the external circuit and these electrons reduce the liquid elemental sulphur $S_{8(l)}$, which is in contact with the cathode structure, to form the sulphide ion S_8^{2-}.

Positive lithium ions at the anode migrate through the electrolyte towards the cathode and negative sulphide ions migrate towards the anode.

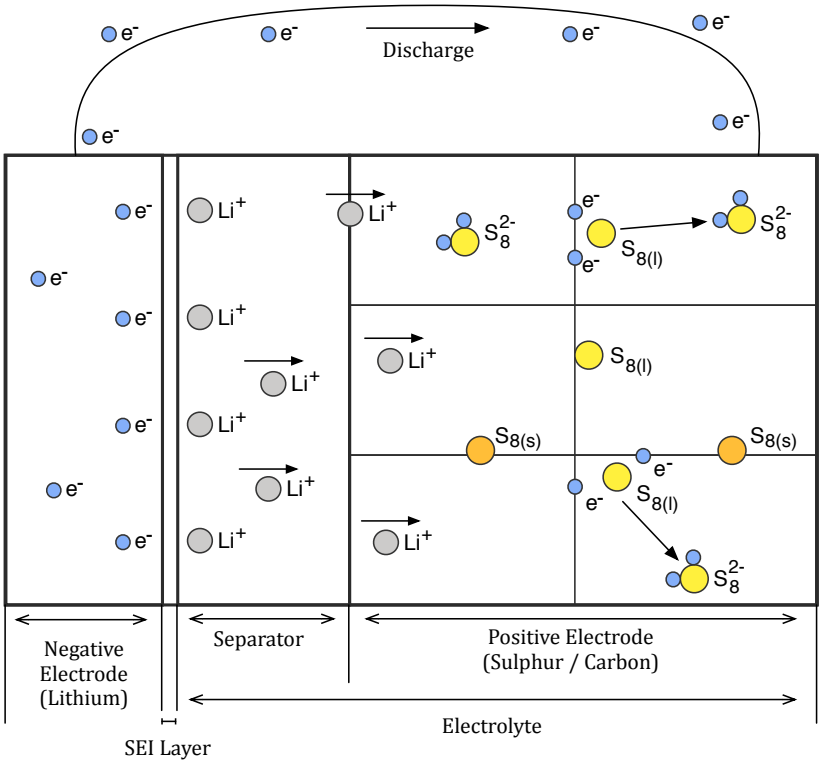

Figure 3.4: Sulphur is reduced at the cathode as electrons are received

As discharge continues the sulphide ions that remain in contact with the cathode structure are further reduced, by facile electron transfer, to increasingly lower states of oxidation given by Equations 3.5-3.9 [28]:

$$\frac{1}{2}S_{8(l)} + e^- \leftrightarrows \frac{1}{2}S_8^{2-} \quad [3.5]$$

$$\frac{3}{2}S_8^{2-} + e^- \leftrightarrows 2S_6^{2-} \quad [3.6]$$

$$S_6^{2-} + e^- \leftrightarrows \frac{3}{2}S_4^{2-} \quad [3.7]$$

$$\frac{1}{2}S_4^{2-} + e^- \leftrightarrows S_2^{2-} \quad [3.8]$$

$$\frac{1}{2}S_2^{2-} + e^- \leftrightarrows S^{2-} \quad [3.9]$$

Throughout discharge the concentrations of these different species of ion vary widely. Kumaresan, Mikhaylik and White reported these concentration variations in 2008 [28] and the results of their model are reproduced in Figure 3.5.

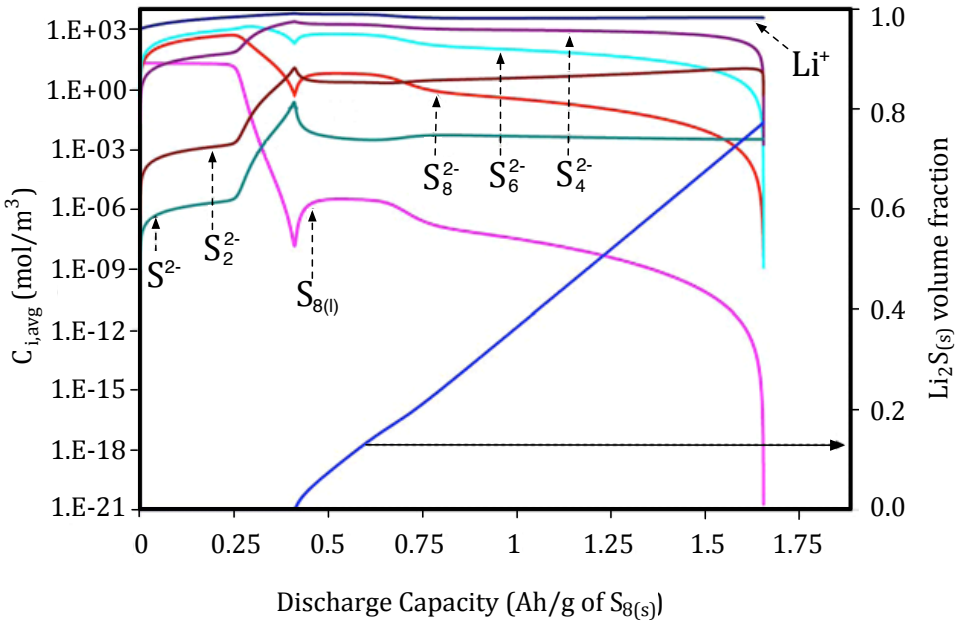

Figure 3.5: Average concentrations of species ($C_{i,avg}$) and average volume fraction of $Li_2S_{(s)}$ in the cathode as a function of discharge capacity [28].

The first discharge region, in Figure 3.2, can be attributed to the reduction of elemental sulphur to the higher order polysulphides, S_8^{2-}, S_6^{2-} and S_4^{2-}, and the second discharge region can be attributed to the reduction of these polysulphides to those of a lower order, $S_2^{2-}$and S^{2-}. In the first discharge region, where solid elemental sulphur is eventually reduced to S_4^{2-}, the overall reaction can be described by Equation 3.10 [31]:

$$S_8 + 4e^- \rightarrow 2S_4^{2-} \qquad [3.10]$$

The EMF of an electrochemical cell is related to the concentrations of the species involved in the reactions by the Nernst equation [26]. The corresponding Nernst equation for the above equation in the high plateau is given by:

$$E_H = E_H^O + \frac{R_g T}{n_H F} ln \frac{[S_8^0]}{[S_4^{2-}]^2} \qquad [3.11]$$

Where E is equal to the EMF, E^0 is the EMF under standard conditions, R_g is the ideal gas constant, T is the temperature in Kelvin, F is Faraday's constant and n is the number of electrons. The subscript H denotes that the equation represents the reactions at the high plateau. As the concentration of the higher order species decreases and the concentration of the lower order species increases during discharge, the value of the logarithm becomes increasingly negative, indicating a lower value of EMF at lower states of charge. For the low voltage plateau where the reactants are different and the high order sulphide ions are reduced to low order sulphide ions, the following equation is obeyed [31]:

$$S_4^{2-} + 4e^- \rightarrow 2S^{2-} + S_2^{2-} \qquad [3.12]$$

The corresponding low plateau (denoted by subscript L) Nernst equation, is given by:

$$E_L = E_L^O + \frac{R_g T}{n_L F} ln \frac{[S_4^{2-}]}{[S^{2-}]^2 [S_2^{2-}]} \qquad [3.13]$$

The concentrations of the three species in this equation do not vary greatly during the second discharge region, as evidenced in Figure 3.5, and so the value of E_L remains close to constant.

The reduction of sulphide ions during discharge is actually more complex than first appears and sulphide chain length does not necessarily reduce systematically. The various discharge reactions described in the remainder of this section are all depicted in Figure 3.6. As previously shown, the ion S_8^{2-} can remain in contact with the carbon structure of the cathode and facile electron transfer reduces it further to a sulphide ion of shorter chain length, S_6^{2-}. However, the S_8^{2-} ion might instead diffuse away from the cathode making it impossible for it to directly receive more electrons from the cathode structure. Once diffused into the electrolyte, it is free to react with two lithium ions to produce the long chain lithium polysulphide Li_2S_8. In fact at any point during systematic reduction, sulphide ions may dissolve away from physical contact with the carbon matrix and migrate towards the lithium ions in the electrolyte, reacting to form one of the following precipitates:

$$Li_2S_{8(s)}, Li_2S_{6(s)}, Li_2S_{4(s)}, Li_2S_{2(s)}, Li_2S_{(s)}$$

Precipitates of the form Li_2S_x where x>2 are highly soluble in the electrolyte while $Li_2S_{2(s)}$ (lithium disulphide) and $Li_2S_{(s)}$ (lithium sulphide) are highly insoluble.

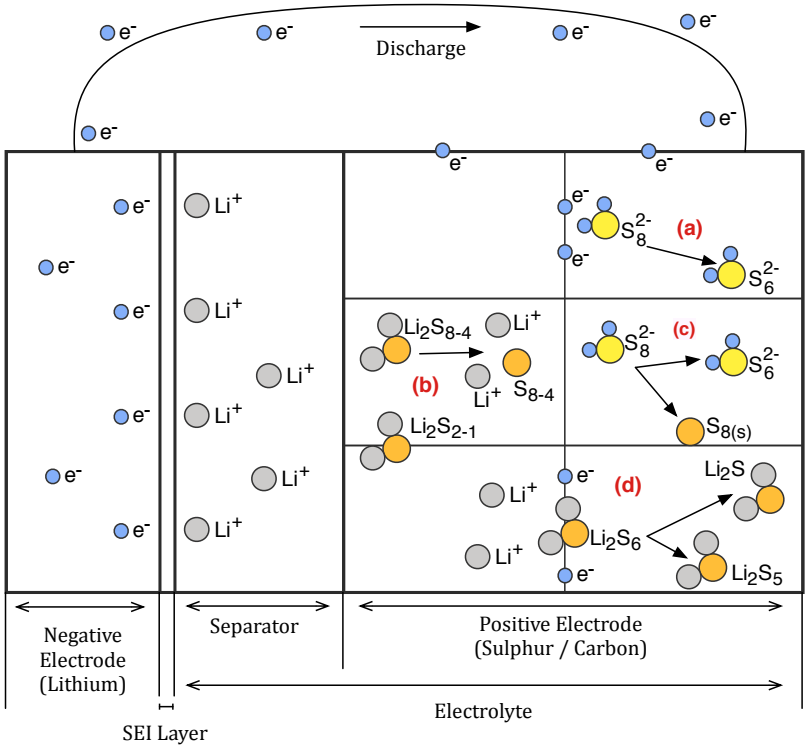

Figure 3.6: Possible reactions during discharge (a) systematic reduction, (b) precipitation/dissolution, (c) dissociation and (d) disproportionation.

In the first discharge region only the first three of these precipitates are formed in abundance. As they are highly soluble in the electrolyte, they are subject to the following precipitation/dissolution reactions:

$$2Li^+ + S_8^{2-} \leftrightarrows Li_2S_{8(s)} \quad [3.14]$$

$$2Li^+ + S_6^{2-} \leftrightarrows Li_2S_{6(s)} \quad [3.15]$$

$$2Li^+ + S_4^{2-} \leftrightarrows Li_2S_{4(s)} \quad [3.16]$$

Figure 3.5 shows an increase in concentration of these three sulphide ions throughout the high plateau (point U, Figure 3.2). In contrast, the concentration of dissolved elemental sulphur stays constant because as soon as it is reduced to S_8^{2-} it is replenished by more elemental sulphur dissolving from the cathode. This constant value of $S_{8(l)}$ is the reason that a

plateau can be seen in the first discharge region, nevertheless, the increase in more negative ions throughout this region means that there is an overall negative gradient to the plateau.

Chemical activity of polysulphides increases with chain length [19]. Subsequently, the longer chain sulphide ions that form in the first discharge region are relatively unstable and can readily dissociate into lower order sulphide ions, leaving behind elemental sulphur, as shown in Equations 3.17 and 3.18 [19,32,33]. The elemental sulphur formed in these reactions continues to be electrochemically reduced and the average polysulphide chain length continues to get smaller.

$$S_8^{2-} \leftrightarrows S_6^{2-} + \frac{1}{4}S_8 \qquad [3.17]$$

$$S_6^{2-} \leftrightarrows S_4^{2-} + \frac{1}{4}S_8 \qquad [3.18]$$

As solid elemental sulphur is used up by these reactions there is more cathode surface area for dissolved lithium polysulphides to be adsorbed to and the rate of reduction during the first plateau is very high. However, the active surface area of the cathode varies throughout discharge as the soluble polysulphides form solid precipitates, which block the pores of the structure [28]. The knee in the discharge curve (point V) signifies that all of the solid elemental sulphur is depleted from the cathode and the concentration of $S_{8(l)}$ decreases sharply as it continues to be reduced, without being replenished.

Reactions may also take place between higher order lithium polysulphides that are adsorbed to the carbon cathode. These lithium polysulphides do not follow the systematic reduction in chain length but instead undergo disproportionation reactions where a lithium polysulphide of a high chain length can both oxidise and reduce at the same time. For example [29]:

$$Li_2S_6 + 2Li^+ + 2e^- \rightarrow Li_2S + Li_2S_5 \qquad [3.19]$$

$$xLi_2S_5 \rightarrow Li_2S + yLi_2S_6 \qquad [3.20]$$

These reactions show that high order lithium polysulphides can directly form the final discharge product $Li_2S_{(s)}$ whilst retaining their average chain length. This process is evidenced in the flatness of the discharge profile, which would otherwise show distinct plateaus for each polysulphide species if polysulphide reduction were strictly systematic [29].

At around point W, in Figure 3.2, insoluble $Li_2S_{(s)}$ begins to precipitate out of solution and the reaction soon becomes kinetically limited [28,34]. The porosity of the cathode and the viscosity of the electrolyte are both at their maximum between points V and W. This theory was verified by Cheon et al in [32] as their SEM images showed that mainly carbon matrix was visible at point W.

During region 2 of the discharge profile, the concentration levels of $S_{8(l)}$ and the higher order polysulphides decrease steadily as they are further reduced to the lower order polysulphides, without being replenished. In addition to direct electron transfer to sulphide ions adsorbed to the cathode structure, chemical dissociation reactions continue to occur (Equations 3.17, 3.18), albeit at a slower rate than in the high voltage plateau as chemical activity is reduced. The disproportionation reactions of the various lithium polysulphides (Equations 3.19, 3.20) also continue to occur during the second discharge region. The final discharge products, $Li_2S_{2(s)}$ and $Li_2S_{(s)}$, are highly insoluble in the electrolyte and they start to precipitate out of solution in the second discharge region, shown in Equations 3.21 and 3.22.

$$2Li^+ + S_2^{2-} \rightarrow Li_2S_{2(s)} \quad [3.21]$$

$$2Li^+ + S^{2-} \rightarrow Li_2S_{(s)} \quad [3.22]$$

At low discharge rates these precipitates accumulate and are distributed evenly throughout the carbon matrix of the cathode, forming an insulating passivation layer, increasing the internal resistance of the cell [35]. The $Li_2S_{2(s)}$ that deposits directly onto the carbon matrix may additionally undergo the following electrochemical reaction [30]:

$$Li_2S_2 + 2Li^+ + 2e^- \rightarrow 2Li_2S \quad [3.23]$$

The idea that $Li_2S_{(s)}$ can be further reduced in this way is supported by the SEM measurements reported by Cheon et al. in [32], taken at around point Y on Figure 3.2, which shows that the passivation layer predominantly consists of a solid film of $Li_2S_{(s)}$ and that it becomes increasingly more severe as the voltage drops to point Z.

At the end of the low voltage plateau, in the section between points Y and Z, the passivation layer rapidly builds up and no further reduction of the sulphide ion is possible. This is reflected in the steep voltage drop in the discharge profile. The end of discharge occurs at point Z where the build up of the $Li_2S_{(s)}$ solid passivation layer blocks any useful electrical contact with the cathode. At higher discharge rates this layer may tend to accumulate on the surface of the cathode, rather than filling its pores, causing the end of discharge resistance increase to occur prematurely. If a discharge current continues to be applied after this point, the $Li_2S_{(s)}$ on the cathode structure may be further reduced depositing a layer of metallic lithium on the cathode, after which the cathode becomes unstable [36].

$$Li_2S + 2e^- \rightarrow 2Li^0 + S^{2-} \qquad [3.24]$$

3.2.2 Charge characteristics

Figure 3.7 shows a typical charge profile for a lithium-sulphur cell as a function of state of charge, produced from data taken during characterisation testing at 0.315A, where some points of interest have been highlighted. A cell that has been discharged to 1.7V will, after a period of rest, show a voltage recovery to its EMF value of about 2.13V and so charging begins at this voltage. As Figure 3.7 shows, there is a sharp rise in voltage at the very beginning of charge (point A) followed by two shallow plateau regions (regions B & C) and another sharp voltage rise at the end of charge (point D). This profile contrasts greatly with the discharge profile. Studies on the various concentrations of ion species in the electrolyte have not been as extensive as for the discharge profile of this cell, and were not covered in [28]. However, information in the literature allows assumptions to be made about electrochemical characteristics during charge.

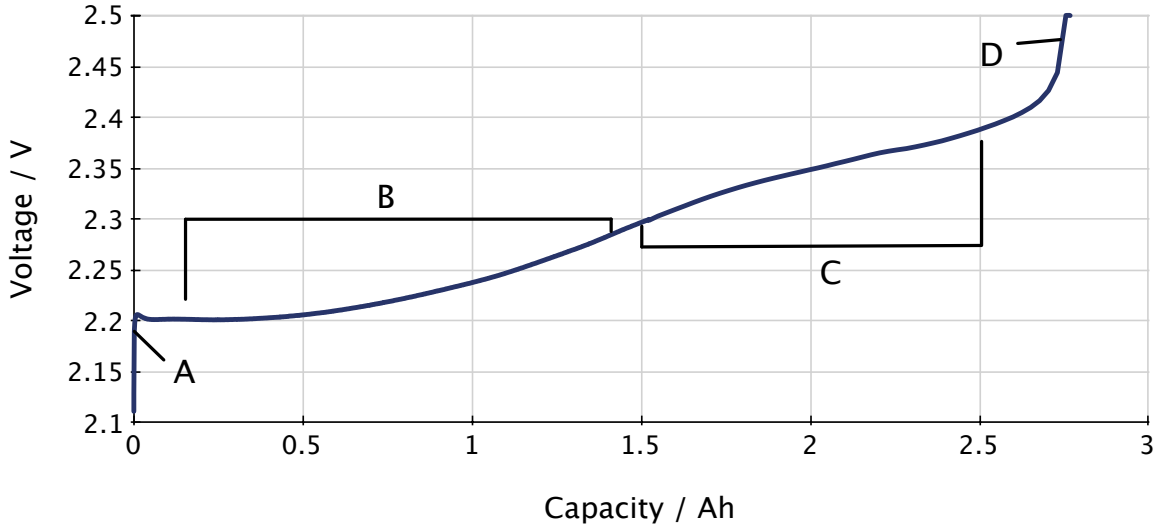

Figure 3.7: Charge profile of the lithium-sulphur cell as a function of state of charge

When a cell has been fully discharged using a low current rate, a dense solid passivation layer of $Li_2S_{(s)}$ evenly fills the pores of the carbon matrix of the cathode [32]. A charger or power supply attached to the terminals of the cell supplies electrons to the lithium electrode causing species there to reduce, while electrons are simultaneously removed from the sulphur electrode causing species there to oxidise. This process occurs by a combination of electrochemical oxidation of the solid $Li_2S_{(s)}$ layer (filling the pores of the carbon matrix) to medium and long chain polysulphides, as in Equation 3.25 [29,30], and by the reversible reactions given by Equations 3.5-3.9 and 3.14-3.16.

$$nLi_2S \rightarrow Li_2S_n + (2n-2)Li^+ + (2n-2)e^- \qquad [3.25]$$

At point A on Figure 3.7, there is an immediate jump to nearly 2.2V before the voltage makes a slight dip again. This initial steep rise in voltage is due to the resistance of the $Li_2S_{(s)}$ passivation layer on the cathode and the subsequent dip may be due to a slight lowering of resistance as the layer begins to be removed [30] as shown in Figure 3.8. The two shallow voltage plateaus that can be identified in the charge profile can be related to two peaks in oxidation at 2.36V and 2.22V [37]. The first plateau, identified by region B, can be attributed to the oxidation of the solid passivation layer to long chain polysulphides and by the end of this region it has been shown that the majority of this layer is depleted [32].

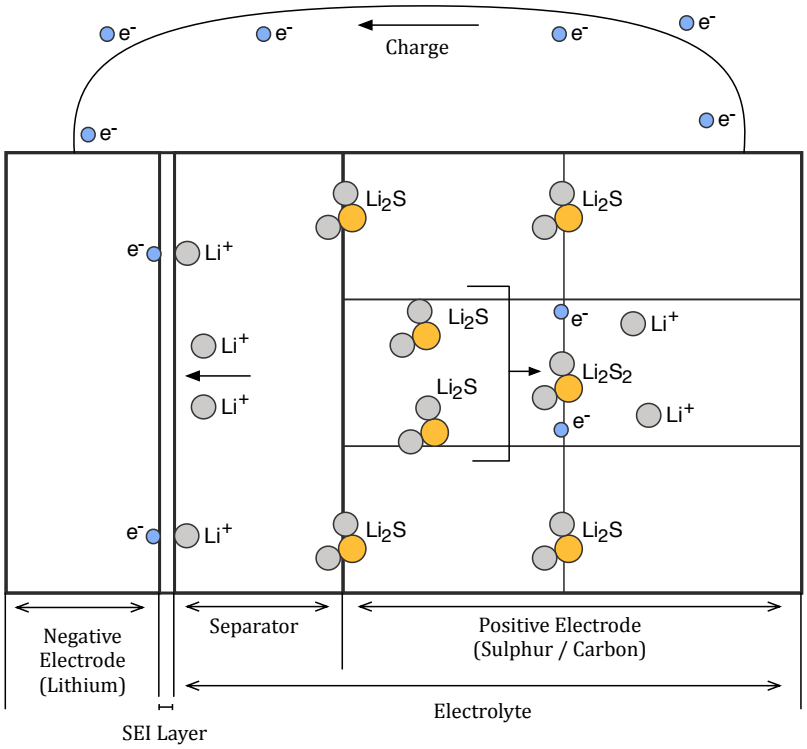

Figure 3.8: Charging begins in a fully discharged Li-S cell

Long chain lithium polysulphides that form in this oxidation reaction also react with the remaining insoluble polysulphides in the passivation layer, creating lithium polysulphides with chain lengths of an intermediate value, such as in Equations 3.26 and 3.27 [29]:

$$Li_2S + Li_2S_n \rightarrow Li_2S_k + Li_2S_{n-k+1} \quad [3.26]$$

$$Li_2S_2 + Li_2S_n \rightarrow Li_2S_k + Li_2S_{n-k+2} \quad [3.27]$$

The medium length polysulphides then go on to be oxidised into longer chain length polysulphides at the cathode surface, as more active surface becomes available through the dissolution of the solid layer. In this plateau region there is a shallow rise in potential, which can be attributed to the overall increasing concentration in longer chain polysulphides.

As the solid passivation layer loses its electrons to the external circuit, positive lithium ions become freely available and they take part in the precipitation/dissolution reactions with the longer chain polysulphides as in Equations 3.14-3.16. Because these polysulphides are highly soluble the lithium ions can diffuse through the electrolyte away from the cathode. As electrons enter the lithium anode, from the external circuit, they attract the lithium ions that

are in the electrolyte. Li^+ ions migrate to the anode, pass through the SEI layer and recombine with electrons to plate lithium metal onto the anode surface.

Cheon et al [32] showed that the bulk of the solid passivation layer was severely depleted at 30% SoC (around the end of plateau region B) and the layer had all but disappeared at 100% SoC. In the second plateau (region C) long chain polysulphides begin to oxidise to elemental sulphur [19,29]. This can be achieved by facile electron transfer because the carbon cathode matrix is now free from $Li_2S_{(s)}$ obstruction and the following reaction is observed [29]:

$$mLi_2S_n - 2Li^+ - 2e^- \rightarrow (m-1)\,Li_2S_{n-k} + S \qquad [3.28]$$

Where:

$$mn = (m-1)((n-k)+1) \qquad [3.29]$$

Where m, n and k are constants. The increase in the concentration of sulphide ions during charge significantly increases the electrical conductivity of the electrolyte [38,39] but this means the viscosity of the electrolyte also increases. At the stage at which solid elemental sulphur begins to precipitate, at the end of region B, the concentration of lithium polysulphides in the electrolyte is at a maximum. This means that, as in discharge, when the high viscosity electrolyte fills the pores of the carbon matrix the electrochemical reactions are displaced from the bulk to the surface of the electrode as current increases [29]. Highly porous carbon matrices are used for this type of cell to try to minimise this effect.

At the end of charge there is a voltage spike between approximately 2.4V and 2.5V. There is very little capacity delivered in this region and as soon as the power supply is removed the voltage relaxes to 2.45V. This is due to a surface layer of solid sulphur dissolving into the electrolyte and chemical dissociation reactions occurring after the current is removed.

3.2.3 Solid electrolyte interphase (SEI)

As described in Section 3.1.2 the chemical make up of the electrolyte can be carefully engineered so that it reacts with the lithium anode in a way that forms a passivating film on its surface. This protective layer acts as an interphase between an electrode surface and the

electrolyte and has the properties of a solid electrolyte, hence is known as the solid electrolyte interphase (SEI). An ideal SEI layer must have good ionic conductivity but must also be an excellent electrical insulator [40]. In lithium-ion batteries the SEI layer is formed on the carbon intercalation anode, consuming a small amount of lithium in the process.

In a Li-S cell a similar effect occurs, where the pure lithium anode reacts with the components of the electrolyte to form a stable SEI layer. Nitrate additives can be used to strengthen the SEI making the anode more robust against corrosive reactions with polysulphides in the electrolyte [12]. Although the SEI increases cell resistance and lowers rate capability, it is essential for protecting the anode against further reaction with the electrolyte, preventing the consumption and corrosion of useful lithium [3]. Manufacturers do not release details of the exact composition of the electrolyte so the chemistry of the SEI layer cannot be determined. However, it is known that its composition changes during cycling of the Li-S cell because of the polysulphides present during the intermediate stages of cycling [36]. During the formation of the SEI layer, lithium polysulphides that reach the surface of the anode react with lithium metal and reduce to insoluble lithium disulphide and lithium sulphide, as in the following reactions [36]:

$$2Li + Li_2S_n \rightarrow Li_2S + Li_2S_{n-1} \quad [3.30]$$

$$2Li + Li_2S_n \rightarrow Li_2S_2 + Li_2S_{n-2} \quad [3.31]$$

The result is that the metallic lithium anode is coated in an SEI layer that slows further reaction with the polysulphide and electrolyte components, improving safety. Any metallic lithium that threatens to form dangerous dendrites spanning between electrodes is quickly coated in this layer, protecting the cell from internal shorts [29]. This SEI layer improves the cycling ability of the cell because dendrites are prevented from forming and lithium deposition during charge is smooth, evidenced by SEM micrographs taken by Wagner et al. in [41]. In addition, parasitic reactions between lithium metal and polysulphides in the electrolyte are greatly reduced, once the SEI layer has been formed.

3.2.4 Polysulphide shuttle mechanism

There is another consequence of the reaction between lithium and sulphur that occurs within this cell type. During cycling, a parasitic chemical shuttle of polysulphide species occurs between the electrodes in a way that does not contribute to energy generation. The result of leaving these reactions to proceed unimpeded has consequences for the self-discharge, obtainable capacity and energy density of the cell.

Shuttle mechanism during charge

It has been shown that high order polysulphides are generated at the cathode surface during charge as they are oxidised by losing electrons to the external circuit (Equation 3.25). Due to concentration gradients in the electrolyte these newly formed polysulphides may diffuse across the electrolyte and interact with the insoluble lithium polysulphides and the lithium metal on surface of the anode, as in Equations 3.26, 3.27, 3.30 and 3.31. When a high order soluble polysulphide makes contact with lithium metal the reaction that occurs reproduces the low order polysulphides. These low order polysulphides may then diffuse back to the cathode surface where they are either oxidised at the cathode surface (Equations 3.5-3.9) or react with solid sulphur (Equation 3.32) [29] to create higher order polysulphides once more.

$$Li_2S_{n-1} + S \rightarrow Li_2S_{\mathrm{n}} \qquad [3.32]$$

The process then repeats itself causing a shuttle mechanism between the electrodes [31]. The protective SEI layer on the anode hinders these parasitic reactions and so the effect is not large, but it could cause incomplete conversion of polysulphides to elemental sulphur under certain charge conditions. This reduces the capacity of the cell on subsequent discharges [12].

The rate of the shuttle reaction is limited by the rate of reaction of polysulphides on the anode surface [42] but is also affected by the solubility of the lithium polysulphides in the electrolyte, the mobility of polysulphides through the electrolyte and the dissolution rates on the electrodes [29]. It follows that at high states of charge, where the solubility and activity of the polysulphides is it its highest, the shuttle reaction is at its strongest. Mikhaylik and

Akridge of Sion Power Corporation have extensively studied this shuttle phenomenon [31]. They have found that the way the cell under their investigation behaves when charged depends on the composition of the electrolyte and the current used to charge the cell. Cells showed high shuttle reaction rates when the viscosity of the electrolyte was low, as there is less physical material to oppose the mobility of the dissolved polysulphides, and also when the charge current was low. The addition of certain salts to the electrolyte can increase electrolyte viscosity, inhibiting the shuttle mechanism. Low charge currents mean that the cell takes longer to charge and so there is ample time for the diffusion of polysulphide species across to the anode, thus increasing the chemical shuttle effect. Unfortunately, increasing the viscosity of the electrolyte can never completely stop the shuttle mechanism, although it can be slowed in this way. This method also comes at the cost of reducing the rate capability of the cell as ion flow between electrodes is inhibited [12]. State of the art cells that now have nitrate additives, which encourage a stable SEI layer on the anode, reduces the chemical shuttle effect by three orders of magnitude [12,21,43].

Therefore, instead of increasing the salt content to raise the viscosity of the electrolyte and thus inhibiting the flow of the chemical shuttle via resistance, the chemical shuttle is hindered by the protective layer on the lithium metal anode. With the ability of polysulphides to react on the anode severely reduced in this way, the chemical shuttle can be interrupted without loss of discharge capacity and the high rate capability of the cell is maintained. In the next generation of Li-S cells the lithium anode may be further protected by a physical polymer barrier that will not only help to minimise the parasitic chemical shuttle but it will also help to control thermal runaway in the cell [12].

Shuttle mechanism during discharge

The reduction of high order polysulphides on the anode may occur on discharge as well as charge and, with no anode protection, this would have a measureable effect on the discharge capacity. The reduction of high order polysulphides proceeds in the normal way, which is attributed to the gaining of electrons at the cathode when the cell is discharging. In parallel

with this, polysulphides that diffuse to the surface of the anode react with the lithium there, causing them to reduce to lower order polysulphides. This parasitic reaction reduces polysulphides in a way that does not contribute to energy generation. The experiments conducted in [31] show that the discharge capacity could only reach the maximum value (i.e. the charge capacity) when the shuttle is completely inhibited.

3.2.5 Swelling and self-discharge

A swelling battery can be dangerous because it usually signifies the final stage before explosion [44]. Even if swelling can be controlled it should be avoided for reasons of performance, which is likely to deteriorate rapidly in the event of swelling. Lithium-sulphur cells may experience volume changes, or swell, under two separate circumstances. The first occurs during normal cycling of the cell when a variation in cell dimensions is observed. The second swelling condition may occur when the cell is left to rest within 30mV of 2.35V for extended periods of time [45], which makes it unusable. It is highly unusual for a danger point such as this to occur within the normal operating range of a battery.

In the first circumstance the swelling of the cell may be attributed to the reaction of the lithium metal anode with polysulphide species present in the electrolyte [46]. This action causes the surface of the lithium to become rough and increase in porosity [12]. Under such circumstances the anode increases in size and electrolyte moves to fill the newly porous areas of the anode, causing the cathode and separator to be depleted of electrolyte [12]. Inhibiting the shuttle mechanism is key to limiting this kind of swelling. Reducing these reactions can be accomplished by improving the protection of the anode, which inhibits the reactions that cause swelling and improves the cycling ability of the cell [46].

He et al. reported that a sulphur composite electrode expands when discharging and shrinks when charging [47]. It was determined that a complementary movement of the lithium anode may compensate this action and so the overall swelling of the cell is not severe. He et al. also conclude that a wound cell would suffer capacity fade at a higher rate than a stacked cell due to the damage caused to the separator as it moved during cycling. A stacked cell would

recover from this movement more readily. The volume change of the cathode during cycling can be attributed to the increase in volume of species on the surface of the electrode. The final discharge product $Li_2S_{(s)}$ has a higher volume than elemental sulphur [42] and so the cathode structure must be porous enough to accommodate this volume change. A build up of $Li_2S_{(s)}$ may also cause stress to the cathode structure, breaking pieces away from the main body. This damage not only reduces the active area of the cathode, but any polysulphide species attached to the broken pieces are no longer able to take part in electrochemical reactions, reducing the capacity of the cell. It is also possible that gases formed from the reaction of lithium metal with trace water or from low boiling hydrocarbons, which result from the reaction of lithium with salts in the electrolyte, may also contribute to the swelling of the cell during cycling [48].

The second type of swelling occurs during periods of rest. Manufacturer's safety guidelines stipulate that Li-S cells should not rest at 2.35V ± 0.03V for extended period of times as this may cause cells to swell [45]. There is insufficient data in the literature to describe or predict this phenomenon and the cause is not well understood.

At 2.35V, whether in charge or discharge, the chemical species present in the cell are similar. In both cases there are virtually no insoluble lithium polysulphides present, only high order, high activity (2.35V corresponds to a peak in reduction activity in the cathode [49]), soluble lithium polysulphides and elemental sulphur. If no current is flowing, the cell is in rest and no exchange of electrons can occur between electrodes via the external circuit. Chemical dissociation reactions may still occur, as in Equations 3.17 and 3.18. In addition, with modern cells having less than 100% protection of the anode, it is possible that high order lithium polysulphides from the cathode may diffuse to the surface of the anode and participate in reactions with lithium metal as in Equations 3.30 and 3.31. The high volume product of these reactions, lithium disulphide and lithium sulphide, may be a cause for this type of swelling.

Chemical reactions occur at a slower rate than electrochemical reactions [19], so the swelling effect may take time to become noticeable. The amount of swelling seen in cells is likely to be

temperature dependent and so, as chemical activity increases with temperature, swelling may take longer to manifest in cells of lower temperature [44]. For cells stored at the critical voltages in high temperatures, swelling may occur much faster and may be more severe.

In a patent for an anti-swell protection circuit put forward by Nexergy [44] it is implied that swelling may occur at a lower voltage in addition to the known swelling range but this voltage is not specified. The peak in reduction that occurs at 2.35V also occurs at 1.9V [49], which may hold some significance but there is no literature to corroborate this, nor are there any safety guidelines from Li-S cell manufacturers that warn against resting the cell at any other voltage than the higher voltage specified here.

The literature also reveals that the Li-S cell has a notable level of self-discharge, at 4-6% per month [42,12], which is caused by parasitic shuttle reactions. Mikhaylik and Akridge showed that inhibiting the polysulphide shuttle mechanism reduces self-discharge [31]. Ryu et al. showed that cells stored at full charge exhibit high levels of self-discharge (16% per month), which were shown to be due to the conversion of elemental sulphur to Li_2S and intermediate lithium polysulphides resulting in a decrease in discharge capacity and of open circuit voltage [23]. The lithium in these reactions was shown to originate from the lithium salts in the electrolyte. They also postulate that the corrosion of the current collector could be a source of electrons that facilitate the reactions [23,22]. The values given for self-discharge in these papers do not differentiate between irreversible and reversible capacity losses and so the values should be considered as total capacity loss rather than self-discharge only. There is no literature published that discusses self-discharge characteristics at states of charge other than 100%. This may be because self-discharge is SoC dependent, reducing rapidly as a cell discharges and so only high states of charge are of interest. This hypothesis is supported with results found by Mikhaylik and Akridge [31] which shows that the higher order polysulphides found at high states of charge (in the first discharge region) have a higher activity than the lower order polysulphides found in the second discharge region.

3.2.6 Origins of capacity fade

It was shown in [32] that some of the Li_2S that forms during discharge remains on the cathode even after full charge. This Li_2S does not contribute to any future electrochemical reactions causing irreversible capacity loss. It is also possible that localised build-up of Li_2S can cause the carbon matrix, to which it is attached, to break away. This decreases the active area of the cathode and removes the Li_2S, to which it is attached, from future electrochemical reaction. When Li-S cells are discharged at high current rates, Li_2S is not uniformly distributed on the cathode structure and tends to accumulate on the outer surface of the cathode [35]. This would imply a more severe localisation of Li_2S at the cathode surface and higher levels of cathode structure destruction at high current rates, which is confirmed by results given in [35]. This reasoning has also been used to explain why there is less capacity available at higher current rates, i.e. the build up of the Li_2S layer on the outer surface of the cathode restricts ionic transport to the sulphur contained in the cathode, decreasing sulphur utilization and lowering the available capacity of the cell. In the Sion Li-S cell the final volume of Li_2S is $\sim$1.79 times greater than that of the original volume of elemental sulphur [12]. This would imply that any localisation also occurring within the pores of the cathode might cause the destruction of the cathode if the pore volume is lower than that of the final discharge product.

The solubility of the high order lithium polysulphides means that they are able to migrate away from the cathode, making them unavailable for further electrochemical reactions at the cathode [24,17]. The shuttle mechanism explains how these dissolved higher order lithium polysulphides can diffuse to and react with the lithium metal anode, recreating the lower order lithium polysulphides. If those lower order lithium polysulphides are themselves soluble then they are able to diffuse back to the cathode and participate in further reaction. If the initial reaction with the lithium anode results in Li_2S_2 or Li_2S then these species are irreversibly deposited on the anode [40] and constitute an irreversible capacity loss.

3.2.7 Scope for improving chemical composition

The chemical composition of lithium-sulphur cells has yet to be optimised. Cycle life remains a limiting factor for these cells with only 30-60 cycles at 80% DoD reported in the literature [12]. It is hoped that the degradation in cycle life as well as the chemical shuttle, self-discharge and swelling phenomenon can all be addressed by either protection of the anode surface or various design changes to the cathode composition. In [12] it was suggested that a physical membrane, comprising ceramic or polymer materials could be employed on the lithium anode surface to aid the restriction of parasitic reactions with lithium metal. Other cell construction options are also being explored, such as a stacked formation of cell components, which accommodates swelling more effectively than wound cells [50].

Various international universities are currently researching improvements of the cathodes structure using silicon nanowire technologies, as detailed further in Chapter 4, Section 4.1.1. [51,52,53]. This technology may increase the cells' tolerance to swelling and decrease capacity degradation. Specific energy densities for Li-S cells remain between 350-390Wh/kg [42,54] but it is believed that an improvement to at least 450Wh/kg is possible in the near future [12]. Larger capacity cells may also be developed [50] and changes to cycling guidelines, such as reducing the operating voltage range of the cell, may have advantages for the cycle life of the cell [54].

3.3 Comparison to State of the Art Technology

In Chapter 2 the state of the art in spacecraft batteries was described. As previously explained, the state of the art can be defined in different ways depending on the mission requirements for the battery. High power batteries are valued for launch vehicle applications whereas batteries with a long cycle life are necessary for LEO satellites, for example.

It is not only electrical performance that needs to be taken into account when comparing a new battery type to the existing state of the art, but other factors such as mechanical design and the electronic protection the cells require. However, the first two hurdles that Li-S cells

must overcome is qualification and heritage. No matter how advanced any new technology is there is always an older technology that is already better understood, known to be reliable and is predictable, i.e. it has heritage. Lithium-ion batteries were first manufactured in the early nineties but it still took several years for them to be flown in space and even longer before they became preferable to the older nickel-based technologies. New cells technologies must also undergo rigorous qualification and life testing in order to characterise the cell, make sure that it can survive the space environment whilst still delivering excellent cell performance and predict the behaviour of the battery under specific mission conditions.

Cell	**Type**	**Voltage Range/ V**	**Max Cont. Discharge Current Rate**	**Cell Capacity/ Ah**	**Mass/ kg**	**Specific Energy / Wh/kg**	**Cont. Power/ W**
ABSL 18650HC	Small Cylindrical	2.5 - 4.2	1C	1.5	0.0405	133	≈5
SAFT VL34P	Large High Power	2.5 - 4.2	15C	34	0.94	129	1250
SAFT VES 180	Large High Energy	2.5 - 4.2	2C	50	1.11	175	≈360
Sion Li-S	Small Pouch	1.7 - 2.5	2C	2.8	0.016	≈350	≈12

Table 3.1: State of the art space battery (2012) and Li-S electrical and physical parameters

In terms of electrical performance the Li-S cell can be compared to both small cell and large cell batteries and also to high power batteries. Table 3.1 summarizes the parameters of some batteries that are currently in use in space (and have a great deal of heritage) and the Li-S cell manufactured by Sion Power Corporation, with information taken from manufacturer's data sheets [27,55,56,57]. The data sheets of all cells used for comparison in this chapter are reproduced in Appendix B. It is important to recognise that this is a comparison to the current position in spacecraft battery technology, not to the emerging state of the art in terrestrial batteries, which was discussed in Section 2.1.

The specific energy of the Li-S battery stands out as being far higher than that of any of the other batteries currently used in space, while its voltage range is notably narrower and of lower value. Aside from these differences it is difficult to usefully compare the technologies

unless equivalently sized batteries are compared. For example, an 8s10p ABSL 18650HC battery is a relatively common size for a satellite battery. A battery made of Li-S cells with near-equivalent voltage and capacity to the 18650HC battery is over 2.5 times lighter, when battery casing and management electronics are not taken into account, and of a similar volume. The Li-S battery can also handle twice the continuous discharge current, as can be seen by the comparison in Table 3.2, although the effect that high current has on the capacity of the battery must also be accounted for. The Li-S battery requires more cells connected in series to obtain an equivalent voltage and, as Li-S cells are not currently made in large batches, cells cannot be well matched, making the need for cell-balancing electronics likely.

Cell	Type	Battery Size	Voltage Range/V	Max Cont. Discharge Current/A	Capacity/ Ah	Mass/kg
ABSL 18650HC	Small Cylindrical	8s10p (80 cells)	20-33.6	15	15	3.24
Sion Li-S	Small Pouch	13s6p (78 cells)	22.1-32.5	33.6	16.8	1.25

Table 3.2: Comparison of 18650HC and Li-S batteries

The pouch cell design also means a Li-S battery would need robust casing to protect the cells from the rigours of launch and the vacuum of space. The 18650HC battery does not require balancing electronics and the cells are of hard-cased cylindrical designs so they do not require as much structural support. The difference in mass between the two batteries shown in Table 3.2 is reduced when these factors are taken into account.

Cell	Type	Battery Size	Voltage Range/ V	Max Cont. Discharge Current	Capacity/ Ah	Cont. Power/ W	Mass/ kg
SAFT VL34P	Large High Power	1s1p	2.5-4.2	15C (500A)	34	1250	0.94
Sion Li-S (Equivalent V & Ah)	Small Pouch	2s12p	3.4-5	2C (67.2A)	33.6	228	0.384
Sion Li-S (Equivalent Power)	Small Pouch	2s66p	3.4-5	2C (370A)	184.8	1256	2.112

Table 3.3: Comparison of equivalent VL34P and Li-S batteries

The Li-S is not a high power cell, when compared to state of the art in high power space batteries, as Table 3.3 shows. A Li-S battery of equivalent voltage and capacity to a SAFT VL34P has less than a fifth of the power, while a Li-S battery scaled to the equivalent power needs 66 parallel cells and weighs over twice as much.

A VL34P battery may require numerous cells in series to obtain the required voltage and these cells would require cell-balancing electronics. An equivalent Sion Li-S battery would need up to twice the number of series cells to make up the correct voltage and hence would require up to twice the number of balancing circuits.

Comparing a SAFT 'very high energy' VES180 battery to a Li-S battery of equivalent voltage and capacity in Table 3.4 shows that the two batteries have very similar properties but the Li-S battery weighs half that of the SAFT equivalent. As with the VL34P comparison, the Li-S battery would require up to twice as many balancing circuits and additional casing. This would affect the specific energy of the battery pack as a whole but there could still be an advantageous mass saving.

Cell	**Type**	**Battery Size**	**Voltage Range/ V**	**Max Cont. Discharge Current/A**	**Capacity/ Ah**	**Mass/ kg**	**Specific Energy / Wh/kg**
SAFT VES180	Large High Energy	1s1p	2.5 - 4.2	100	50	1.11	175
Sion Li-S (Equivalent V & Ah)	Small Pouch	2s18p (36 cells)	3.4-5	100.8	50.4	0.576	≈350

Table 3.4: Comparison of equivalent VES180 and Li-S batteries

The cycle life of the various batteries also needs to be accounted for. While Li-ion cells can endure many thousands of cycles, the cycle life of Li-S (cells currently in production) at high depth of discharge has been reported as less than 100 cycles [12]. The literature does not contain data for low DoD cycles so a direct comparison cannot be made but capacity degradation in Li-S cells is still much more significant than in Li-ion cells. The self-discharge

of Li-S cells is currently higher than Li-ion and Li-ion cells also do not contain a 'swelling voltage' in their normal operating range. Despite these apparent drawbacks, future developments in chemical composition, which aim to fully protect the lithium anode, are expected to benefit cycle life, self-discharge, current rate ability, swelling and cell degradation because these effects can be mainly attributed to parasitic reactions at the anode. Improvements to the cathode composite material may aid recovery after swelling [52,53] and as cell design changes, from small capacity, wound pouch cells to large capacity, stacked prismatic cells, they will become more robust to spacecraft environments. Manufacturing cells in larger batch numbers and reducing impurities facilitate better cell matching, reducing the need for cell-balancing electronics and improving specific energy and energy density. If the chemical composition can be optimised and batch sizes increased, these aspects of cell performance will be improved and there is the potential for Li-S cell technology to compete with Li-ion. Li-ion cell technology did itself start out with low cycle life and a dangerous lithium anode before the chemistry was optimised.

Despite these apparent advantages, lithium-ion cells at the research level are beginning to close the specific energy gap that has always been the main advantage of the Li-S cell. The 233Wh/kg NCR-18650A cell is already in production. Cycle life is still low and capacity degradation still high in silicon based research level cells but cylindrical 18650 type cells have a large mechanical advantage over their Li-S pouch cell counterparts. Li-S cell technology will only be a real contender for next-generation spacecraft batteries if they can meet their projected performance swiftly.

3.4 Conclusions

In this chapter the lithium-sulphur electrochemistry was described in detail. This included a description of the constituent components of the cell, its fundamental design and operation, and its theoretical performance characteristics. The discharge and charge characteristics of the cell were explained by indicating the various chemical and electrochemical reactions that are thought to take place, with reference made to the evidence in the literature that supports such assertions.

Other attributes that define the Li-S cell chemistry are the polysulphide chemical shuttle and the swelling that occurs during the normal operation of the cell. Both of these phenomena were discussed although the literature available on these subjects is not plentiful, especially for the swelling event, which is not well understood.

It was established that there is scope for improvement of the Li-S cell chemistry, which is yet to be optimised by cell manufacturers. Future improvements to chemical composition and cell design were discussed with a view to reducing the parasitic reactions that cause cell degradation and internal damage caused by swelling.

A comparison between examples of various state of the art lithium-ion space batteries was made with Sion Li-S batteries of equivalent voltage and capacity or power. In summary, the Li-S cell is not yet competitive with its lithium-ion counterparts in terms of cycle life or power, but if the improvements to cell performance that have been predicted do come to fruition then the extremely large specific energy of the Li-S could be exploited in a lightweight, high energy space battery.

REFERENCES

[1] C.A. Vincent and B. Scrosati, *Modern Batteries: An Introduction to Electrochemical Power Sources*, 2nd ed.: Butterworth-Heinemann, 1997.

[2] M-Y. Chu, L. C. De Jonghe, S. J. Visco, and B. D. Katz, "Liquid electrolyte lithium-sulfur batteries," US Patent 6030720, February 29, 2000.

[3] SAFT, *Lithium Batteries*, 1st ed., J-P. Gabano, Ed.: Academic Press, 1983.

[4] J.R. Coleman and M.W. Bates, "The Sulfur Electrode," in *6th Internaltional Symposium on Power Sources*, 1968, pp. 289-302.

[5] L.C. Dejonghe, S.J. Visco, C.C. Mailhe, and M.B. Armand, "Metal-Sulfur type cell having improved positive electrode," US Patent 4,833,048, May 23, 1989.

[6] D. Peramunage and S. Licht, "A Solid Sulfur Cathode for Aqueous Batteries," *Science, New Series*, vol. 261, no. 5124, pp. 1029-1032, 1993.

[7] W. Fischer, H. Kleinschmager, W. Haar, G. Weddigen, and F-J Rohr, "Electrochemical storage cell," 4018969, April 19, 1977.

[8] E. T. Seo, H. P. Silverman, and R. J. Day, "Low temperature primary electrolyte cell," 4020246, April 26, 1977.

[9] R. D. Rauh, K. M. Abraham, G. F. Pearson, J. K. Surprenant, and S. B. Brummer, "A Lithium/Dissolved Sulfur Battery with an Organic Electrolyte," *J. Electrochem. Soc.: ELECTROCHEMICAL SCIENCE AND TECHNOLOGY*, vol. 126, no. 4, pp. 523-527, April 1979.

[10] M-Y. Chu, "Rechargeable positive electrodes," US Patent 5523179, June 4, 1996.

[11] M-Y. Chu, "Methods of fabricating rechargeable positive electrodes," US Patent 5582623, December 10, 1996.

[12] Y. V. Mikhaylik et al., "High Energy Rechargeable Li-S Cells for EV Application: Status, Remaining Problems and Solutions," *ECS Transactions*, vol. 25, no. 35, pp. 23-34, 2010.

[13] B. D. Katz, M-Y Chu, L. C. DeJonghe, and S. J. Visco, "Liquid electrolyte lithium-sulfur batteries," US Patent 6358643, March 19, 2002.

[14] M-Y. Chu, "Rechargeable positive electrodes," US Patent 5789108, August 4, 1998.

[15] M-Y. Chu, "Rechargeable positive electrodes," US Patent 5814420, September 29, 1998.

[16] R. D. Rauh, G.F. Pearson, and S.B Brummer, "Rechargeability studies of ambient temperature lithium sulfur batteries," in *12th Intersociety Energy Conversion Engineering Conference*, vol. 1, Washington, D.C., 1977, pp. 283-287.

[17] J. Shim, K. A. Striebel, and E. J. Cairns, "The Lithium/Sulfur Rechargeable Cell," *Journal of The Electrochemical Society*, vol. 149, no. 10, pp. A1321-A1325, 2002.

[18] E. Peled, Y. Sternberg, A. Gorenshtein, and Y. Lavi, "Lithium-Sulfur Battery: Evaluation of Dioxolane-Based Electrolytes," *Journal of The Electrochemical Society,* vol. 136, no. 6, pp. 1621-1625, 1989.

[19] V. S. Kolosnitsyn, E. V. Karaseva, D. Y. Seung, and M. D. Cho, "Cycling a Sulfur Electrode in Mixed Electrolytes Based on Sulfolane: Effect of Ethers," *Russian Journal of Electrochemistry*, vol. 38, no. 12, pp. 1314-1318, 2002.

[20] W. Wang et al., "The electrochemical performance of lithium–sulfur batteries with LiClO4 DOL/DME electrolyte," *J. Appl. Electrochem*, vol. 40, pp. 321-325, 2010.

[21] Y. V. Mikhaylik, "Electrolytes for lithium sulfur cells," US Patent 58144207358012, April 15, 2008.

[22] H.S. Ryu et al., "Self-discharge characteristics of lithium/sulfur batteries using TEGDME liquid electrolyte," *Electrochimica Acta*, vol. 52, pp. 1563-1566, 2006.

[23] H.S. Ryu et al., "Self-discharge of lithium–sulfur cells using stainless-steel current-collectors," *Journal of Power Sources*, vol. 140, pp. 365-369, 2005.

[24] H-J. Ahn, K-W. Kim, J-H. Ahn, and G. Cheruvally, "Secondary Batteries - Lithium Rechargeable Systems | Lithium-Sulfur," in *Encyclopedia of Electrochemical Power Sources.*: Elsevier, 2009, pp. 155-161.

[25] P. Atkins and J de Paula, *Atkins Physical Chemistry*: Oxford University Press, 2010.

[26] F. Walsh, *A First Course in Electrochemical Engineering*. Hants, England: Electrochemical Consultancy, 1993.

[27] Sion Power Corporation. (2008, October) Lithium Sulfur Rechargeable Battery Data Sheet. [Online]. http://sionpower.com/pdf/articles/LIS%20Spec%20Sheet%2010-3-08.pdf

[28] K. Kumaresan, Y. Mikhaylik, and R. E. White, "A Mathematical Model for a Lithium–Sulfur Cell," *Journal of The Electrochemical Society*, vol. 155, no. 8, pp. A576-A582, 2008.

[29] V. S. Kolosnitsyn and E. V. Karaseva, "Lithium–Sulfur Batteries: Problems and Solutions," *Russian Journal of Electrochemistry*, vol. 44, no. 5, pp. 506-509, 2008.

[30] V.S. Kolosnitsyn, E.V. Kuzmina, E.V. Karaseva, and S.E. Mochalov, "A study of the electrochemical processes in lithium sulphur cells by impedance spectroscopy," *Journal of Power Sources*, vol. 196, pp. 1478-1482, 2011.

[31] Y. V. Mikhaylik and J. R. Akridge, "Polysulfide Shuttle Study in the Li/S Battery System," *Journal of The Electrochemical Society*, vol. 151, no. 11, pp. A1969-A1976, 2004.

[32] S-E. Cheon, K-S. Ko, J-H. Cho, S-W. Kim, and E-Y. Chin, "Rechargeable Lithium Sulfur Battery: I. Structural Change of Sulfur Cathode During Discharge and Charge," *Journal of The Electrochemical Society*, vol. 150, no. 6, pp. A796-A799, 2003.

[33] V.S. Kolosnitsyn, E.V. Karaseva, N.A. Amineva, and G.A. Batyrshina, "Cycling Lithium-Sulfur Batteries," *Russian Journal of Electrochemistry*, vol. 38, no. 3, pp. 329-331, 2002.

[34] B. Jina, J-U. Kimb, and H-B. Gua, "Electrochemical properties of lithium-sulfur batteries," *Journal of Power Sources*, vol. 117, pp. 148-152, 2003.

[35] S-E. Cheon, K-S. Ko, J-H. Cho, S-W. Kim, and E-Y. Chin, "Rechargeable Lithium Sulfur Battery: II. Rate Capability and Cycle Characteristics," *Journal of The Electrochemical Society*, vol. 150, no. 6, pp. A800-A805, 2003.

[36] V. S. Kolosnitsyn, E. V. Karaseva, and A. L. Ivanov, "Electrochemistry of a lithium electrode in lithium polysulfide solutions," *Russian Journal of Electrochemistry*, vol. 44, no. 5, pp. 564-569, 2008.

[37] X. He et al., "Charge/discharge characteristics of sulfur composite cathode materials in rechargeable lithium batteries," *Electrochimica Acta*, vol. 52, pp. 7372-7376, 2007.

[38] H. Yamin and E.Peled, "Electrochemistry of a Nonaqueous Lithium/Sulfur Cell," *Journal of Power Sources*, vol. 9, pp. 281-287, 1983.

[39] D-R. Changa, S-H. Lee, S-W. Kim, and H-T. Kim, "Binary electrolyte based on tetra(ethylene glycol) dimethyl ether and 1,3-dioxolane for lithium–sulfur battery," *Journal of Power Sources*, vol. 112, no. 2, pp. 452-460, 2002.

[40] E. Peled, "The Electrochemical Behavior of Alkali and Alkaline Earth Metals in Nonaqueous Battery Systems - The Solid Electrolyte Interphase Model," *Journal of the Electrochemical Society*, vol. 126, no. 12, pp. 2047-2051, 1979.

[41] M.W. Wagner, C. Liebenow, and J.O. Besenhard, "Effect of polysulfide-containing electrolyte on the film formation of the negative electrode," *Journal of Power Sources*, vol. 68, no. 2, pp. 329-332, 1997.

[42] Y. Mikhaylik, "Fundamental Chemistry of Sion Power Li/S Battery," in *IBA-HBC*, Waikoloa, Hawaii, 2006.

[43] D. Aurbach et al., "On the Surface Chemical Aspects of Very High Energy Density, Rechargeable Li–Sulfur Batteries," *Journal of The Electrochemical Society*, vol. 156, no. 8, pp. A694-A702, 2009.

[44] R. A. Ibrahim, "Anti-swell protection circuit for battery cells," US Patent 7830125, November 9, 2010.

[45] Sion Power Corporation, "Lithium Sulfur Cell Safety Guidelines", Private Communication, 2011.

[46] Y. V. Mikhaylik and I. Kovalev, "Swelling inhibition in batteries," US2009/0035646 A1 (Patent Application), July 31, 2007.

[47] X. He et al., "Expansion and shrinkage of the sulfur composite electrode in rechargeable lithium batteries," *Journal of Power Sources*, vol. 190, pp. 154-156, 2009.

[48] Y.Mikhaylik, "Storage life enhancement in lithium-sulfur batteries," US Patent 6436583, August 20, 2002.

[49] J-W. Choi et al., "Rechargeable lithium/sulfur battery with liquid electrolytes containing toluene as additive," *Journal of Power Sources*, vol. 183, no. 1, pp. 441-445, 2008.

[50] Chris Pearson, "Status of Sion Power Corporation Li/S cells," ABSL Space Products, Internal Report 2010.

[51] Kyu Tae Lee and Linda F. Nazar Xiulei Ji, "A highly ordered nanostructured carbon-sulphur cathode for lithium sulphur batteries," *Nature Materials* , vol. 8, pp. 500-506, 2009.

[52] Y. Yang et al., "New Nanostructured Li2S/Silicon Rechargeable Battery with High Specific Energy," *Nano Letters*, vol. 10, pp. 1486-1491, 2010.

[53] Y. Yao et al., "Interconnected Silicon Hollow Nanospheres for Lithium-Ion Battery Anodes with Long Cycle Life," *Nano Letters*, vol. 11, pp. 2949-2954, 2011.

[54] J. Jeevarajan and B. Duffield, "Performance and saftey studies on COTS Li-ion cells of cylindrical and pouch cell designs," in *NASA Battery Workshop*, Huntsville, Alabama, November 2011.

[55] SAFT. (2009, July) Rechargeable lithium-ion battery, VL34P - High power cell. [Online]. http://www.saftbatteries.com/doc/Documents/defence/Cube769/VL34P_cell_data_sheet.a2df63d5-f58d-4eff-9760-0370d5487ae2.pdf

[56] SAFT. (2008, June) Rechargeable lithium battery, VES 180 – Very high specific energy space cell. [Online]. http://www.saftbatteries.com/doc/Documents/space/Cube712/VES%20180.e9cf5d8f-3cbd-4921-8ac0-89d7b13bd0c0.pdf

[57] ABSL Space Products, "ABSL 18650HC Cell Datasheet,"(2008).

CHAPTER 4

INVESTIGATION OF CELL CHARACTERISTICS

In this chapter, a review of the available Li-S cell technologies is made and the cell chosen for characterisation in this study is described. Furthermore, the choice of modelling technique chosen for the Li-S cell is justified. The characterisation tests chosen for this study are then defined and related to the objectives of the work. These tests comprise characterisation tests to collect data for the cell model and tests to aid in the design of the battery management system. The test descriptions include the development of the testing methodology, the experimental setup and implementation of the test.

4.1 Cell Selection

4.1.1 Lithium-sulphur cell technologies

There are several Li-S cell technologies undergoing intense research by different institutions today. Sion Power Corporation has been researching the lithium-sulphur couple since 1994 [1] and has manufactured an advanced Li-S pouch cell that has an energy density of at least 350Wh/kg [2]. These cells use a pure lithium metal anode and a sulphur/carbon composite cathode, with a non-aqueous electrolyte and have a high sulphur utilization [3], as well as a good safety record [4].

Oxis energy has been working on Li-S cell technology since 2004 and holds several key patents in the field [5]. Their cell is similar to the Sion cell and has a similar specific energy, but uses a polymer electrolyte that improves battery performance at low temperatures [6]. Both the Sion and the Oxis cells suffer from capacity degradation; low cycle life and their energy densities remain much lower than the theoretical 2600Wh/kg due to the limitations of the surface area of the cathode [3,7].

In an attempt to address these problems a considerable amount of research has focussed on novel electrode nano-materials, although these cells are still at the research level. Researchers at the University of Waterloo have made advancements with a mesoporous carbon structure as a cathode material [8]. Carbon nanotubes are arranged hexagonally and are spanned by carbon nanofibre support structures. Molten sulphur is infused into the pores and is allowed to solidify onto the carbon structure. Electrolyte is used to fill the remaining volume in the structure. The channels created between the nanotubes have uniform porosity and allow for expansion and contraction of the electrode, which reduces degradation of the cell during repeated cycling. This porosity is carefully tuned to allow enough room for expansion as the high-volume Li_2S forms on discharge, whilst not compromising the volume of active sulphur mass. Coulombic efficiencies of 99.9%, low capacity fading and high reversible capacities of 1320mAh per gram of sulphur have been seen in this cell [9].

Stanford University have also been researching novel electrode materials in order to improve the cycle life and cycling efficiency of lithium-sulphur based batteries. They have made several advancements in silicon anode technology [10] coupled with lithium-sulphur mesoporous carbon composite cathodes [11]. Their Li-S/Si battery [12], despite having a lower theoretical capacity than the Li-S battery (1550Wh/kg in comparison to 2600Wh/kg), has a reported specific energy of 630Wh/kg on the initial discharge.

4.1.2 Cell availability and selection

At the time this project was undertaken, lithium-sulphur cells were not available on the open market, despite the promising prospects of the above mentioned institutions. An objective review showed that Sion Power Corporation (hereafter Sion) and Oxis Energy are the most advanced in the manufacture of Li-S cells, and are the closest to commercialisation of their respective technologies. Of these manufacturers only Sion's cells, shown in Figure 4.1, were obtainable for testing, and then under restricted conditions. Therefore the testing undertaken in this project and the models derived from the results of those tests are specific to the lithium-sulphur cell chemistry used by Sion.

Figure 4.1: The Sion lithium-sulphur pouch cell [2].

4.1.3 The Sion Power Corporation cell

Fresh cells measure 55mm in length, 37mm in width and are 11.5mm thick as indicated in Figure 4.2 (a)-(c). This measurement is of the cell bulk and does not include the seams, which add a border ~ 7mm wide along three sides of the cell.

(a)

(b)

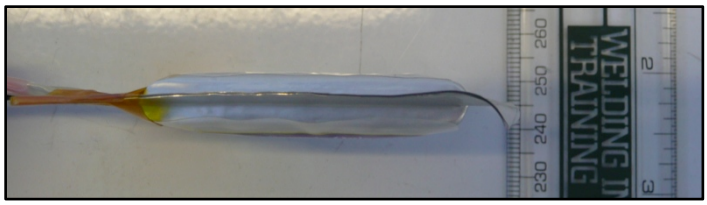

(c)

Figure 4.2: Dimensions of the Sion lithium-sulphur cell

A detailed description of the chemical make up of the Sion Li-S cell is given by Mikhaylik et al. in several papers [3,13,14]. Some information, such as the specific chemicals used in the electrolyte, remains proprietary. In summary, the cell comprises layers of lithium metal foil (anode), porous polyolefin separator material, and a mixture of elemental sulphur, graphite and acetylene black (cathode), all of which are sandwiched between an aluminised substrate

that acts as a current collector. The liquid electrolyte is entirely incorporated into the porous structure of the cathode and separator while remaining in contact with the surface of the anode [13]. The elements of the cell are layered, wound and compressed to form a pouch cell with nickel tags extruding from the case. A cross-section of this arrangement is shown in Figure 4.3.

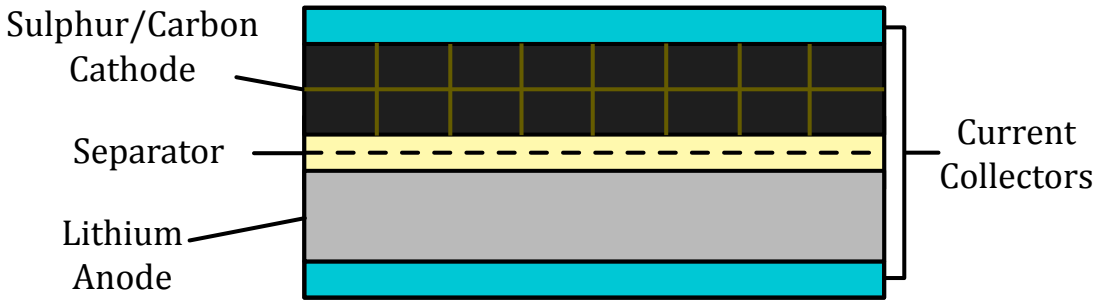

Figure 4.3: Cross-section of a Sion lithium-sulphur cell

4.2 Testing Strategy

4.2.1 Choice of modelling technique

A review of battery modelling techniques was given in Chapter 2. In choosing the ideal modelling technique for this work several factors have to be accounted for, including the accuracy required of the model, comprehension of the electrochemistry and the testing facilities available.

The purpose of this lithium-sulphur battery model is to assist a power system designer in accurately predicting the behaviour of the Li-S cell in a full power system. The model needs to return reliable information on state of charge, capacity, temperature, current and terminal voltage from power and temperature profile inputs. An equivalent circuit model is not only the most intuitive solution for a power system designer but has the advantage of having a reasonable simulation time whist retaining accuracy, can be implemented in circuit simulation software, is adaptable to a wide range of conditions and can be adapted to the programming language of choice.

Electrochemical models of other cell types can be very accurate, but only under very specific conditions, and do not predict cell behaviour precisely [15,16]. Establishing a precise electrochemical model of a Li-S cell would require comprehensive knowledge of the electrochemical reactions occurring within the cell and the calculation of a large number of constants and parameters, including the diffusion coefficients of all chemical species present at all states of charge through all materials. In Chapter 3 the chemical composition of the Li-S cell was described and there are evidently a multitude of species present, in addition to the various chemicals found in the electrolyte. The use of Sion's cells for this project was bound by strict terms of use, including the prohibition of cell destruction and chemical analysis, and so an investigation to determine the exact chemical composition of the cells and the concentrations of each intermediate species at different states of charge was impossible. Furthermore, the intermediate reduction stages of discharge are not yet fully understood and are much more complicated than in the Li-ion chemistry [17]. An electrochemical model of a cell with an unknown chemical composition would therefore be primitive and inaccurate and does not serve the objectives of this thesis. The inability to investigate the internal structure and composition of the cells meant that characterisation methods such as cyclic voltammetry and impedance spectroscopy, which require the use of a reference electrode, were not exploitable. Battery testers, however, were available for use and can acquire empirical measurements of time, cell voltage, current, capacity and power that can then be manipulated into empirical look up tables for the (more intuitive) equivalent circuit model. It was for these reasons that an equivalent circuit model based on empirical electrical characterisation was chosen for this project. One of the main advantages of this method is that the resultant model does not rely on total comprehension of the electrochemistry involved and may be adaptable to improved cell versions, with no chemical analysis required.

In addition to the characterisation of the cell's electrical properties, thermal characterisation is also required in order to analyse the temperature dependencies of properties such as internal resistance and open circuit voltage. Thermal chambers were available to keep cells at

the required temperature and T-type thermocouples could be connected to the battery testers in order to empirically measure the temperature changes on the surface of the cell. Dedicated battery calorimeter equipment was unavailable for these tests.

4.2.2 Experimental equipment and preparation

The testing performed on the Sion Li-S cells was carried out at ABSL Space Products Ltd in Abingdon, Oxfordshire. One hundred lithium-sulphur cells were shipped from Sion Power Corporation and arrived at ABSL in January 2011.

Figure 4.4: Cells were packaged in individual plastic bags contained within small tins.

Figure 4.5: The cells were shipped in drums of vermiculite.

The cells were shipped in individual sealed plastic bags and contained in small tins, two cells per tin as in Figure 4.4. Ten tins were contained in larger drums filled with vermiculite and the drums were bolted shut as shown in Figure 4.5. After removing the cells from their packaging the cells were checked for signs of damage or heating and, when none was found, they were individually numbered and resealed in their plastic bags.

The cells were prepared for testing by soldering two 20 gauge wires to each protruding electrode, black to the negative and red to the positive, so each electrode had a power line and a sense line. The exposed electrodes were shrink wrapped with plastic insulation in order to reduce the risk of shorting the electrodes.

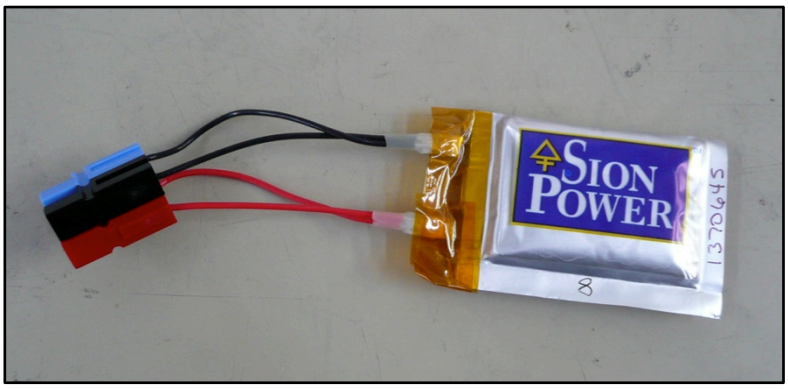

Figure 4.6: The electrodes were insulated with shrink wrap and kapton tape

A layer of kapton tape (gold coloured) was wrapped around the area between the cell body and where the shrink-wrap ends in order to lower the risk of shorting as shown in Figure 4.6.

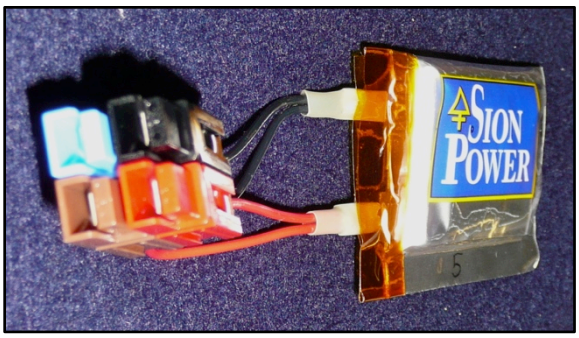

Figure 4.7: The electrodes were wired to Anderson connectors. Black: Negative power, Blue: Negative sense. Red: Positive power. Brown: Positive sense.

Anderson connectors were connected to the end of each wire in the configuration, as shown in Figure 4.7. These connectors were chosen because of their compatibility with the connections on the battery testers. All 100 cells were prepared in this way so that they could be screened before the specific characterisation testing began.

During testing the cells were contained in thermal chambers (Figure 4.10) to ensure that their temperature was controlled to ± 2°C. Three brands of thermal chamber were used during testing; Vötsch, TAS, and Design Environmental. T-type thermocouples were attached to the side of the cell using kapton tape, as in Figure 4.8, and were wired to auxiliary channels that corresponded to the test channel.

Figure 4.8: A thermocouple attached to a cell using kapton tape

Figure 4.9: The Maccor battery tester

Figure 4.10: Vötsch (left) and Design Environmental (right) thermal chambers

Test data was logged using Maccor battery testers (Figure 4.9) and each cell or battery was connected to a Maccor channel via a custom-made harness cable constructed from four-core 1.5mm^2 wire. These battery testers are highly accurate data loggers and are calibrated to 1mV for voltage and 1mA for 5A current channels and 2mA for 10A current channels.

The tests were programmed using the Maccor Build Test program and included measurements for test and step time, voltage, capacity, power, current, voltage, cell state and auxiliary channels were able to measure temperature if required.

In between tests the cells were stored in sealed plastic bags inside sealed plastic boxes, which were contained in a heavy-duty freezer chest at (uncontrolled) ambient temperatures. Because the cells have both positive and negative tags protruding from the same side of the cell, care was always taken to remove any jewellery before handling the cells in order to minimise the risk of shorts.

The details of equipment used to carry out the tests described in this chapter are given in Appendix C. An example Maccor test program is provided in full in Appendix D.

4.2.3 Test methodology

In order to accurately model a Li-S cell using an equivalent circuit method a range of empirical characterisation tests are required to populate the relevant lookup tables. However, the layout of the equivalent circuit cannot be optimised until the cell has been characterised and its voltage, capacity and thermal responses understood. Consequently, the testing methodology was developed over the course of the testing, as the model was refined, and more was learnt about the cell.

As was shown in Section 2.4 an equivalent circuit model of any battery type is generally composed of a voltage source and various resistors and capacitors that describe the transient voltage response. Therefore it was logical to begin with an initial set of tests that were based on those used to characterise Li-ion cells. As such, the initial test plan was based on those tests used to characterise the ABSL 18650HC cell [18] for use in ABSL's modelling software, BEAST [19].

In Section 4.3 the tests used to characterise data for the model are described. Each test description includes, where applicable, an account of how the test was developed from the original, based on 18650HC characterisation tests or from information on Li-S cells in the literature, to one that would more accurately characterise the Sion Li-S cell. Following this, each test procedure, including a description of the voltage and temperature ranges and test period, are detailed. The following tests were used to characterise the Sion Li-S cell:

- Screening and capacity checks
- EMF characterisation
- Internal resistance characterisation
- Dependency of EMF on temperature
- Hysteresis between charge and discharge EMF profiles
- Life tests

In addition to cell characterisation for modelling purposes, the objectives of this work also require that the protection requirements of the cell are determined and that the cells' suitability for space related applications is established. The information gleaned from the results of the aforementioned tests contributes to these last two objectives, especially in determining the predicted performance of the cells. However, additional tests are also required to aid in meeting these objectives. In Section 4.4 the development and implementation of the following tests are described:

- Open Circuit Voltage (OCV) decline
- Swelling characterisation
- Series string cycling
- Overcharge/overdischarge tests

4.3 Model Characterisation

In this section the tests used to characterise the cell and gain data for a Li-S equivalent circuit model are described. When developing these tests, the data sheet that accompanied the cells was used to determine their basic operating conditions and limits. The data sheet that accompanies the Sion Li-S cell contains the information given in Table 4.1 [2]. In addition to this operational data, Sion also issued safety guidelines to stipulate that the cells were not to be held within the range 2.35V ± 0.03V due to the safety risks associated with swelling, and gave an ideal operating current of 0.315A (~C/9).

Maximum operating voltage limit	2.5V
Minimum operating voltage limit	1.7V
Maximum charge rate	C/5
Maximum continuous discharge rate	2C
Operating temperature range	-20°C to 45°C
Maximum voltage safety limit	2.8V
Minimum voltage safety limit	1.05V
Cell Capacity @ C/5 and 20°C	2.5Ah
Specific Energy	350Wh/kg
Energy Density	320Wh/l
Cell Impedance	25mΩ

Table 4.1: Sion Li-S data sheet information

4.3.1 Screening and capacity checks

It is common practice to perform screening assessments on each cell prior to any characterisation tests. This ensures that the manufacturer's specifications are met, that any defective cells are found and that the variation in cell characteristics across the batch are determined. This is especially necessary for the Li-S cell batch used in this work, as the cell is produced in low batch numbers and so batch uniformity may be variable. The capacity found in a screening cycle can also be used to define a "standard capacity measurement" (SCM), which tells the user how much of the full capacity is available using a predefined current rate.

For the Li-S cell it was important that the screening tests provided as much information about the cell as possible with minimal impact on its future performance. As such, the following screening test algorithm was completed on each Li-S cell:

1. Charge cell at the manufacturer's recommended current rate of 0.315A to 2.3V.
2. Rest for 2 seconds.
3. Charge cell at the manufacturer's recommended current rate of 0.315A to 2.5V.
4. Hold at 2.5V and allow current to taper down to a pre-set limit of 50mA.

5. Rest for 6 hours.
6. Discharge cell at the manufacturer's recommended current rate of 0.315A to 2.3V.
7. Rest for 2 seconds.
8. Discharge cell at the manufacturer's recommended current rate of 0.315A to 1.7V.
9. Rest for 6 hours.
10. Repeat steps 1-9 once.

From this test the following information about each individual cell could be determined:

1. Nominal charge and discharge capacity.
2. Charge efficiency.
3. Ohmic resistance estimate, for both charge and discharge (from 2 second rests).
4. Severity of self-discharge (from 6 hour rests).
5. Cell-to-cell variation of above parameters.

Due to the limited availability of thermocouple data logging channels only approximately 10% of cells had temperature monitoring. If a cell were to have overheated, it would have been likely to show visible signs of failure, such as swelling, and the screening data would have been unusual. Thus, it was not necessary to monitor the temperature of all the cells. A cell was deemed to have passed the screening test if the test completed within specified safety limits and there was no evidence of swelling or internal shorting.

Reference to an 'SCM' cycle in the remaining tests shall from hereon mean the following:

1. Charge to 2.5V at a current rate of 0.315A.
2. Taper charge at 2.5V until current diminishes to 0.05A.
3. Rest for 30 minutes.
4. Discharge to 1.7V at a current rate of 0.315A.

Reference to a cell being charged to 100% SoC in the remainder of this thesis shall mean steps one and two of the above program.

4.3.2 Standard capacity measurement

A standard capacity measurement (SCM) is used to determine a cell's nominal capacity at a predetermined current rate and is referenced as a percentage of the cell's total capacity. For example, a Li-S cell discharged at and SCM rate of C/9 may yield 97% of its total capacity. This is useful information because determining an accurate measurement of the total capacity of a cell requires a very slow discharge (~2 days) in order to minimise resistive losses. If it were necessary to perform a full capacity measurement each time a cell was used in a test, that test would be very time consuming. Therefore, knowing what percentage of capacity an SCM cycle yields means the total capacity can be accurately determined from a much shorter test (~9 hours in the case of the C/9 rate).

Knowing the total capacity of the cell means that the cell's state of charge can be calculated when the current is monitored into and out of the cell. All of the lookup tables used in the cell model are dependent on state of charge. In order to determine the full capacity of the Li-S cell the following test was performed on a set of 5 cells connected in parallel:

1. Charge to 2.5V at a current rate of C/48.
2. Rest for 30 minutes.
3. Discharge to 1.7V at a current rate of C/48.

Using 5 cells in parallel reduces the error of the Maccor logging system at low currents. This is because a current 5 times as large as that used on a single cell is needed.

4.3.3 Self-discharge and capacity degradation

Chemical side reactions occur within a cell when it is stored with no load across its terminals. These side reactions use up active chemicals in the cell that then can't be used for energy generation in a subsequent discharge. The amount of capacity lost to side reactions is recoverable because the reactions are reversible on the application of a charge current. The process of losing recoverable capacity through internal chemical reactions is known as self-discharge. The level and uniformity of the self-discharge characteristics of the Sion Li-S cells

was unknown before testing began, although the literature suggested a level of 4-6% per month could be expected [3]. In addition to the recoverable capacity lost to self-discharge, electrochemical cells also suffer from various irreversible capacity losses, which are caused by cell aging and the effects of cycling, as was described in Chapter 3.

Understanding self-discharge characteristics is of importance for the Li-S cell type. Firstly, self-discharge affects the way that cells perform in a battery pack, where non-uniform self-discharge characteristics add to cell imbalance. Additionally, for the Li-S cell chemistry, the drop in cell open circuit voltage caused by self-discharge must be closely monitored to prevent the cell from passing from 100% SoC into the swelling voltage range and resting there for extended periods of time. The results from these tests, when compared to current state of the art spacecraft batteries will help to determine their suitability for space applications, where batteries are routinely stored for long periods of time before launch. Characterisation of irreversible capacity losses is important for the prediction of the cells' performance degradation with age and their cycle life.

Tests were performed on Li-S cells to characterise the reversible and irreversible capacity losses that occur during both use and storage for inclusion in the cell model. However, due to limited resources the range of tests had to be restricted. This meant that these features were characterised only at 100% and 40% SoC and temperature effects were not considered.

Test implementation: Self-discharge and aging (100% SoC)

A set of 10 cells underwent the following test at 20°C:

1. Perform SCM cycle to determine initial discharge capacities (D_1).
2. Recharge to 100% SoC.

To determine the self-discharge and aging characteristics of cells stored at 100% SoC as a function of storage time the following test was performed on 2 randomly selected cells from the storage batch after N days:

1. Discharge to 1.7V at a current rate of 0.315A to obtain new discharge capacity (D_2).
2. Charge to 100% SoC.
3. Discharge to 1.7V at a current rate of 0.315A to obtain new discharge capacity (D_3).

In this case N is equal to 1 and 8 days. Longer duration tests (N>8days) were abandoned as the remaining cells had fallen into the swelling voltage range and additional cycling of these cells was not permitted.

The difference between the pre-storage (D_1) and post-storage (D_2) discharge capacities gives the total capacity lost (C_t) due to storage at 100% SoC, as depicted in Figure 4.11.

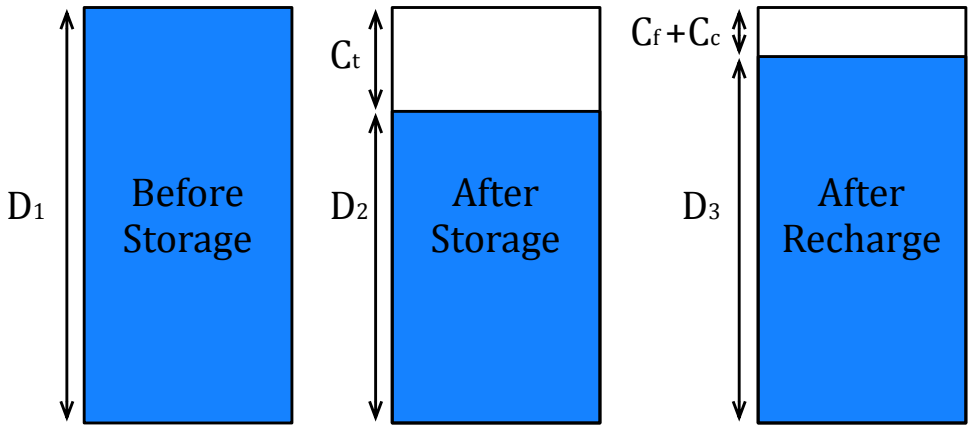

Figure 4.11: The various discharge capacities obtained before and after storage at 100% SoC

C_t is a summation of the reversible capacity loss due to self-discharge (C_{sd}), which is regained on the next charge, the irreversible capacity fade due to the cell's age (C_f), and the irreversible capacity loss due to the cycling of the cell (C_c). These relationships are shown in Equation 4.1.

$$C_t = D_1 - D_2 = C_{sd} + C_f + C_c \quad [4.1]$$

The difference in capacity between D_1 and D_3 is due to the effects of C_f and C_c as in Equation 4.2. The capacity lost to self-discharge is therefore calculated as in Equation 4.3.

$$D_3 = D_1 - (C_f + C_c) \quad [4.2]$$

$$C_{sd} = D_3 - D_2 \quad [4.3]$$

Test implementation: Self-discharge and aging (40% SoC)

In order to characterise the self-discharge characteristics of cells resting at 40% SoC the following test was implemented, again at a test temperature of 20°C, on a set of 8 cells:

1. Perform SCM cycle to determine initial discharge capacities (D_1).
2. Recharge to 40% SoC.

The following test was then performed on 2 randomly selected cells from the storage batch after a period of 1 day, 1 week, 1 month and 5 months of storage and, as the cell voltages were already below 2.32V, there was no risk of swelling.

1. Discharge to 1.7V at a current rate of 0.315A to obtain new discharge capacity (D_2).
2. Charge to 100% SoC.
3. Discharge to 1.7V at a current rate of 0.315A to obtain new discharge capacity (D_3).

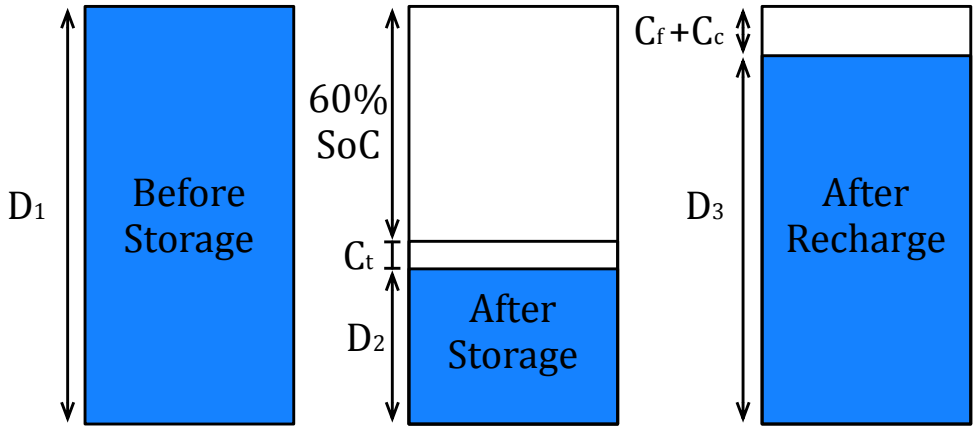

Figure 4.12: The various discharge capacities obtained before and after storage at 40% SoC

In this case the difference between the original discharge capacity (D_1) and the final discharge capacity (D_3) also gives the total irreversible capacity fade (C_f + C_c) due to cycling and age effects, as depicted in Figure 4.12. Although the self discharge at 40% SoC cannot be calculated in the same way as for the 100% SoC tests (because the discharge capacities are not comparable), an estimate of the expected discharge capacity in relation to the 40% SoC charge capacity can be compared to the actual discharge capacity D_2 and the self-discharge may be approximated. Results of these tests are given in Section 5.3.

Test methodology development

In the results of the aforementioned tests, the contribution to irreversible capacity losses appeared to be quite severe. It was therefore proposed to look at this effect in more detail and to separate out the effects of C_f and C_c to determine whether the act of performing cycling after storage contributed greatly to the overall irreversible capacity fade seen in the cells. In order to do this the capacity loss per cycle should be known and, as such, a repetitive cycling test to characterise this effect was performed. Data from the first cycles, when the capacity loss due to the age of the cell is at a minimum, is most accurate for separating C_f and C_c.

Test implementation: Repetitive cycling

Five individual cells underwent the following test whilst at an ambient temperature of 20°C:

1. Charge all cells to 100% SoC (at a current rate of 0.315A for all cells)
2. Discharge Cell 1 at 2C, Cell 2 at C, Cell 3 at C/2, Cell 4 at C/5 and Cell 5 at C/9 until 1.7V is reached.
3. Repeat steps for a maximum of 100 cycles.

In addition to the determination of capacity fade per cycle this test also gives important results on the rate dependency of available capacity (the Peukert effect) and cell degradation, as well as the general effect of continual cycling.

4.3.4 EMF

The open circuit voltage (OCV), or EMF, is a fundamental quantity that varies with a cell's state of charge in a way characteristic to its chemistry. When a load is connected to a cell the voltage seen at the terminals (V_{term}) is different to the EMF by an amount that depends on current rate, I, and internal resistance, R:

$$V_{term} = EMF + I.R \qquad [4.4]$$

The EMF value changes as the cell cycles. Therefore, a lookup table of EMF vs. SoC is required as the basis for the cell model for determining the terminal voltage in Equation 4.4.

Test methodology development

It is known that if a cell is cycled at a very slow constant rate such as C/50 [13,17] the voltage drop due to the internal resistance and current rate is greatly reduced and the terminal voltage should give a good representation of the EMF. At first it was thought that the EMF of the cells could be accurately characterised in this way, as is the case with the characterisation of the 18650HC cell. Preliminary tests of this nature were conducted and included hour long rests at intermittent points in the cycle. These rests indicated that there was a non-trivial voltage recovery to the true EMF value and showed the slow C/48 cycle did not indicate the true EMF as seen in Figure 4.13.

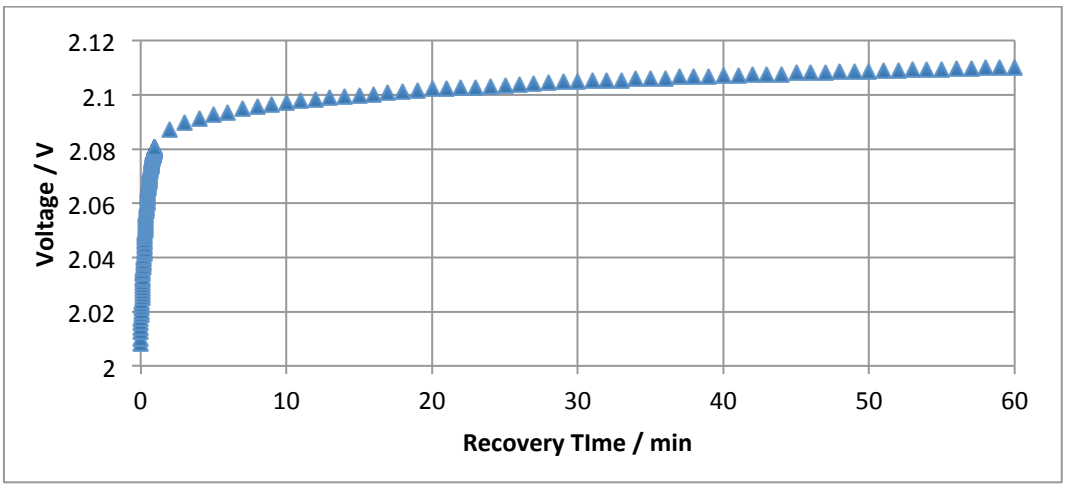

Figure 4.13: A C/48 current is removed from a discharging cell

Following this realisation, the EMF test was modified to include periodic rest points during the cycle that allowed the voltage to recover to its true EMF value. Monitoring the current into and out of the cell allows the state of charge of the cell to be known at each rest point and an EMF vs. SoC lookup table can be generated.

Test implementation

A set of 5 cells was connected in a parallel, as in the total capacity measurement test. There is a trade off between using several individual cells (to determine similarity) and a module of parallel cells (better current accuracy). Because the characteristics of the cells in the batch were thought to be quite non-uniform before testing commenced, it was decided that the

average values gained from a module test would be of more value for modelling purposes. The module was placed inside a thermal chamber set to a temperature of 20°C and the following test program commenced:

1. Perform SCM cycle.
2. Charge to 100% SoC.
3. Discharge by 0.05Ah/cell at a rate of C/48.
4. Rest for 2 hours.
5. Repeat steps 3 and 4 until 1.7V has been reached.
6. Charge by 0.05Ah/cell at a rate of C/48
7. Rest for 2 hours.
8. Repeat steps 6 and 7 until 2.5V has been reached.
9. Discharge at C/9 until 1.7V has been reached.

Due to the limited number of cells available for the testing only one module could be used for all of the EMF tests, repeated at additional temperatures of 0°C, -20°C and +40°C (in this order). The order is important as the high temperature tests, where the cells are more likely to be damaged, are completed last. The results of these tests can be found in Section 5.5.

4.3.5 Internal resistance

Characterisation of the internal resistance of a cell is vital to the battery model as the value of internal resistance dictates how the battery will respond to different current rates, states of charge and temperatures and how the battery voltage recovers during rest phases. Applying a current change ΔI, measuring the corresponding change in voltage ΔV and then applying Ohm's Law can be used to calculate the internal resistance of a cell, R.

$$R = \frac{\Delta V}{\Delta I} \qquad [4.5]$$

Test methodology development

The first set of tests used to characterise resistance employed a current pulse during cycling so as to measure the voltage response to a change in current, as shown in Equation 4.5, at

different states of charge. This was because, originally, internal resistance was thought to be a good indicator of state of charge, due to information found in the literature and also in a patent filed by Sion [20,21]. The aim of the pulse test was to determine if the resistance had a strong SoC dependency and if so, could a pulse test predict this with accuracy? In theory, a current pulse could be used by the BMS to determine state of charge without having to put the battery into a rest condition and could be superimposed over any current profile that was already running on the battery. The results showed that not only did the internal resistance of the cell not have a strong state of charge dependency but that the results would not be useful for modelling the transient behaviour of the battery.

The test was therefore modified, in an attempt to capture this transient behaviour. The resistance characterisation tests used on the 18650HC cell only seek to describe the Ohmic resistance of the cell and the transient response is not addressed. The Ohmic response is characterised by periodic 2 second rests in a C/10 cycle where the voltage change divided by the cycling current gives the resistance at the rest point. To capture the transient voltage recovery of the Li-S cell the rest length was increased so that the recovery to the EMF value could be fully characterised, and therefore modelled. These tests were expanded to include characterisation at a range of temperatures and current rates.

Test implementation

- **Rate dependency rest test**: Three individual cells were charged to 100% SoC and kept at a temperature of 20°C. They were then cycled at one of the following current rates: C/20, C/9 and C/5. During the cycling the current was interrupted at every 0.1Ah and the cells were left open circuit for 1 hour in order to monitor the rate dependency of the voltage response.
- **Temperature dependent resistance characterisation**: Two individual cells underwent 3 SCM cycles. These cycles enabled an accurate capacity and cycling efficiency to be calculated. The cells were then charged to 100% SoC and underwent another standard cycle except that in this final standard cycle, the cells were left to

rest for 2 hours after every 0.05Ah of capacity had been removed or added. The test was conducted on three different sets of cells (two cells per set) at a different temperature for each set (0°C, 20°C and +40°C). This allows a comparison of the internal resistance of the cells over a range of temperatures.

The results of these tests can be found in Section 5.6.

4.3.6 Dependency of EMF on temperature

When a battery discharges it generates an amount of heat that is the sum of the heat generated by polarization (Joule heating, q_p), entropy effects (q_s) and other sources such as self-discharge (q_{other}). For the purposes of modelling, it is important to know how the temperature of a battery varies as it charges and discharges as some components of the battery model are temperature dependent. Equation 4.6 describes the power dissipated by a cell P_{diss} during its operation [22]. The full derivation of this equation, from first principles, is given in Appendix A.

$$P_{diss} = I^2R + I.T.\frac{dE}{dT} \quad [4.6]$$

Where E is the cell's EMF, T is cell temperature, I is the load current and R is its total internal resistance. This value of power dissipation is used in the standard heat transfer equation to model the temperature of a Li-S cell during operation. In order to evaluate power dissipation, it is necessary to characterise the differential term in Equation 4.6, which represents the rate that the open circuit voltage varies with temperature.

Test methodology development

This test was based on a similar test used to characterise the 18650HC cell. In that test a selection of cells were charged to different states of charge and thermally cycled at a rate of 10°C per hour and their voltage response monitored. The gradient of the resultant voltage vs. temperature line for each cell gives the value of $\frac{dE}{dT}$ at the state of charge at which that cell is resting. Tests on the Li-S cells showed that the voltage vs. temperature graph showed a slight

hysteresis in the final results. It was thought that the thermal cycling could have been too fast and the cell could not adapt to the temperature change quickly enough. The testing method was then modified so that the thermal cycle was much slower, but in fact a slower thermal cycle created a greater hysteresis effect. It was subsequently realised the hysteresis effect was due to the cells not having reached an equilibrium voltage value before the thermal cycling commenced. The cells that underwent the slower thermal cycling had markedly less time to reach an equilibrium value before the cycling started and the greater hysteresis seen in the results was likely to be due to this. Although the hysteresis could not be completely eliminated, allowing the cell voltage to relax to equilibrium minimises the effect.

Test implementation

The tests to determine how EMF changes with temperature were completed in two parts.

	Cell Number	**1**	**2**	**3**	**4**	**5**	**6**	**7**	**8**
Capacity Removed / Ah	**Part 1**	0	0.4	0.8	1.2	1.6	2.0	2.4	X*
	Part 2	0.2	0.6	1.0	1.4	1.8	2.2	2.5	2.6

Table 4.2: Capacity removed from a fully charged cell for each $\frac{dE}{dT}$ test. *Cells were discharged to 1.7V and so X represents full discharge capacity.

Part 1: Eight cells were charged to 100% SoC and then each had a fixed number of amp-hours removed as the data in Table 4.2 shows. The cells were placed in a thermal chamber at 20°C and their voltages and temperatures were recorded. After a period of rest at their respective states of charge, the thermal chamber was cycled between the temperatures of -20°C and +40°C at a rate of 10°C per hour for a total of 6 cycles.

Part 2: The same test was repeated using the same set of cells but for this part, the cells had intermediate amounts of charge removed so that they were at different states of charge, as can be seen in Table 4.2. This was in order to gain more data for the look up table and also to determine any effect that cell degradation had on the results.

The results for these tests can be found in Section 5.7.

4.3.7 Hysteresis

An important aspect of the battery model is to accurately account for changes in the direction of current. The charge and discharge EMF profiles of the Li-S cell have shown to be highly asymmetrical and so switching the current from charge to discharge (or vice versa) with no rest period in between does not mean the cell voltage instantaneously jumps from one voltage profile to the other. A test is therefore required to characterise the effect of voltage transition between these curves for inclusion in the cell model.

Test methodology development

The hysteresis effect is not something that is modelled in the BEAST tool, although it is considered for future updates, as the effect can be significant, especially at low states of charge [23]. Dudley et al. described a test for the Li-ion cell in which a cell is cycled at a rate of C/50 and this current is reversed at several points during the cycle. This test has been modified for the Li-S cell by using a higher current rate (to reduce test length) and including roughly twice as many reversal points. In addition, the charge to discharge hysteresis was characterised using a separate cell from the discharge to charge hysteresis cell. The purpose of this test was to observe the voltage transition between charge and discharge at different states of charge, at a temperature of 20°C. The following two tests characterised this effect:

- **Charge hysteresis**: A cell was charged to 100% SoC and then discharged to 1.7V where the current was allowed to taper to 50mA while the voltage was held constant. Following this, the cell program continued as follows:
    1. Charge at a rate of 0.315A for 30 minutes.
    2. Discharge at a rate of 0.315A to 1.7V, then allow current to taper to 50mA.
    3. Rest for 2 hours.

    These steps were continually repeated but at each cycle the charge time was increased by 30 minutes. This continued until the cell reached 2.5V.
- **Discharge hysteresis**: A different cell was charged to 100% SoC and then continued as follows:

1. Discharge at a rate of 0.315A for 30 minutes.
2. Charge to 100% SoC
3. Rest for 2 hours.

These steps were continually repeated but at each cycle the charge time was increased by 30 minutes. This continued until the cell reached 1.7V.

These hysteresis tests allow the model to show an accurate transition between charge and discharge curves should a sudden change in current direction occur. This is important for real-life applications where a satellite battery may abruptly switch from charge to discharge modes as the satellite enters or emerges from eclipse. Results for these tests are found in Section 5.8.

4.4 BMS Specification Testing

In order to create a specification for the battery management system certain tests must be completed in order to establish a cell's operating limits. Recommended safety ranges from the cell manufacturer were given for the Li-S cell in Table 4.1. By exceeding these limits or entering forbidden ranges during testing, information can be obtained about a cell's reaction to certain abusive conditions and steps can be made, when designing the battery management system, to avoid or minimise the risks involved. Information on how a battery is expected to perform, should an unplanned abusive event occur, would also be available to the end user of the battery.

In this section the tests used to specify the battery management system are described. Tolerance to repeated overcharge and undercharge conditions were tested as well as the rate and severity of cell swelling and the level of imbalance in a series string of cells was investigated. Due to safety concerns regarding the use of excessive current and the unknown consequences of continually over-charging or over-discharging a cell to the point of destruction, some tests that had been planned could not go ahead. These tests would have been used to verify the voltage and current limits placed on the cell by the manufacturer and

are given in the further work section of Chapter 8. Nevertheless, because the cell manufacturer had already provided these limits it was thought that these tests were not critical to the specification of the battery management system. The tests described in this section were not based on any documented Li-ion testing but were designed specifically for the Li-S cell for the purposes described above.

4.4.1 Open circuit voltage decline

Two cells were used to determine the rate that EMF declines if a Li-S cell is left open circuit for extended periods of time. One cell was charged to 100% SoC and another to 40% SoC. Their voltage and temperature were monitored over a period of months. These tests show the rate at which the voltage declines at different states of charge. Monitoring of the 100% SoC cell also indicated how long it took for the cell to reach the high swelling voltage limit (2.38V) from full capacity, emerge at the other end of the swelling range (2.32V) and what happened to the cell over this range. Monitoring the cell at 40% SoC indicates how stable the cell is when resting at this SoC and if there is any danger of the self-discharge mechanism over-discharging the cell. Results for this test can be found in Section 7.1.1.

4.4.2 Over/under voltage abuse tests

The operating ranges specified by the manufacturer for the Li-S cell were given in Table 4.1 [4.2]. The cells should normally be operated between voltages of 1.7V and 2.5V, but they should also be safe to use between the wider safety limits of 1.05V and 2.8V, even though this may severely affect the performance of the cell. The tests devised to test these limits are summarised in Table 4.3.

Test Number	Test Name	Description
Abuse 1	Repeated overcharge	Cell is cycled between operating voltage lower limit (1.7V) and safety voltage upper limit (2.8V) for 20 cycles at 0.315A.
Abuse 2	Repeated overdischarge	Cell is cycled between safety voltage lower limit (1.05V) and operating voltage upper limit (2.5V) for 20 cycles at 0.315A.

Table 4.3: Summary of abuse tests

If cells in a battery pack become unbalanced their individual voltages may stray over the normal operating limits (if they are not adequately protected). This test will show the Li-S cells' tolerance to repeated overcharge or overdischarge (within it's safety limits) and the effect this has on the retained capacity of the cell. This will help to determine what level of balancing protection the cells need, how much overcharge or overdischarge they can accommodate and how the cells degrade under these conditions.

Each test was conducted on a single cell contained in a thermal chamber set at 20°C. Both tests were split into two parts. The first part of each test cycled the cells between their normal operating limits (a standard cycle) for 3 cycles and then one cycle at the respective abuse cycle. The voltage profile of the cell outside of its operating limits was unknown before completion of this test and so after the first part of the test the data-logging rate was checked in order to make sure that the detail of the extended voltage profile was suitably recorded. In the second part of the test the cells were cycled between the appropriate voltage limits (as given in Table 4.4) for 20 cycles (chosen as a preliminary value). Cycle number could have been extended if cell response was minimal. Abuse test results can be found in Section 7.1.2.

4.4.3 Series string cycling

As described in Chapter 2, a battery of cells connected together in series may require additional protection to that of a single cell, due to the possibility of cell imbalance. A test was devised in order to determine cell voltage divergence in a series connected string. This helps to define the level of balancing, if any, that Li-S cells would require during normal operation.

Test implementation

A set of 5 cells was chosen for this test. These cells were selected from a batch of 25 cells and were chosen for their similarity in capacity and cycling efficiency. The test was split into two parts where the cells were first tested individually before being connected in series. This initially defined individual cell features so that if any imbalance occurs it might be attributed to one cell having a higher resistance, or another cell having slightly lower capacity.

Part 1: Each cell was subject to two SCM cycles. A resistance cycle was then completed (a standard cycle with 5 second rests every 0.2Ah) and the cells were recharged to 100% SoC in preparation for part two of the test.

Part 2: All 5 cells were connected in a series arrangement as in Figure 4.14. Individual cell voltages and temperatures were logged as well as string voltage and current. Once in this arrangement the cells were subject to 20 SCM cycles. The battery voltage was limited to 12.5V (2.5V x 5 cells), however in order to monitor the natural behaviour of the cells as closely as possible, but still with regard to safety, the individual cell voltages were limited to their safety charge voltage of 2.8V as they were expected to exceed their normal limit of 2.5V. If no imbalance had been noted, the test could have been extended for further cycling. Results for the series string tests can be found in Section 7.1.3.

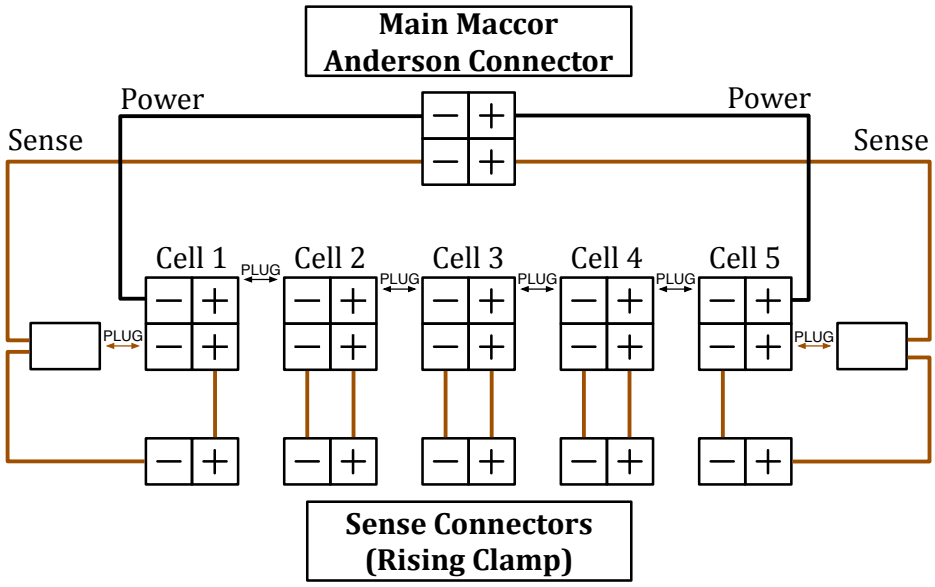

Figure 4.14: Series string test set up of 5 Li-S cells

4.4.4 Swelling

As explained in Chapter 3, a lithium-sulphur cell can swell if left to rest open circuit in the range of 2.35V ± 0.03V, which is well within the normal operating range for this cell. It is a unique feature of this cell chemistry to have a hazard point of this nature within the cell's normal operating range. As instructed by the manufacturer, any cell that expands beyond a thickness of 15mm is deemed to have "swelled", is thus unsafe to use and should be safely

disposed of. If the Li-S cell were to become commercialised, this feature must be explored (or resolved) and the battery management electronics, designed to protect the cell from abuse conditions, must be able to prevent cells from swelling.

A situation could be envisaged where a spacecraft battery is left to rest at an undesired voltage. This may occur during a fault condition, where the charge or discharge current is abruptly cut from the battery. Cells may become unbalanced during cycling and if the balancing electronics do not actively rectify the imbalance adequately, or they develop a fault, then it would be hard to keep all cells out of the swelling range after a recharge. Furthermore, depending on the mission, the battery may only need to be partially discharged during eclipse, or it may not receive a full charge during sunlight. Also, the battery could be left at full charge for extended periods of time, on the launch pad for example, where there is a risk of the voltage falling into the swelling range as the cell self-discharges. Any one of these conditions may result in a cell being at rest inside the swelling voltage range. Swelling can be a dangerous event if not controlled properly as it is usually the last stage before venting. It also needs to be avoided for reasons of performance, which is likely to deteriorate rapidly in the event that a cell swells.

Because the swelling effect has not been reported in detail in the literature, the BMS could be designed to protect the cells in a number of ways. For example, the BMS may need to monitor the time that the cell is in the swelling range, its thickness or its pressure in order to prevent damage. Swelling may also be temperature dependent [24]. It is the purpose of this test to quantify the swelling effect to determine the BMS requirements.

Test implementation

Several important features can be determined from observing the swelling effect. Consequently, the test was split into several parts, in order to characterise the following attributes:

1. The rapidity with which a Li-S cell begins to swell once it is in the swelling range.
2. Whether the severity/rapidity of swelling depends on how deep into the swelling voltage range the cell is.
3. Whether the severity of swelling depends on how long the cell has spent in the swelling voltage range.
4. How cell degradation is affected by the above factors.
5. The effect that temperature has on the above factors.
6. Variation between cells.

Seven cells were used in this test. Cells 1-5 were placed in a thermal chamber set at 20°C while cells 6 and 7 were placed in a separate thermal chamber also set at 20°C.

All 7 cells were cycled 3 times using the SCM cycle at 20°C to determine the discharge capacities and cycling efficiencies of the cells. Another cycle, interrupted by 5 second rests at intervals of 0.2Ah, was also performed on all cells in order to determine pre-test Ohmic resistance. Each cell was then charged to voltage *W*, given for each cell in Table 4.4.

Cell Number	**1**	**2**	**3**	**4**	**5**	**6**	**7**
Swelling Voltage V / Volts	2.35	2.35	2.35	2.37	2.33	2.35	2.35
Charge to Voltage W/ Volts	2.39	2.39	2.39	2.4	2.375	2.39	2.39
Swelling Temp T/ °C	20	20	20	20	20	40	40
Time in Swelling Range S / hours	144	144	28	144	144	28	28

Table 4.4: Summary of cell conditions for swelling tests

These voltages were determined from pre-test checks to define the best voltage to aim for when requiring the cell voltage to relax into the swelling range. The final voltage, within the swelling range, that each cell was intended to rest at is also given in Table 4.4, as swelling voltage V. All cells were left in the swelling voltage range for the specified period of time, *S*. After such a time had elapsed the cells underwent a series of 'post-swelling tests', as follows:

1. Cells are discharged to 1.7V at a rate of 0.315A.
2. An SCM cycle is performed.
3. A resistance cycle is performed (an SCM cycle with 5 second rests every 0.2Ah).
4. Cells are cycled 10 times using an SCM cycle.

As Table 4.4 shows, cells 1-3 were all left in the same condition, at the centre of the swelling voltage range, for different amounts of time. These tests are designed to show the correlation between cell degradation and severity of swelling with the time left in the swelling voltage range. Also the rapidity of swelling once at the desired voltage is determined. They also show the variation between two cells (1 and 2) under the same conditions.

Cells 4 and 5 were left to rest at voltages on the limits of the swelling voltage range. The post-swelling tests were performed on these cells at the same time as cells 1 and 2 (after 144 hours) and were used to compare the severity of swelling and cell degradation in relation to the position in the voltage range.

As soon as Cells 6 and 7 began to rest, after charging to voltage *W*, the thermal chamber temperature was increased from 20°C to 40°C. Due to the limited number of thermal chambers available and the fact that the temperature of the chamber had to be reduced back to 20°C for the post-swelling tests both cells were subject to the same test conditions. The post-swelling tests were conducted at the same time as cell 3 (after 28 hours) and so a direct comparison between the two test results can be made. The temperature dependency of swelling rate and cell degradation may thus be deduced. Results for all the swelling tests can be found in Section 7.1.4.

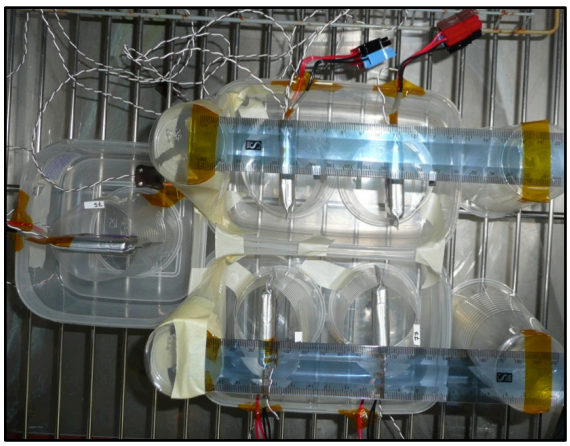

Figure 4.15: Arrangement of 20°C swelling tests

At all points during testing the cells were observed closely. The 20°C cells were monitored via webcam for any signs of danger and were arranged so that rulers, positioned over the cells,

could show cell thickness to the viewer, as shown in Figure 4.15. This was also done so that a significant event could be recorded if it occurred overnight while the cells were not being monitored in person. The equipment used to monitor the 20°C tests was not available for use on the 40°C tests. Calliper measurements of cell thickness were taken every 30 minutes on all seven cells whilst in the swelling range (during the day). Aside from exploring the electrical aspects of a swollen cell, observing the cells during swelling gives information about its mechanical design. This is useful for future battery casing design, internal cell protection mechanisms and mechanical restraints.

4.5 Conclusions

Lithium-sulphur cells manufactured by Sion Power Corporation were chosen for study in this work due to these cells being the only ones made available to ABSL at the time the project was undertaken.

In this chapter several common methods used for modelling batteries were discussed. Different cell characterisation methods were also considered and it was explained why, mainly due to equipment availability and constraints on the use of Sion's cells, an equivalent circuit modelling method and an empirical testing regime were chosen. Development of the model is presented in Chapter 6. Cell testing was divided into two main areas and detailed descriptions of each test carried out were given. They are summarised as follows:

Cell characterisation: The cells were characterised in order to populate lookup tables for a cell model. Tests to characterise properties of EMF, internal resistance, EMF dependency on temperature, self-discharge, storage and hysteresis were described.

BMS specification: Tests to aid the specification of the battery management system were used to characterise properties of open circuit voltage decline, swelling, string cycling and overcharge/overdischarge abuse conditions.

The results of the tests described in this chapter and the conclusions drawn from the data are presented in the remaining chapters of this thesis.

REFERENCES

[1] Sion Power Corporation. (2011, November) Sion Power About Us. [Online]. http://www.sionpower.com/about.html

[2] Sion Power Corporation. (2008, October) Lithium Sulfur Rechargeable Battery Data Sheet. [Online]. http://sionpower.com/pdf/articles/LIS%20Spec%20Sheet%2010-3-08.pdf

[3] Y. Mikhaylik et al., "High energy rechargeable Li-S cells for EV applications," *ECS Transactions*, vol. 25, no. 35, pp. 23-34, 2010.

[4] J.R. Akridge, "Lithium Sulfur Rechargeable Battery Safety," *Battery Power Products & Technology*, October 2001.

[5] Oxis Energy. (2011, December) Oxis Energy: Technology. [Online]. http://www.oxisenergy.com/html/technology.html

[6] V. Kolosnitsyn and E. Karaseva, "Electrolyte for lithium-sulphur batteries and lithium-sulphur batteries using the same," Int. Patent WO2006059085, 2006.

[7] G. Ivanov. (2010, January) Recent Progress in Polymer Lithium-Sulphur Batteries. [Online].http://www.oxisenergy.com/downloads/Recent%20progress%20Polymer%20Li-S_2010.pdf

[8] X. Ji, K. T. Lee, and L. F. Nazar, "A highly ordered nanostructured carbon-sulphur cathode for lithium sulphur batteries," *Nature Materials*, vol. 8, pp. 500-506, June 2009.

[9] B. L. Ellis, K. T. Lee, and L. F. Nazar, "Positive electrode materials for Li-ion and Li-batteries," *Chemical Materials*, vol. 22, pp. 691-714, 2010.

[10] Y. Yao et al., "Interconnected Silicon Hollow Nanospheres for Lithium-Ion Battery Anodes with Long Cycle Life," *Nano Letters*, vol. 11, pp. 2949-2954, 2011.

[11] G. Zheng, Y. Yang, J.J. Cha, S.S. Hong, and Y. Cui, "Hollow Carbon Nanofiber-Encapsulated Sulfur Cathodes for High Specific Capacity Rechargeable Lithium Batteries," *Nano Letters*, vol. 11, no. 10, pp. 4462-4467, 2011.

[12] Y. Yang et al., "New Nanostructured Li2S/Silicon Rechargeable Battery with High Specific Energy," *Nano Letters*, vol. 10, pp. 1486-1491, 2010.

[13] Y.V. Mikhaylik and J.R. Akridge, "Polysulfide Shuttle Study in the LiS Battery System," *Journal of the Electrochemical Society*, vol. 151, no. 11, pp. A1969-A1976, 2004.

[14] Y. Mikhaylik, "Fundamental Chemistry of Sion Power Li/S Battery," in *IBA-HBC*, Waikoloa, Hawaii, 2006.

[15] P.M. Gomadam, J.W. Weidner, R.A. Dougal, and R.E. White, "Mathematical modelling of lithium ion and nickel battery systems," *Journal of Power Sources*, vol. 110, pp. 267-284, 2002.

[16] J. Newman, K.E. Thomas, H. Hafezi, and D.R. Wheeler, "Modeling of lithium-ion batteries," *Journal of Power Sources*, vol. 119–121, pp. 838–843, 2003.

[17] K. Kumaresan, Y. Mikhaylik, and R. E. White, "A Mathematical Model for a Lithium–Sulfur Cell," *Journal of The Electrochemical Society*, vol. 155, no. 8, pp. A576-A582, 2008.

[18] R. Buckle, "Characterisation of ABSL 18650HC for BEAST," ABSL Space Products, Engineering Note LION-ABS-BD-EN-0243/01, 2008.

[19] ABSL Space Products. (2007) Battery Electrical Analysis and Simulation Tool (BEAST) V1.2. Software.

[20] T. E. Kelley, C. Scordilis-Kelley, and V. J. Puglisi, "Lithium sulfur rechargeable battery fuel gauge systems and methods," US Patent 7688075 B2, 2010.

[21] M. Coleman, W. G. Hurley, and C. K. Lee, "An Improved Battery Characterization Method Using a Two-Pulse Load Test," *IEEE Transactions on Energy Conversion*, vol. 23, no. 2, pp. 708-713, June 2008.

[22] N. A. Godshall and J. R. Driscoll, "Determination of the Thermoneutral Potential of Li/SOCl2 Cells," *Journal of the Electrochemical Society*, vol. 131, no. 10, pp. 2221-2226, 1984.

[23] G. J. Dudley, J. De Roche, F. Tonicello, and C. Thwaite, "Electrical/Thermal Model of a Sony 18650HC Li-ion Cell," in *Proc. 'Seventh European Space Power Conference'*, Stresa, Italy, 2005.

[24] R. Ibrahim, "Anti-Swell Protection Circuit for Battery Cells," US Patent 7830125 B2, 2010.

CHAPTER 5

CELL CHARACTERISATION RESULTS

In this chapter the results from the cell characterisation tests, which were described in Chapter 4, are presented. The test data is analysed and compared to results found in the literature and where possible the electrochemistry of the cell is used to explain the findings. The development of these results into the cell model will be discussed in Chapter 6.

5.1 Preliminaries

The following information was recorded during the tests described in Chapter 4 (unless otherwise stated):

- Cycle Number
- Program Step Number
- Test Time (min)
- Step Time (min)
- Capacity (Ah)
- Temperature (°C)
- Energy (Wh)
- Current (A)
- Voltage (V)
- State (e.g. Charge, Discharge, Rest)
- Test Start Date
- Test Start Time

The data logged on the Maccor system was recorded in a format compatible with Excel, with one column for each of the parameters given above, in its raw form. This enabled simple manipulation of the data through the use of standard Excel tools and macros.

In results where the age of the cell was important, the age is taken as number of days since 8th January 2011, the date when pre-shipping voltage readings were recorded, as no specific prior history of the cells was known. The cells were shipped in a discharged condition, between 0% and 10% SoC, and were all at a voltage of 2.16V ± 0.02V when they arrived [1].

5.2 Screening and Capacity Checks

Due to the large number of cells received for testing, cells had to be screened in batches of approximately 10, with 48-hour periods between the start of each set of tests. There was an additional gap of about 4 months between the screening of the first 63 cells and the remaining 36, due to other characterisation tests taking priority over screening. Figure 5.1 compares the charge and discharge voltages of a Li-S cell, obtained from screening, using a 15 second sample rate. The spikes at 2.3V show where 2 second rests were used to estimate internal resistances. At a rate of 0.315A each charge or discharge took approximately 9 hours.

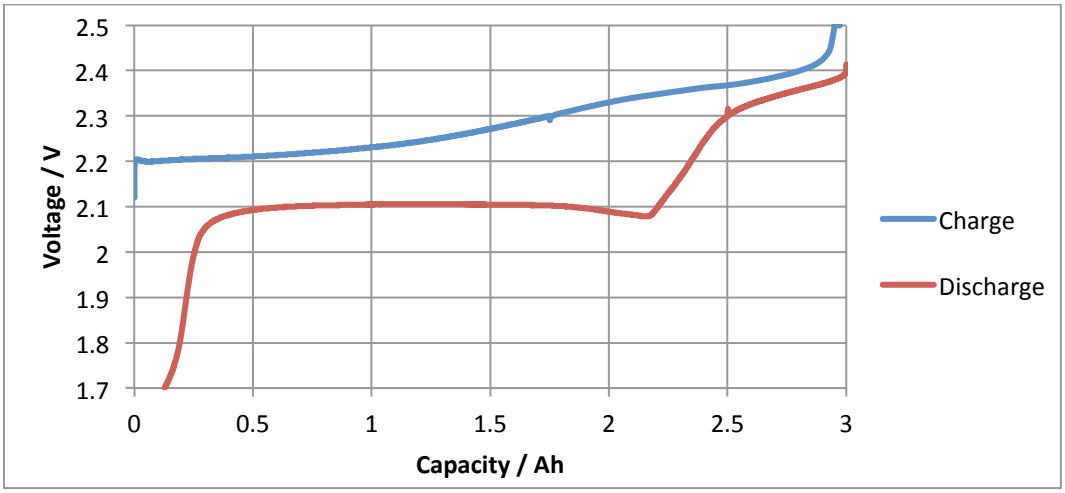

Figure 5.1: 0.315A charge and discharge voltage profiles as a function of capacity

The coulombic efficiency (E_c) is a measure of the total amount of charge available from a cell compared to the charge required to fully charge it and is described by Equation 5.1.

$$E_c = \frac{Discharge\ Capacity\ (Ah)}{Charge\ Capacity\ (Ah)} \quad [5.1]$$

Figure 5.2 shows the coulombic efficiency vs. the age of the Li-S cell batch. Two sets of coulombic efficiency results can be taken from the screening tests as each test consisted of two cycles. The average coulombic efficiency of a cell in its second cycle was 96.7% irrespective of time spent in storage, however the efficiency of the first cycle declines with age. This is well explained by the variation of the SEI layer present on the anode. In Chapter 3 the SEI layer was described as a protective layer that forms when the lithium anode reacts

with chemicals present in the electrolyte. This layer is modified further by the soluble lithium polysulphide species that occur during discharge, providing additional protection against reaction with the lithium anode. If the cell has been left open circuit in a fully discharged condition for a number of days the protection that this layer provides may degrade, causing a possible increase in self-discharge reactions. The first charge after a period of rest is also less protected against parasitic shuttle reactions, requiring substantially more charge to be input into the cell before full charge is reached, reducing the coulombic efficiency of the first cycle. In the subsequent discharge the SEI layer is again modified by the lithium polysulphide species and so an immediate charge following this would not suffer the same level of parasitic reactions and the coulombic efficiency is improved.

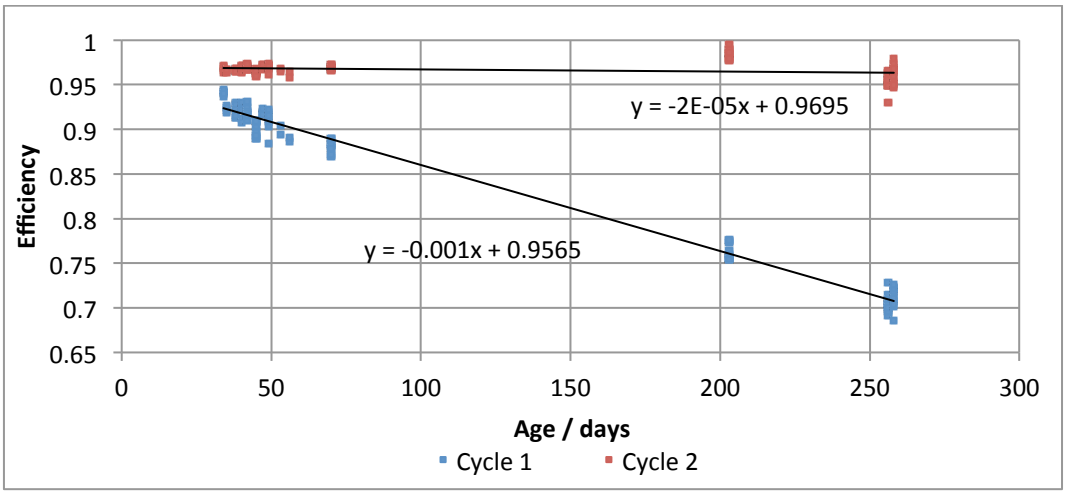

Figure 5.2: Coulombic efficiencies of all screened cells plotted against cell age

In reality the coulombic efficiency is likely to be higher than 96.7%. In these tests a 30-minute rest was taken between charge and discharge. This rest has the effect of reducing the efficiency slightly from its true value because of the self-discharge that occurs. The results of the life tests (see Section 5.4) show that coulombic efficiency decreases with cycle number and the screening tests showed that coulombic efficiency is age independent. The hysteresis tests, where the cells were discharged immediately following a partial charge, showed that the efficiency for a 40% cycle was 97.6%. This number is higher than the screening test results because of the lack of rest between charge and discharge and is probably a smaller percentage than would be obtained for a new cell due to the previous cycles performed on

the cell in the hysteresis test. An expected efficiency closer to, but less than, 100% would not be unreasonable for a brand new cell with zero rest between charge and discharge, but this would require further investigation. The average value of 96.7% is used as the value of coulombic efficiency for a new cell in this work, but should be seen as a worst-case value.

The charge and discharge capacities for the second screening cycle are displayed in Figure 5.3 as a function of age. These results show that, even for cells stored at a low state of charge, capacity irreversibly degrades with calendar age. Assuming the rate of degradation is linear[1] there is a loss of approximately 1.7mAh per day for both charge and discharge capacities when cells are stored at less than 10% SoC. It should be noted that the cells were stored in a non-temperature-controlled chamber, which could have affected these results.

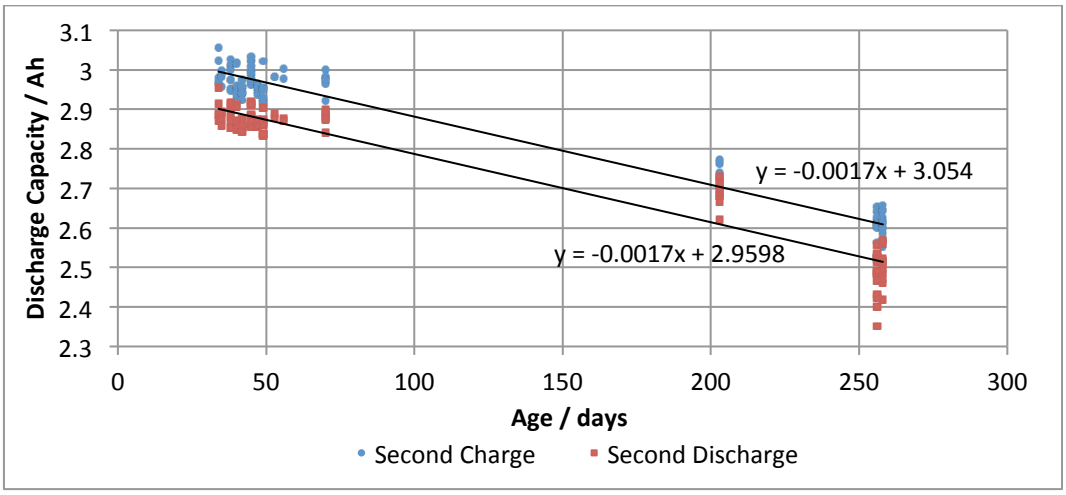

Figure 5.3: Capacities of the second screening cycle performed on each cell as a function of calendar age.

For the set of cells screened first (from day 34 to day 70), the average discharge capacity was 2.88Ah and the average charge capacity was 2.97Ah, on their second cycle. There was a capacity variation of 4.5% across the batch, which is not unreasonable considering the small-scale manufacture of the cells.

[1] The spread of capacity values and the relatively short storage time mean that linearity is assumed. A suitable fit is also achieved assuming a correlation with the square root of time.

During the second screening cycle, a 2 second rest was included when the cells reached 2.3V, during both charge and discharge, so that the internal resistance could be measured. The change in voltage divided by the change in current gives a measure of internal resistance at that point. The results are given in Figure 5.4 and show a somewhat higher resistance than the 25mΩ value given in the data sheet [2].

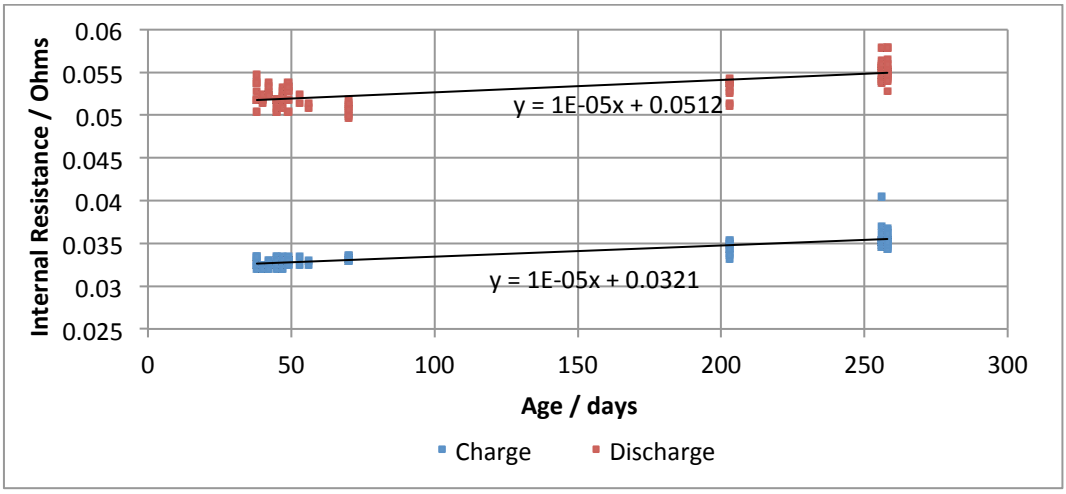

Figure 5.4: Internal resistance of screened cells taken during the second screening cycle

It is clear that the resistance during discharge is higher than the resistance during charge and there is a tendency for resistance to increase with calendar age at a rate of about 10$\mu\Omega$ per day, as the trend line in Figure 5.4 shows.

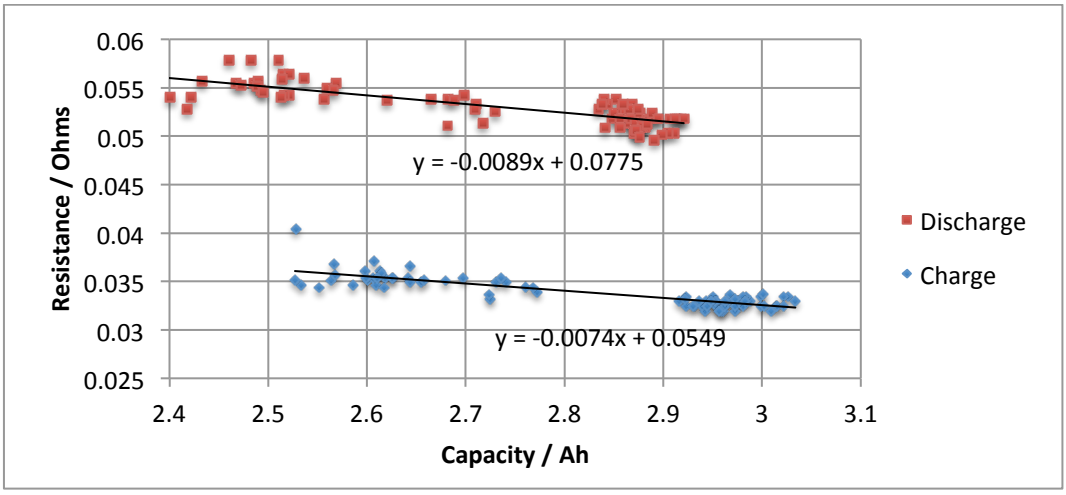

Figure 5.5: Correlation between internal resistance and capacity in the second screening cycle for both charge and discharge.

The results also show that the cells are reasonably uniform in resistance at the point the measurement was taken, with the first cells screened displaying a 5% variation in charge resistance and a 10% variation in discharge resistance. An increase in resistance is accompanied by a reduction in capacity, as shown in Figure 5.5. This active capacity loss can be explained by the deposition of irreversible Li_2S on both electrodes, which also acts to increase the resistance of the cell.

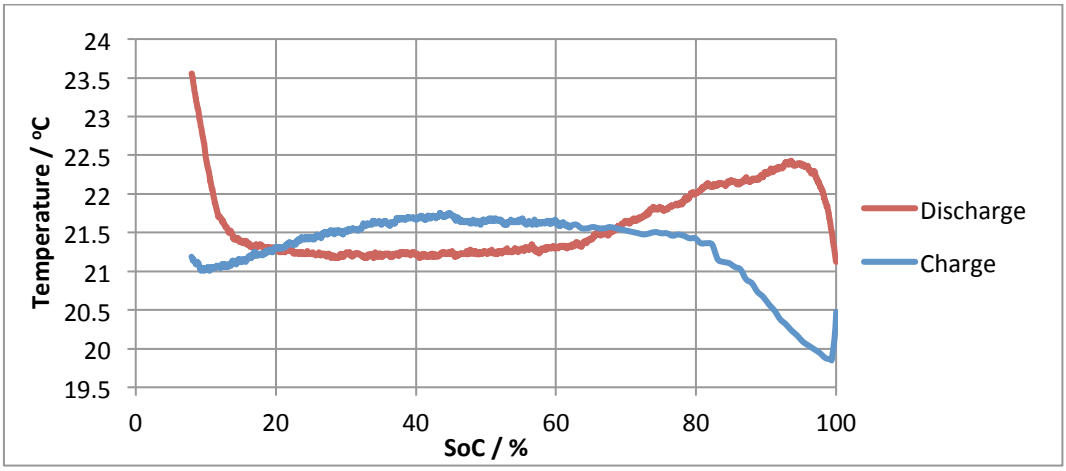

Figure 5.6: Temperature changes of a Li-S cell during a 0.315A cycle. Thermal chamber temperature was measured at 21°C.

There were clear temperature variations during cycling, depicted in Figure 5.6, which were comparable to results found in the literature [3]. The cells returned to ambient temperature within 30 minutes of the removal of current. During charge, the temperature of the cell gradually increased, indicating an exothermic cell reaction, peaking at a temperature of less than 1°C above ambient at about 50% charge. In the second half of charge the temperature decreased dipping to just below 1°C of ambient at the end of charge. The electrochemical cell reaction is thus endothermic in the second half of charge, absorbing heat from its surroundings.

In reversible cell reactions the opposite flow of current invokes the opposite temperature profile. The discharge temperature profile of the Li-S cell is almost the inverse of the charge profile. The asymmetrical nature of the profiles, at the very end of discharge where cell temperature increases steeply to 23.5°C, can be attributed to the formation of the Li_2S layer

on the cathode at low states of charge. This layer causes a sharp increase in internal resistance, which in turn causes more of the energy entering the cell to be dissipated as heat. Although this layer is still present at the beginning of charge, it is depleted before the cell can heat up to appreciable levels.

5.2.1 Standard capacity measurement (SCM) analysis

Five cells were connected in parallel and cycled at the very low rate of C/48, with no current interruptions, in order to determine the average beginning of life (BoL) total capacity of the Li-S cells. The total charge capacity obtained in this test was 3.21Ah while the total discharge capacity was 3.13Ah. A comparison of these values to the average charge and discharge capacities of the same cells in the screening cycles is given in Table 5.1 (taking into account the expected capacity fade due to cycling and storage). It shows that an SCM cycle, as defined in Section 4.3.1, where the cells begin at 100% SoC, gives around 92% of the total capacity.

	Slow Cycle / Ah	Expected capacity at 0.315A/Ah	Percentage of slow cycle capacity
Charge Capacity/Ah	3.21 ± 0.01	2.97 ± 0.01	92.5 ± 0.6%
Discharge Capacity/Ah	3.14 ± 0.01	2.91 ± 0.01	92.7 ± 0.6%

Table 5.1: Comparison between capacities obtained during a C/48 cycle and the average of the capacities obtained for the same cells during screening, modified to match cycle number.

In support of this result, a single cell was charged to 100% SoC and then discharged at a rate of 0.315A until 1.7V was reached, after which the cell was taper discharged until the current reached a value of 0.058A; the same current value as used in the C/48 test. The capacity removed from the cell down to 1.7V was 92.1% of the capacity removed from the cell in total. The uncertainty in the Maccor readings (±0.02% of full current scale) gives an error in the capacity measurements of ±0.6%. These values could be affected by self-discharge occurring during both cycling and during the rests between cycles.

The low current used means that the slow cycle test took a number of days to complete, in which time self-discharge may have occurred to decrease the capacity of the cell. If the

maximum self-discharge current occurred over all states of charge then the storage test results (given in Section 5.3) show that the reversible capacity lost over 48 hours would be 2% of the total capacity. However, self-discharge may not be constant over all states of charge and could decline as SoC decreases. Therefore, the discrepancy in capacity from self-discharge reactions is likely to fall within the noise of the measurements and will be disregarded in the results of this test.

Taking into account the above complications, and accepting a certain level of error in these results, in the remainder of this work the SCM cycle will be taken as 92% of the full capacity of the cell. This conclusion can be used to process the results of other tests, where a 0.315A SCM cycle can be used to estimate total capacity of a cell rather than using a time consuming 4-day slow cycle.

5.3 Storage and Self-Discharge Tests

Two series of storage tests were described in Section 4.3.3. Cells were stored at both 100% SoC and 40% SoC at 20°C for different amounts of time while their storage characteristics were acquired. The purpose of these tests was to determine both the rate of self-discharge and the amount of irreversible capacity fade for inclusion in the cell model.

5.3.1 40% SoC storage tests

Table 5.2 shows the data obtained in the 40% SoC storage tests. It is possible to determine the irreversible capacity loss due to cycling and age by substituting D_1 and D_3 into Equation 4.2, the results of which are shown in the final row of the table. Because the cells were stored at 40% SoC, the discharge capacity (D_2) is not comparable to D_1 and D_3. To determine the total capacity loss an expected value of D_2 was calculated based on the charge put into the cell to reach 40% SoC and a coulombic efficiency of 96.7%. Comparing the actual discharge capacity after rest (D_2), with the expected discharge capacity (had there been no rest) gives an estimation of the total capacity loss. This data shows some interesting results. All capacity losses are clearly a function of the square root of time, as depicted in Figure 5.7, indicating

that the reactions that cause capacity losses are self-limiting. Results presented by Ryu et al. in [4] show a similar trend, where capacity loss is more significant in the first 80 days of storage, reducing down to insignificance thereafter.

Cell Number	42	43	44	45	46	47	48	49
Days in storage	1	1	7	7	41	41	140	140
Initial Discharge Capacity, D_1 / Ah	2.811	2.802	2.822	2.803	2.805	2.789	2.839	2.819
Charge to 40% SoC Capacity / Ah	1.208	1.208	1.208	1.208	1.208	1.208	1.208	1.208
Expected D_2 / Ah	1.168	1.168	1.168	1.168	1.168	1.168	1.168	1.168
Actual Discharge Capacity after Rest, D_2 / Ah	1.377	1.384	1.213	1.213	0.852	0.877	0.403	0.428
Discharge Capacity after Recharge, D_3 /Ah	2.763	2.760	2.738	2.721	2.618	2.611	2.543	2.517
Irreversible Capacity Loss (D_1-D_3) / Ah	0.048	0.042	0.084	0.082	0.187	0.178	0.296	0.302

Table 5.2: 40% SoC storage test results

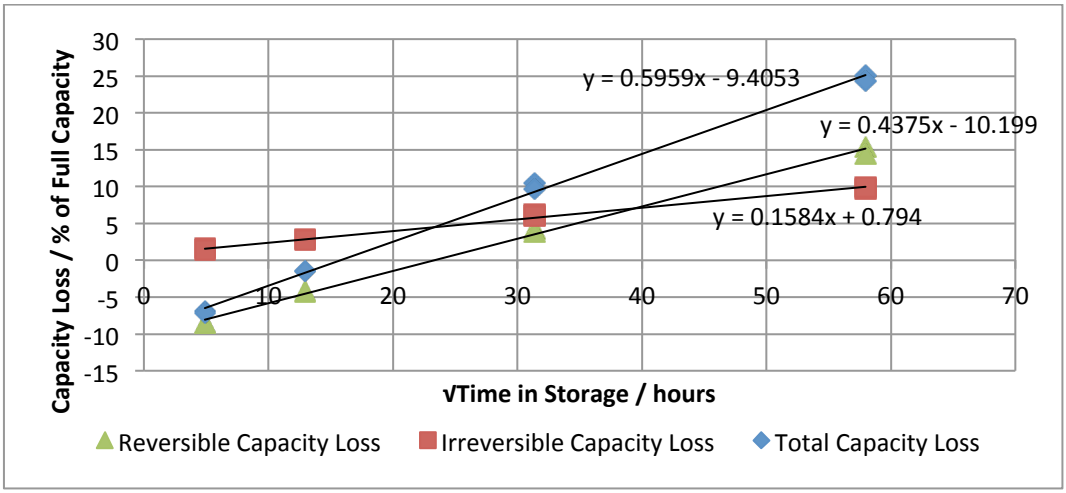

Figure 5.7: Irreversible, reversible and total capacity losses in cells stored at 40% SoC

Extrapolating to zero days in the irreversible loss trend line gives the intercept of the graph, which represents the percentage of capacity lost due to the act of cycling, as 0.8%. In the case of the cells stored at 40% SoC, this loss can be attributed to 1.4 cycles occurring between the initial discharge and the final discharge. The actual discharge capacity after 1 day and 7 days of rest, D_2, was higher than the charge put into the cell. This indicates that, when the load current is removed, the concentration gradients that have built up decrease, and possibly disappear, very slowly and that this effect masks any results that could be obtained to

determine self-discharge in this time period. Self-discharge reactions do occur however and are more apparent over longer periods of time, once the concentration gradients have settled. It is not until at least 20 days of rest that the self-discharge reactions become dominant.

Consequently, the experiments intended to characterise the self-discharge reactions, were actually a combination of reversible capacity changes incorporating the sum of both self-discharge capacity losses and capacity recovery "gains". This presents a number of issues. Separating the two effects is important for modelling purposes as the capacity gain witnessed during rest only occurs after the removal (and possibly reversal) of current, whereas self-discharge reactions may occur regardless of whether the cell is connected to a load or not. It is possible that the level of self-discharge remains constant over the entire SoC range of the cell although this is unlikely because of the reduction of chemical activity of polysulphides as chain length decreases at lower states of charge [5]. The effect that storage of the cell has on the protective SEI layer may also affect these results. As storage time continues, the SEI layer starts to degrade, possibly leading to an increase in parasitic self-discharge reactions that may eventually become self-limiting. The mechanisms behind the storage effects of Li-S cells at states of charge other than during rest at 100% SoC are not described in the literature, the only implication being that self-discharge decreases with decreasing states of charge [5].

5.3.2 100% SoC storage tests

It was intended to repeat the above tests on cells stored at 100% SoC. The test was in fact only completed on cells stored for 1 and 8 days because the remaining cells had begun to swell by the time they were due for testing at 40 days. Due to safety concerns these cells were discharged out of the swelling range and no further cycling on these cells was permitted. The results obtained for the 1 and 8 day storage tests are given in Table 5.3. The two time points available from this data does not indicate the relationship between self-discharge and the time in storage. However it is not unreasonable to assume the same self-limiting nature of the cell reactions as with the cells stored at 40% SoC and as described in the literature. Ryu et al. noted that the rate of capacity loss due to self-discharge diminishes as time progresses [4].

	Cell 28	Cell 29	Cell 30	Cell 31
Days in storage	1	1	8	8
Initial Discharge Capacity, D_1/Ah	2.810	2.774	2.801	2.850
Discharge Capacity after Rest, D_2/Ah	2.711	2.690	2.598	2.624
Discharge Capacity after Recharge, D_3/Ah	2.759	2.731	2.716	2.743
Irreversible Capacity Loss / Ah	0.052	0.043	0.084	0.107
Reversible Capacity Loss / Ah	0.048	0.040	0.118	0.119

Table 5.3: Test results for cells stored at 100% SoC for 1 and 8 days

Assuming proportionalilty with the square root of time gives the relationships displayed in Figure 5.8. The intercept of the irreversible capacity loss trend line represents the percentage of initial capacity lost due to the act of 2 cycles. The intercept occurs at 0.7%, which is in agreement with the value of 0.8% found in the 40% SoC tests. The total capacity loss is always positive at 100% SoC indicating that self-discharge losses occur soon after resting begins. Extrapolating the self-discharge trend line shows a capacity loss of 7.6% after 1 month in storage. This is comparable to the literature [3,6], which states values of 4-6% per month. However, the temperature at which these values were arrived at is not stipulated and a cooler temperature could be the reason for this discrepancy.

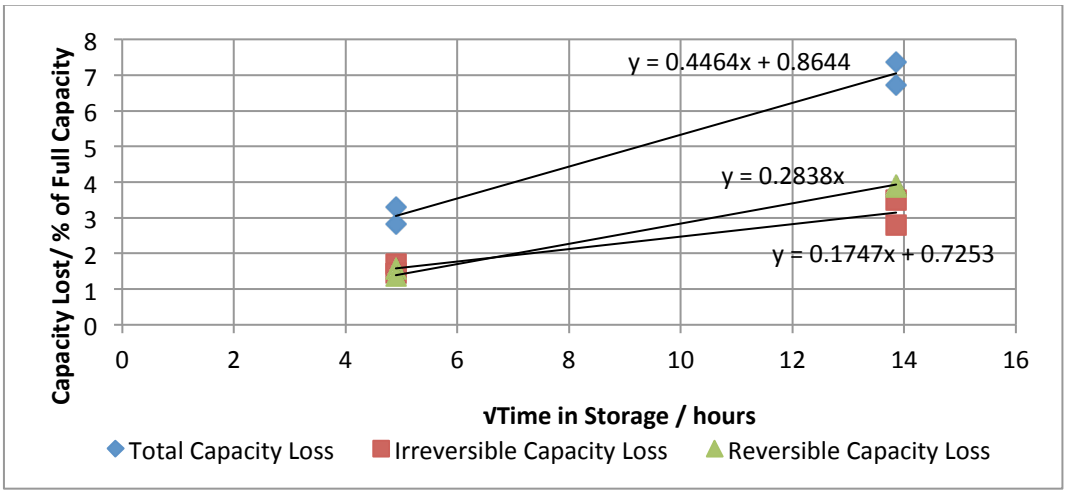

Figure 5.8: Relationship between capacity losses and time spent in storage at 100% SoC

The results of these tests clearly show that there is a significant capacity loss at medium to high states of charge, and these losses are not profoundly larger at 100% SoC. In Chapter 6 the reversible and irreversible capacity changes are analysed for inclusion in the cell model.

5.4 Life Tests

A series of repeated cycling tests were conducted on 5 individual cells. Each cell was taper charged to 100% SoC at a rate of 0.315A and discharged at a rate of 5.6A (2C), 2.8A (C), 1.4A (C/2), 0.56A (C/5) or 0.315A (~C/9). These values were chosen to span the current range that is acceptable to use on the cell. These tests indicate the capacity losses due to cycling and reveal the short term cycling behaviour of the cells, which helps to determine their suitability for space industry applications. The results of these tests can be incorporated into the cell model to predict cell degradation and may be used by the BMS to predict a cell failure.

5.4.1 Cell failure

The cells undergoing C/9 discharge and C/5 discharge both ruptured during cycling, as shown in Figure 5.9. The analysis of life test data given in this section indicates why these failures may have occurred and examines the possibility of predicting such a failure.

Figure 5.9: A ruptured Li-S cell

5.4.2 Capacity fade

Figure 5.10 shows the capacities of the life test cells as a function of cycle number. There are some discontinuities in the data where the capacities change sharply from one cycle to the next before recovering again. This is due to the fact that the tests had to be suspended for a period of 10 days to accommodate restructuring of the facilities. Despite a slight increase in capacities of the C/2 and C/5 cells during the first 5 or so cycles there is an overall trend of

capacity fade with cycling, as expected. In [7] this initial increase in capacity was attributed to slow penetration of electrolyte into the pores of the carbon structure. However, the results given here show that the initial capacity increase did not occur in all cells and only at intermediate rates. As expected, the available capacity decreases with increasing current rate.

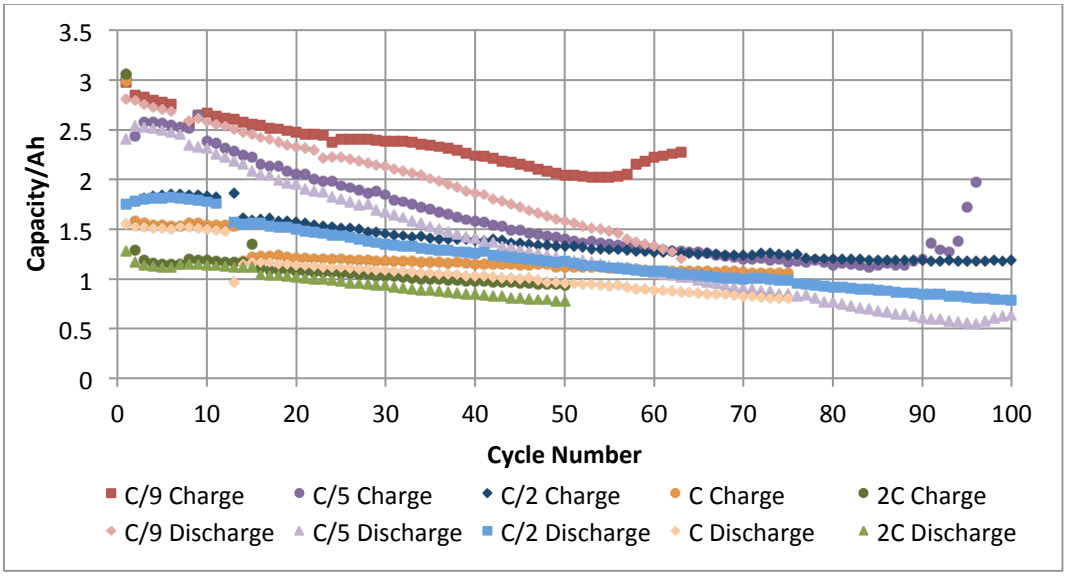

Figure 5.10: Charge and discharge capacities of life test cells

Figure 5.11 shows the average capacity loss per cycle as a function of rate. These values were calculated by taking the expected loss due to calendar age into account, due to the varying amounts of time the tests took to complete.

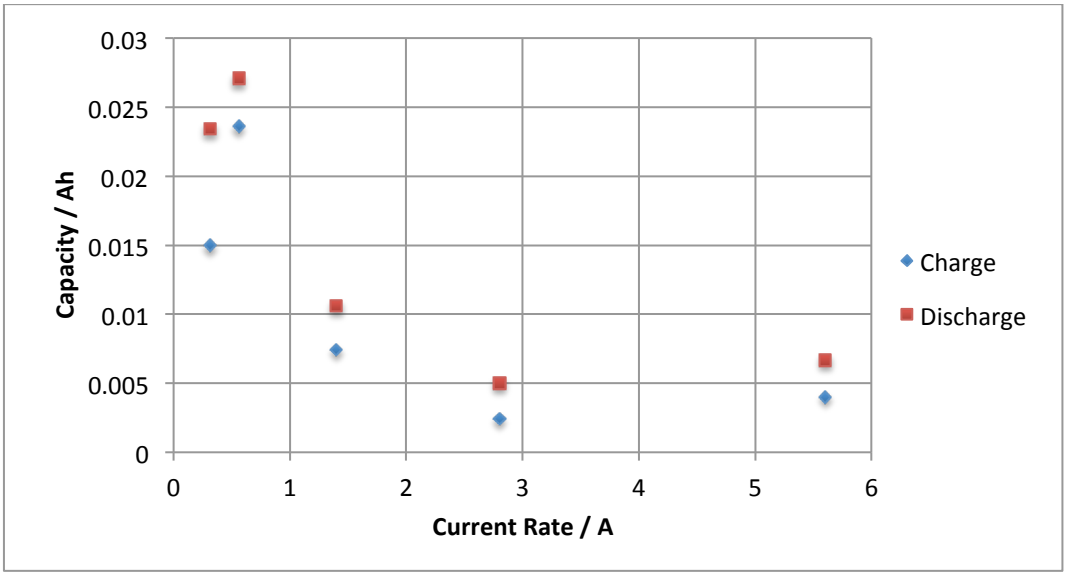

Figure 5.11: Capacity (Ah) lost per cycle as a function of current rate

These results show that capacity fade rate generally decreases as current rate increases, and possibly starts to increase again at very high rates, which could indicate a current rate threshold of ~2C at which point cathode destruction becomes a dominant factor. This result appears to conflict with results found in [8], which state that the rate of capacity fade increases from 0.1Ah per cycle to 0.18Ah per cycle as current rate increases from ~C/10 to ~C/1.4 respectively. However, in that paper the fade rates are both significantly larger than in the Sion cells cycled at similar rates, indicating a significant variation in chemical composition. In this work, the cells discharged at the C/9 and C/5 rate both ruptured after approximately 60 and 90 cycles respectively, which may have been preceded by the increased capacity degradation seen in Figure 5.11. However, many C/9 conditioning cycles were performed in a range of other tests and all showed similar levels of capacity fade to those of this test, which would imply that the results are not anomalous and the rate of capacity fade is indeed larger at low current rates for the Sion cells. This hypothesis is further corroborated in literature concerning lithium metal cells [9], which establishes that cycle life is longer for cells cycled at high discharge rates in comparison to lower rates. The storage test results predicted approximately 0.4% capacity fade (due to cycling) per 0.315A cycle, however these cells had time for recovery between cycles. The life tests predict a capacity fade of 0.9% per 0.315A cycle when cells are cycled continuously.

The conflict with the results given in [8] may be due to varying cell compositions, as the Sion cell uses a different electrolyte to the TEGDME electrolyte of the cell in [8], and there may be different levels of parasitic reactions present. In addition, the results in this work give the capacity when the cells are discharged to a cut off voltage of 1.7V. In [8] the cut-off voltage is 1.5V, which may influence capacity fade (see results of abuse tests in Section 7.1.2). At low current rates the cells experience a higher depth of discharge compared to higher current rates. Hence, there is more opportunity for Li_2S to form and even though it is deposited more evenly throughout the cathode, the additional volume may be destructive to the pores of the carbon matrix.

In Chapter 3 it was shown that the precipitation of Li_2S begins at the start of the second discharge region. If Li_2S increasingly tends to deposit on the surface of the cathode as current rate increases [8], obstructing access to the inner cathode, then the available capacity in the second discharge region declines as current rate increases. This is supported by the voltage profiles given in Figure 5.12, which shows that the current rate only affects the capacity available in the second discharge region. The capacity available from the first discharge region is independent of the current rate used.

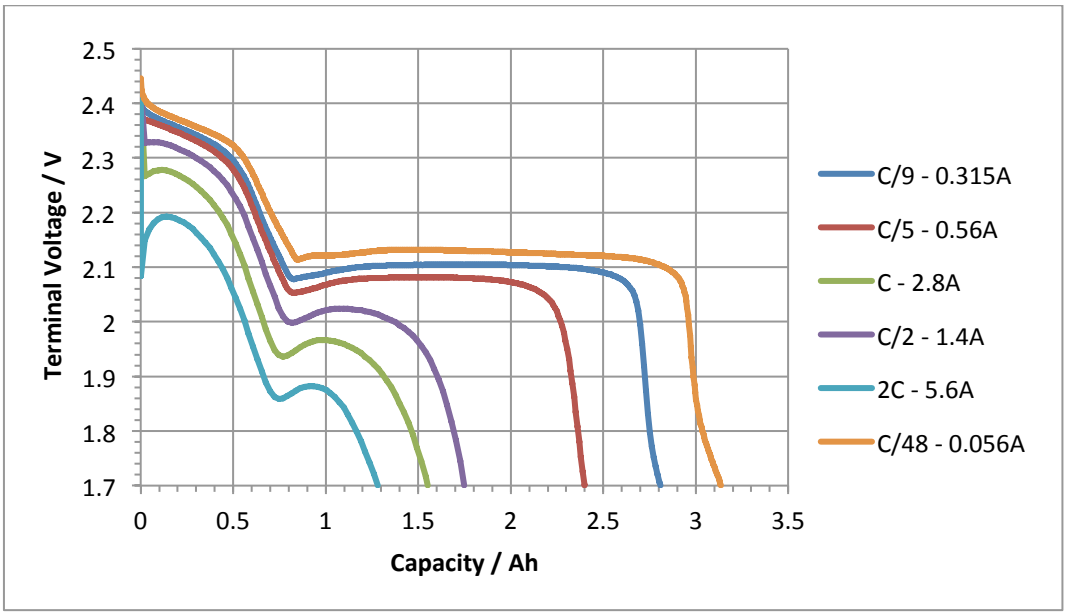

Figure 5.12: Voltage profiles of cells discharged at various current rates

Figure 5.13 shows that the capacity available in both the first and second discharge region decreases with cycle number, complementing results found in the literature [10]. This supports the theory that the total level of irreversible capacity (i.e. irreversible Li_2S deposited on the anode and cathode) increases with cycle number [11,8]. Irreversible Li_2S accumulating on the electrodes during cycling would not only lower the total capacity available in the cell but would also increase the resistance of the surface layers as cycle number increased. This is evidenced in Figure 5.13 by the fall in voltage of both the first and second plateaux.

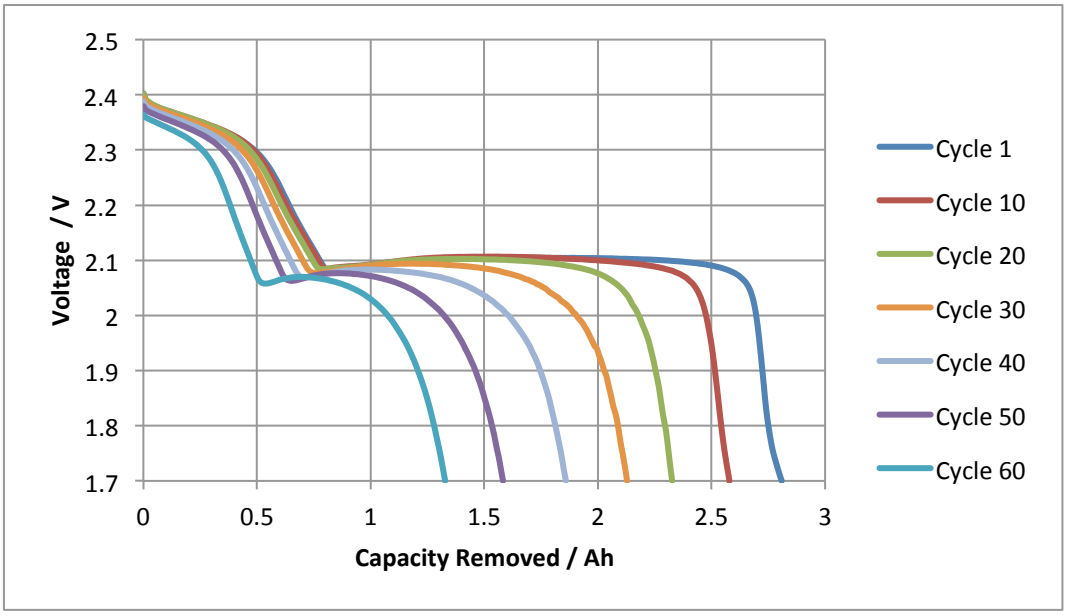

Figure 5.13: The 0.315A discharge voltage profiles at different cycle numbers

The specific energy of the cell is calculated using Equation 5.2.

$$Specific\ Energy\ (\text{Wh/kg}) = \frac{V_{av} \cdot Q_t}{m} \qquad [5.2]$$

Where V_{av} is the average voltage during discharge, Q_t is the total capacity of the cell and m is its mass. Mass can be interchanged for volume to find the energy density of the cell. For a Li-S cell cycled at C/9 and C/5 these energy values, taken at cycle 1 and cycle 60, are given in Table 5.4. The mass of the cell is taken as 16g and its volume as 0.023l.

	C/9		**C/5**	
Cycle Number	1	60	1	60
Average Voltage (V)	2.14	2.1	2.13	2.07
Capacity (Ah)	2.809	1.33	2.4	1.05
Specific Energy (Wh/kg)	376	175	320	136
Energy Density (Wh/l)	257	119	218	93
Capacity loss after 60 cycles (%)	53%		56%	

Table 5.4: Energy parameters of the Sion Li-S cell

The values given here are comparable to those found on the publically available data sheet provided by Sion [2], which states a nominal voltage of 2.15V and a capacity of 2.5Ah at C/5. However, in a presentation made at the 2011 NASA Battery Workshop by J. Jeevarajan [12], improved values were reported for cells also manufactured by Sion. Nominal capacities of

around 4.55Ah were stated along with a capacity fade of around 30% for 92 cycles. The specific energy of those cells were reported as 393Wh/kg for a fresh cell, which implies that larger capacity cells with a mass of ~25g are in production, assuming equivalent voltages.

5.4.3 Efficiency degradation

Figure 5.14 plots the coulombic efficiency of the life test cells. The data for the cells that did not rupture shows a possible rate dependency where the cycling efficiency reduces faster at higher current rates especially after the initial 20 cycles, but this could also be due to the non-uniformities and temperature variations of the cells. The data shows that there is, on average, a linear 0.3% decrease in cycling efficiency per cycle. The anomalous data points can be attributed to the charge capacity being much higher than normal after a period of rest, reducing coulombic efficiency. In [13] it was reported that cycling efficiency decreases more rapidly in cells discharged to a lower cut-off voltage of 1.5V.

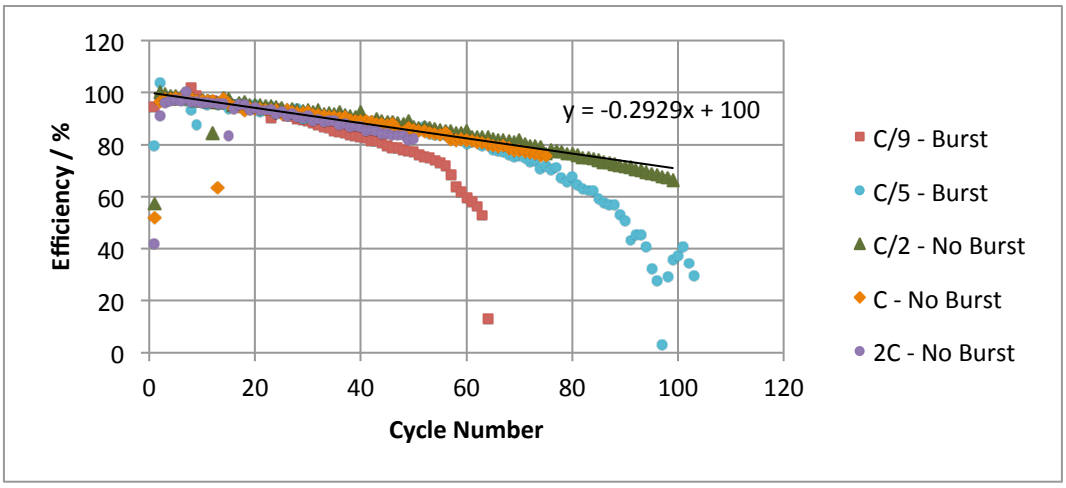

Figure 5.14: Cycling efficiency of life test cells

Looking at the efficiencies of the cells that did burst and comparing them to those that didn't, it would appear that a gradual drop in coulombic efficiency precedes the burst event. The fall in coulombic efficiency implies that there was possibly an internal soft short between the electrodes in the cell providing a path for current to bleed off without contributing to the capacity of the cell. In certain applications this result could be used as an early warning for possible cell failures.

5.5 EMF Characterisation Test

The aim of the main EMF vs. SoC tests was to obtain a look up table containing a single value of EMF for each uniform increment in SoC. The resulting lookup table can be mathematically interpolated so that the EMF of a Li-S cell at any intermediate state of charge can be known. The EMF was found by recording the open circuit voltage at the end of each rest period, after a fixed amount of charge is added to or removed from the cell.

As explained in Section 2.2.2 the state of charge is defined as the capacity remaining in the cell as a percentage of some reference point. In these tests the reference point will refer to the cell's total capacity at 100% SoC, which changes as the cell degrades. Monitoring the current, *I*, that goes into and out of the cell allows us to compute the changing state of charge as the cell cycles, as given in Equation 5.3:

$$SoC = SoC_0 + \frac{\int I_1 dt}{Q_t} \qquad [5.3]$$

Where SoC_0 is the initial state of charge, SoC is the present state of charge and recalling that load current I_1 was defined as negative for discharge and positive for charge. For this test the cells were pre-cycled at 0.315A (SCM cycle), in order to estimate their full capacity Q_t. The capacities relating to this test are given in Table 5.5.

SCM charge capacity (92% of total capacity)	2.58 Ah
SCM discharge capacity (92% of total capacity)	2.54 Ah
Estimated total charge capacity (no rests)	2.80 Ah
Estimated total discharge capacity (no rests)	2.76 Ah
Actual charge capacity (with rests)	3.43 Ah
Actual discharge capacity (with rests)	3.02 Ah
Charge capacity gained (in 69 2hr rests)	0.63 Ah
Discharge capacity gained (in 60 2hr rests)	0.26 Ah

Table 5.5: Capacity data obtained from EMF vs. SoC test

As these results show, there is a significant difference between the estimated full capacity and the capacity when rests were incorporated. The storage tests showed that self-discharge and capacity recovery affect these results, particularly because the state of charge cannot be said to be constant during each 2 hour rest period, falling due to self-discharge at high states of charge and increasing at lower states of charge as capacity recovers.

From the storage test results, the estimated reversible capacity changes (the sum of gains and losses) after 2 hours rest at 100% and 40% SoC vary, as depicted in Figure 5.15. Further testing is required to populate this graph in more detail and to determine the exact relationship between reversible capacity loss and SoC. Factors such as temperature and current rate also affect these values as the capacity recovery effect is due to the diffusion and relaxation of chemicals inside the cell. At 40% SoC the capacity gain after two hours of rest is predicted to be ~0.02Ah. The full cell capacity is estimated to be 2.76Ah and so this capacity change then represents a change in SoC of less than 0.8%. At 100% SoC the discrepancy in SoC is around 0.1%.

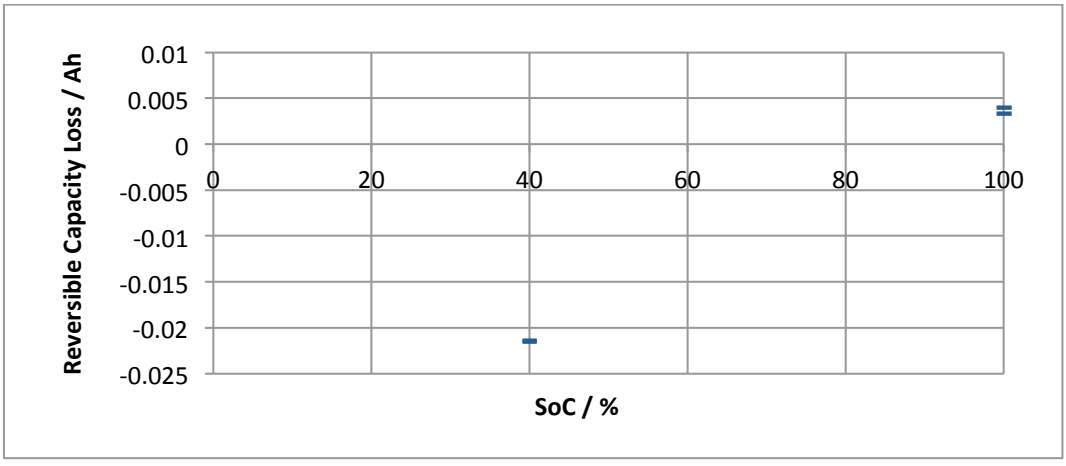

Figure 5.15: Predicted reversible capacity losses after 2 hours storage at 40% and 100% SoC

The gain in total capacity, due to the rest periods, was incorporated into the SoC calculation by scaling the data so that the final rest point corresponded to 0% SoC. This means that the state of charge at each rest point is adjusted to account for the total capacity change during the rest. Because it is only the end of rest voltage that is of concern, and the state of charge changes by less than 1% during rest, this method gives a good description of the EMF vs. SoC.

The capacity recovery phenomenon occurs in all battery types, however it needs to be addressed for modelling purposes and is discussed in more detail in Section 6.3.4.

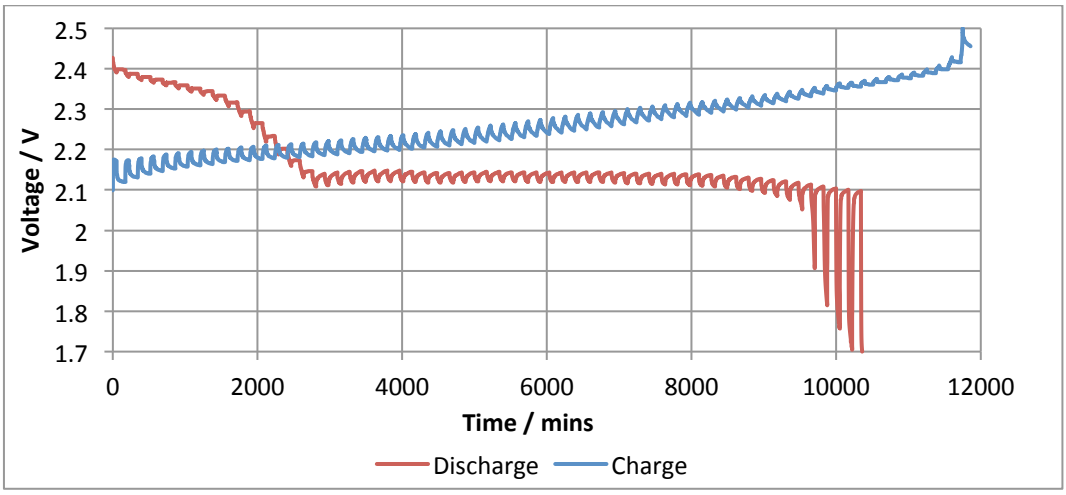

Figure 5.16: Discharge and charge EMF test results at 20°C

Figure 5.16 shows this voltage response for both a discharging and charging cell, as a function of time and at an ambient temperature of 20°C. The voltage gradient in the rest periods approaches zero rapidly at higher states of charge (>70%) for both curves, as expected. This indicates that the solid Li_2S layer that exists at lower states of charge has a noticeable effect on the voltage recovery by hindering the chemicals in the cell from reaching equilibrium quickly. The fundamental EMF vs. SoC look up table resulting from the end of rest voltage values can be found, along with all other model look up tables, in Appendix E. Figure 5.17 is a graphical representation of this table.

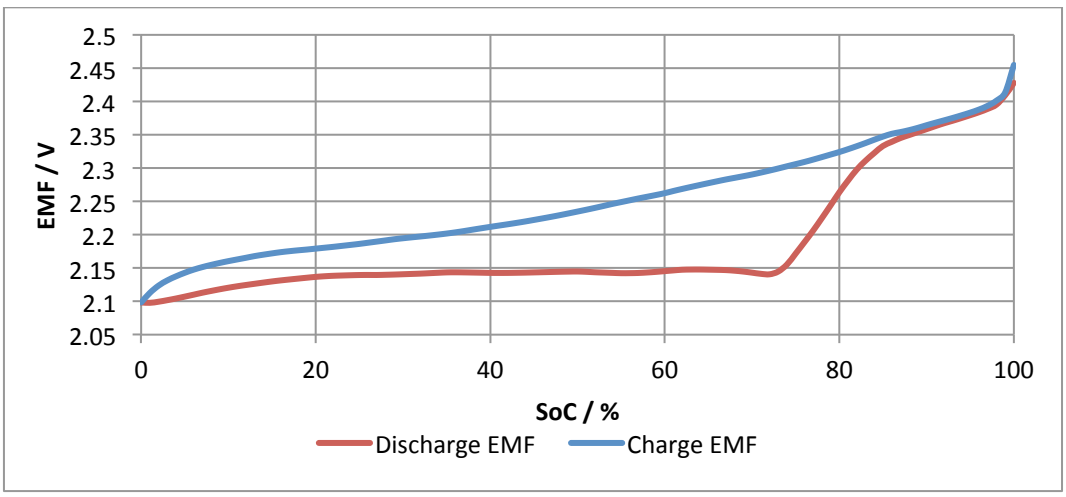

Figure 5.17: Fundamental charge and discharge EMF curves for the Li-S cell

The same 5 cells were used for all of the EMF tests repeated at each test temperature, which affects the results given in Figures 5.18 and 5.19. Less capacity is available at 0°C because of the increased viscosity (and hence resistance) of the electrolyte at low temperatures. The residual effect of this may affect the full conversion of the Li_2S discharge product back to elemental sulphur, hence also reducing the capacity available at 40°C. There is also less capacity available at 40°C because of the history of the cells, as deep DoDs cause an increased level of degradation, and this was the final test.

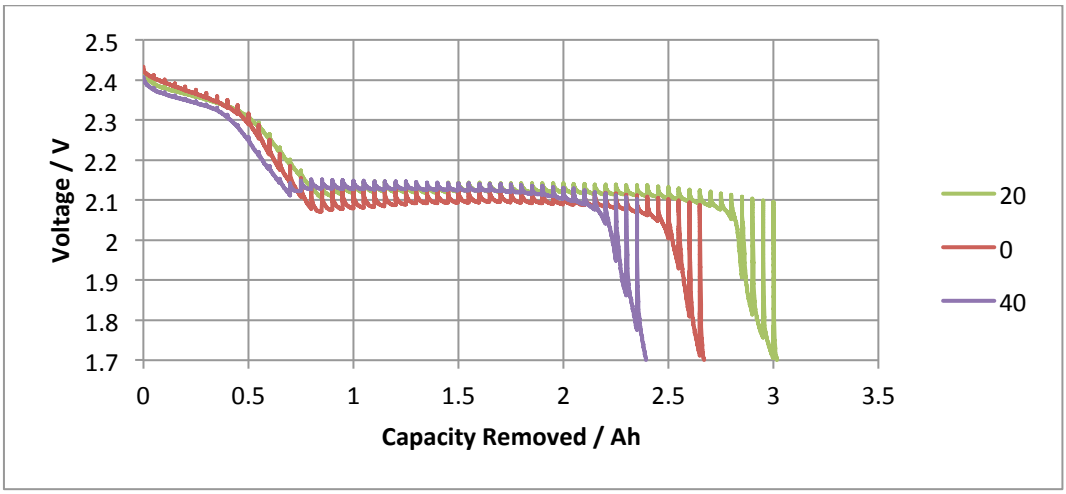

Figure 5.18: Discharge EMF test results at 0°C, 20°C and 40°C

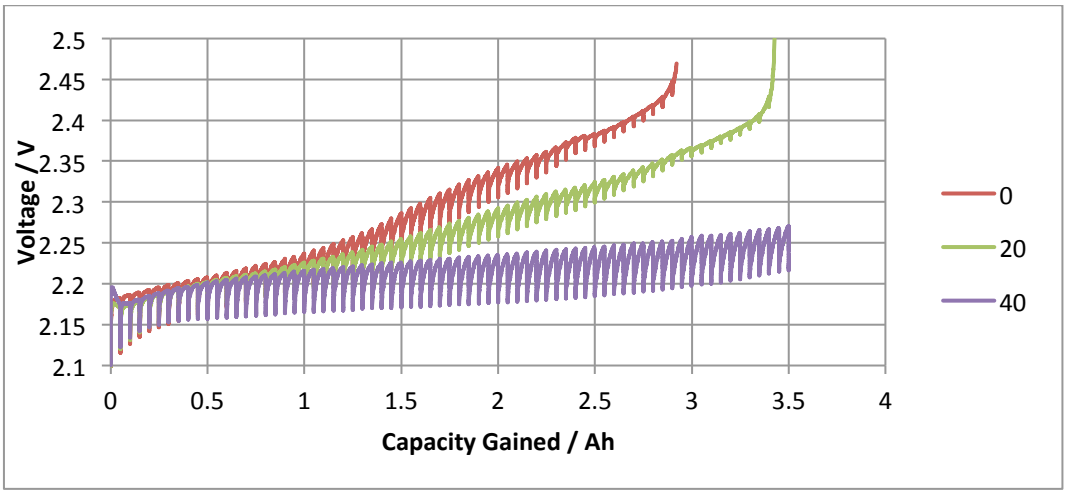

Figure 5.19: Charge EMF test results at 0°C, 20°C and 40°C

In addition, the cells underwent an SCM cycle before each test began, but this cycle was completed at the same temperature as the test condition, so the SoC at which the tests began was not known accurately. The 40°C charge tests were not permitted to complete as the input

capacity far exceeded the expected charge capacity of the cell. This was likely due to an increased level of self-discharge at these high temperatures, preventing the full conversion of polysulphides to solid sulphur during the long rest periods. Because of the potential for error, the results of the 0°C and 40°C tests were not used in the model but were used to compare to the "EMF dependency on temperature" test results, given in Section 5.7.

5.6 Resistance Characterisation Tests

The origins of resistance of a Li-S cell were described in Chapter 3. Ohmic resistances are governed by the physical elements of the cell such as electrodes, tags and current collectors, and also by the conductivity of the electrolyte. The conductivity of the electrolyte changes during cycling because of the varying concentrations of lithium polysulphide species. Although a higher concentration of ions in the electrolyte should, in theory, improve conductivity, the increase in dissolved lithium polysulphides increases the viscosity of the electrolyte, which in turn increases resistance to mass transport. The SEI layer on the anode and the Li_2S layer deposited on the cathode also contribute to the resistance of the cell. The form of these surface layers is both state of charge and temperature dependent and, as previous results imply, may also depend on storage time. These surface layers impede the movement of lithium ions and lithium polysulphides dissolved in the electrolyte. When the load current stops or changes direction, the forces on the ions in the electrolyte change, but the surface layer and electrolyte resistances cause a time delay before the ions can fully respond to the current change. In addition to the surface layer resistances there is a charge transfer resistance associated with electrochemical reactions on the surface of an electrode. This resistance occurs when electrons are transferred to reactants present on the electrode and the product of this reaction must be transported away from the electrode so that other reactants can take its place. The mass transport processes of lithium polysulphide species in the electrolyte limit the rate at which these reactions can take place. In this section the results of the resistance tests are given and the voltage relaxation curves are analysed with respect to the contributions to resistance described above.

5.6.1 Rate dependency rest test

When a Li-S cell is subject to a discharge current that is suddenly stopped, the voltage recovery takes the form shown in Figure 5.20. In the first instant of rest there is an immediate steep rise in voltage that can be mostly attributed to the removal of the current and hence the Ohmic resistance of the cell.

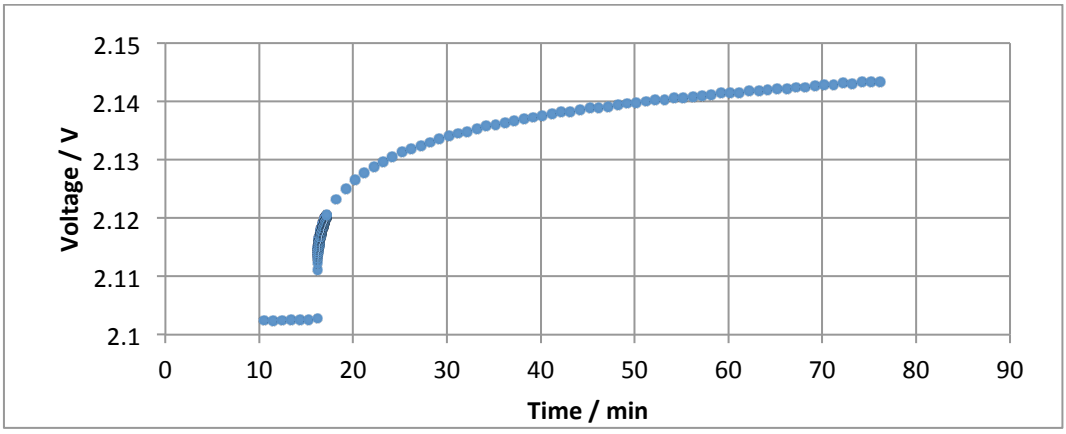

Figure 5.20: Voltage recovery of a discharging Li-S cell after the current is abruptly stopped

The remaining slow voltage recovery to the EMF value is depicted by the curved portion of the graph and is attributed to the time dependent recovery of the concentration gradient as the chemical species diffuse back to equilibrium. In this test, individual cells were cycled at a rate of C/20, C/9 or C/5 with periodic 1-hour rests incorporated so as to study and compare the voltage recovery effect.

In Li-ion cells Ohmic resistance is largely independent of current rate used [14] but it was important to determine if the same could be said for Li-S. The Ohmic resistance contribution is dominant in the instant the current is removed. Therefore, the Ohmic resistance was defined as the change in voltage after 1 second[2] of rest, divided by the current change, a technique commonly used to define Ohmic resistance [15]. This calculation was repeated for each rest period and so a value for the Ohmic resistance at each SoC was found for each rate. The results of this test are displayed in Figures 5.21 and 5.22.

[2] This 1-second definition is nominal. The effects of Ohmic resistance are dominant in this first second of rest, but in reality diffusion resistances occur throughout the entirety of the rest period.

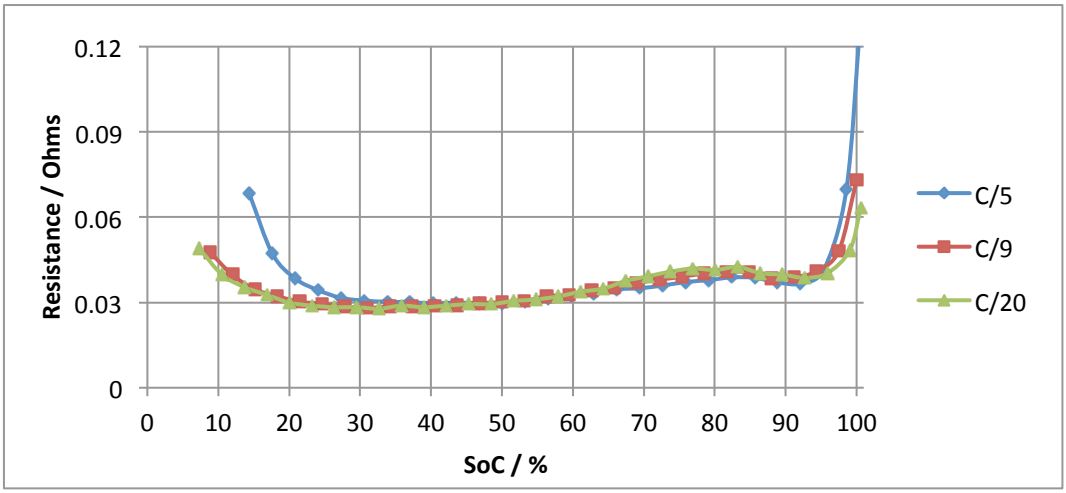

Figure 5.21: Ohmic resistance during charge for cells cycled at various rates

It is clear that for the lower current rates (<0.315A) the Ohmic resistance of the cells is largely rate independent. For the cell cycled at the higher rate of 0.56A (C/5) the Ohmic resistance is larger at low states of charge. The values of Ohmic resistance between the lower and higher rate starts to diverge at around 40% SoC, the difference increasing as DoD increases.

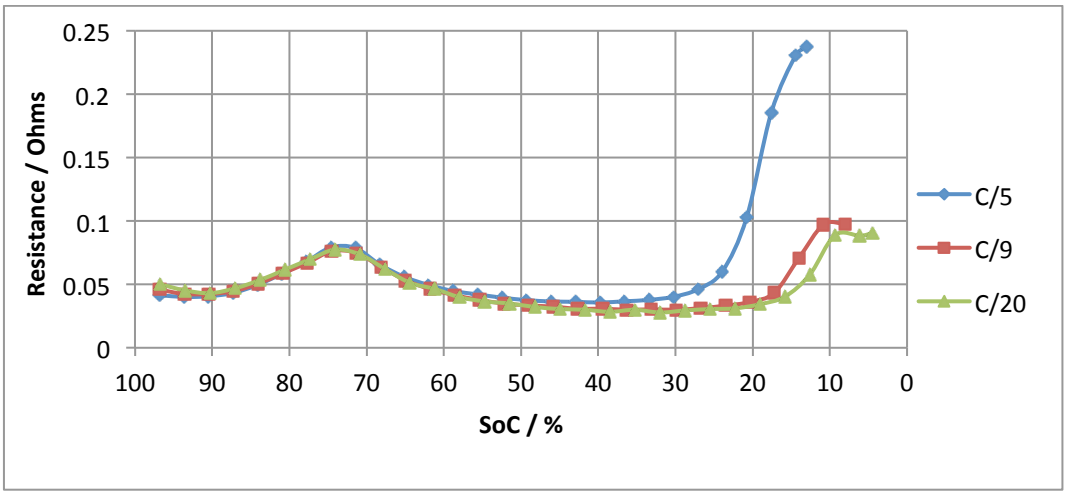

Figure 5.22: Ohmic resistance during discharge for cells cycled at various rates

The 1-hour rests and short periods of current flow means that these differences cannot be attributed to any temperature effects, as cell temperatures did not exceed the ambient 20°C ± 2°C. However, the differences could be due to how the chemicals respond to high current. Electrochemical analysis presented in the literature states that sulphur utilization is dependent on current rate [8]. As discharge current rate increases, the Li_2S layer, which

builds up uniformly inside the structure of the cathode at low current rates, increasingly tends to precipitate onto the surface of the cathode, blocking ionic transport to the bulk of the cathode. A proportion of the sulphur contained in the bulk of the cathode is not utilized and the cathode remains porous after discharge as evidenced by SEM images taken by Cheon et al. in [11]. A rate dependent increase in Ohmic resistance at low states of charge affects the capacity available during discharge, and so could be the reason why Sion recommends 0.315A as the optimum operating current.

Analysis of the total resistance of the cells at different current rates broadens the picture. Figure 5.23 and 5.24 shows a clear rate dependency on the total resistance of each cell, which is again independent of temperature. The total resistance was calculated by taking the total voltage difference between the EMF (i.e. open circuit voltage, taken after each rest period) and the terminal voltage, then dividing by the current.

The total cell resistance was higher in the second discharge region for cells discharged at low current rates and the steep rise in resistance at the end of charge occurred earlier at higher current rates. These variations can be attributed to the conversion of sulphur to low order lithium polysulphides. Figure 5.22 shows that Ohmic resistance is rate independent down to 40% SoC. At high current rates access to the cathode is blocked earlier resulting in the steep rise occurring sooner. At lower currents the rate of diffusion must be lower due to a more complete conversion of elemental sulphur into lower order lithium polysulphides.

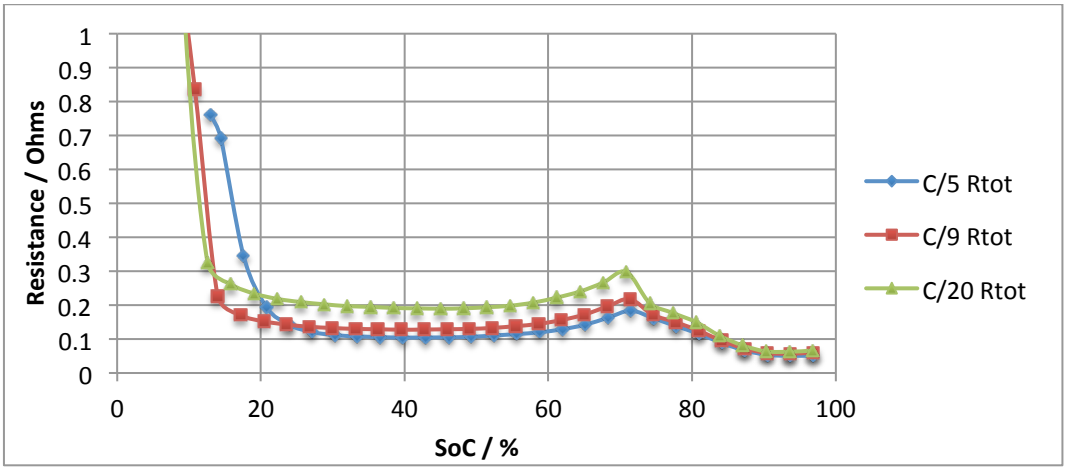

Figure 5.23: Total internal resistance of Li-S cells discharged at various current rates

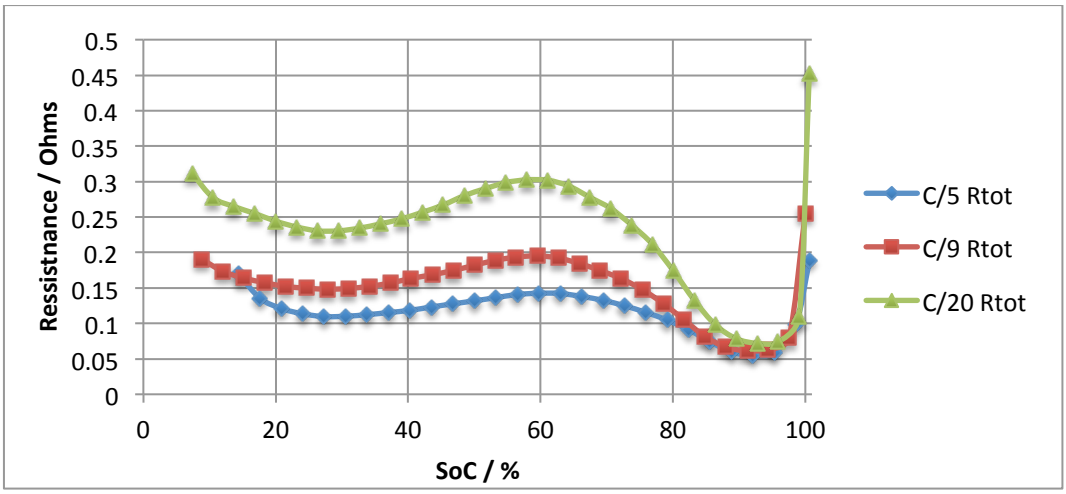

Figure 5.24: Total internal resistance of Li-S cells charged at various current rates

Figure 5.25 shows the voltage recovery curves, for cells discharged at different rates, taken at around 70% SoC. The curves do appear to have a slight rate dependency, although this dependency is small and does not change significantly over the state of charge of the cell. After the initial steep rise, the voltage recovery takes an exponential form and it is this form that determines the topology of the circuit equivalent model. Serially connected resistors in the circuit determine the total voltage difference between terminal voltage and EMF while the capacitors in the circuit determine the length of time it takes to reach that total voltage difference and the time dependency of the voltage recovery during rest periods.

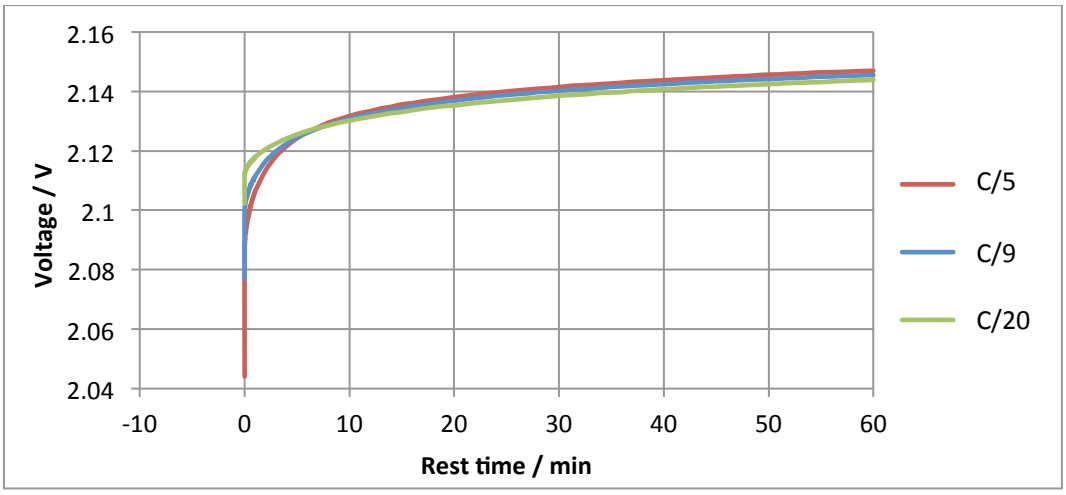

Figure 5.25: Voltage recovery curves at 70±2% SoC for various discharge current rates

5.6.2 Temperature dependency rest test

The temperature dependent resistance tests described in this section were conducted at the 0.315A rate, as this rate is fast enough so that the tests do not take an unnecessary amount of time to complete and slow enough so as to have a negligible effect on the uniformity of the distribution of Li_2S on the cathode during discharge.

In order to characterise cell resistance at different temperatures, a test similar to the rate dependency test was conducted with some modifications. Firstly, more rest periods were added in order to increase the number of data points in the results. Also, the length of each rest period was doubled to two hours so as to further characterise the capacitive effects of the voltage recovery. The test was repeated on different cells at temperatures of 0°C, 20°C and 40°C. A comparison of the first three SCM cycles and the 'rest cycle' included at 20°C is given for discharge in Figure 5.26 and charge in Figure 5.27. In all of the results shown in this section the voltage profile that contained rests was scaled to match the capacity of the continuous voltage profiles.

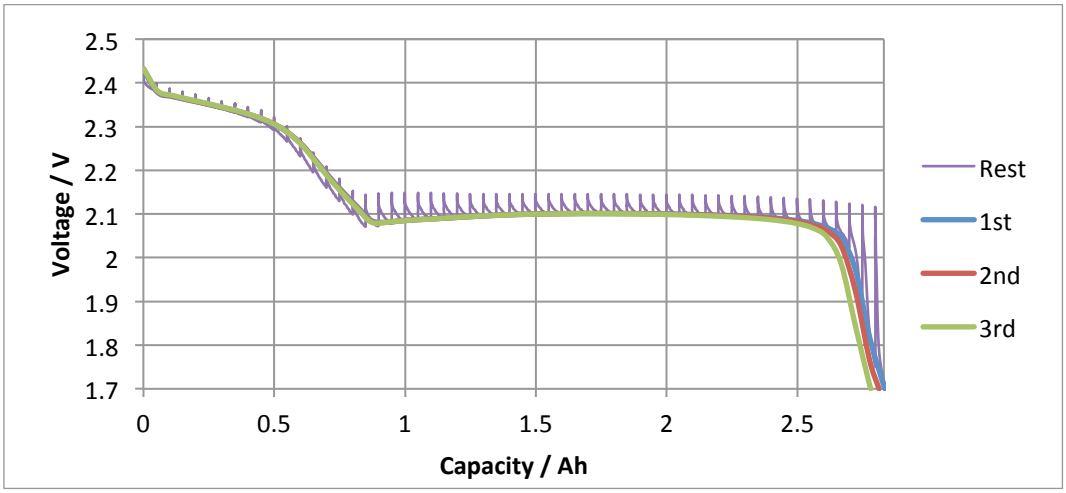

Figure 5.26: Discharge profiles for 20°C resistance tests

In Figure 5.26 the discharge rest profile shows that the voltage of the cell increases to the EMF value during rest and drops to the continuous terminal voltage profile when under load. The difference between the EMF and the voltage that the cell returns to under load (ΔV) predicts the total internal resistance (R) of the cell, at each rest point, using Ohm's Law.

$$V_{term} = EMF + \Delta V \quad [5.4]$$

$$\Delta V = IR \quad [5.5]$$

The fact that the voltage returns to the continuous voltage profile, when the cell is under load, means that the resistances predicted by the voltage difference is a good match, except for a small deviation in the second half of the first discharge region.

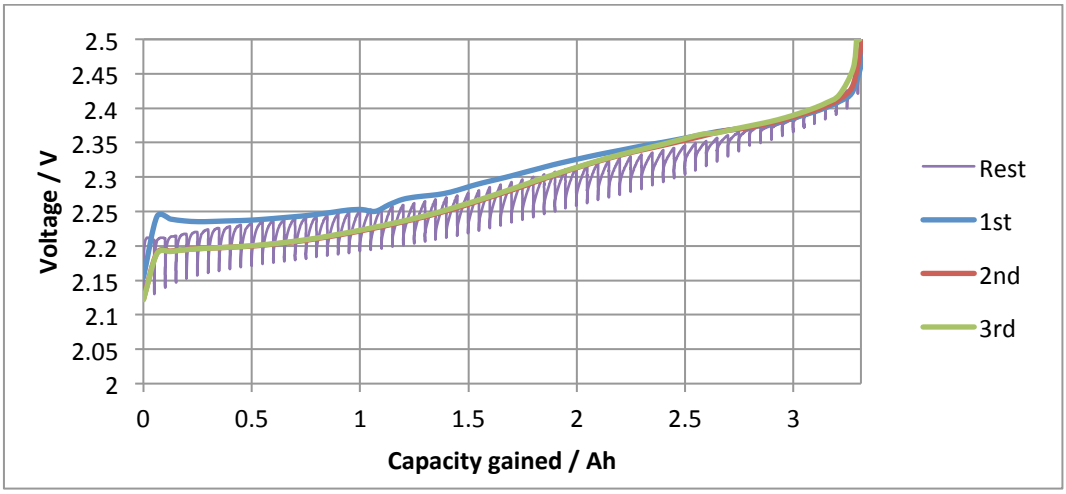

Figure 5.27: Charge profiles for 20°C resistance tests

Figure 5.27 shows the corresponding charge voltage profiles. It is evident that on the first charge the cell has a higher voltage than in subsequent charges. This implies a temporarily higher charge resistance on the first charge, which may be related to the products of parasitic reactions that cause reversible capacity loss during the storage time before charge.

In the rest profile the voltage falls to the EMF during rest periods and increases when the charge current is applied. However, the voltage does not return to the continuous voltage profile and is instead closer to the higher voltage of the initial charge indicating that the resistances predicted by ΔV overestimates the terminal voltage during charge. The reason for this increased resistance could be due to the step-discharge profile that the cell was subjected to immediately prior to the step-charge profile. The interrupted current applied in discharge may affect the amount and uniformity of the deposition of Li_2S, which would in turn affect the charge resistance of the cell until all of the Li_2S is depleted. The results support this hypothesis as the voltages, and hence resistances, converge at high states of charge.

The tests repeated at 40°C gave similar results, albeit returning to a slightly lower terminal voltage than in the continuous discharge tests, and a slightly higher voltage than in the continuous first charge profile. As with the EMF tests, the 40°C charge test did not complete due to the action of self-discharge that occurred during the rest periods.

The voltage profiles for the 0°C tests are given in Figures 5.28 and 5.29. Both the charge and discharge profiles show that the total resistances that would be calculated using these results would not give a representative terminal voltage for a continuous current load. Therefore, results of these resistance characterisation tests show that only the 20°C discharge rest test gives an accurate representation of the resistances and recovery voltages of the cell.

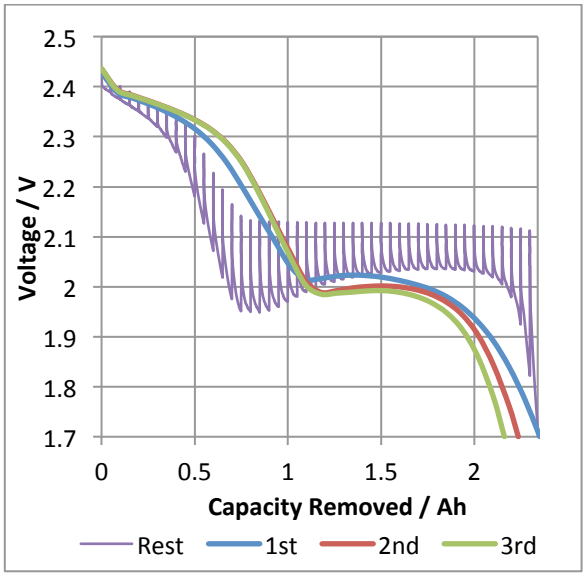

Figure 5.28: Discharge profiles for 0°C resistance tests

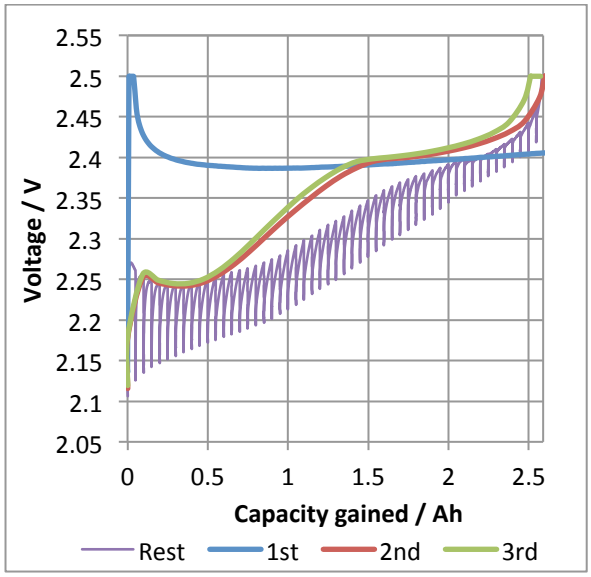

Figure 5.29: Charge profiles for 0°C resistance tests

In Chapter 6, the results of the 20°C discharge resistance tests are manipulated into look up tables for the model. Because the charge tests and varying temperature tests proved to be unacceptable for the purpose intended, and because the tests could not be repeated, another method was devised for approximating internal resistances for both charge and discharge in a 0°C to 40°C temperature range, using the data available. In Chapter 8, these tests are analysed and an improved method for determining internal resistances at different temperatures is suggested.

5.7 Dependence of EMF on Temperature

In Section 4.3.4 an investigation into the dependency of EMF on temperature was described. Two sets of tests, identical except for the state of charge at which the cells rested, were conducted. Once the data had been collected for each cell in a set, a graph of EMF vs. temperature for the final thermal cycle was plotted. Examples of two of these graphs are given in Figure 5.30.

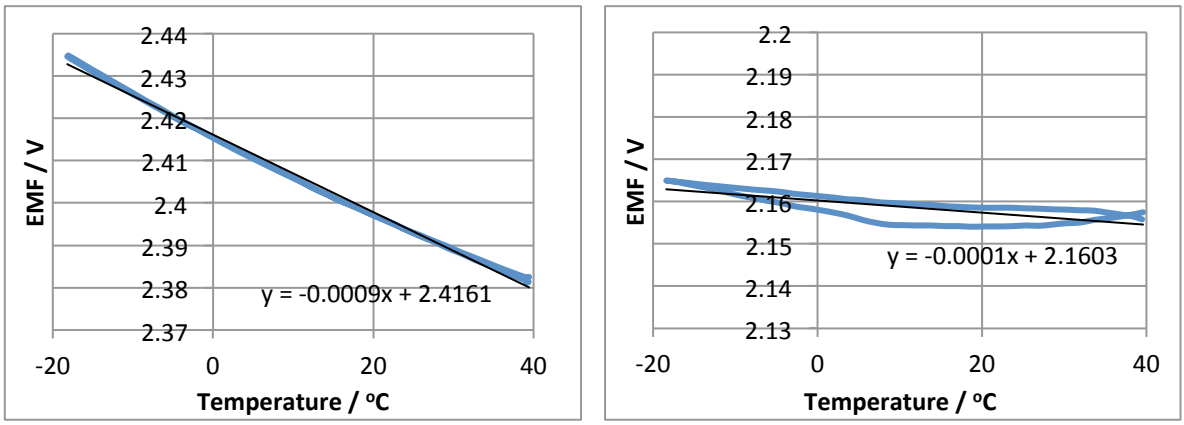

(a) (b)

Figure 5.30: EMF varying with temperature at (a) 100% SoC and (b) 30% SoC

At lower states of charge a hysteresis effect occurs although variation is small. The gradient of the linear fit through the data gives the rate at which EMF varies with temperature $\left(\frac{dE}{dT}\right)$ at that particular state of charge. Once the gradient is calculated for each graph the collective results show how $\left(\frac{dE}{dT}\right)$ varies with SoC, the results of which are displayed in Figure 5.31.

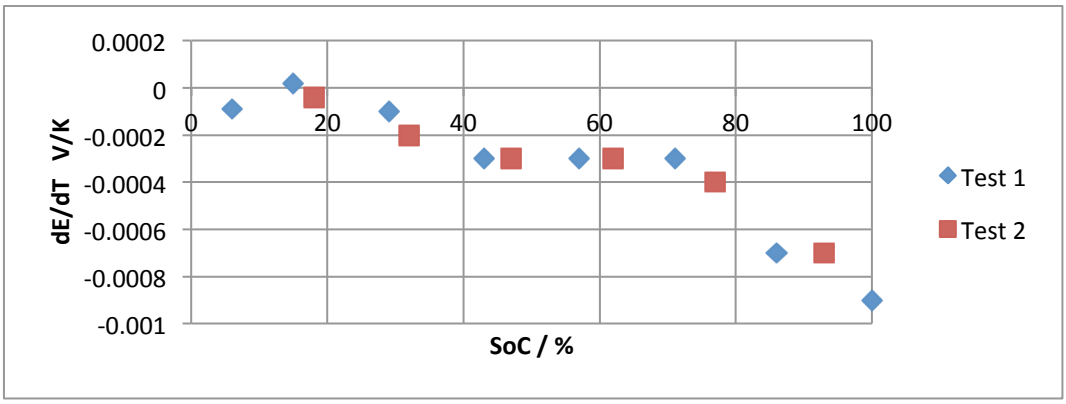

Figure 5.31: The variation of $\left(\frac{dE}{dT}\right)$ with state of charge

It is clear that the results of the second test complement those of the first, and a definite pattern has emerged. Interpolating this data gives a value for $\left(\frac{dE}{dT}\right)$ at all states of charge.

The value of $\frac{dE}{dT}$ is largely negative meaning that an increase in temperature will show a lowering of EMF. Looking back to the EMF tests conducted at different temperatures (Figures 5.18 and 5.19) it is evident that the charge profile complements the results found in this test. In the discharge profiles, the EMF is lower at higher temperatures in the first discharge region, as expected, but in the second discharge region the voltage recovers to a higher EMF value at 40°C than at 0°C. At 0°C the voltage was still increasing even after 2 hours rest. The slow dynamics of the chemicals at lower temperatures means that diffusion through the electrolyte and surface layers, that begin to form in the second discharge region, prevent the relaxation to the final EMF value in the 2 hour time that was given.

5.8 Hysteresis

Tests showed a large hysteresis between charge and discharge voltages when the current was changed abruptly. A portion of the discharge to charge hysteresis curve is depicted in Figure 5.32.

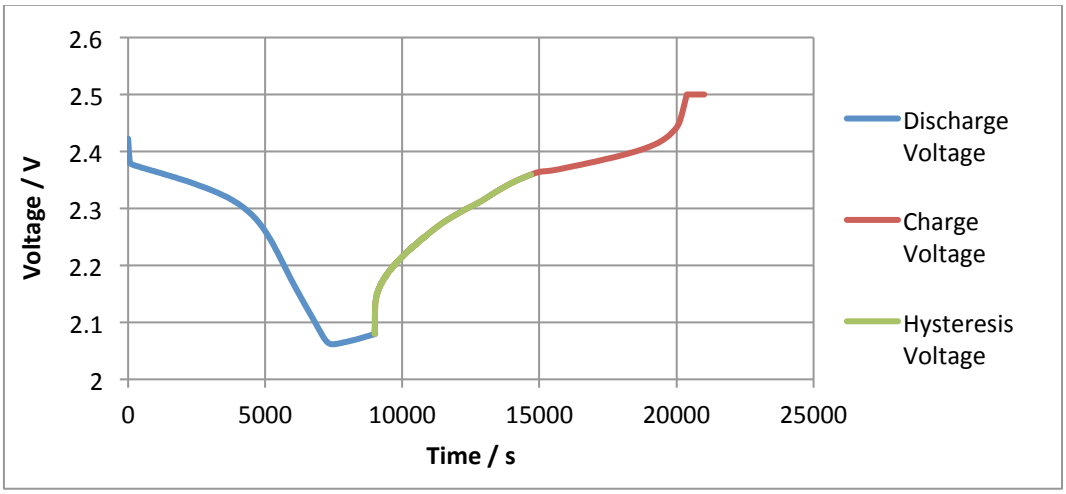

Figure 5.32: Voltage transient when current is reversed from discharge to charge

Similar results for the charge to discharge direction are shown in Figure 5.33. The figures show that the length of time the voltage profile is in the intermediate range before it matches

the standard charge profile is significant. In order to model this intermediate range, the voltage data was analysed at each current reversal point.

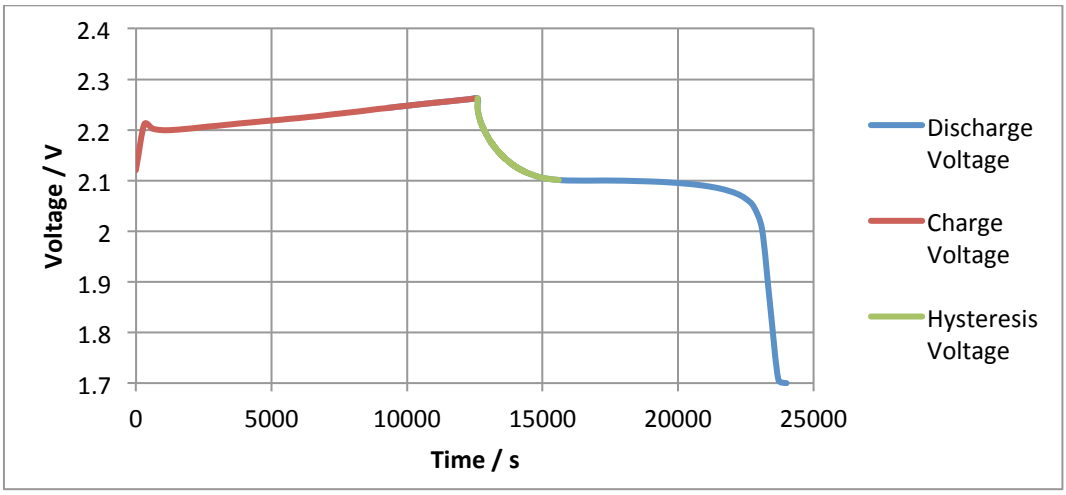

Figure 5.33: Voltage transient when current is reversed from charge to discharge

Firstly it was noted that the difference between charge and discharge EMF curves is state of charge dependent with the maximum difference occurring at around 70% SoC, as can be seen in Figure 5.34. The internal resistances cause the value of dV to increase with current rate.

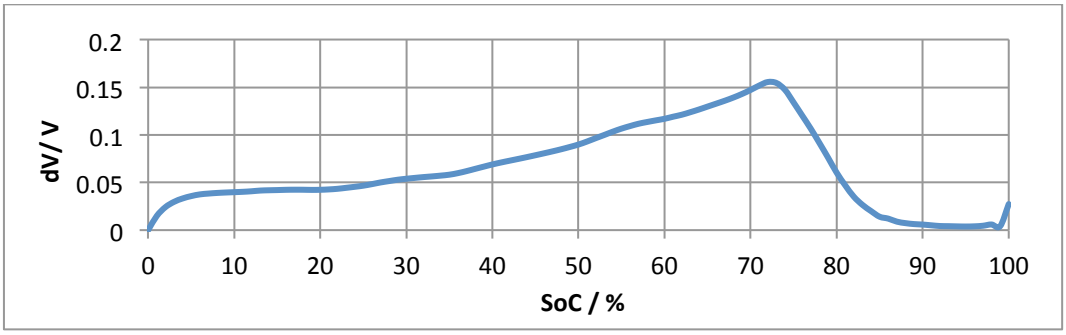

Figure 5.34: Voltage difference, dV, between charge and discharge EMF

It was also noted that the hysteresis voltage could be represented by a combination of exponential functions that depend on state of charge. The literature states that hysteresis is also dependent on the previous cycling history of the cell, however this was not part of the characterisation testing for this cell and may warrant further investigation, as discussed in Section 8.3.2. A model devised by Geoff Dudley et al. [16] for a lithium-ion cell also describes an exponential relationship between the hysteresis voltage and state of charge. The cell's cycling history is also ignored in this paper, with the error in results being negligible.

Using the curve-fitting tool Origin[3] the properties of the hysteresis voltage were analysed. It was apparent that, due to the large transient, a second order exponential function fits the data more accurately than a first order function. Equation 5.6 was fitted to each hysteresis voltage curve.

$$V = A_0 + A_1.exp^{x/t_1} + A_2.exp^{x/t_2} \quad [5.6]$$

At each state of charge where a current reversal occurred a value for A_1, A_2, t_1 and t_2 was recorded where the sign of each value depends on the current direction. The A_0 term corresponds to the final voltage value where the hysteresis voltage meets the standard voltage profile after the transition has occurred. The values of these constants for the discharge to charge direction are shown in Figure 5.35. The values for the charge to discharge direction are shown in Figure 5.36[4].

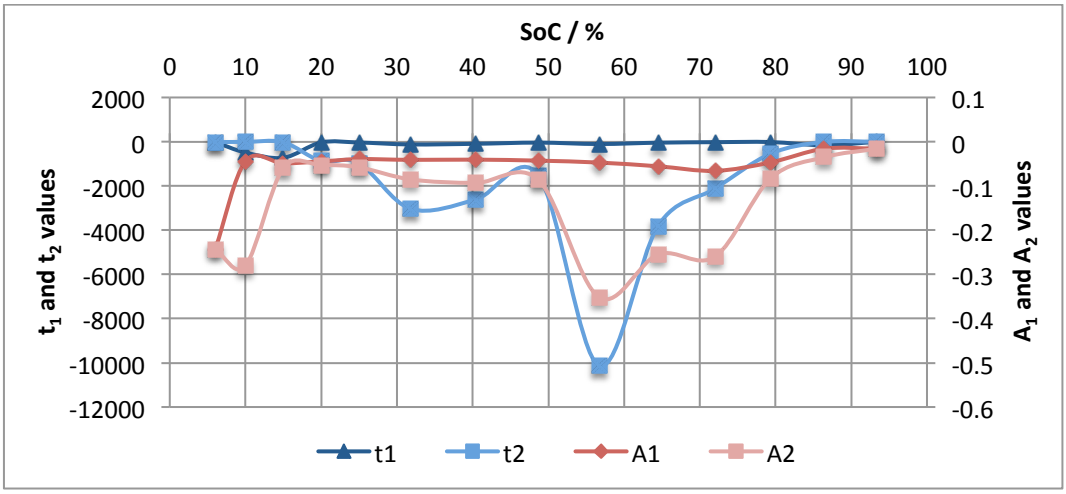

Figure 5.35: Fitted values for A_1, A_2, t_2 and t_2 constants (discharge to charge direction)

In order to incorporate these constant values into the model they need to be related to known cell parameters. In fact, the constants A_1 and A_2 sum to the delta voltage between the charge and discharge voltage profiles and vary depending on current rate. In addition, the time constants t_1 and t_2 can be related to the capacity transferred during to or from the cell in the

[3] OriginPro 8.5.0 (Academic), OriginLab Corporation

[4] Only results up to 70% SoC are available for this test due to a file corruption that occurred in the Maccor data logging system.

voltage hysteresis period. This is explained in more detail in Section 6.1.3, where the values are manipulated for inclusion into the cell model.

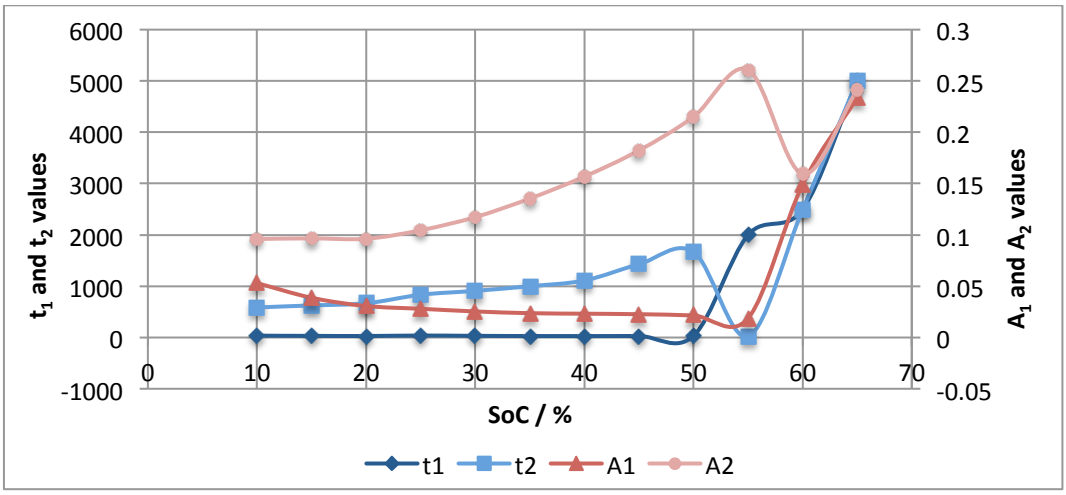

Figure 5.36: Fitted values for A_1, A_2, t_2 and t_2 constants (charge to discharge direction)

The cause of the hysteresis is not documented for Li-S but is most likely due to the chemical diffusion processes reacting to a change in current direction. Diffusion processes are affected by the current rate and by the temperature of the cell. This implies that the voltage could transition between the two profiles faster when the chemicals recover more quickly, i.e. at higher temperatures current rates. Further analysis at different temperatures and current rates are required to characterise the hysteresis effect fully as discussed in Section 8.3.2.

5.9 Conclusions

Numerous tests were conducted in order to characterise cell characteristics at different current rates and temperatures and the results were presented in this chapter. Several conclusions can be made regarding the characteristics of Sion Li-S cells as a result of the testing conducted in this work.

General Characteristics: In the first cycle, after a period of storage, the Li-S has a low coulombic efficiency and a higher than average charge resistance. This points to the temporary degradation of the SEI layer, which is subsequently restored in the following discharge. Disregarding the first cycle, the average coulombic efficiency of the Li_2S cell during

an SCM cycle was 96.7%. This value is age independent but declines with cycle number at a rate of 0.3% per cycle.

The cell batch was reasonably uniform, with a 4.5% variation in capacity. There was a 10% variation in discharge resistance and a 5% variation in charge resistance.

The cells have a BoL specific energy of 380Wh/kg, energy density of 257Wh/l and average voltage of 2.14V. These values degrade over the life of the cell.

In a standard capacity measurement (SCM) cycle, 92% of the cell's full capacity is available.

Storage: Capacity losses due to storage can be separated into irreversible and reversible variants. Irreversible losses are a result of cycling and calendar age of the cell whereas reversible losses are due to self-discharge and capacity recovery effects. The capacity losses appeared to act proportionally to the square root of time. Irreversible capacity losses are roughly equal in severity over 40%-100% SoC, a feature which has not been published in the literature. Self–discharge results predict a 7.6% reversible capacity loss over a period of 1 month. This figure is slightly higher than results published in the literature.

Life: Capacity fade generally decreases with current rate although additional testing is required to further validate this. The capacity available in the second discharge region is rate dependent, while the capacity available in the first discharge region is rate independent. The capacity in both regions degrades with cycle number and cell resistance increases.

Observing a non-linear degradation in coulombic efficiency could be an early warning sign for a cell that will eventually fail.

EMF: The EMF was taken as the voltage that the cell relaxed to after 2 hours rest at periodic states of charge. A full set of results was obtained from the 20℃ tests although testing at other temperatures revealed flaws in the testing methodology.

Resistance: Resistance contributions can be split into Ohmic and capacitive contributions. The Ohmic contributions are taken to be the change in voltage after 1 second of rest divided

by the change in current. The capacitive effects take an exponential form as the voltage recovers to the EMF. Resistance is current rate dependent in the second discharge region. This is due to the non-uniform deposition of Li_2S on the cathode during discharge at high rates, which confirms results given in the literature.

The resistance increase seen in the Li-S during storage was estimated to be $10\mu\Omega$ per day for both charge and discharge resistances. The correlation seen between resistance increase and capacity fade indicates the deposition of irreversible Li_2S on the electrodes.

The resistance values did not accurately predict the continuous voltage at 0°C for both charge and discharge. There were minor discrepancies in the discharge profiles at 20°C and 40°C. The charge profiles at these temperatures predict a higher continuous voltage than is true. These results give a good basis for the implementation of a cell model but also show room for improvement in the testing methodology at varying temperatures and current rates.

EMF dependence on temperature: the values found for $\frac{dE}{dT}$ are negative indicating that EMF falls as temperature increases. These results are compared to the EMF tests to show that the Li_2S layer formed in the second discharge region severely affects voltage recovery.

Hysteresis: Cells showed a large hysteresis between charge and discharge voltage profiles and it was found that this hysteresis voltage could be fitted to a second order exponential equation.

The results found in these tests were validated by looking at the electrochemistry of the cell presented in the literature. Some of the results given in this chapter require further investigation, which is discussed in Chapter 8. By comparing the general characteristics to results presented at the 2011 NASA Battery Workshop it appears that the manufacturer has already improved upon the cells used in this work. A higher capacity cell with a better cycle life was reported which shows that the problems that this cell type experiences are continually being improved upon [12]. The data that was obtained from these tests forms the basis of a novel Li-S cell model, which is presented in Chapter 6.

REFERENCES

[1] Sion Power Corporation, "Cell Shipping Documentation," 2011.

[2] Sion Power Corporation. (2008, October) Lithium Sulfur Rechargeable Battery Data Sheet. [Online]. http://sionpower.com/pdf/articles/LIS%20Spec%20Sheet%2010-3-08.pdf

[3] Y. Mikhaylik, "Fundamental Chemistry of Sion Power Li/S Battery," in *IBA-HBC*, Waikoloa, Hawaii, 2006.

[4] H.S. Ryu et al., "Self-discharge characteristics of lithium/sulfur batteries using TEGDME liquid electrolyte," *Electrochimica Acta*, vol. 52, pp. 1563-1566, 2006.

[5] Y. V. Mikhaylik and J. R. Akridge, "Polysulfide Shuttle Study in the Li/S Battery System," *Journal of The Electrochemical Society*, vol. 151, no. 11, pp. A1969-A1976, 2004.

[6] Y. V. Mikhaylik et al., "High Energy Rechargeable Li-S Cells for EV Application: Status, Remaining Problems and Solutions," *ECS Transactions*, vol. 25, no. 35, pp. 23-34, 2010.

[7] J. Shim, K. A. Striebel, and E. J. Cairns, "The Lithium/Sulfur Rechargeable Cell," *Journal of The Electrochemical Society*, vol. 149, no. 10, pp. A1321-A1325, 2002.

[8] S-E. Cheon, K-S. Ko, J-H. Cho, S-W. Kim and E-Y. Chin, "Rechargeable Lithium Sulfur Battery: II. Rate Capability and Cycle Characteristics," *Journal of The Electrochemical Society*, vol. 150, no. 6, pp. A800-A805, 2003.

[9] K. Saito, M. Arakawa, S. Tobishima, and J. Yamaki, "Specific surface-area measurement of lithium anode in rechargeable lithium cells," *Journal of Power Sources*, vol. 72, no. 2, pp. 111-117, April 1998.

[10] J-W. Choi et al., "Rechargeable lithium/sulfur battery with suitable mixed liquid electrolytes," *Electrochimica Acta*, vol. 52, no. 5, pp. 2075-2082, 2007.

[11] S-E. Cheon, K-S. Ko, J-H. Cho, S-W. Kim and E-Y. Chin, "Rechargeable Lithium Sulfur Battery: I. Structural Change of Sulfur Cathode During Discharge and Charge," *Journal of The Electrochemical Society*, vol. 150, no. 6, pp. A796-A799, 2003.

[12] J. Jeevarajan and B. Duffield, "Performance and saftey studies on COTS Li-ion cells of cylindrical and pouch cell designs," in *NASA Battery Workshop*, Huntsville, AL, November 2011.

[13] R. D. Rauh, G. F. Pearson, and S. B. Brummer, "Rechargeability studies of ambient temperature lithium sulfur batteries," in *12th Intersociety Energy Conversion Engineering Conference*, vol. 1, Washington, D.C., 1977, pp. 283-287.

[14] M. Dubarry, N. Vuillaume, and B-Y. Liaw, "From single cell model to battery pack simulation for Li-ion batteries," *Journal of Power Sources*, vol. 186, no. 2, pp. 500–507, January 2009, E29.

[15] H-G. Schweiger et al., "Comparison of Several Methods for Determining the Internal Resistance of Lithium Ion Cells ," *Sensors*, vol. 10, pp. 5604-5625, 2010.

[16] G. J. Dudley, J. De Roche, F. Tonicello, and C. Thwaite, "Electrical/Thermal Model of a Sony 18650HC Li-ion Cell," in *Proceedings of the Seventh European Space Power Conference*, Stresa, Italy, 2005.

CHAPTER 6

DEVELOPMENT AND DESIGN OF A LITHIUM-SULPHUR BATTERY MODEL

In this chapter the test results given in Chapter 5 are used to develop an equivalent circuit model of the electrical response of a Sion Li-S cell. The thermal response of the cell is also included in this model and, furthermore, an investigation is made into the capacity variations that occur during normal use of the cell. The individual parts of the model are discussed prior to considering the integrated system model. The conversion of the test results into useful lookup tables is also described along with their implementation into the system model. Finally, the model is verified against test data and a critical analysis of the model is made.

6.1 Electrical Modelling

Each circuit element in an equivalent circuit model can be described by an empirical lookup table, which gives the value of the element at the given state i.e. what state of charge, temperature or rate it is operating at. In this section an electrical equivalent circuit of the Li-S cell is developed and lookup tables for each circuit element are produced from the testing results that were given in Chapter 5.

6.1.1 EMF

The basis of an equivalent circuit model is the relationship between EMF and state of charge. This relationship was characterised at 20°C by the results given in Section 5.5. The same test, repeated at different temperatures, could not be relied upon for accurate determination of EMF. This was partly due to the effect that temperature has on the viscosity of the electrolyte and hence the voltage recovery. However, the EMF's temperature dependence was additionally characterised in a separate test, which did not rely on periodic voltage recovery

(results given in Section 5.7). In order to use the results of this test (in conjunction with the EMF values found at 20°C) to find the EMF at different temperatures, Equation 6.1 was implemented at 1% increments of SoC to form a lookup table that finds the EMF of the cell at any state of charge in the 0°C- 40°C temperature range.

$$EMF(T) = EMF(20) + (T - 20)\frac{dE}{dT} \quad [6.1]$$

Where T is the desired temperature (0°C and 40°C in this case in order to compare with the results in Section 5.5) and $\frac{dE}{dT}$ is the EMF dependency on temperature function found in Section 5.7 and is a function of SoC. The results of applying this equation to both charge and discharge EMF curve at 20°C are displayed in Figure 6.1 and Figure 6.2.

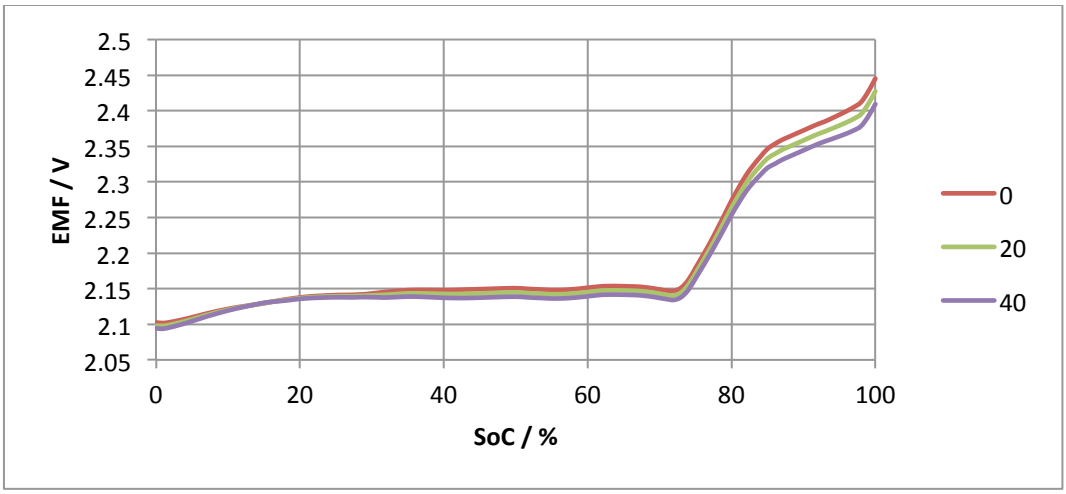

Figure 6.1: Discharge EMF at temperatures of 0°C, 20°C and 40°C

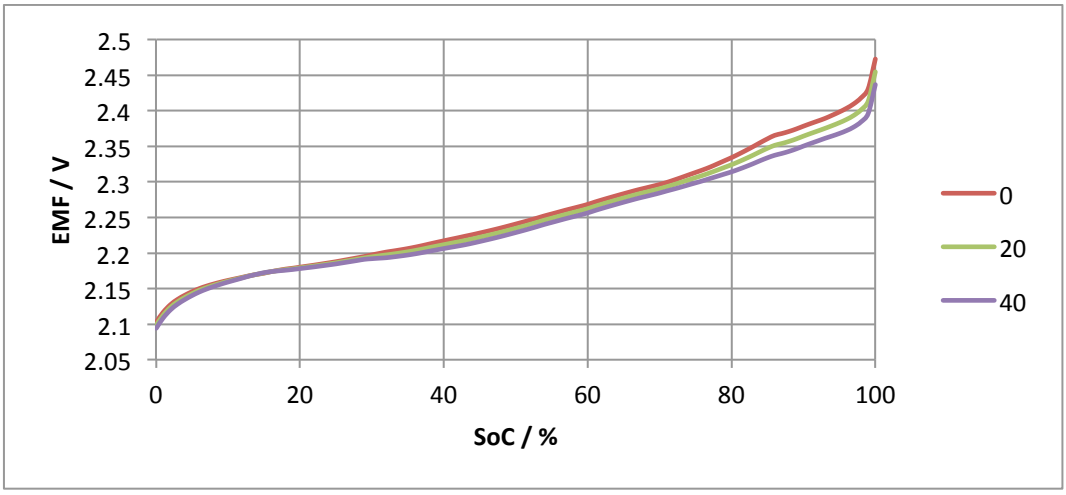

Figure 6.2: Charge EMF at temperatures of 0°C, 20°C and 40°C

When comparing these graphs to those found in the dedicated EMF tests (Figures 5.18 and 5.19) it is clear that the two methods produce conflicting results in the second discharge region. In the above results the EMF recovers to a higher value at lower temperatures, whereas in Figures 5.18 and 5.19 this was only true in the first discharge region. However, in the second discharge region the results are affected by the build up of the Li_2S layer. This slows diffusion of the chemicals, especially at low temperatures where the electrolyte is more viscous. Because of the length of the rests in the dedicated EMF tests, it appears to have been difficult for the cell to return to equilibrium in the given time. Therefore, for the purposes of modelling, Equation 6.1 is used to calculate EMF at different temperatures.

6.1.2 Resistance

As previously discussed, the deviation of the terminal voltage of a cell from its EMF is a function of the cell's internal resistance. In Section 5.6.1 a cell's Ohmic resistance was found at 20°C by assuming that its contribution to total resistance is dominant in the instant that the current is removed during a rest period. That "instant" was defined as 1 second and so the Ohmic resistance R_1 is defined as in Equation 6.2.

$$R_1 = \frac{V_{term} - V_{1sec}}{I} \qquad [6.2]$$

In an equivalent circuit a resistor placed in series with the EMF source represents the Ohmic resistance as shown by the diagram in Figure 6.3; the simple equivalent circuit model that was described in Section 2.4.

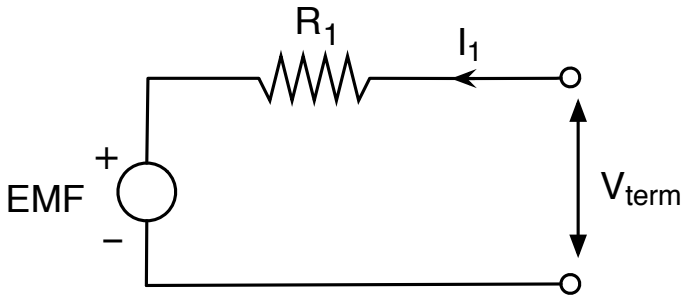

Figure 6.3: Equivalent circuit diagram of the terminal voltage of a cell, which deviates from the EMF by an amount proportional to the Ohmic resistance, R_1.

The results in Chapter 5 showed that an additional time-dependent voltage recovery follows the initial steep rise in voltage caused by the Ohmic resistance. The cell resistance is affected by dynamic surface layers, which depend on SoC, temperature and current rate. These surface layers also affect the rate of diffusion and migration of species across the cell. This effect on the movement of chemicals in the cell causes the time dependent voltage recovery seen in the results. Using the curve-fitting tool Origin[1] it was concluded that a second-order exponential curve was far superior to a first-order fit of the voltage recovery data. A third order exponential did not significantly improve upon this fit and so a second order exponential was deemed suitable enough for the purpose of the model. A second-order exponential voltage recovery can be modelled as an equivalent circuit in two ways, either a Cauer or a Foster network of resistors and capacitors. Incorporating these networks into the simple circuit described above, results in the equivalent circuits shown in Figure 6.4.

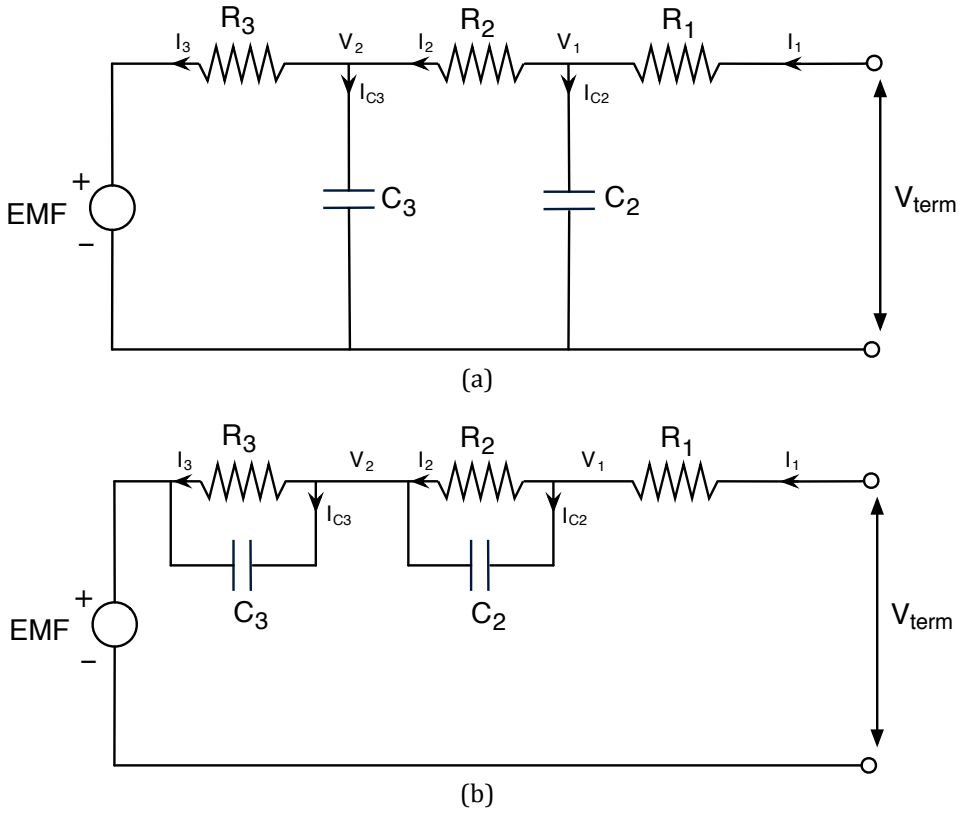

Figure 6.4: Equivalent circuit model of a second order exponential voltage recovery by (a) A Cauer network or (b) A Foster network.

[1] OriginPro 8.5.0 (Academic), OriginLab Corporation

In Figure 6.4, I_1 is the load current defined by the user and the direction indicated in the diagrams specifies a charging current. In both circuits the total voltage difference between EMF and V_{term} is given by the sum of the voltage drop across the resistances R_1, R_2 and R_3. The voltage drop across R_1 is immediate, following the addition or removal of a load current. However, the voltage drop across both R_2 and R_3 is affected by the charge and discharge of their associated capacitors C_2 and C_3, causing the potential difference across each resistor to build up to its maximum value as the capacitors charge, or diminish to zero as the capacitors discharge. This models the exponential time-dependent voltage response of the battery.

Analysis of the Foster network circuit at the instant the current is removed gives the form of the voltage recovery curve as in Equation 6.3.

$$V_{term} = EMF - I_1 R_1 - V_{Bmax} e^{-t/R_2 C_2} - V_{Cmax} e^{-t/R_3 C_3} \quad [6.3]$$

Where t is recovery time, V_{Bmax} is the maximum potential difference over resistor R_2 and V_{Cmax} is the maximum potential difference over resistor R_3. This solution is easily arrived at because the RC time constants are independent of one another.

For the Cauer network, assuming that R_1 can be calculated using Equation 6.2, the remaining recovery curve can be fitted to the following equation:

$$V_{term} + (R_2.C_2 + R_3.C_2 + R_3.C_3).\frac{dV_{term}}{dt} + R_3.C_3.R_2.C_2.\frac{d^2V_{term}}{dt^2} = EMF \quad [6.4]$$

This second-order differential equation can be solved with respect to V_{term} to give the following solution:

$$V_{term} = EMF + K_1.e^{\lambda_- t} + K_2.e^{\lambda_+ t} \quad [6.5]$$

Where:

$$\lambda_- = \frac{\alpha - \sqrt{\beta}}{\gamma} \quad [6.5a]$$

$$\lambda_+ = \frac{\alpha + \sqrt{\beta}}{\gamma} \quad [6.5b]$$

$$\alpha = -(R_2.C_2 + R_3.C_2 + R_3.C_3) \quad [6.5c]$$

$$\beta = (R_2.C_2 + R_3.C_2 + R_3.C_3)^2 - 4.R_2.R_3.C_2.C_3 \quad [6.5d]$$

$$\gamma = 2.R_2.R_3.C_2.C_3 \quad [6.5e]$$

This result shows that the time constants of the voltage recovery curves are not simple *RC* relations and the circuit is not straightforward to solve analytically, especially for networks with more than two RC branches. The only way to calculate suitable resistor and capacitor values is by defining a tailored linear regression algorithm. This is possible, but can be unstable, meaning that the results found at each SoC do not necessarily relate to one another if many solutions are possible. However, because both equivalent circuits are suitable representations of the transient voltage response the Foster network has been chosen as the best approach to modelling the Li-S cell. It has been shown that the performance of the specific Li-S cells tested in this work has not yet been maximised and it is probable that changes to the cell chemistry and cell format will occur. Consequently, using the Foster network will allow future cell versions to be simply incorporated into the cell model with minimal manipulation of test results. Additionally, the Foster network allows additional RC branches to be added without significant consequence to the mathematics. The solution to a higher order Cauer circuit is not necessarily solvable and the required linear regression algorithm would be extremely overcomplicated in relation to the purpose it serves.

Using the Origin graphing tool, Equation 6.3 was fitted to each voltage recovery curve found in the resistance tests. R_1 was calculated using Equation 6.2 and so the portion of the curve used for the exponential fit was between the terminal voltage recorded after 1 second (V_{1sec}) and the EMF value that the cell relaxed to after 2 hours. From these curve fits, values for the constants K_1 and K_2 and the time constants R_1C_1 and R_2C_2 were found. The K constants sum to the maximum voltage difference between EMF and V_{1sec} and, in terms of the equivalent circuit,

can be thought of as the sum of the voltage drops across resistors R_2 and R_3 when the capacitors C_2 and C_3 are fully charged. Dividing K_1 and K_2 by the load current gives a value for R_2 and R_3. In knowing these resistance values the capacitance values were then obtained from the fitted time constant values. Therefore, at each state of charge all values for each circuit element in Figure 6.4(b) can be calculated. The results of these calculations are given graphically in Figure 6.5 and Figure 6.6 and in numerical form in Appendix E. For states of charge below 8% the values were extrapolated.

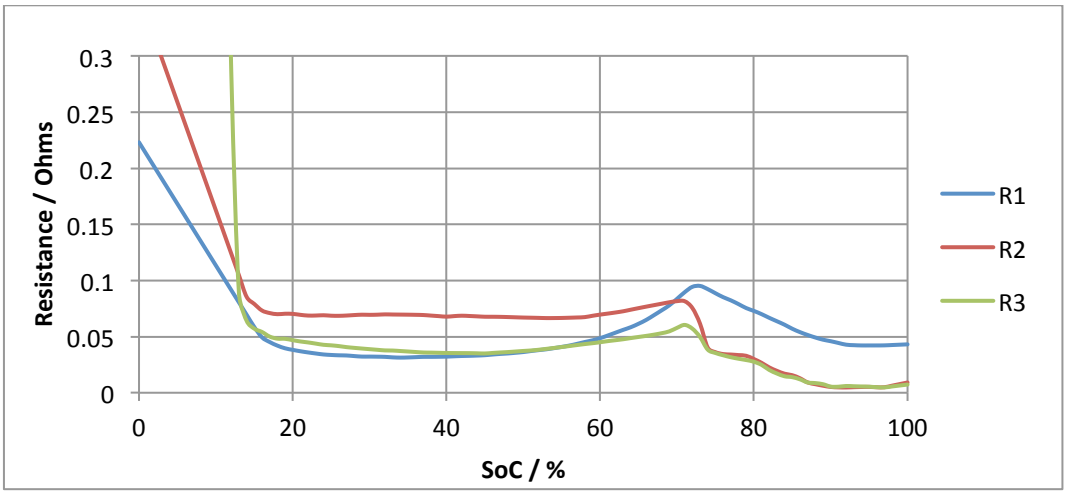

Figure 6.5: Discharge resistances R_1, R_2 and R_3 found for a 0.315A current at 20°C

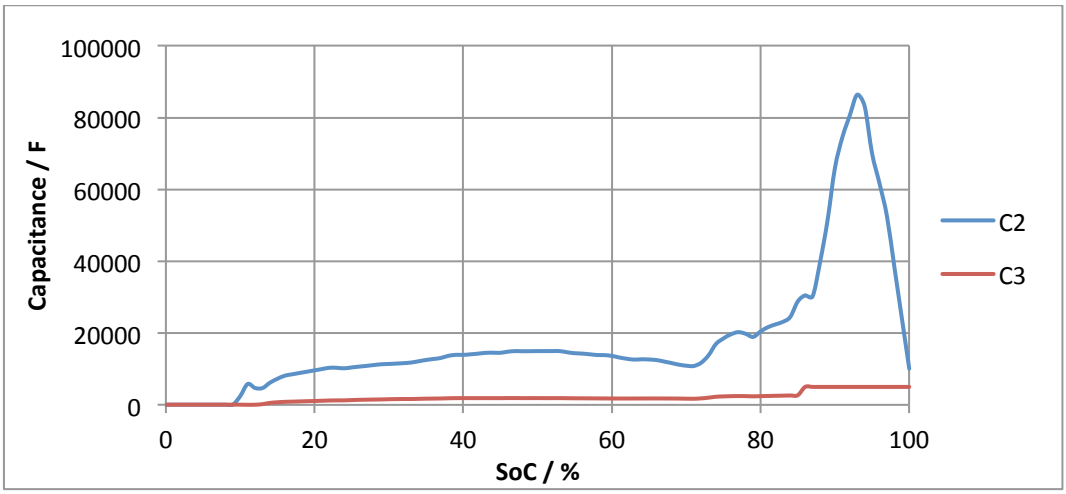

Figure 6.6: Discharge capacitances C_2 and C_3 found for a 0.315A current at 20°C

In Chapter 5 it was shown that the charge resistance test and the equivalent charge and discharge tests completed at 0°C and 40°C did not provide accurate means for determining cell resistance under those conditions. Because these tests could not be repeated another

method of estimating these resistances was therefore devised, using the data that was available. An improved methodology for calculating these resistances in future work is outlined in Chapter 8, however, for the purpose of broadening the usability of the model, the method described below provides a good approximation.

The EMF of the cell was calculated for the range 0°C-40°C using the method described in Section 6.1.1. Additionally, the continuous 0.315A charge and discharge voltage profiles are known at these temperatures. Therefore, the total voltage difference between the EMF and the continuous voltage profiles at each test temperature and for each increment in SoC can be calculated. Using the same ratio for R_1:R_2:R_3 as found in the 20°C discharge tests approximates their true values. Because the sum of the resistances is relatively accurate, modelling of a continuous current condition will not be heavily affected by the splitting of the resistances in this way. The model still includes transient behaviour but the accuracy of the voltage recovery is affected using this method, however this is not vital to the overall objective or usability of the model, and can be refined in future work. The C_2 and C_3 values cannot be calculated under these conditions and are assumed to be the same for all rates and temperatures, although in reality are likely to be dependent on rate and temperature.

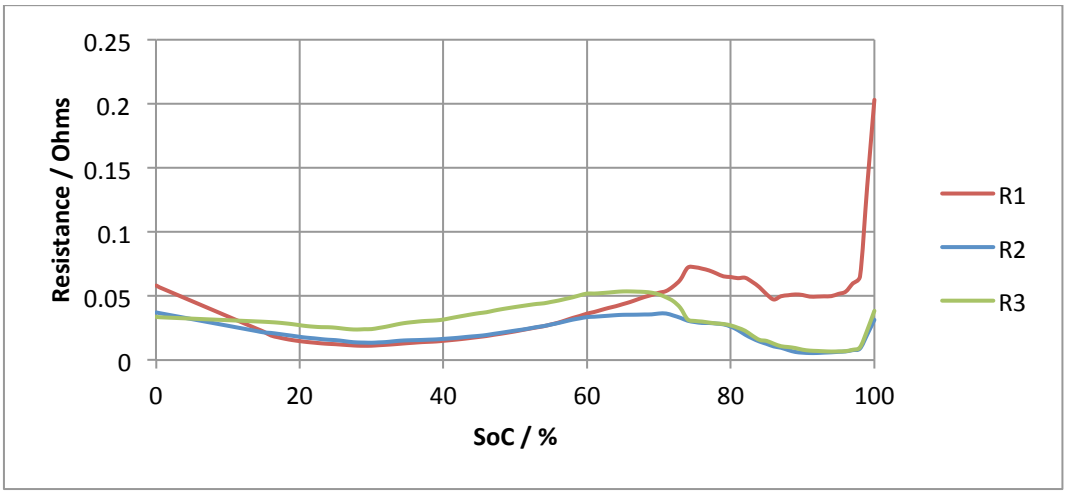

Figure 6.7: Charge resistances R_1, R_2 and R_3 at 20°C

The same method as described above was used to find the cell resistances during charge. The results found for charge resistances are given in Figure 6.7 while the discharge resistances at

various temperatures are given in Figure 6.8. As with other cell technologies, cell resistance increases with decreasing temperature. This is due to the increase in the viscosity of the electrolyte, which affects the diffusivity of the ions.

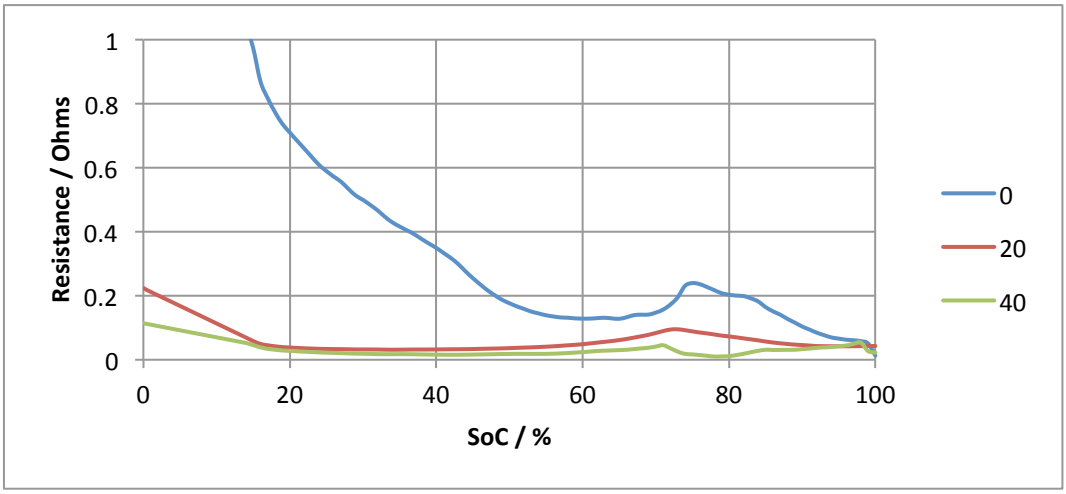

Figure 6.8: Discharge resistance R_1 at 0°C, 20°C and 40°C

In Chapter 5 it was shown that the "diffusion" resistances are dependent on the current rate used. A higher current rate produced a lower cell resistance while a lower current rate produced a higher cell resistance. This result was independent of any increase in temperature caused by the higher current rate, as the periodic rests ensured that cell temperature remained at ambient. In order to incorporate this rate dependency into the model two approaches could be made. Firstly, the resistance and capacitance values could be found for a wide range of current rates, as with the method used for the C/9 tests, and the resistance lookup tables could incorporate another dimension to include current dependency. However, the resistance testing completed in this work was limited to the C/9, C/5 and C/20 current rates, with only 20°C data available for the latter two. Using this method with the available data would leave the lookup tables severely depleted and would limit the model to the range of currents tested unless further extensive testing is carried out. The second approach is to compare the total resistance calculated at each rate with the standard C/9 resistances and observe the mathematical relationship between them. Using an equation to determine a rate dependent resistance factor allows the C/9 resistances to be extrapolated at any rate outside of the range that was tested. The average rate dependent resistance factor, or division factor

(*DF*) required to transform the resistances found at the C/9 rate to the resistances found at the C/5 and C/20 rates is plotted against rate in Figure 6.9.

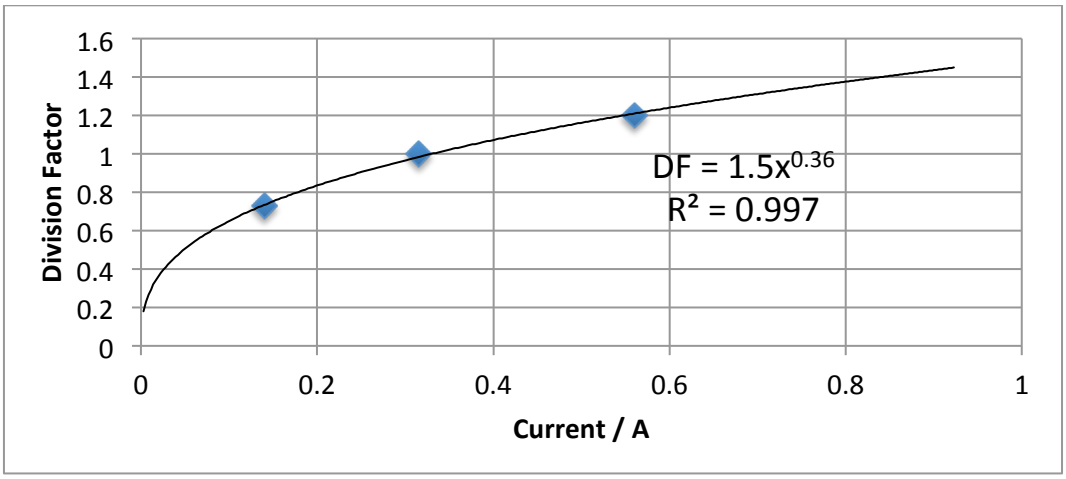

Figure 6.9: Resistance division factor (*DF*) as a function of current rate

It is important to note that this method was used as an indication of the resistance changes that occur when varying current rates are used, using the data that was available. This testing could be extended in future work so as to fully characterise the effect that current rate has on resistance, including any state of charge dependencies that also arise.

6.1.3 Hysteresis

The results of the hysteresis tests showed that the transfer between EMF profiles for charge and discharge varied with state of charge. The data at each current reversal point was fitted to Equation 5.6, which is repeated below.

$$V = A_0 + A_1.exp^{x/t_1} + A_2.exp^{x/t_2} \quad [5.6]$$

In this equation, V represents the voltage as it transients between the 0.315A charge and discharge curves, A_0 is the final voltage after the transient is complete and A_1 and A_2 sum to the total voltage difference between the curves. In addition, the x terms represent time in seconds and the t terms are time constants.

In a basic cell model with no correction for hysteresis, the EMF of the cell is taken from the lookup table that corresponds to the direction of current at any given moment, with no

regard to the previous current profile applied to the cell. At the moment before a charge current is applied, if the cell is discharging, the EMF of the cell in the model is found from the discharge EMF lookup table (*EMFdchg*). At the moment after the charge current is applied the EMF of the cell changes immediately to the charge EMF lookup table (*EMFchg*). In order that the EMF is modelled more accurately the cell EMF (during charge) should instead be modelled as that given in Equation 6.6.

$$EMF = EMFchg - B_1.exp^{-SoCtrans/\tau_1} - B_2.exp^{-SoCtrans/\tau_2} \quad [6.6]$$

Where *SoCtrans* is the SoC transferred since the current direction change, B_1 and B_2 are constants and $\tau_1$and τ_2 are time constants. At the moment of current change the exponential terms are equal to 1 because there has been zero capacity transferred and the sum of B_1 and B_2 is such that it equals the voltage difference between *EMFchg* and *EMFdchg* at that SoC. As time progresses, the capacity transferred increases and the exponential terms fall to zero so EMF tends to *EMFchg*. For the opposite change in current direction the EMF is given in Equation 6.7.

$$EMF = EMFdchg + B_1.exp^{-SoCtrans/\tau_1} + B_2.exp^{-SoCtrans/\tau_2} \quad [6.7]$$

The results of the tests given in Section 5.8 provided values for A_1, A_2, t_1 and t_2, which were taken for a current rate of 0.315A. To transform the A terms into the equivalent B terms the following conversions must be made:

$$B_1 = \frac{A_1}{A_1 + A_2}.(EMFchg - EMFdchg) \quad [6.8]$$

$$B_2 = \frac{A_2}{A_1 + A_2}.(EMFchg - EMFdchg) \quad [6.9]$$

These conversions mean that the sum of B_1 and B_2 is equal to the difference between the EMF curves, whilst retaining the proportions that the results from the 0.315A test gave.

To convert the exponential terms it must be noted that the test results gave values for t_1 and t_2 that were based on the transition time (x) between voltage curves. The transition time

depends on the current rate, and hence the capacity transferred during transition. Therefore, the following relationship between the time constants and the state of charge transferred since the current change, *SoCtrans*, is made:

$$\frac{x(\mathrm{s})}{t_1} = \frac{SoCtrans}{\tau_1} \qquad [6.10]$$

$$\frac{time(\mathrm{s})}{t_1(\mathrm{s})} = \frac{0.315\ (\mathrm{A})\ .\ time(\mathrm{hr})\ .\ 100}{Q_t(\mathrm{Ah})} . \frac{1}{\tau_1} \qquad [6.11]$$

$$\frac{time(\mathrm{s})}{t_1(\mathrm{s})} = \frac{0.315\ (\mathrm{A})\ .\ time(\mathrm{s})\ .\ 100}{3600\ (\mathrm{s\ hr^{-1}}).\ Q_t(\mathrm{Ah})} . \frac{1}{\tau_1} \qquad [6.12]$$

Where Q_t is the total capacity of the cell. Therefore the new time constants are given in Equations 6.13 and 6.14 below. By using these equations, the EMF predicted by the model gives a smooth transition between charge and discharge.

$$\tau_1 = \frac{8.75 \times 10^{-3}\ t_1}{Q_t} \qquad [6.13]$$

$$\tau_2 = \frac{8.75 \times 10^{-3}\ t_2}{Q_t} \qquad [6.14]$$

6.2 Thermal Modelling

In Chapter 3 the spacecraft environment was described. Due to the vacuum of space, conduction and radiation are the only means of heat transfer between a cell and its environment. To simulate this effect, all cells in this work were placed in individual sealed plastic bags to minimise the effects of convection caused by the fans inside the thermal chamber. In Chapter 4 the power dissipated by a cell as heat (P_{diss}) was given by Equation 4.6, repeated below, where $\frac{dE}{dT}$ is the EMF dependence on temperature factor, I is the load current, R is the total internal resistance and T is cell temperature.

$$P_{diss} = I^2R + I.T.\frac{dE}{dT} \quad [4.6]$$

This generated heat is transferred to the surrounding environment via conductive and radiative heat transfer. In order to determine how the cell responds thermally to its environment the thermal properties of the cell must be considered.

Some thermal properties of Sion Li-S cells were discussed in a paper published in 2003 [1], which refers to an earlier cell prototype than the one tested in this work. The cell that was analysed had a thickness of 7mm and a mass of 9.8g while the cell tested in this work was somewhat thicker at 11.5mm and had a mass of 16g. This corresponds to a 39% increase in thickness and a 39% increase in mass between the older and newer prototypes. The tests completed in the paper were not fully repeatable due to the restrictions placed on the use of the Sion Li-S cell, and therefore it was impossible to determine the temperature difference between the inside and the surface of the cell. In the paper this temperature difference was found to be ~1°C and consequently was considered as lumped mass with uniform temperature. It is not unreasonable to assume that the increase in cell thickness does not increase this difference by any more than ~0.5°C, provided the ratio of cell components remain about the same. Hence, the cell will be considered as a lumped mass of uniform temperature with only heat transfer at the surface of the cell being relevant to the model.

The heat capacity, C, of an object determines the amount of thermal energy, Q, required to change the temperature of the object by 1K and is described by Equation 6.15.

$$C = \frac{dQ}{dT} \quad [6.15]$$

In [1] the heat capacity per unit mass, or the specific heat capacity (C_p), of the cell was calculated to be $1.65 \text{Jg}^{-1}\text{K}^{-1}$ based on the heat capacities of the cell components. On the assumption that the actual cell components and the proportion of cell components do not differ significantly between the older and newer cell prototypes the heat capacity of the newer cell (of mass 16g) can be approximated to be 26.4JK^{-1} using Equation 6.16.

$$C = m.C_p \quad [6.16]$$

Specific heat capacity can also be thought of as thermal capacitance, which is analogous to electrical capacitance. The rate at which heat is transferred into or away from the cell is equal to the change in thermal energy with respect to time $\frac{dQ}{dt}$, which has units Js^{-1} or W. Differentiating Equation 6.15 with respect to time gives the change in thermal energy in terms of the lumped heat capacity of the cell and the change in temperature of the cell over time:

$$C\,\frac{dT}{dt} = \frac{dQ}{dt} \quad [6.17]$$

In order to calculate exactly how the temperature of the cell changes with time, the power into and out of the cell must be known. Equation 4.3 already describes the power that the cell dissipates as heat and so it is only necessary to determine the conductive and radiative flow of heat energy across the cell's surface. Fourier's Law, given in Equation 6.18, describes the temperature change that occurs as heat is conducted away from the surface of a cell.

$$\frac{dQ_c}{dt} = Q_c\,(T_1 - T_{env}) \quad [6.18]$$

Where $\frac{dQ_c}{dt}$ is the rate of heat conduction (W), Q_c is thermal conductance (WK^{-1}) (the reciprocal of thermal resistance), T_1 is the temperature of the cell and T_{env} is the temperature of the environment into which the conduction link is connected (i.e. the battery casing or the spacecraft structure).

The heat thermally radiated from the cell to the surrounding environment does not follow this Ohmic (linear) relationship and instead depends on the difference of the fourth powers of the surface temperatures. Thus, Equation 6.19 gives the heat radiated away from the cell.

$$\frac{dQ_r}{dt} = Q_r\,(T_1^4 - T_{env}^4) \quad [6.19]$$

Where $\frac{dQ_r}{dt}$ is the rate of heat radiation and Q_r is the thermal radiance (WK^{-4}). Summing Equations 4.9, 6.18 and 6.19 give the total power generated, absorbed and dissipated by the cell as heat, which can be equated to Equation 6.17 to give:

$$\frac{dT_1}{dt} = \frac{P_{diss} - Q_c\,(T_1 - T_{env}) - \ Q_r\,(T_1^4 - T_{env}^4)}{m.C_p} \qquad [6.20]$$

Equation 6.20 uses the convention that heat into (or generated by) the cell is positive while heat leaving the cell is negative. This equation cannot be solved analytically for T_1, however the rate of change of T_1 can still be modelled so long as Q_c and Q_r are known. Equations 6.21 and 6.22 govern these heat transfer coefficients.

$$Q_c = \frac{k.A}{l} \qquad [6.21]$$

$$Q_r = \ \sigma.A.\varepsilon.VF \qquad [6.22]$$

Where k is the thermal conductivity of the cell ($Wm^{-1}K^{-1}$), which is a property of the physical cell components, A is the surface area over which the heat transfer takes place (m^2), l is length over which the temperature gradient acts (m), σ is the Stefan-Boltzmann constant ($Wm^{-2}K^{-4}$) and ε is the emissivity of the surface of the cell (dimensionless). VF is the view factor (dimensionless) and gives the proportion of the surface that radiates to the environment.

The thermal radiance Q_r is straightforward to calculate. It is believed that the foil pouch that encases the cell is made of aluminium, thus the emissivity can be taken to be 0.11. The surface area of the cell is calculated to be $0.006186m^2$, the Stefan-Boltzmann constant is 5.670373 x $10^{-8}Wm^{-2}K^{-4}$, and the view factor for a single cell is 1, assuming all sides can radiate to the environment. Using these figures in Equation 6.22, the thermal radiance is calculated to be $3.86\times10^{-11}WK^{-4}$.

An experiment completed in [1] showed a method of determining the thermal conductance of the cell by the 'shock cooling' method, where the temperature change of a cell, which starts at

ambient and is plunged into a thermal environment of a significantly lower temperature, is monitored. This experiment was repeated on the newer Li-S cell, which started at an initial temperature of 30°C and was then placed in a thermal chamber of -20°C. The results are plotted in Figure 6.10.

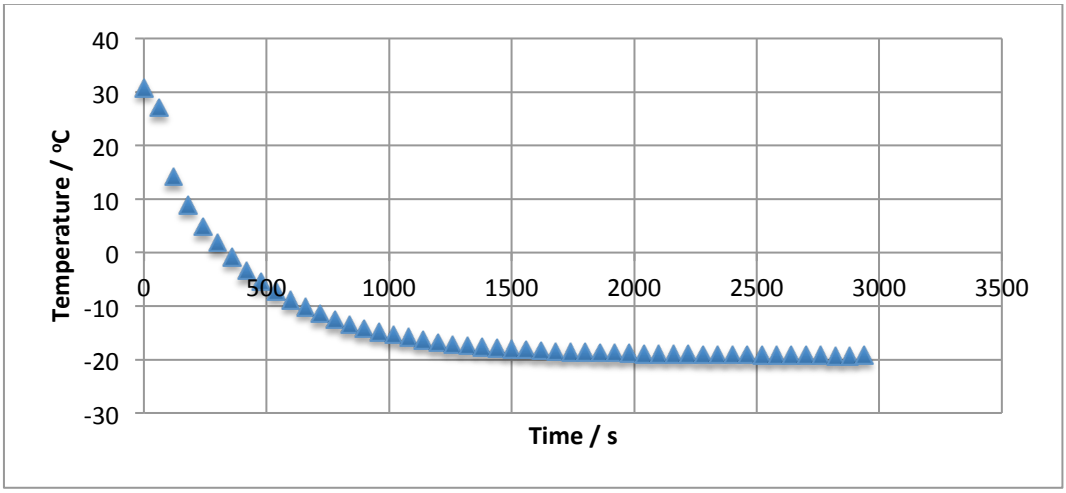

Figure 6.10: Response of Sion Li-S cell to -20°C shock cooling

The result for Q_r found above shows that the effect of thermal radiance is very small, mainly due to the small surface area of the cell. Taking into account that the cell is not producing any heat of its own during rest and using the assumption that conductive heat transfer is the dominant effect and radiative effects are negligible, Equation 6.20 can be reduced to:

$$\frac{dT_1}{dt} = \frac{-Q_c\,(T_1 - T_{env})}{m.\,C_p} \qquad [6.23]$$

This equation can be rearranged to form the following differential equation:

$$\frac{1}{(T_1 - T_{env})}\frac{dT_1}{dt} = \frac{-Q_c}{m.\,C_p} \qquad [6.24]$$

The solution to Equation 6.24 takes the form:

$$T_1 = T_{env} + K_3.\,e^{\left(\frac{-Q_c.t}{m.C_p}\right)} \qquad [6.25]$$

Where K_3 is a constant of integration. At t = 0, K_3 is equal to $(T_0 - T_{env})$, where T_0 is the cell's initial temperature, hence the temperature of the cell as it responds to shock cooling is:

$$T_1 = T_{env} + (T_0 - T_{env}).\, e^{\left(\frac{-Q_c.t}{m.C_p}\right)} \quad [6.26]$$

Fitting this equation to the test data reveals the following results:

$$e^{\left(\frac{-Q_c.t}{m.C_p}\right)} = e^{-0.002527.t}$$

$$Q_c = \ 0.002527.m.C_p \ \mathrm{WK^{-1}}$$

Using 1.65 $\mathrm{Wg^{-1}K^{-1}}$ as an estimate for specific heat capacity, as stated in [1], and a cell mass of 16g gives a thermal conductance value of 0.07 $\mathrm{WK^{-1}}$. In [1] Q_c was found to be 0.08 $\mathrm{WK^{-1}}$ for conditions that included convection and estimated to be around 0.015-0.02 $\mathrm{WK^{-1}}$ for conditions that did not include convection. These values were calculated empirically and ultimately depend on the area over which conduction is allowed to take place, the cell tested in this work, for example, may have had a different surface area in contact with its surroundings which would affect these values. For the cells tested in this work heat conduction was limited to one side of the cell and the connectors attached to the tags. In addition, the effects of convection could not be wholly eliminated.

In a full scale battery the thermal response of the Li-S cell will vary due to the interaction between cells packed together, as the structure and topology of the battery itself is the dominating factor. The heat transfer equations described above are used to model the response of single cells in the test environment but can be extended for the simulation of the thermal response of a full battery. For example, a thermocouple placed at the hottest point and one placed at the coolest point can provide additional information on the internal thermal gradient in the shock-cooling test. Depending on the size of battery chosen for the mission, this information can be used to extend the thermal model to include extra nodes (for large batteries) or, for smaller batteries, the average cell response can be used. In Chapter 8, further testing is suggested to improve the thermal model when it is scaled to a full battery.

6.3 Degradation and Capacity Changes

The electrical response of the Sion Li-S cell was described in Section 6.1. In the equivalent circuit used to describe the transient electrical characteristics (Figure 6.4(b)) the EMF of the cell is described by a state of charge dependent voltage source. Equation 5.3 gave the state of charge of the cell and is repeated below.

$$SoC = SoC_0 + \frac{\int I_1 \, dt}{Q_t} \quad [5.3]$$

Where I_1 is the load current, Q_t is the total capacity of the cell and SoC_0 is the initial state of charge of the cell. The results of the storage tests given in Chapter 5 clearly show that the total capacity of the cell is affected by irreversible capacity changes. The capacity available from the cell is also affected by the current rate at which it is being operated and reversible capacity changes that occur during rest periods. In this section the cell model is improved by taking these capacity variations into consideration. However, it should be noted that the topic of cell capacity degradation is highly complex and an extended analysis requires many hours of data at many different operating conditions using many more cells than were available in this work. The results presented in this section are the best that could be achieved with the available cells and knowledge at the time of testing.

6.3.1 Coulombic efficiency

The total capacity of the Li-S cell is dependent on whether the cell is charging or discharging. More Ah are required to charge the cell than are available on discharge, determined by the Coulombic efficiency, which has a BoL value of 96.7%. Test results showed that this efficiency degrades during repeated cycling by 0.3% per cycle and is considered to be rate independent. It is assumed that the end user of the battery model will perform an SCM cycle on the cell to determine its most recent discharge capacity Q_D, which is known to be 92% of the full capacity. The total capacity of the cell during charge (Q_{tC}) and discharge (Q_{tD}) is therefore calculated as:

Discharge: $$Q_{tD} = {}^{Q_D}/_{0.92} \quad [6.27]$$

Charge: $$Q_{tC} = \frac{Q_D}{0.967 - (0.003 * CycNo)}\Big/_{0.92} \quad [6.28]$$

Where *CycNo* is the number of full cycles that the cell has completed.

6.3.2 Capacity fade due to calendar age and cycling

The efficiency calculations in the previous subsection are only valid if the cell undergoes a 0.315A discharge from 100% SoC to obtain the most recent value of Q_D and the cycle history of the cell is known. In a more likely situation, the value of Q_D may need to be predicted from BoL data so that the relevant charge and discharge capacities can also be predicted.

Total cell capacity is irreversibly diminished by age and cycling losses. In Chapter 5 it was shown that there was a state of charge dependent capacity loss associated with a cell's age that was proportional to the square root of its age. Furthermore, there was an additional loss associated with cycling that was dependent on the current rate used. The total capacity of the cell (Q_t) after these losses are accounted for is given by Equation 6.29.

$$Q_{t1} = Q_{tD} - Q_{age} - Q_{cyc} \quad [6.29]$$

Where Q_{tD} represents the full capacity of the cell determined by the SCM. Q_{age} is the capacity lost due to the age of the cell and was determined to be proportional to the square root of time. Q_{cyc} is the rate-dependent capacity lost per cycle that is due to cycling. Q_{age} and Q_{cyc} are given by:

$$Q_{age} = A_{age} * t^{0.5} \quad [6.30]$$

$$Q_{cyc} = A_{cyc} e^{-k_{cyc} * I} * CycNo \quad [6.31]$$

Where t is given in hours and A_{age} is a coefficient (with units $A.h^{0.5}$) and is calculated to be 0.0017*Q_{tD}. This figure is derived from the gradient of the trend line in Figure 5.8, which was

expressed as a percentage of Q_{tD}. The results for the storage tests showed that A_{age} is in fact likely to be both SoC dependent and affected by temperature.

Converting the test data given in Figure 5.11 into a percentage of full capacity and subsequently fitting Equation 6.31 to this data shows that A_{cyc} has a value of 0.9 ± 0.1 Ah while k_{cyc} has a value of 0.7 ± 0.1 A^{-1}. These values were taken from the average fade between charge and discharge. Again these values could change with temperature and do not account for the fact that cycling fade showed signs of improvement at the 5.6A rate. In addition the fade rate was taken for full cycles, where the cut-off voltage was 1.7V for all tests. These capacity losses can be modelled by representing the capacity of the cell with a variable capacitor, the capacitance of which is dependent on the conditions and history of the cell. The state of charge of the cell is calculated using this variable capacitance, which is then converted into a corresponding EMF value using the EMF vs. SoC lookup table to be used by the electrical equivalent circuit.

6.3.3 Self-discharge

The self-discharge of a cell can be modelled by a small current drain, of the order 0.5mA, that occurs regardless of there being no load at the terminals. Because the capacity lost due to self-discharge is reversible it is replenished once the cell is recharged. This effect can be modelled by placing a high value resistor in parallel with the variable capacitor that represents the capacity of the cell, depicted in Figure 6.11. This ensures that the state of charge of the cell is dynamic even when the cell is at rest, as with the real cell.

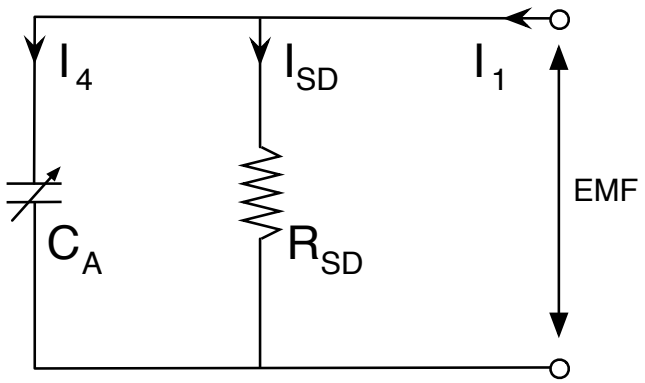

Figure 6.11: Equivalent circuit of cell capacity with a self-discharge leakage current

To incorporate these effects, the state of charge equation is thus altered to a new form given in Equation 6.32, where the value of I_{SD} is always negative, irrespective of the sign of the load current.

$$SoC = SoC_0 + \frac{\int I_1 + I_{SD}\, dt}{Q_t} \quad [6.32]$$

In order to define the self-discharge current, its relationship with the amount of charge lost to self-discharge reactions Q_{SD}, which is proportional to the square root of the time spent at rest, t (hours), must be known. Plotting the capacity lost to self-discharge at 100% SoC against time in hours and fitting to an equation of the form $Q = A.t^{0.5}$ gives a value of 0.01 for the A coefficient. The capacity lost to self-discharge reactions can thus be modelled as:

$$Q_{SD} = 0.01t^{0.5} \quad [6.33]$$

Using the relationship between charge and current, the self-discharge current I_{SD} that causes this capacity loss has the form of Equation 6.34, where the value of A_{SD} is 0.005 A($h^{0.5}$).

$$\frac{dQ_{SD}}{dt} = I_{SD} = A_{SD}.t^{-0.5} \quad [6.34]$$

Displayed graphically in Figure 6.12, the self-discharge current is seen to diminish as storage time at 100% SoC increases.

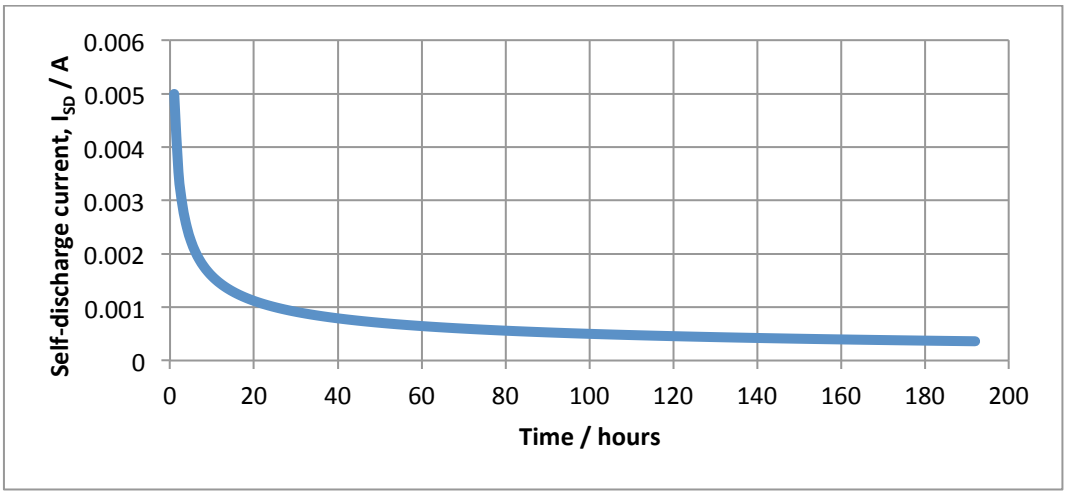

Figure 6.12: Self-discharge current as a function of rest time at 100% SoC

Equation 6.34 gives a simple relationship, which can be incorporated into Equation 6.32, provided that the storage time of the cell is known (in hours). The value for A_{SD} calculated here should be seen as a worst-case value. In reality, the self-discharge current may change over the full SoC range. The self-discharge current did appear to be similar between 100% and 40% SoC, but tests at lower states of charge could yield different results. Further to this, these values are valid only for long-term storage. The results given in Figure 5.7 show that the effect of the relaxation of the concentration gradient, or apparent "capacity recovery", immediately after the current is removed, conceals the self-discharge effect in the first hours, or even days, of rest. In order to accurately model the cell's response during rest this capacity recovery affect also needs to be accounted for and is addressed in the following subsection.

6.3.4 Capacity recovery and rate effect

So far, the model does not account for the fact that the current rate used on the cell directly affects the capacity available from the cell. This is due to the Li_2S layer forming on the cathode surface at higher current rates, as opposed to uniformly depositing throughout the cathode, causing access to the active materials to be restricted. The current rate therefore directly affects the capacity available from the cell. In addition, the available capacity is increased when the cell is rested part way through discharge, caused by the relaxation of the concentration gradient or the "capacity recovery effect". Both of these effects have implications for the cell model.

In the proposed model the full capacity is the value of the capacitor C_A shown in Figure 6.11 for a given cycle and age. This value decreases in accordance with the irreversible capacity losses that occur during the cell's lifetime. The changes to cell capacity that are due to the current rate and the recovery periods, however, are considered to be reversible. If the variable capacitor shown in Figure 6.11 adapts its value as a function of current rate, rest time and temperature, this would provide a more accurate representation of cell performance. The implication of this is that the state of charge of the cell is actively recalculated to be a percentage of a changing capacity.

Capacity rate effect

A plot of a cell's available capacity against the rate used to obtain that capacity (Figure 5.12) shows that capacity diminishes as current rate increases. The relationship between available capacity, Q_A, and current rate, I, was found from life test data and is given by Equation 6.35.

$$Q_A = 2.02 * I^{-0.273} \quad [6.35]$$

A rate dependent capacity correction can be simply modelled by Peukert's Law, which is an equation that shows the relationship between obtainable discharge capacity and current rate. All battery types have a characteristic Peukert number that defines this relationship. A Peukert number of 1 indicates that the amount of capacity obtainable is independent of current rate. Lithium-ion cells have a number very close to 1 whereas lead acid cells have a number closer to 1.3. Peukert's law can be written as:

$$I.t = Q_{SCM}\left(\frac{Q_{SCM}}{IH}\right)^{P-1} \quad [6.36]$$

Where P is the Peukert number, Q_{SCM} is the SCM capacity (Ah) obtained after H hours of discharge and t is the time, in hours, that the cell can supply a current of I, which is different from the current used to obtain Q_{SCM}. It transpires that Equation 6.35 is analogous to Equation 6.36 and so the capacity obtainable at any discharge rate can be related to the rate using the following relationship:

$$Q_{rate} = Q * 0.315^{0.273} * I^{-0.273} \quad [6.37]$$

Where Q_{rate} is the capacity available at current rate I and the Peukert number for the Li-S cell is calculated to be 1.273. This calculation could be used to modify the available capacity of the cell, depending on the current rate being used.

Although the Peukert number found above provides a way to calculate the total available capacity from the cell, the Li-S chemistry exhibits fundamentally more complex behaviour than other cell types. Recalling the comparison of rates in Figure 5.12 it is evident that the

available discharge capacity is largely rate independent in the first discharge region and rate dependent only in the second discharge region, where the Li_2S layer begins to form. This has implications for the use of the Peukert correction because this solution results in the scaling down of both discharge regions and ultimately provides an inaccurate representation of power output. A novel solution to this problem, not used in equivalent circuit models for other battery types, is to model the total capacity of the cell as two separate capacitors. The first capacitor represents the total capacity of the cell when the voltage is in the first discharge region, and is not affected by the current rate being used. The second capacitor represents the capacity of the cell as it enters the second discharge region and is affected by the current rate. Applying the Peukert correction factor to the second discharge region only gives an increasingly accurate representation of the Li-S discharge profile.

Capacity recovery effect

The 40% SoC storage test results showed that the apparent capacity available from the cell was increased after 24 hours of rest, indicating that the relaxation of the concentration gradient, and hence the capacity recovery effect, is dominant over any self-discharge reactions that may also be occurring. Around 10% capacity was recovered during 24 hours rest at 40% SoC; a significant amount. This recovery effect occurs in other battery types [2] and has been modelled in the literature using stochastic methods [3,4]. A detailed review of variations on this method is given in [5]. Capacity recovery is complicated to model due to the interdependency of state of charge, current rate and temperature; factors that determine how much and how quickly capacity is recovered during rest periods. For example, the percentage of capacity recovery is likely to be higher should a higher current rate be used preceding the rest [4]. In addition, the recovery would be faster at high temperatures and slowed at lower temperatures caused by an increasingly viscous electrolyte. Stochastic modelling is an unsuitable method for use in this work due to its abstract nature relative to the equivalent circuit model, although results using this method can be accurate for predetermined, specific load profiles. In other work [6] the capacity recovery effect has been incorporated into an

equivalent circuit model by defining a mathematical relationship between the amount of discharged capacity and the maximum recoverable capacity, however, the limited storage tests that were performed in this work prevent the characterisation of the parameters required for an accurate description. Nevertheless, it would be beneficial to incorporate a description of the capacity recovery effect for completeness and seek to increase the available test data in future work.

One method of modelling this effect in the equivalent circuit model described above is to assume that intermittent rests do not affect the total capacity of the cell but that a small amount of charge is recovered during those rests, as the concentration gradient relaxes. The maximum amount of charge recoverable depends on the state of charge of the cell, the current rate and the temperature and the actual amount that is recovered also depends on the length of time in rest. If the maximum recoverable charge available to the cell is denoted by Q_{max} then the amount of capacity recovered, Q_R, after a period of time t following the removal of the load current, can be modelled by Equation 6.38.

$$Q_R = Q_{max}(1 - e^{-k_R t}) \quad [6.38]$$

Where k_R is a temperature and current dependent constant that determines the rate at which charge is recovered. This charge can be modelled by an internal equivalent current, I_R, which delivers the recoverable capacity. It is found by differentiating Equation 6.38 to obtain Equation 6.39.

$$I_R = \frac{dQ_R}{dt} = k_R . Q_{max} e^{-k_R t} \quad [6.39]$$

An extended set of characterisation tests is required to determine precise values of Q_{max} and k_R. Using the data provided by the 40% SoC tests, and assuming that there is no recoverable capacity available at 100% SoC, Q_{max} is given as a proportion of the total capacity and can be estimated to be:

$$Q_{max} = \frac{(17 - 0.17.SoC) * Q_t}{100} \quad [6.40]$$

There is some difficulty in determining the value of k_R. However, using data from step-cycling tests, k_R was given a preliminary value of 0.02hr^{-1}. If an application, which required multiple rests during cycling, became desirable for this cell type, then these values could be characterised further in tests described in Chapter 8.

6.3.5 Combined capacity model

In the previous subsections several different types of capacity variations were evaluated and modelled. The total capacity of the Li-S cell when irreversible capacity losses are accounted for was given in Equation 6.29 and is repeated below:

$$Q_{t1} = Q_{tD} - Q_{age} - Q_{cyc} \quad [6.29]$$

Where:

$$Q_{tD} = \frac{Q_D}{0.92} \quad [6.41]$$

$$Q_{age} = 0.8 * t^{0.5} \quad [6.42]$$

$$Q_{cyc} = 0.9e^{-0.7t} * CycNo \quad [6.43]$$

Here, Q_{t1} represents the capacity in the first discharge region. To account for the dependency that available capacity has on current rate, the available capacity in the second discharge region Q_{t2} is given in Equation 6.44, where the additional Q_{rate} factor was given in Equation 6.37.

$$Q_{t2} = Q_{tD} - Q_{age} - Q_{cyc} - Q_{rate} \quad [6.44]$$

The state of charge of the cell can be modelled by:

$$SoC = SoC_0 + \frac{\int I_1 + I_{SD} + I_R \, dt}{Q_t} \quad [6.45]$$

Where I_1 is the load current, I_{SD} is the self-discharge current and I_R is the equivalent capacity recovery current given by:

$$I_{SD} = 0.005 * t^{-0.5} \quad [6.46]$$

$$I_R = 0.02 * Q_{max} e^{-0.02t} \quad [6.47]$$

The use of I_{SD} and I_R are conditional to the power profile used on the cell.

6.4 Model Implementation

In the preceding sections it was shown how the various contributions to the Li-S cell characteristics are modelled. In this section, those concepts are brought together to show how a coherent battery model is created, using modelling tool MatLab[2]. The code used to implement the model can be found, fully annotated, in Appendix F.

6.4.1 Consolidation of model elements

In Section 6.1 a Foster network of resistors and capacitors was chosen as the best way to represent the relationship between EMF and the various contributions to resistance in the cell. In the Foster network that was shown in Figure 6.4(b) there is a SoC controlled voltage source representing the cell's open circuit voltage, or EMF. It was shown in Section 6.3 that this EMF is calculated by first knowing the SoC of the cell and using a lookup table to find the corresponding EMF value. However, the SoC must first be calculated using Equation 6.45, where the parasitic self-discharge current and capacity recovery current are accounted for. In Section 6.3.3 it was shown that a resistor placed across the terminals of the cell would act as a parasitic current drain to represent cell self-discharge and this current drain was predicted using empirical testing. The equivalent capacity recovery current can be modelled by a parallel capacitor (C_R), which recharges the main capacitor (C_A) when the applied current is stopped. This configuration is shown in Figure 6.13. It should be noted that the currents I_R and I_{SD} were modelled rather than the actual values of the circuit components C_R and R_{SD}. The total capacity Q_t, also used to determine SoC, is calculated using Equations 6.25 and 6.44, taking into account the degradation of capacity due to age and cycling, and also the capacity

[2] MatLab R2009b, Version 7.9.0.529, The MathWorks Inc. US.

rate effect seen in the second discharge region. In calculating an accurate, dynamic value of SoC as it changes with current flow and degradation, the EMF vs. SoC lookup table can then be used to determine the corresponding EMF value for each time step. This EMF value is then coupled with the Foster network and, along with the SoC dependent values of resistance and capacitance also found in lookup tables, the cell's terminal voltage response is determined. Figure 6.13 shows how these two parts of the model are combined.

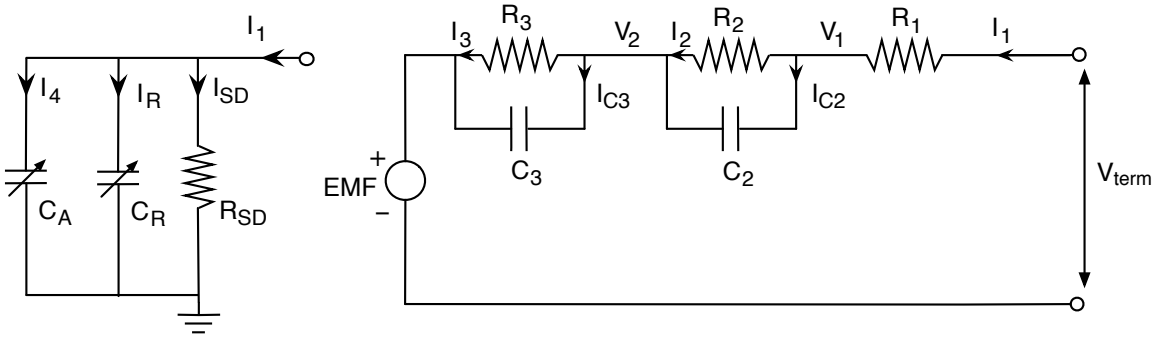

Figure 6.13: Combined Li-S cell model

When the resistor and capacitor values in the Foster network are selected from the relevant lookup tables, both SoC and temperature are used as lookup criteria and so the temperature effects on terminal voltage are also included. The hysteresis factor is incorporated into the model code and modifies the EMF value when a change of current occurs. The EMF is found using the lookup table in the usual way but is adjusted by Equations 6.6 and 6.7, ensuring that the transition between charge and discharge EMF is a realistic representation of the smooth voltage transient that occurs.

6.4.2 Model execution

MatLab was used to implement the various lookup tables, equations and circuit elements in the way described above. A simple Runge-Kutta method was used to perform the integration over each time period so that a dynamic value of SoC could be calculated with current flow. The basic algorithm for the model is described in the steps below.

- **Import battery data** – The first task is to set up all the model parameters which are either inherent to the battery type or set by the user. In future applications of this

model the user will be able to select the particular version of the Li-S cell they wish to model and the associated parameters characteristic to that cell type will be called. The following characteristics specific to the cell type are imported:

  - Maximum and minimum voltage.
  - Thermal properties such as thermal capacity and thermal conductance.
  - Battery topology (number and arrangement of cells).
  - Cell history, comprising age and cycle history.

- **Import user defined data** – the power profile defined by the user is imported as well as initial cell and ambient temperatures and initial state of charge. The user may also define the time step to be used.
- **Lookup tables** containing the specific cell data, such as resistances and capacitances, are defined and imported. All of the lookup tables are dependent on both SoC and temperature (except for the $\frac{dE}{dT}$ parameter, which only varies with SoC).
- **Model is initialised** – starting values for all equivalent circuit elements, including resistances, capacitances, EMF, internal voltages and currents are defined based on initial conditions (temperature and state of charge) and the total cell capacity is calculated from the known history of the cell.
- **Runge-Kutta** integration loop is run for each time step for the duration of the test.
  - For each increment in time the current is integrated using Equation 6.45 to calculate the increment in SoC and Equation 6.20 is used to calculate the increment in temperature.
  - The new values of SoC and temperature are fed into the lookup tables and new values for each of the model parameters are calculated.
  - The process is repeated in a loop that continues until the power profile defined by the user is completed or the battery voltage limits are exceeded.
- **Results** are displayed to the user in the form of an Excel spreadsheet and graphs of selected data.

6.5 Model Verification and Analysis

In the remainder of this chapter the model is verified against data collected during testing so its accuracy can be analysed. In addition, this verification exercise will identify possible improvements to the model to be made in future work.

6.5.1 Discharge at 20°C

Figure 6.14 shows a comparison between a random set of screening data and the model for a 0.315A discharge from 100% SoC until the voltage cut-off point at 1.7V.

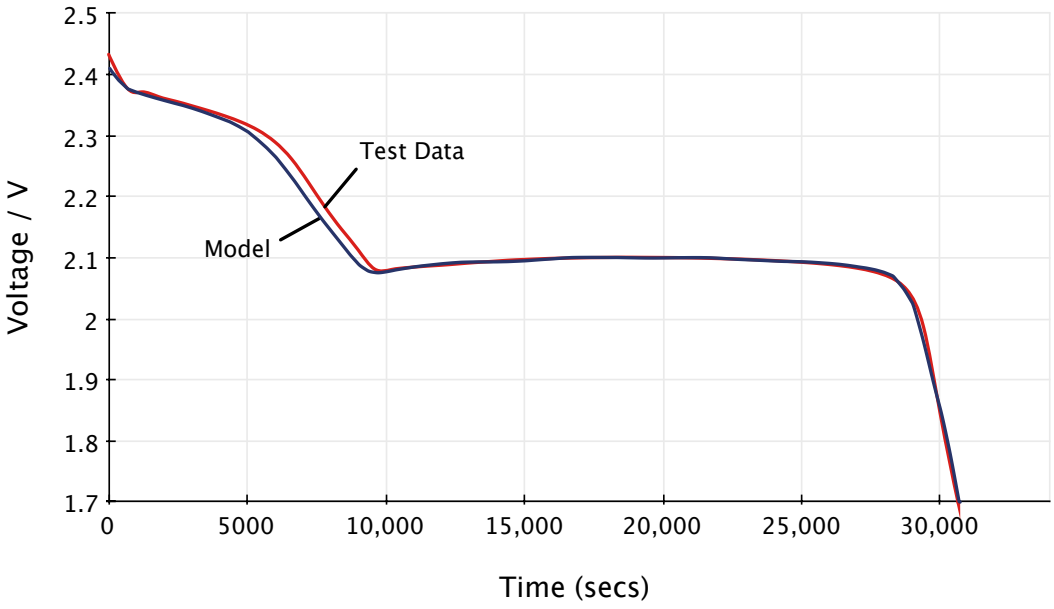

Figure 6.14: Voltage profile of a 0.315A discharge at 20°C

The R^2 value between these two sets of data is 0.99, calculated using the data analysis tool in Excel 2010. The fit is very close for the majority of the curve however there is a larger error of around 3% during part of first discharge region. This inaccuracy is due to the sensitivity of this part of the curve to the rests used to determine internal resistance. The quality of the fit is expected as the majority of the characterisation tests were completed at this temperature and at this current rate. However, the purpose of the model is to predict the cell's behaviour using different temperature and current profiles and at different states of degradation. Discharging at various current rates using a basic version of the model, that does not include any resistance or capacity corrections, gave the result shown in Figure 6.15.

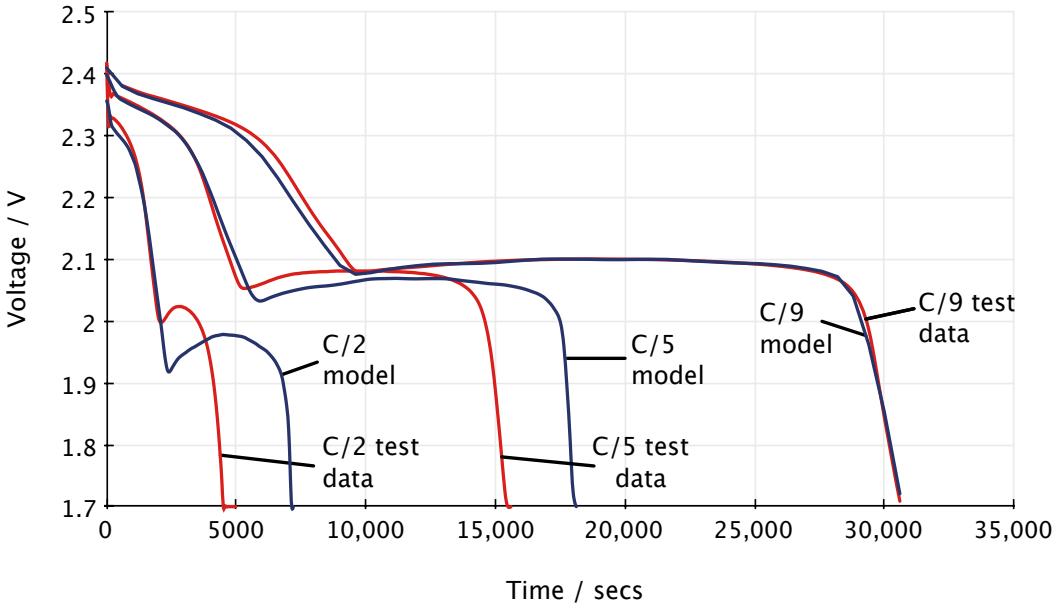

Figure 6.15: Discharge voltage profiles of C/9, C/5 and C/2 rates using basic model

From this figure it is clear that the model overestimates the internal resistance as current rate increases. This is evident in the level of the plateau in the second discharge region, which the model predicts to be lower than the test data implies. Inclusion of the correction factor described in Section 6.1.2, which gives a current rate dependency to the internal resistance, provides a more accurate description of internal resistance, as evidenced by the higher level of the plateau in the second discharge region in Figure 6.16.

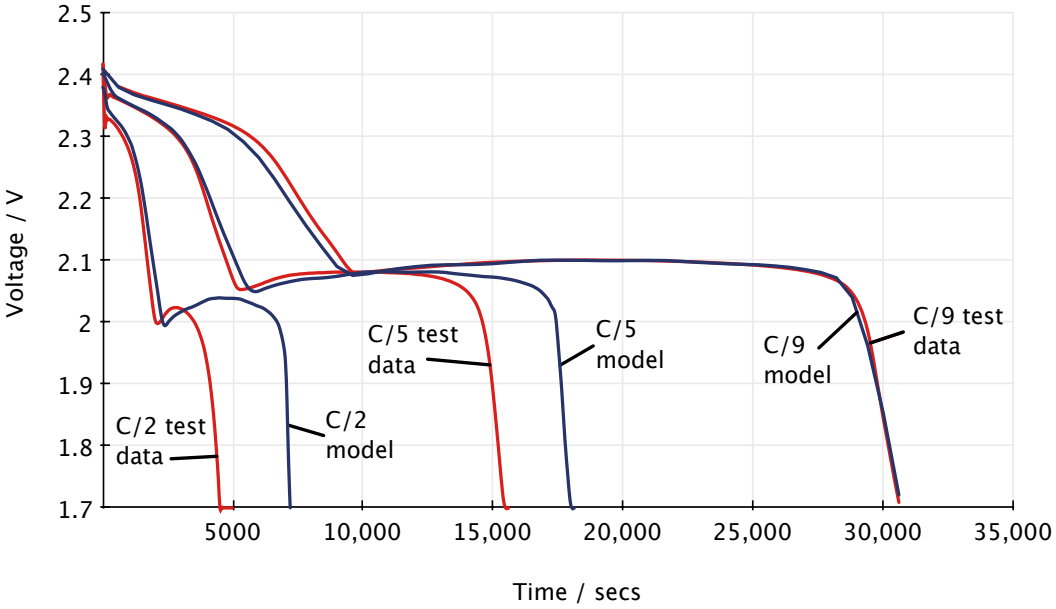

Figure 6.16: Discharge voltage profiles of C/9, C/5 and C/2 rates using current-dependent internal resistance.

Although the model is improved there is still a discrepancy between the available capacity predicted by the model and that of the test data. As expected, the model predicts a larger capacity than the real cells were able to deliver. The available capacity in the second discharge region has been shown to be dependent on the current rate used because of the way in which Li_2S blocks access to active materials in the cathode at high rates. Inclusion of the Peukert effect over the whole capacity gives the data displayed in Figure 6.17.

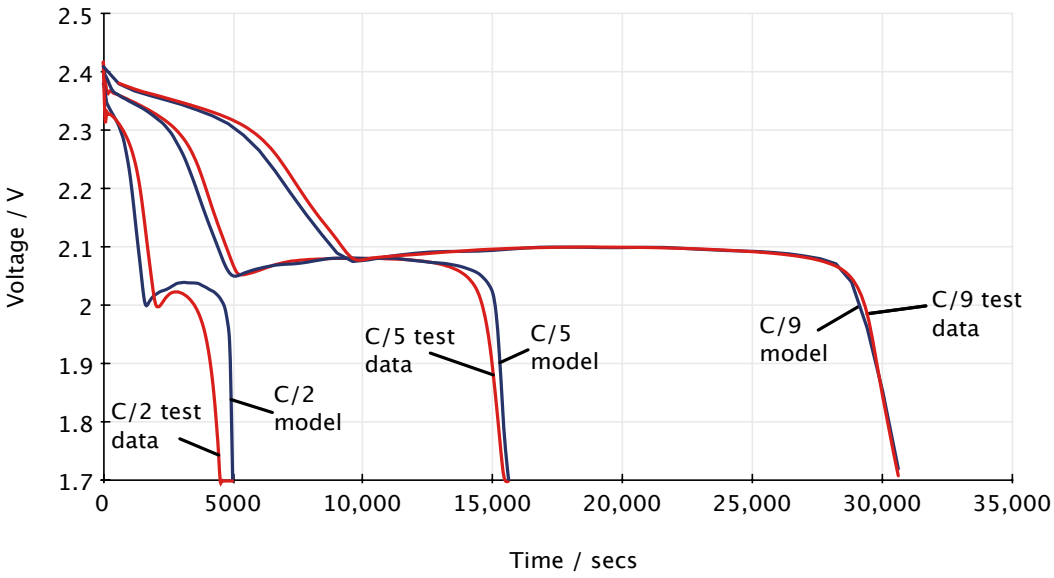

Figure 6.17: Discharge voltage profiles of C/9, C/5 and C/2 rates using current-dependent internal resistance and Peukert effect over the whole capacity.

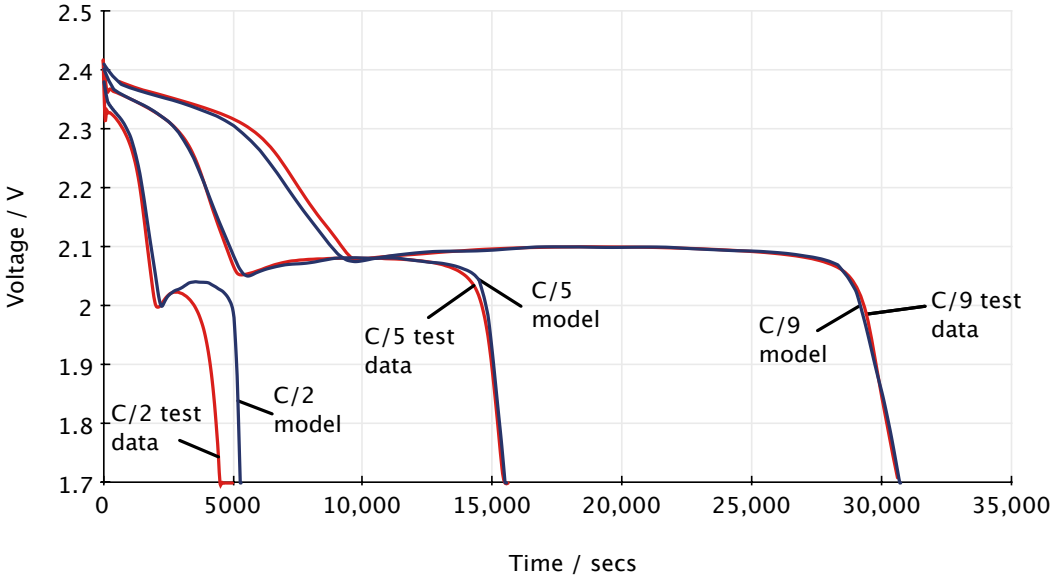

Figure 6.18: Discharge voltage profiles of C/9, C/5 and C/2 rates using current-dependent internal resistance and Peukert effect over the second discharge region.

The result is further improved, as shown in Figure 6.18, when the "split capacity" effect is taken into consideration. The R^2 values for the C/5 discharge are improved from 0.64 to 0.96 once the capacity and resistance correction factors are included, and to 0.99 once the capacity has been split into regional contribution. The R^2 values for the C/2 discharge are improved from 0.68 to 0.72 and again to 0.78 once the capacity has been split. These numbers show that the model accuracy is enhanced when the performance of the cell at varying current rates is accounted for but that this accuracy deteriorates as current rate increases. Further characterisation of the rate dependence resistance and capacity factors at higher current rates should establish better accuracy at high rates.

6.5.2 Charge at 20°C

Using the method described in Section 6.1.2 the charge resistances were incorporated into the model, the results of which are displayed in Figure 6.19. Due to the safety restrictions placed on the cell there is limited data with which to compare charge voltage profiles and only a C/9 charge was accurately recorded.

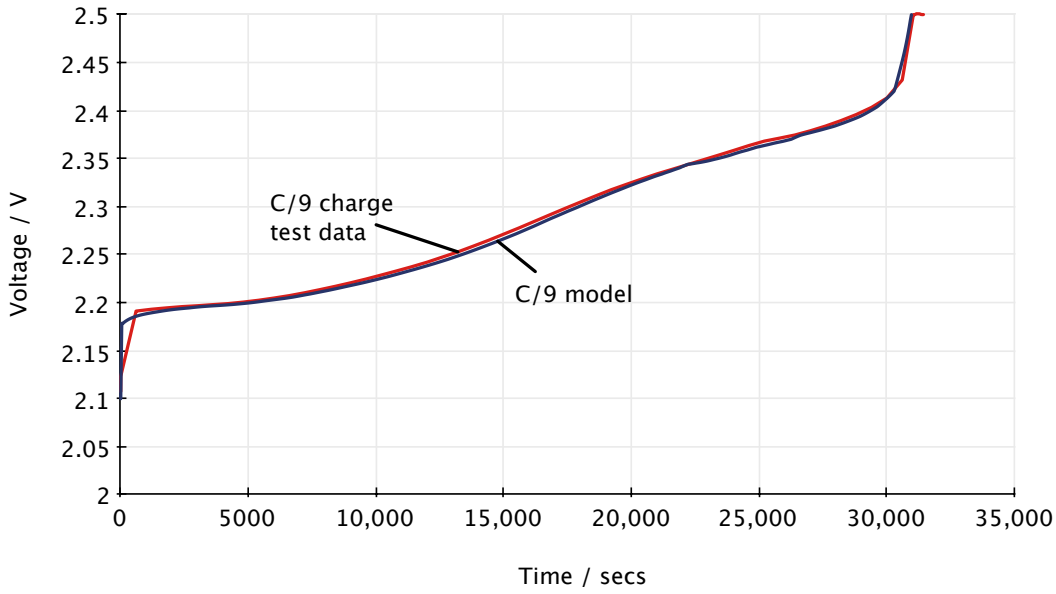

Figure 6.19: C/9 Charge voltage profile rate at 20°C

6.5.3 Hysteresis

The model is able to transition smoothly between charge and discharge in either direction, when there is no rest between current direction changes. Figure 6.20 shows two sets of

preliminary results when performing a discharge to charge transition. In the profile marked as Model 1 the SCM capacity was taken from the screening test as 2.85Ah and no history was assumed for the cell (i.e. no age or cycle history). In the profile marked as Model 2 the number of days between the screening and hysteresis testing (18 days) was added to the history, as well as the number of full or partial cycles (8 cycles) that the cell had undergone prior to the test shown in the figure. These results show that the model accuracy improves when the history of the cell is accounted for but, for this particular cell, the degradation is considerably underestimated.

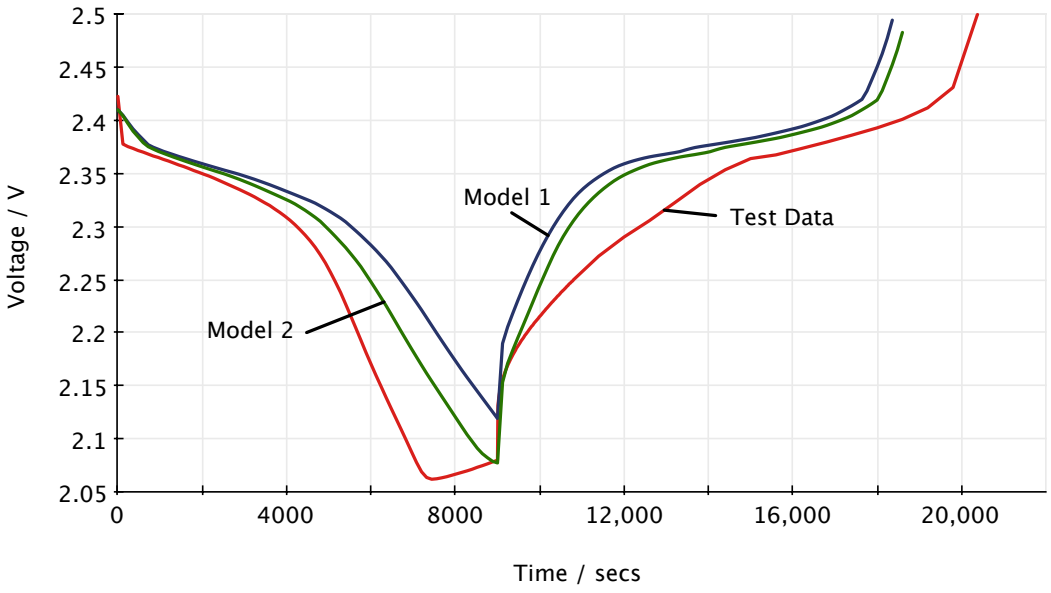

Figure 6.20: Hysteresis voltage transition from discharge to charge without cell history

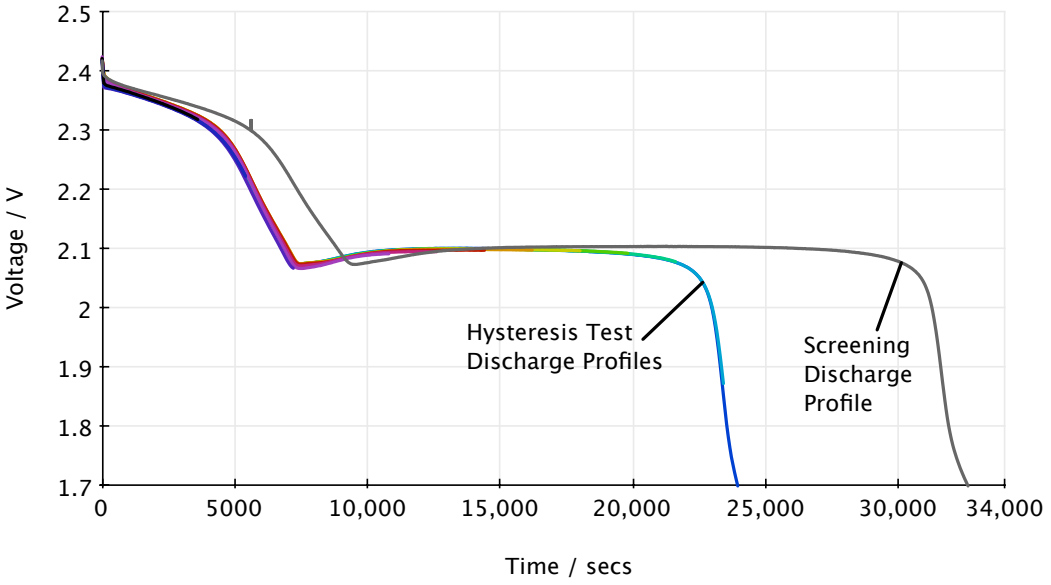

Figure 6.21: Comparison of hysteresis discharge data with screening data from the same cell

Comparing the discharge profile found in screening to the discharge profiles found in the hysteresis test Figure 6.21 shows that the cell capacity was reduced during the 18-day rest between tests and not as a result of the partial cycling conducted in the hysteresis test.

Replacing the SCM capacity found in the screening test with a value closer to that seen in the hysteresis test gives a more accurate representation of the response of this cell, as can be seen by the profile labelled Model 3 in Figure 6.22.

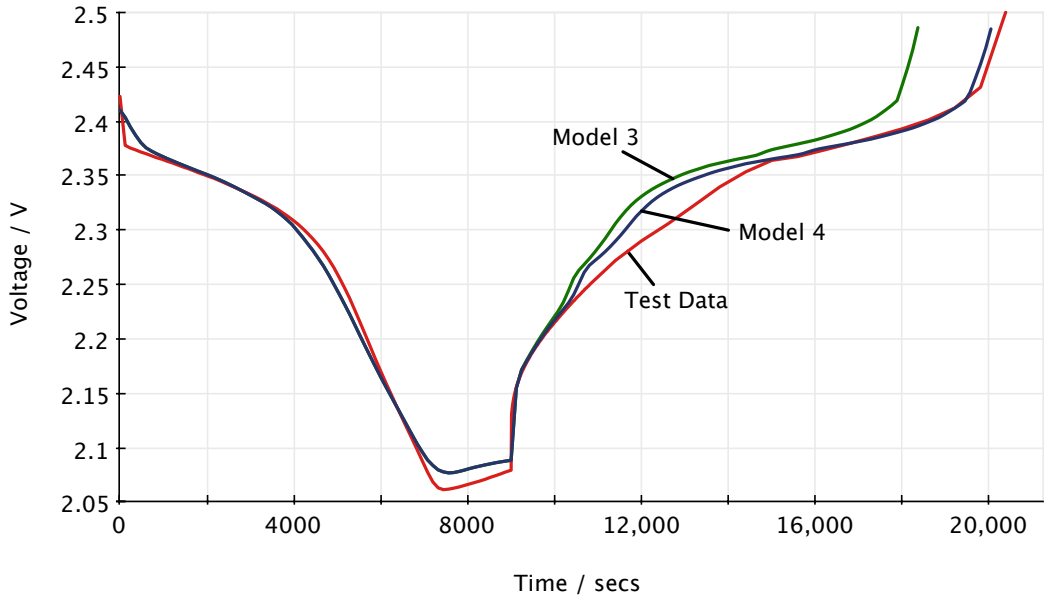

Figure 6.22: Hysteresis voltage transition from discharge to charge using cell history

The Model 3 profile shows that the model also underestimates the cycling efficiency degradation of the cell. Calculating the decrease in the cell's cycling efficiency gives the profile labelled as Model 4. The improvement seen in predicting the behaviour of the cell when the capacity and cycling efficiency of the cell are corrected shows that the model can predict cell performance with accuracy, if the factors affecting cell degradation are well characterised. Degradation predicted by the cell model is indicative only and emphasises the need to perform characterisation tests on a large number of cells so that the spread across a cell batch can be well determined. It also highlights the importance of performing an SCM cycle immediately prior to any characterisation test so that the precise value of capacity and cycling efficiency are known.

The charge profiles of the charge to discharge hysteresis tests are shown in Figure 6.23 with the screening charge profile as a comparison. It is clear that the partial cycling of the hysteresis test affected the cell resistance and hence the charge voltage. Modelling the charge to discharge hysteresis voltage thus encounters problems because the charge resistance of the real cell decreased with each partial cycle that occurred in the test and the cell capacity is also likely to have been reduced.

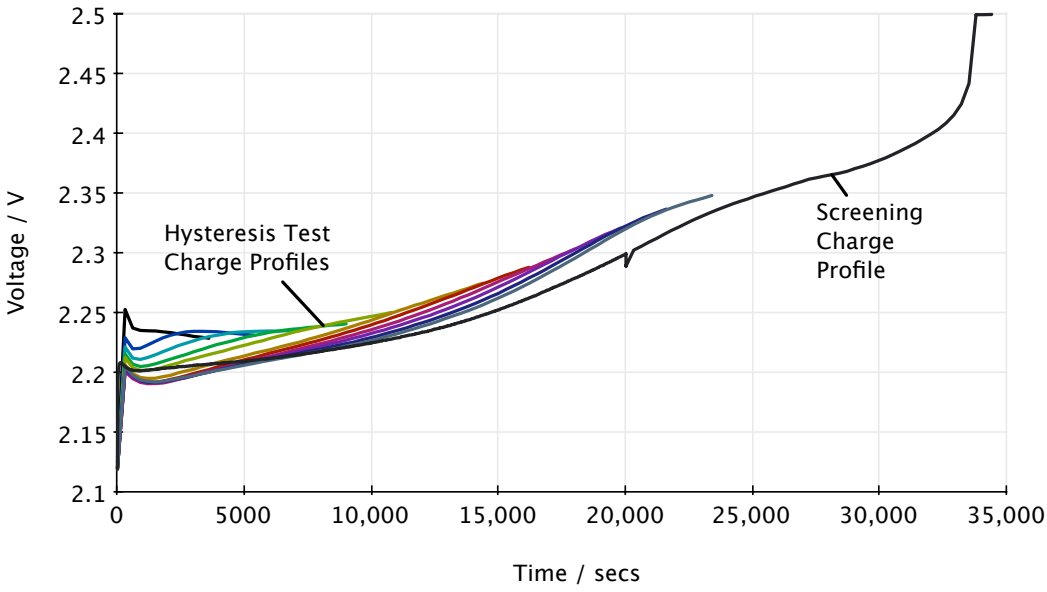

Figure 6.23: Comparison between hysteresis test charge data with screening discharge data of the same cell.

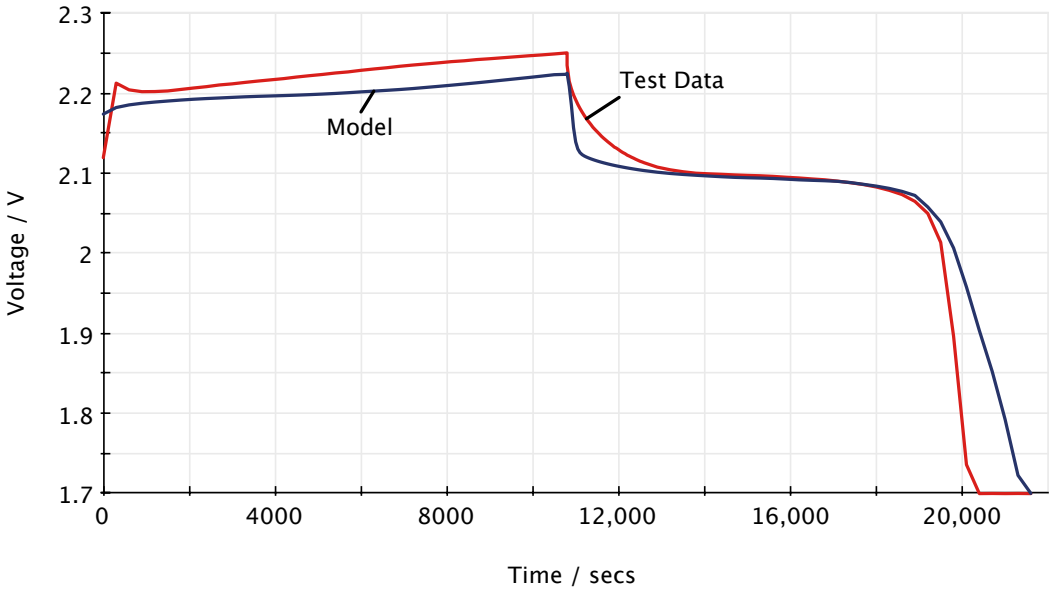

Figure 6.24: Hysteresis voltage transition from charge to discharge

The model thus predicts a lower charge voltage than occurred in the test; an example is seen in Figure 6.24. This increased resistance also affects the voltage on transition from charge to discharge and so the accuracy of the predicted hysteresis voltage is lowered. Modifications to the testing methodology that may improve the accuracy of these tests are described in Section 8.3.

6.5.4 Temperature response

The temperature response for a discharging cell is given in Figure 6.25. The result is highly dependent on the accuracy of $\frac{dE}{dT}$, on the cell's internal resistance and its thermal properties. It is also possible that the thermal properties of the cell are themselves temperature dependent. The figure shows that the thermal model predicts the temperature response of the cell well but an improved $\frac{dE}{dT}$ testing methodology may give more accurate results.

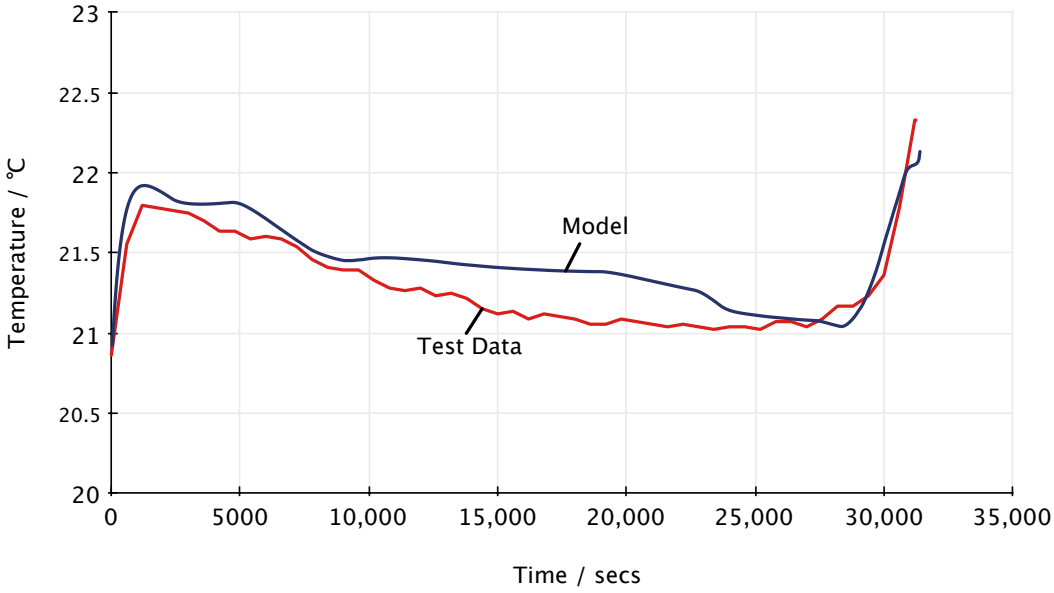

Figure 6.25: Thermal response to a C/9 discharge

The voltage response of the cell whilst discharging at different temperatures is shown in Figure 6.26. There was limited test data at different temperatures to verify the model against and the model also cannot extrapolate outside of the 0°C - 40°C temperature range so a direct comparison was not possible. Therefore Figure 6.26 depicts a 5°C and 35°C model discharge compared to 0°C and 20°C test data.

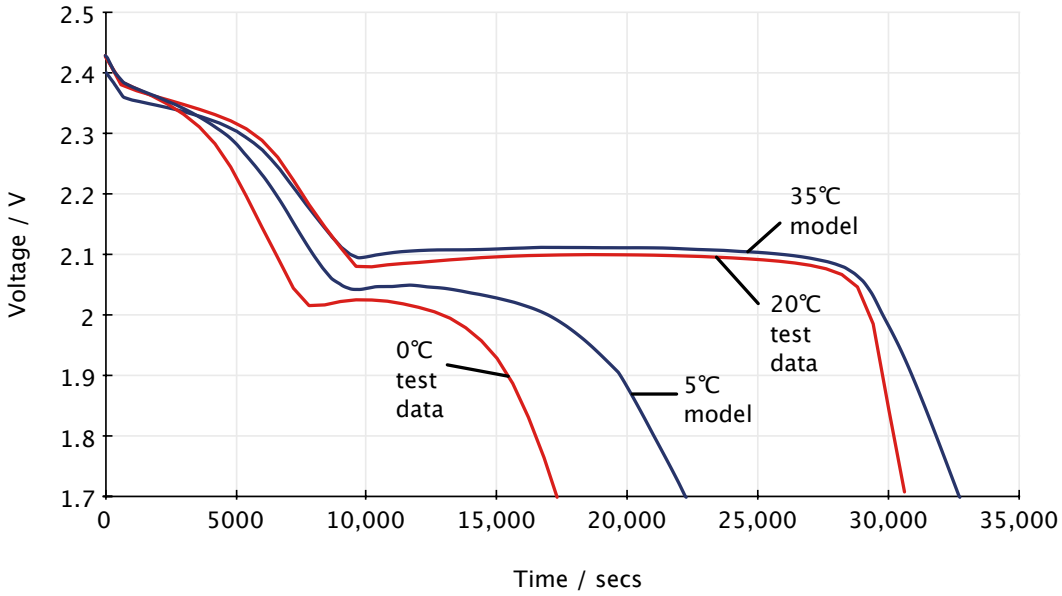

Figure 6.26: Voltage profiles modelled at 35℃ and 5℃ compared to 20℃ and 0℃ test data.

6.5.5 Step cycling

A step cycling program was used to verify the voltage recovery during periodic rests. Figure 6.27 shows the results of comparing test data of a 0.315A discharge with periodic 1 hour rests to a model of the same profile. The model used for this first comparison did not incorporate the capacity recovery effect and, as a result, the model predicts that the discharge ends earlier than the real cell did during test.

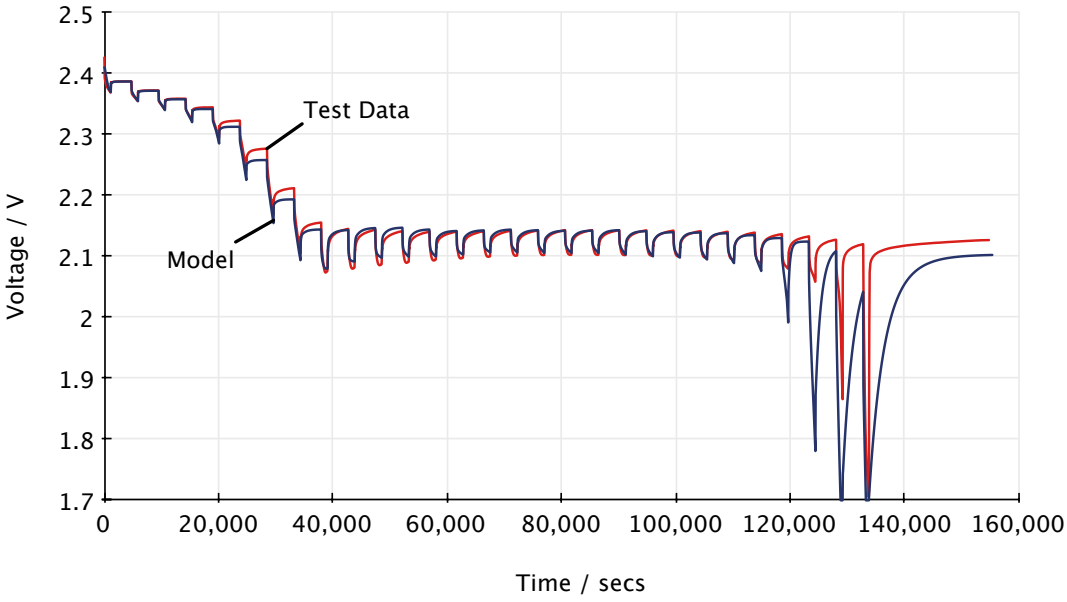

Figure 6.27: Comparison between model and test data of a 0.315A discharge with periodic 1-hour rests. The capacity recovery function is disabled in the model.

Enabling the model's capacity recovery function described in Section 6.3.4 shows an improvement to the prediction of the cell's available capacity, as illustrated in Figure 6.28. The value of the coefficient k_R in Equation 6.39, which determines how quickly capacity is recovered in rest periods, is not well defined and is likely to be rate, SoC and temperature dependent. To obtain the results in Figure 6.28 the value of k_R was taken to be 0.02. A full characterisation of k_R is desired if capacity prediction is to be improved at variable rates and temperatures. A portion of this graph is shown in more detail in Figure 6.29.

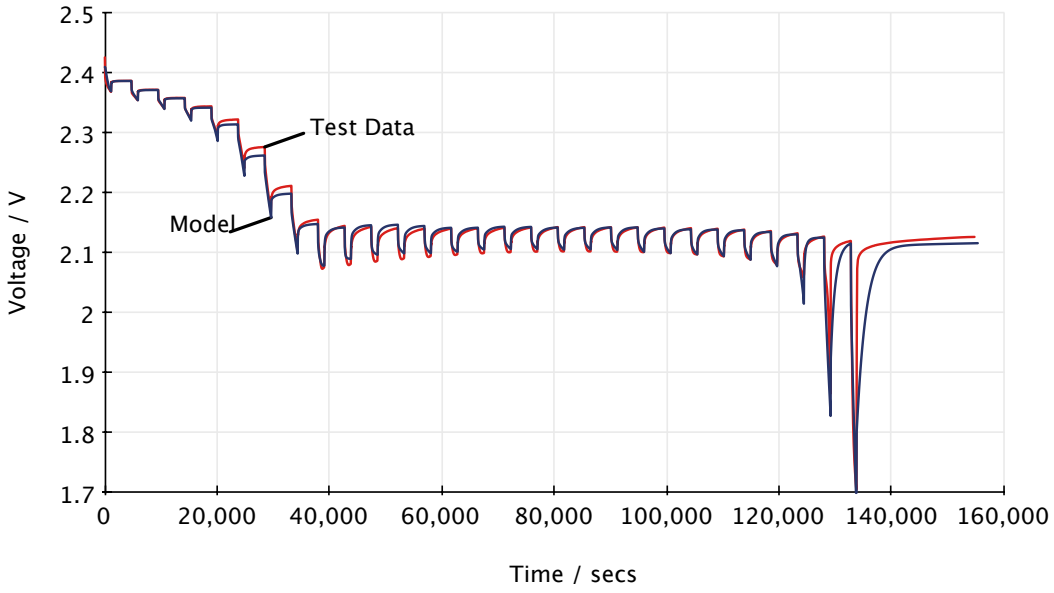

Figure 6.28: Comparison between model and test data of a 0.315A discharge with periodic 1-hour rests. The capacity recovery function is enabled in the model.

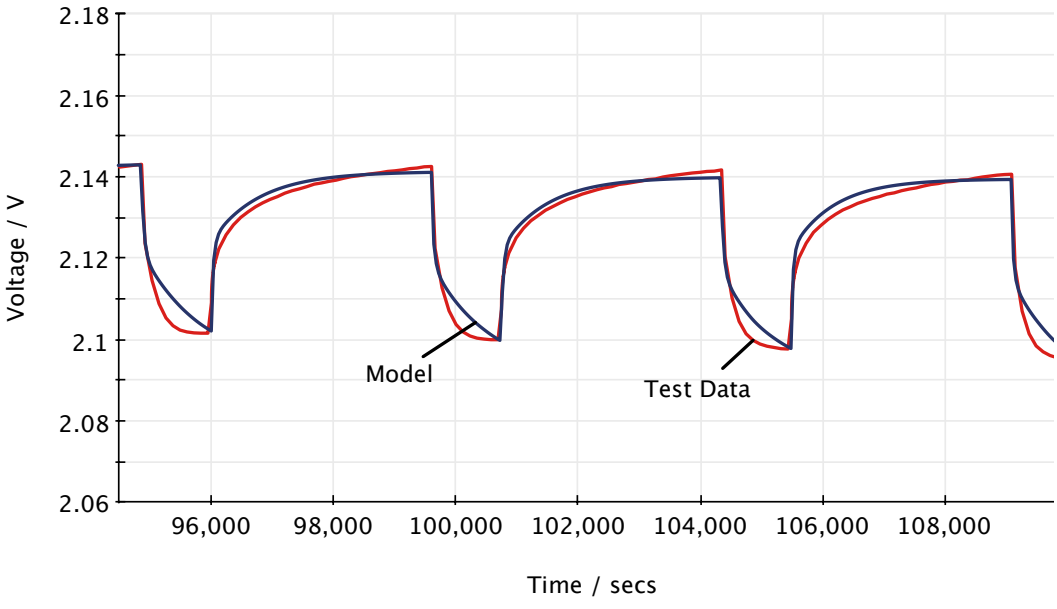

Figure 6.29: A detail of Figure 6.28 to show the accuracy of the resistances and capacitances

6.6 Cell to Battery Conversion

So far, the electrical response of a single cell has been considered. The model has been written to output results of different size or topology of battery such as s-p, p-s or p_1-s-p_2 (addressed in Chapter 7), assuming that, in the future, cells will be manufactured in bulk and be more closely matched. The conversions between cell and battery characteristics are given in Table 6.1, where $p_1 = p$ and $p_2 = 1$ for both the s-p and p-s topologies.

Cell	**Battery**
EMF	$EMF * s$
V_{term}	$V_{term} * s$
$Capacity$	$Capacity * p_1 * p_2$
$Resistance$	$(Resistance * s)/(p_1 * p_2)$

Table 6.1: Cell to battery parameter conversions

6.7 Conclusions

In this chapter an electrical, thermal and capacity model of a lithium-sulphur cell was proposed in an equivalent circuit format, having not been previously described in the literature. Many battery types have been successfully modelled using this approach and, as the equivalent circuit format is the preferred modelling technique for the spacecraft power systems designer, this approach also fits the proposed application well. The equivalent circuit model presented in this chapter showed that the Li-S cell has the ability to be modelled in this format, with useful results. The various resistances and voltage recovery effects were modelled as well as self-discharge and capacity fade effects. However, the complexity of the Li-S chemistry means that the model also has additional complexities not necessarily seen in other cell types.

Several issues affected the final model design. The formation of the Li_2S layer in the second discharge region blocks access to the available active materials, reducing the available capacity as current rate increases. A novel "split capacity" approach was used to address this issue, so that the capacity available in the first discharge region remains unaffected. A rate

dependent resistance factor was also necessary to account for the apparent increase in diffusion resistances at lower current rates, likely due to the increase in dissolved lithium polysulphides in the electrolyte. Figure 6.16 showed that, at high rates, the resistance correction factor begins to be over compensated. The fit given to the data in Figure 6.9 would benefit from additional data points at high current rates to improve accuracy, should a high rate application be deemed necessary.

Another effect that had implications for the modelling of the Li-S cell is the capacity recovery that occurs during rest periods. This recoverable capacity is significantly higher than that found in Li-ion cells, and is often ignored in such models. In the model presented in this work, an internal equivalent current was used to model the capacity recovery effect. The complexity of the recovery processes and the many interdependencies (e.g. temperature, current rate, state of charge) makes this effect extremely difficult to model, especially with restricted information of the specific chemical composition of the cell. The results of the step-cycling tests given at various temperatures and rates in Chapter 5 illustrate the complexity of continual current interruptions and the discernible effect they have on the voltage response. This not only had implications for the testing methodology but may also indicate a limitation on the modelling method, i.e. a more detailed understanding of diffusion coefficients that characterise the chemical species of the specific cell may be needed for a fully accurate model.

In conjunction with the electrical and capacity models the thermal model presented allows the temperature of the cell to be calculated based on its thermal characteristics, the load current and the environment in which it is operating. The result of this calculation allows the temperature dependency of the electrical circuit components to be used.

The degradation of the Li-S cells appeared to vary significantly and sometimes unpredictably, depending on different factors associated with both the use and storage conditions of the cells. These factors have implications for the overall predictability of the cell's performance and its applications. The effect that cell history has on performance, especially partial DoD cycling and high rate cycling, may require further investigation for future cell modifications.

REFERENCES

[1] Y.V. Mikhaylik and J. R. Akridge, "Low Temperature Performance of Li-S Batteries," *Journal of The Electrochemical Society*, vol. 150, no. 3, pp. A306-A311, 2003, A28.

[2] S. Castillo, N. Samala, K. Manwaring, B. Izadi, and D. Radhakrishnan, "Experimental Analysis of Batteries under Continuous and Intermittent Operations," in *Proceedings of the International Conference on Embedded Systems and Applications*, 2004, pp. 18-24.

[3] Venkat Rao, Gaurav Singhal, Anshul Kumar, and Nicolas Navet, "Battery Model for Embedded Systems," in *Proceedings of the 18th International Conference on VLSI Design held jointly with 4th International Conference on Embedded Systems Design (VLSID'05)*, 2005.

[4] Carla F. Chiasserini and Ramesh R. Rao, "A Model for Battery Pulsed Discharge with Recovery Effect ," in *Wireless Communications and Networking Conference, 1999. WCNC.*, vol. 2, 1999, pp. 636 - 639.

[5] M.R. Jongerden and B.R. Haverkort, "Battery Modeling," Centre for Telematics and Information Technology University of Twente, Enschede., Technical Report TR-CTIT-08-01, 2008. [Online]. http://doc.utwente.nl/64556/1/BatteryRep4.pdf

[6] J. Zhang, C. Song, H. Sharif, and M. Alahmad, "An Enhanced Circuit-Based Model for Single-Cell Battery," in *Applied Power Electronics Conference and Exposition (APEC), 2010 Twenty-Fifth Annual IEEE*, 2010, pp. 672 - 675.

CHAPTER 7

FUNCTIONAL REQUIREMENTS FOR A LITHIUM-SULPHUR BATTERY MANAGEMENT SYSTEM

In this chapter the results from the abuse, swelling and string tests are given and analysed. These results are used, in conjunction with the cell level tests, to recommend a battery topology suitable for the Li-S system, to advise on the required functionality of a Li-S battery management system (BMS) system and to propose applications for the Li-S cell in the space industry. Thoughts on the construction of a battery pack suitable for Li-S are also discussed.

7.1 Battery and Abuse Testing

7.1.1 Open circuit voltage tests

Monitoring the open circuit voltage (OCV) of a cell resting at 100% SoC showed that a new cell typically took 15 days to reach the swelling voltage range. Once achieving a swelling potential, the cell remained within the swelling voltage range for an additional 27 days. This information is important for specifying the level that the BMS is required to protect against undesired swelling, as discussed further in Section 7.1.4.

7.1.2 Over/under voltage tests

In Section 4.4.2 a test was described where two cells were repeatedly cycled to either the upper safety voltage limit of 2.8V or lower safety voltage limit of 1.05V. The voltage profiles associated with this abuse testing are given in Figure 7.1. Figure 7.1(a) shows that very little additional capacity enters the cell during the charge period between 2.5V and 2.8V. The overcharged cell was able to continue cycling for the full 20 cycles, reiterating that charging to voltages between 2.5V and 2.8V is not definitively unsafe at low cycle counts. Figure 7.1(b) shows that an additional 10% capacity is available from the cell if the lower cut-off voltage is reduced from 1.7V to 1.05V.

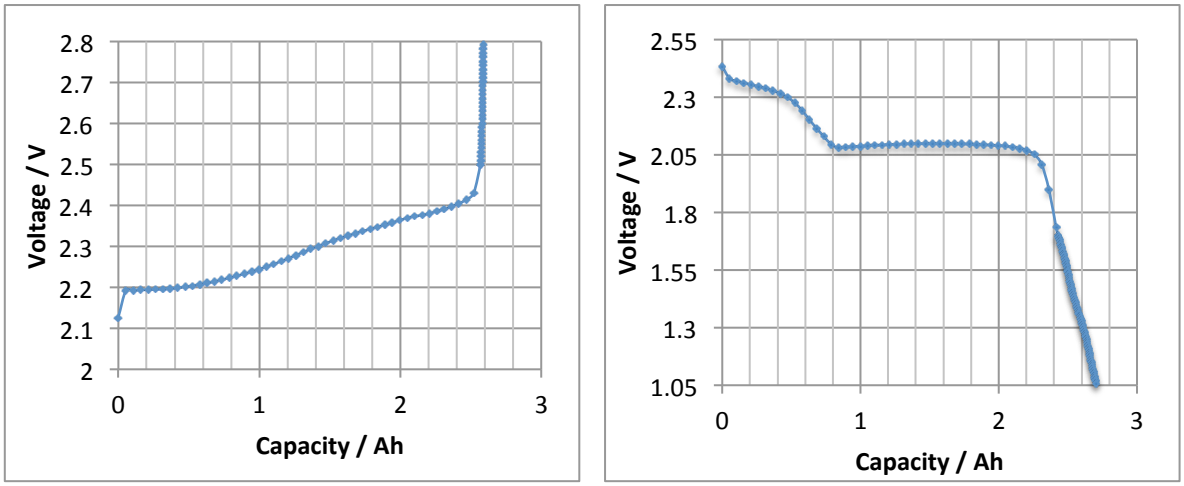

(a) (b)

Figure 7.1: Voltage profile of the Li-S cell during (a) overcharge and (b) overdischarge

The effect that overcharge and overdischarge has on discharge capacity is displayed in Figure 7.2. There was a linear capacity fade of ~37mAh per cycle. This fade rate is over 40% higher than that seen in the repeated SCM cycling (~26mAh per cycle), results of which were given in Section 5.4.2.

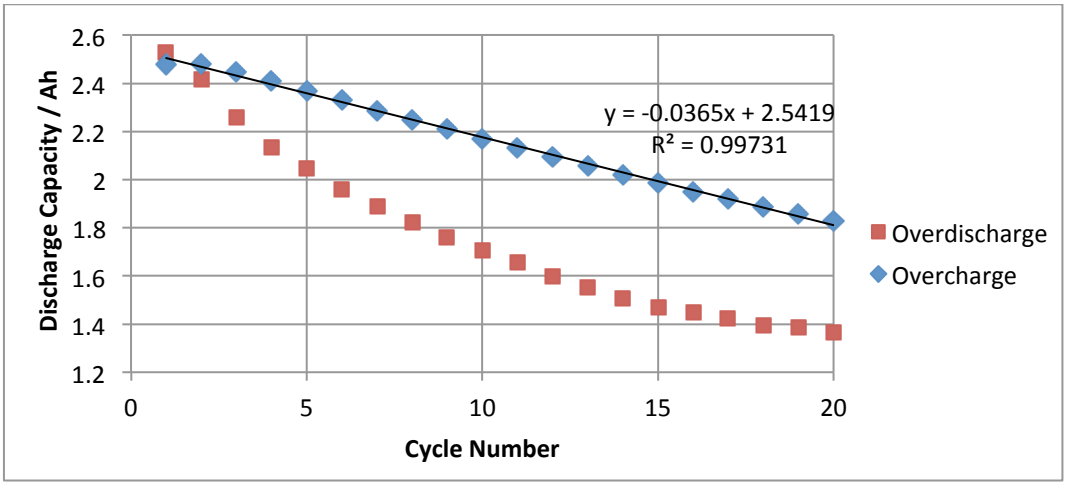

Figure 7.2: Discharge capacity of a Li-S cell following an overcharge to 2.8V (note suppressed zero – differences are magnified)

The cell that was cycled between its lower safety voltage limit of 1.05V and an upper limit of 2.5V similarly completed 20 cycles without rupturing. The discharge capacities found at each cycle are also displayed in Figure 7.2. There is not an obvious linear fade rate as with the overcharged cells, however there is (on average) a capacity loss of 58mAh per cycle, which is more than twice as high as seen in the repeated SCM cycling.

The discharge capacity available between the normal cut-off voltage of 1.7V and the safety cut-off voltage of 1.05V is 0.28Ah, as shown in Figure 7.1(b). Increasing the discharge capacity by ~10% may seem like a benefit, but there is a trade-off between the capacity gain and the increase in degradation to cycle life and possible safety issues. In a cell whose cycle life is already limited this extra capacity gain does not benefit the performance of the cell enough to warrant the additional capacity fade, especially for applications that require a long cycle life. In a work conducted on Sion Li-S cells by J. Jeevarajan [1] the cells were cycled between voltages of 2.5V-1.85V [2], implying that the small amount of capacity lost by not discharging to 1.7V is offset by an increase in cycle life, although this was not explicitly stated.

On test completion the overcharged cell had a thickness of 15.2mm, while the overdischarged cell was 18.9mm thick. Both cells were thus over the 15mm limit of what is considered to be an acceptable level of thickness as indicated by the manufacturer. Cell temperature monitoring showed that temperatures did not exceed 26℃ in the case of the overdischarged cell and did not change by more than 2℃ from the ambient in the case of the overcharged cell.

The results of this test show two things. Firstly, the cells were cycled outside of their normal operating range without rupturing, although an unacceptable level of swelling was seen after 20 cycles, which could be taken as a precursor to rupturing. Overdischarging the cells gives an approximately 10% increase in capacity, which could be seen as an advantage. In launch vehicle applications, where primary batteries are commonly used, there is only the requirement for one discharge. In this case, the extra capacity gained outweighs the degradation caused. This theory requires the cells to undergo stringent safety testing, including how the mechanical structure of the cell casing can accommodate or inhibit swelling. The second point is that, for applications where a good cycle life is required, such as in LEO and GEO, it is very important for the BMS to keep the individual cells in the battery from exceeding their operational voltage limits of 1.7-2.5V. In an unbalanced string of cells, the cells that are allowed to exceed these limits age differently to those kept within them, reducing the life of the battery and increasing the risk of failure.

7.1.3 Series string test

In the series string test described in Section 4.4.3, five cells were connected in series before undergoing twenty 0.315A cycles with their performance monitored. Unfortunately, the Maccor program encountered some problems at the beginning of the test and the cells were forced to remain at rest, in a charged state for a number of days before the test began. This was an undesirable situation because, although the cells had been matched in capacity and coulombic efficiency as closely as possible prior to the test, the self-discharge characteristics of the individual cells were unknown. Varying self-discharge characteristics could have had an effect on the balance of the cells at the beginning of the test. In addition, storage at high states of charge is not ideal and the cells could have degraded in a non-uniform manner. Nevertheless, prior to the first string discharge the difference between the maximum and minimum voltages did not exceed 4mV, indicating that the spread in the severity of self-discharge between cells is low. In support of this, data from the 24 cells that had been stored below 10% SoC for 263 days prior to their first screening showed a voltage spread of only 14mV, although there is no data to suggest the spread of self-discharge values at high states of charge across a cell batch. At high states of charge, EMF is a good indicator of SoC and a 4mV voltage difference represents a SoC variation of less than 1%. Spacecraft cell-balancing electronics can balance Li-ion cells to within ±5mV [3].

In Chapter 2 the main causes of cell imbalance were given as being due to differences in capacity, internal resistance, self-discharge and temperature gradients, assuming that cells do not intentionally start at different states of charge. The cells in this test were physically separated from one another and kept in a thermal chamber of 20°C ± 2°C, so were not subject to thermal gradients. SCM and internal resistance tests conducted on each individual cell prior to the string test gave an indication of the range of internal resistances and discharge capacities. Figure 7.3 shows the charge and discharge capacity of each cell while Figure 7.4 compares their internal resistance. These graphs show that the difference between the highest and the lowest discharge capacity is 0.06Ah, a spread of around 2%. There is a

correlation between results; cells with the lowest resistance have the highest discharge capacity. This is expected, as cells with a lower capacity have been subject to irreversible capacity loss by the precipitation of irreversible Li_2S on the electrodes. This Li_2S layer increases the resistance of the cell.

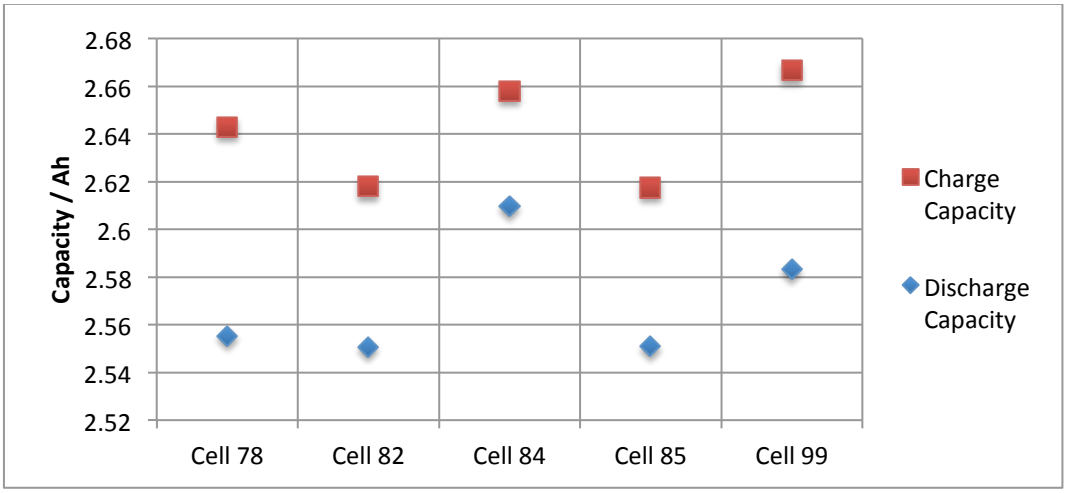

Figure 7.3: Cell capacities of string test cells prior to test.

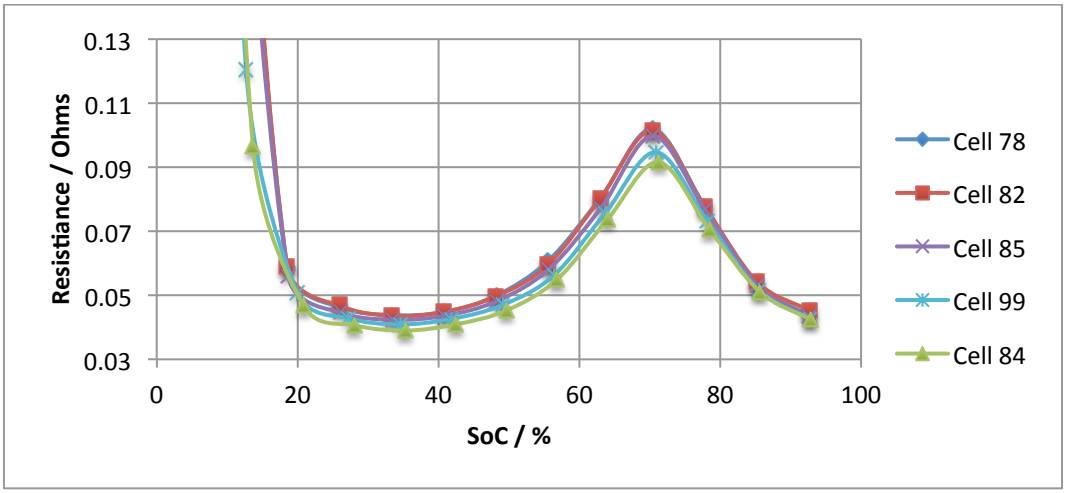

Figure 7.4: Ohmic resistance during discharge of cells prior to string test.

There was a maximum resistance variation of 10% in the 5 cells used for this test, which is comparable to a batch of lithium-ion cells [4]. Internal resistance differences only affect the terminal voltage of the cells under load; they do not affect the cell's state of charge and so any variations in individual cell voltages while the cells are cycling does not necessarily indicate a state of charge imbalance.

The highest discharge capacity was recorded as 2.61Ah for Cell 84 and the lowest at 2.55Ah for Cell 82. Connected in series, the string is dominated by the weakest cell. If the string is discharged from 100% SoC by 2.55Ah, Cell 82 will reach its cut-off voltage before Cell 84 and the current is cut before Cell 84 is fully discharged. This leaves a 2.3% difference in SoC between the highest and lowest cell.

The voltages seen at the end of charge and discharge for each cycle are displayed in Figure 7.5 and Figure 7.6 respectively. At the end of the first discharge, Cell 82 indeed reached the cut-off voltage of 1.7V first because it has the lowest cell capacity and the highest resistance. The discharge current that was applied to the whole string is cut at this point and so the remaining cells in the string are not fully discharged.

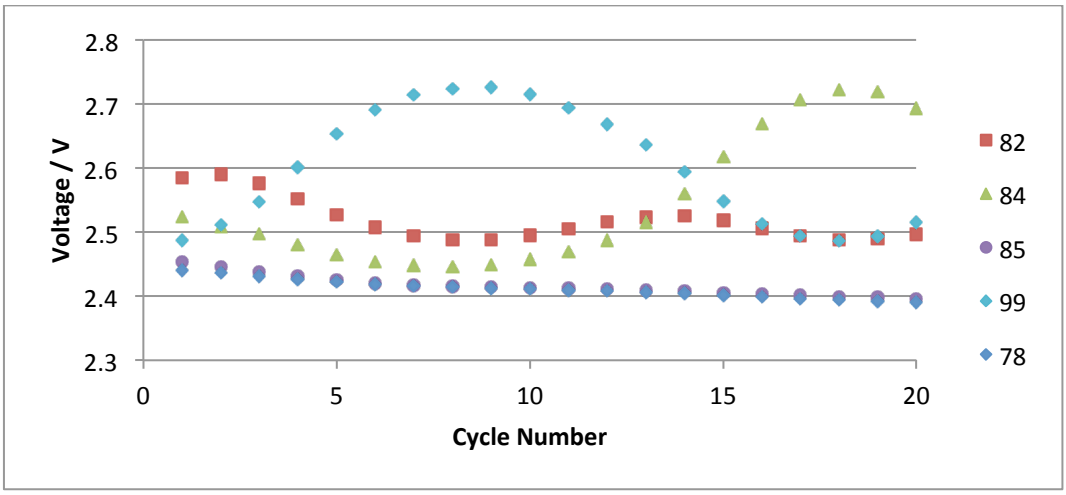

Figure 7.5: End of charge voltages for each cell in the string

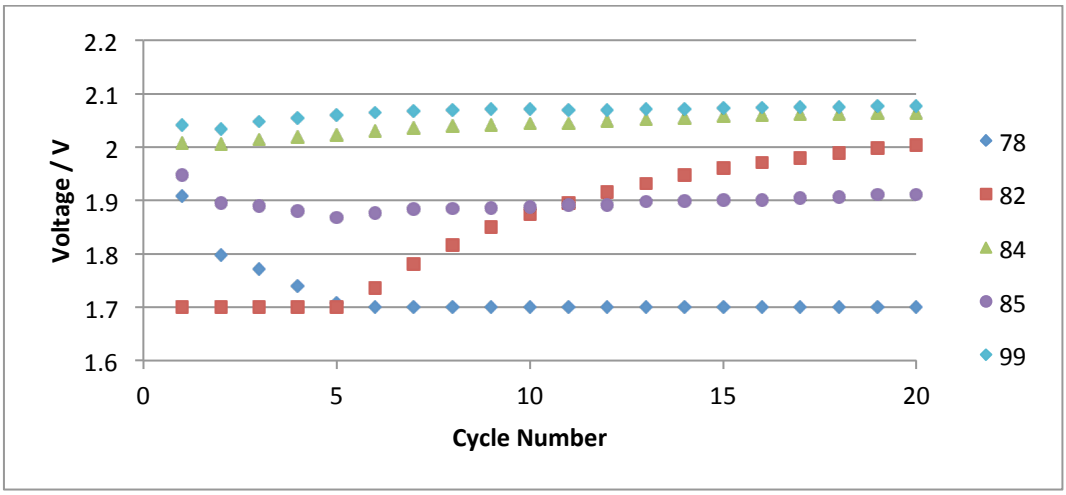

Figure 7.6: End of discharge voltages for each cell in the string

In the subsequent charge Cell 82 reaches the highest voltage, again because of its lower capacity and higher resistance in comparison to the other cells. At this point, Cell 82 and 84 are overcharged while Cells 78, 85 and 99 are undercharged, because the current was stopped when the string voltage reached 12.5V, not when an individual cell reached 2.5V. The upper voltage of individual cells was limited to 2.8V, but this limit was never reached.

The voltages that the cells return to in the rest period following a charge or discharge gives a better indication of the SoC imbalance because the effect of resistance variations are reduced, and can be seen in Figure 7.7 and Figure 7.8.

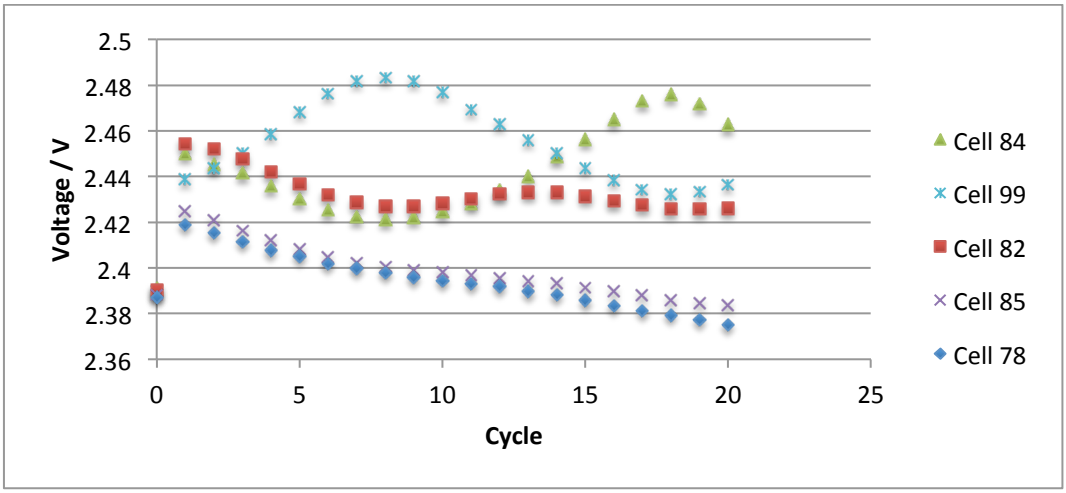

Figure 7.7: EMF values of individual cells at the end of rest before discharge commences

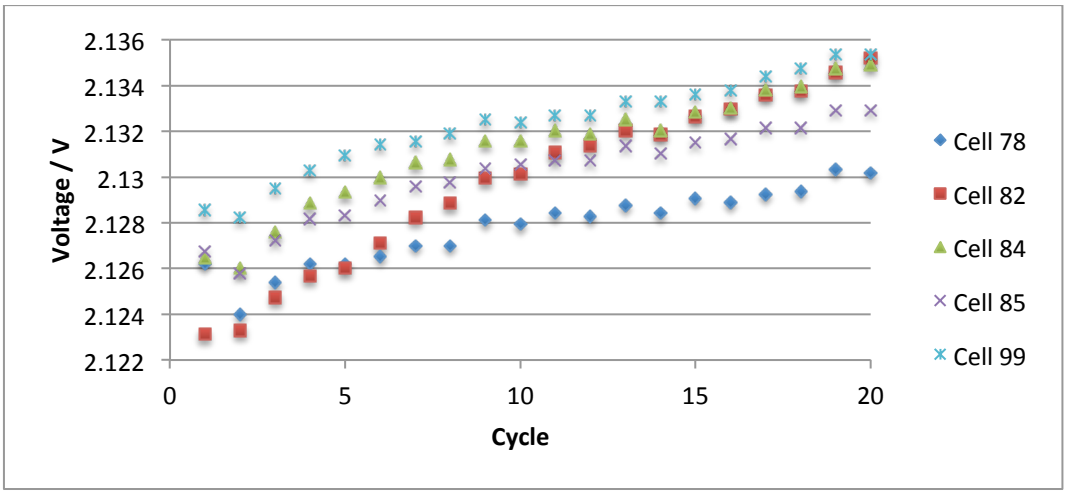

Figure 7.8: EMF values of individual cells at the end of rest before charge commences

These figures show that the terminal voltage imbalance seen in Figure 7.5 and Figure 7.6 has a large contribution from resistance variations but also includes a contribution from capacity and SoC variations. As the results in these figures were taken after only 30 minutes of rest, they may not have fully settled to their final EMF value, and hence the resistance factor cannot be completely excluded. A 30-minute rest was chosen so as to allow cell voltage time to recover and to allow cell temperature to stabilise whilst also limiting the possibility of additional imbalances caused by self-discharge.

An interesting result that arises from these graphs is that the cell behaviour changes during cycling. This is evident in Figure 7.7, which shows that the "weakest" cell changes as cycle number increases. The pre-test resistance and capacity results gave a clear indication of how the first few cycles would emerge, but after continued cycling the cells' behaviour became unpredictable. The underlying reasons for this lie with the electrochemical response to overcharge and the variation in DoD across the string. This result implies that the predictability of battery performance could be limited.

As previously stated, prior to the first discharge there was only a 1% deviation in SoC. The voltage deviation after the first charge was in the region of 35mV and this deviation generally increased with cycle number, as shown in Figure 7.9, to around 100mV. The deviation in EoD voltages remained constant at 5mV, although this is not surprising as EMF is not a good representation of SoC in the second discharge region. At high states of charge, 35mV represents a ~4% difference in SoC whereas 100mV represents a ~10% SoC difference.

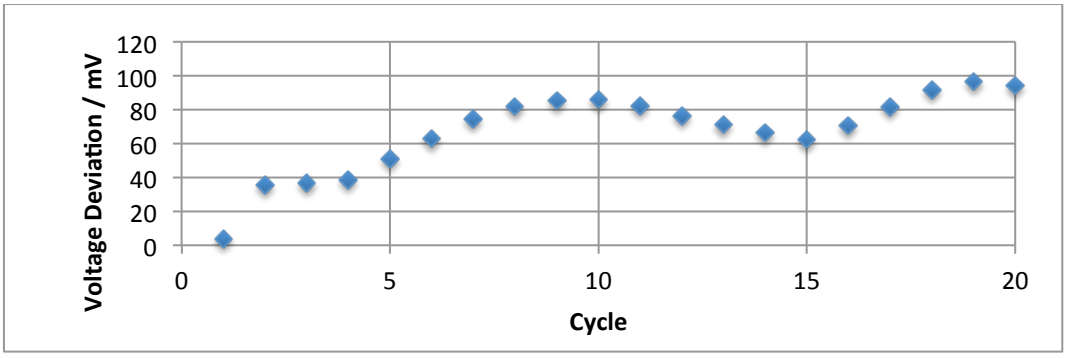

Figure 7.9: Voltage deviation between cells after a 30-minute rest following a charge

LEO cell-balancing electronics generally limit cell voltage spread to within 50mV [5] although smaller values are also seen. With this figure in mind, the voltage deviations seen in the Li-S cells are not unmanageable. A continuation of this test using a larger number of cycles is required to observe the long-term cycling effects and to fully understand the reasons behind the apparent improvement in cell balance between 10 to 15 cycles, and the subsequent decline up to 20 cycles. There appear to be many factors and dependencies that contributed to the imbalance of these cells, such as capacity, coulombic efficiency, resistance, rate of degradation, self-discharge, DoD and level of overcharge. In addition, a real battery pack would have all cells closely packed together and so thermal gradients should be considered as well as any nonlinear current drain the battery management electronics may cause. Cells that are allowed to exceed 2.5V have been shown to degrade faster than cells kept below this voltage and could also have different levels of self-discharge. The voltage at which discharge is cut may also affect the uniformity of cell degradation. In the string test conducted, the cells were not constrained to a maximum of 2.5V each and the voltage deviation generally increased to 100mV after 20 cycles. The usable capacity of the string decreased by 41mAh per cycle, a 60% increase on standard SCM cycling as can be seen in Figure 7.10. The low capacity seen in the first cycle is an indication of the self-discharge that occurred while the cell was rested prior to the test.

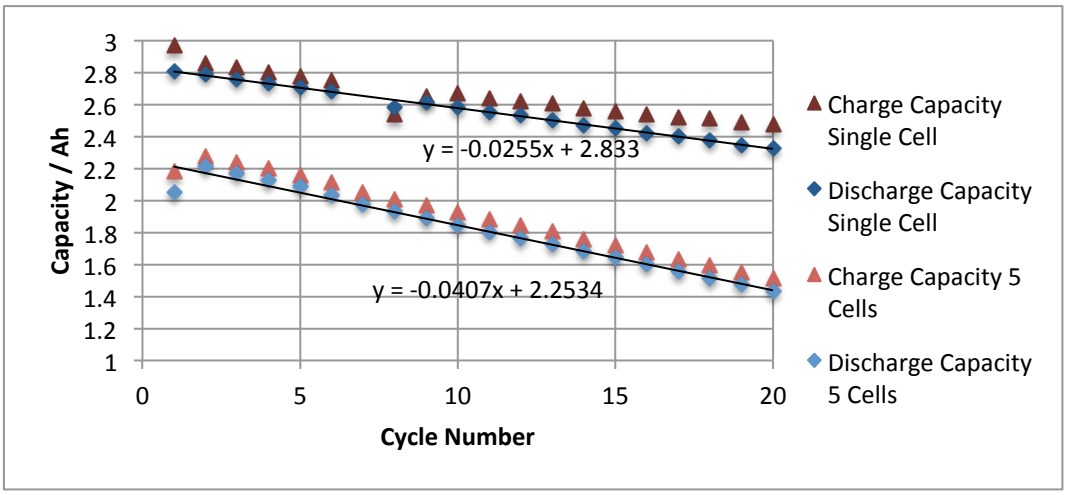

Figure 7.10: Decline in capacity of a serially connected string of 5 cells cycling at 0.315A, compared to that of a single cell.

The increase in fade seen in serially connected cells has major implications for cell to battery performance and, in a cell with an already limited cycle life, could be a major disadvantage. The results therefore indicate that a serially connected string of Li-S cells is highly dependent on circuitry to keep the cells' SoC balanced, if the full capacity of each cell and hence the cycle life of the battery is to be maximised. In Section 7.3.3 appropriate cell-balancing mechanisms are discussed. The results of this test also give criteria by which cells should be matched and restrictions on their handling to prevent causing unbalance accidentally.

- To avoid initial SoC discrepancies and non-uniform cell degradation cells should:
    - Be subject to the same environmental conditions prior to battery assembly.
    - Not be stored above 10% SoC or at temperatures exceeding 20°C.
    - Be chosen from as large a cell batch as possible (>25 cells).
- Cell characteristics to be taken into account when matching are:
    - Discharge capacity
    - Coulombic efficiency
    - Internal resistance
    - Self-discharge
    - Age

7.1.4 Swelling tests

It has been shown that lithium-ion cells tend to swell during charge and contract during discharge [6]. They also show an initial irreversible expansion during the first charge followed by reversible expansion and contraction in subsequent cycles. This natural swelling is due to the normal intercalation processes that occur in the electrodes of a lithium-ion cell and is not dangerous. The Li-S cells tested in this work arrived at the testing facility in an uncycled condition at an average thickness of 11.5mm ± 0.3mm. Measurements of all cells used in the swelling test showed that, prior to starting the test, each cell had remained within this range. This implies that any swelling that followed as a result of the initial screening cycles, which occurred 2 months before the swelling test started, was reversible over this

period of rest. Cell thickness measurements were taken at regular intervals during the SCM cycle, performed at the end of the swelling test. These measurements showed a clear thickness increase during charge followed by a contraction during discharge over a 2mm range, which draws clear comparisons to the lithium-ion chemistry. In [7] He et al. investigated the expansion and shrinkage of the sulphur electrode in Li-S cells during normal cycling. It was found that the sulphur electrode expanded during discharge and contracted during charge. This is due to the volume increase of the discharge products of the cell reaction. Conversely, the thickness of the lithium electrode was found to increase during charge and decrease during discharge, relating to the deposition and dissolution of lithium metal respectively. This work also showed that, on average, the two effects cancelled and that the overall thickness of the cell varied by around 2μm per layer. It is possible that the advancement of the Sion Li-S cell has seen improvements to the sulphur composite electrode that accommodates for high volume discharge products more effectively than in [7]. This may leave the changes to the lithium anode as the dominant effect and be the reason behind the overall expansion seen in charge and the contraction seen in discharge.

The main purpose of the swelling tests was to study the additional swelling effect, which occurs when a cell is rested at a voltage in the range 2.35 ± 0.03V and exceeds the 15mm limit of natural (and safe) fluctuations in cell thickness. Table 4.4 has been modified into Table 7.1 below to show the voltage and temperature at which the cells were rested and how many hours were spent under these conditions before the SCM cycle was implemented.

Cell Number	74	75	76	77	79	80	81
Swelling Voltage V/Volts	2.35	2.35	2.35	2.37	2.33	2.35	2.35
Ambient Temp T/ °C	20	20	20	20	20	40	40
Time spent at V/hours	144	144	28	144	144	28	28

Table 7.1: Summary of cell conditions for swelling tests

Cell thickness measurements began after each cell had undergone the pre-cycling and resistance tests described in Chapter 4 and had begun resting at the voltage V specified in Table 7.1. At this point the average thickness of the cells was 14.0 ± 0.6mm, which was expected as all the cells had been charged to their respective voltages and so were naturally swollen.

From previous experience, it was expected that the cells would begin to swell within 24 hours. As previously discussed, a problem with a harness cable during the first screening tests caused a cell's program to suspend while the cell was at 2.35V. Because this incident occurred over a weekend the cell was not viewed until 1.5 days after the event, by which time the cell had reached ~18mm in thickness, as seen in Figure 7.11.

Figure 7.11: A new Li-S cell left to rest at 2.35V became swollen after less than 2 days

Monitoring of the cells during the dedicated swelling test, however, provided some unforeseen results. Figure 7.12 shows the thickness of cells 74, 75, 77 and 79 over a period of 6 days. Not only did these cells show no signs of swelling, regardless of resting voltage, there was an overall decline in cell thickness. This may be attributed to the self-discharge of the cells at these high states of charge, and the contraction that accompanies a normal discharge. This result was unexpected, both from the experience of the swollen screening cell and the strict operating advice issued by Sion. One hypothesis that could be pursued is that the occurrence and severity of physical swelling in Li-S cells is a function of the age of the cell, a feature that is not discussed in the literature.

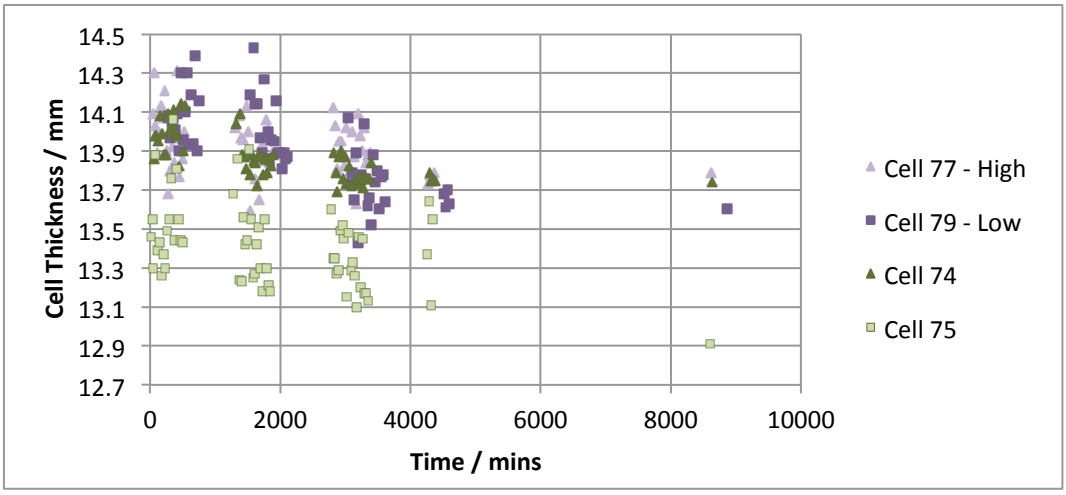

Figure 7.12: Thickness of cells resting in the swelling voltage range, at 20°C, over a period of 6 days. Gaps in the data represent overnight periods where measurements were not taken.

Further tests were conducted on the cells to determine the effects of temperature on the rate and severity of swelling. Cells 80 and 81 completed the pre-cycling and resistance tests in a thermal chamber of 20°C. When they reached their resting voltage of 2.35V the temperature of the thermal chamber was increased to 40°C. Figure 7.13 shows the results of thickness measurements made on these cells from the point at which the temperature was increased. The gap in data is due to measurements only being taken during the daytime.

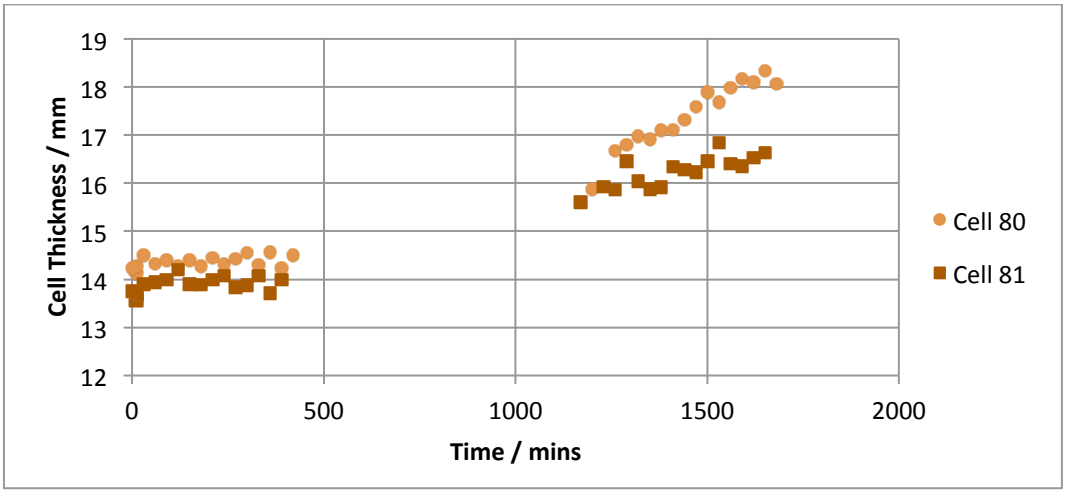

Figure 7.13: Thickness of cells resting at 2.35V, at 40°C, over a period of 28 hours.

It is clear from these results that, despite the age of the cells, swelling over 15mm did occur. The actual point at which swelling began occurred overnight, however it can be said that, at 40°C, the cells began to swell at between 7 to 14 hours of rest inside the swelling voltage range. If the age of the cells affect the rate of swelling at 20°C, then the time before swelling begins in cells stored at 40°C may decrease for newer cells. It should also be noted that the maximum swelling seen here might have been larger had the cells been allowed to rest under these conditions for longer. Indeed, physical swelling may have been seen in cells resting at 20°C had more time been available for the test to proceed.

A comparison of cell capacity and resistance data was made in order to determine if the degradation of the cells was affected by the period of time spent at rest in the swelling voltage range. Each cell tested underwent an SCM cycle and a resistance cycle both before and after the test. A comparison between cells 74, 75 and 76 revealed that cell 74 experienced the largest increase in cell resistance of around 8% while cell 75 showed a 5% increase and cell 76 showed a 3% increase. As cell 76 spent the least time in the swelling voltage range it would indicate that resistance increase might be dependent on time spent in the range.

The disparity between results for cells 74 and 75, which were both subject to equal test conditions, showed that degradation is not uniform. As cell 74 started with a slightly higher resistance than cell 75 before the test, it is also possible that resistance increase is dependent on the level of resistance itself. This effect would be difficult to characterise and a complicated function would be required to accurately predict degradation. Testing should be repeated on a larger number of cells in order to fully characterise degradation in the swelling range. Examples of the resistance increases that occurred in cell 74 are displayed in Figure 7.14 and Figure 7.15.

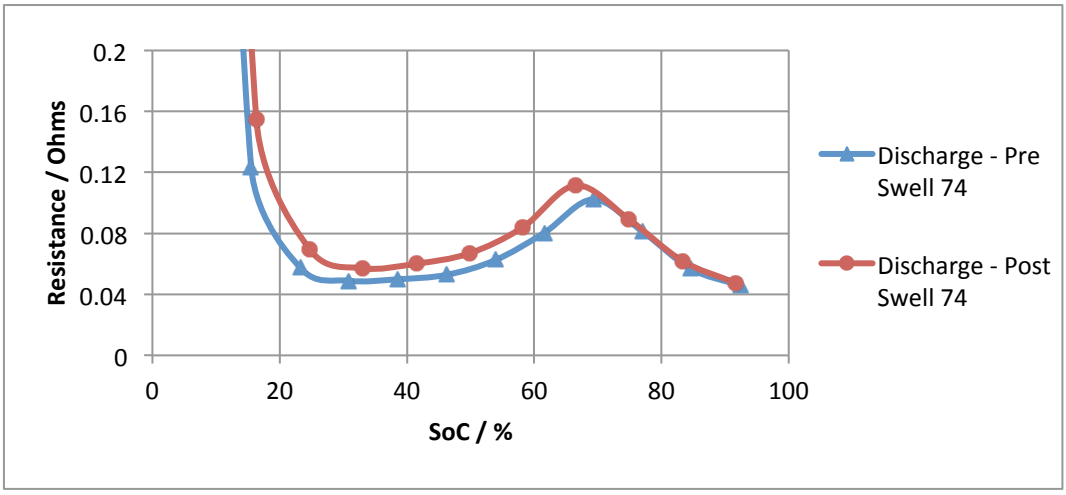

Figure 7.14: Comparison of discharge Ohmic resistance in cell 74, before and after resting in the swelling voltage range for 6 days.

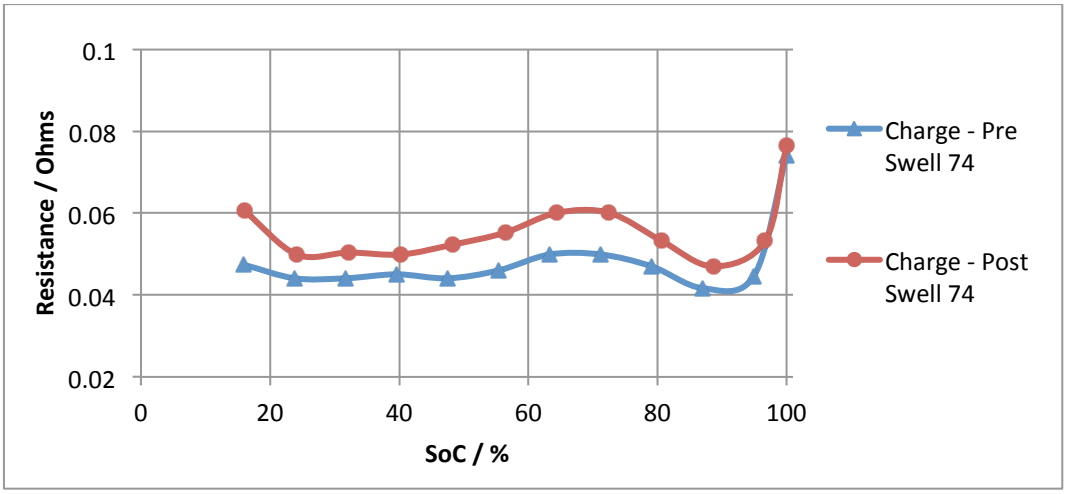

Figure 7.15: Comparison of charge Ohmic resistance in cell 74, before and after resting in the swelling voltage range for 6 days.

During discharge the Ohmic resistance of the cell appears to have increased more severely for the second discharge region. The charge resistance of the cell has increased over all states of charge. In conjunction with these resistance increases a decrease in cell capacity is noted. Figure 7.16 shows the discharge capacities of cells 74, 75 and 76 before and after the rest period at 2.35V. The results of these tests show that, despite there being no evidence of the expected physical swelling of cells resting at 20°C, there was an increase in the cells' resistance and capacity fade. This increase exceeds that of what would be expected of a cell resting for 1-6 days at a voltage outside of 2.35 ± 0.03V.

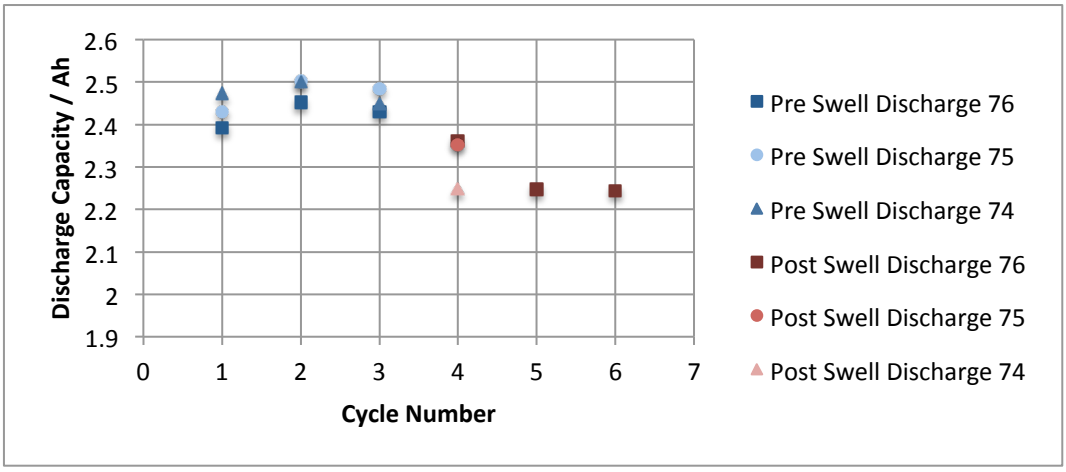

Figure 7.16: Comparison of cell discharge capacities before and after resting at 2.35V

Cells 77 and 79 were tested under the same conditions as cells 74 and 75 except that they were held at different voltages. Cell 77 began resting at 2.37V whereas cell 79 began resting at 2.33V, both within the swelling voltage range. Cell 79 spent only 2.5 hours actually in the lower end of the swelling voltage range before the voltage dropped below the lower threshold. Figure 7.17 shows the discharge resistance of cell 79 before and after the rest. As expected, there is little difference between the two measurements.

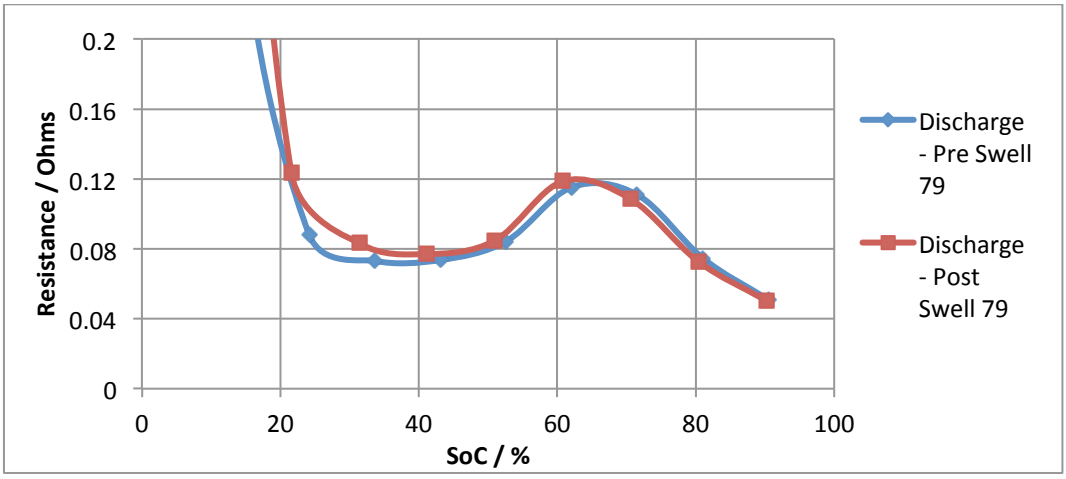

Figure 7.17: Comparison of discharge Ohmic resistance in cell 79, before and after rest.

Figure 7.18 shows the discharge resistance of cell 77 before and after the rest. There is no appreciable difference between these results and the results seen in cells 74 and 75. This implies that the severity of the degradation caused by resting in the swelling voltage range does not have a high dependency on the actual voltage, but that resting at any voltage in that range for extended periods has a similar effect.

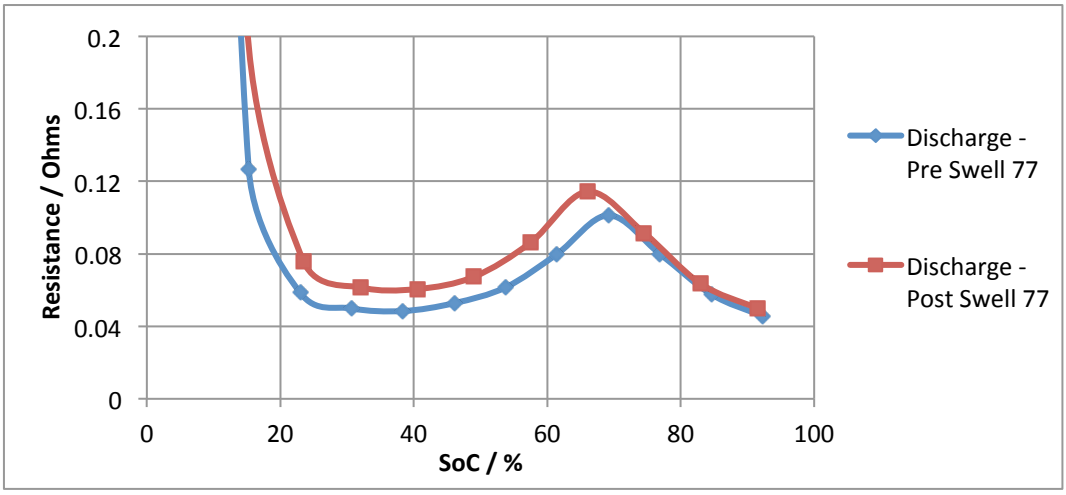

Figure 7.18: Comparison of discharge Ohmic resistance in cell 77, before and after rest

Cells 80 and 81 underwent the same test duration as cell 76, except that the ambient temperature at which the cells rested was 40°C. Figure 7.13 showed that that swelling did occur at 40°C and comparisons of the resistance increases and capacity degradations between cells 76, 80 and 81 indicate that both were more severe in the 40°C environment.

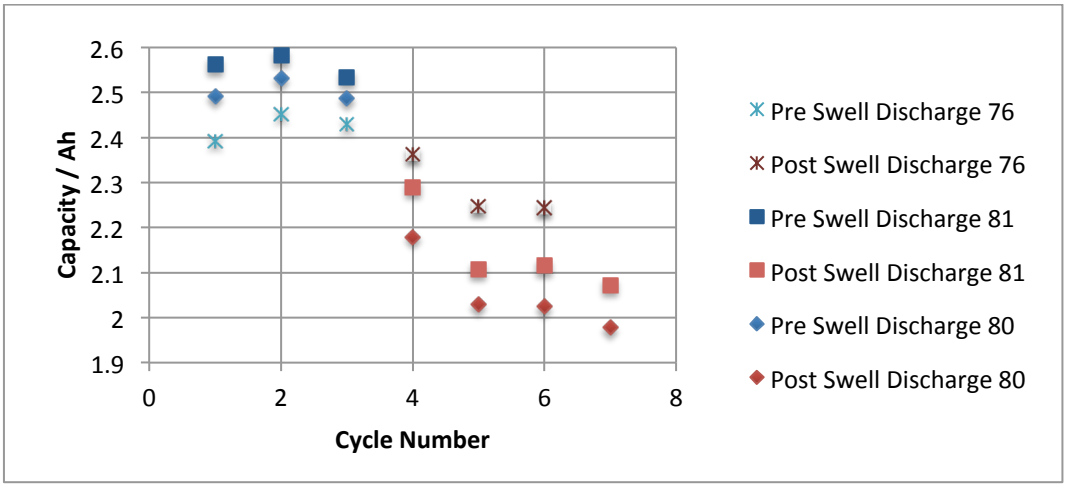

Figure 7.19: Comparison of discharge capacities of cells 76, 80 and 81 before and after rest

The capacity degradation data for these cells are displayed in Figure 7.19. The cells stored at 40°C experienced an increased capacity degradation of around 10% in the subsequent cycles, after the cells had returned to 20°C, when compared to cell 76. Cell 80 showed the greatest level of swelling and capacity degradation, exceeding the thickness of cell 81 by around 1mm. The cells tested at 40°C also showed higher levels of resistance increase, with a peak increase

of over 30%. The results for cell 80 are shown in Figure 7.20 and can be compared to that of cell 76 in Figure 7.21 as both cells spent the same length of time in the swelling range but at different temperatures. In cell 80 the increase in resistance was not limited to the second discharge region but was significant over all states of charge.

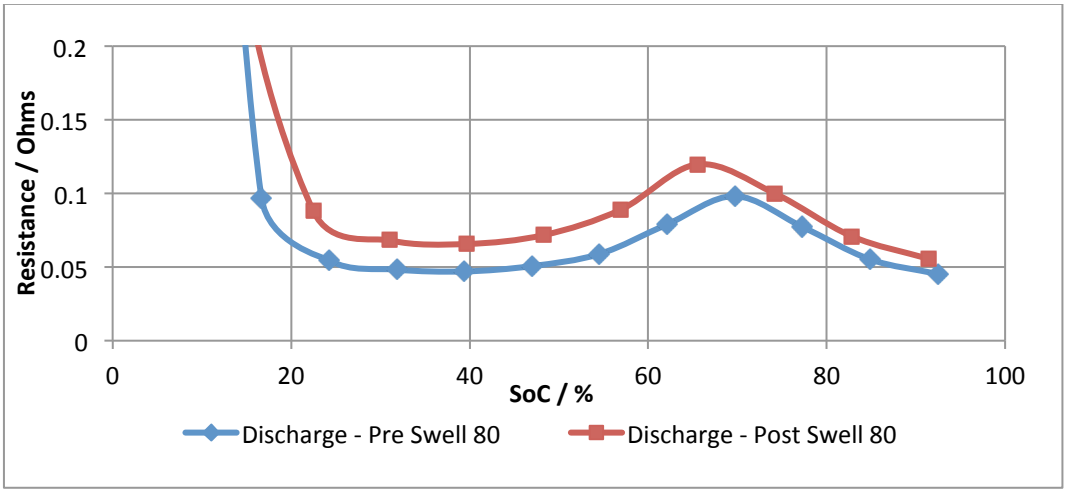

Figure 7.20: Cell 80 resistances, before and after 28-hour storage at 2.35V at 40°C.

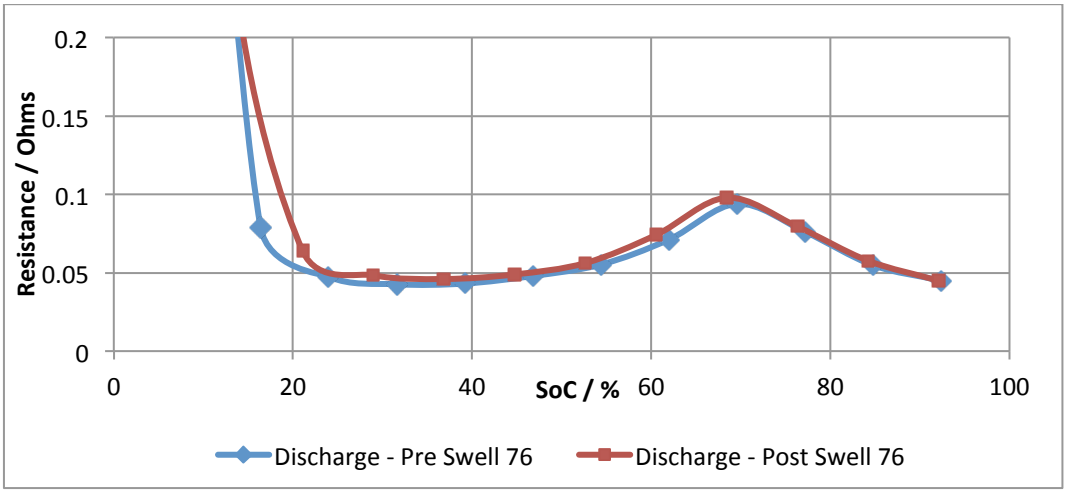

Figure 7.21: Cell 76 resistances, before and after 28-hour storage at 2.35V at 20°C.

7.1.5 Conclusions from testing results

The experiments described in this chapter were completed for a number of key reasons:

- Learning how the Li-S cell responds to abusive conditions.
- Aiding the design of a Li-S battery management system.
- Finding suitable applications for the Li-S cell.
- Providing information on the level of degradation caused by abusive conditions.

The overcharge and overdischarge tests showed that Li-S cells were able to cycle between their upper (2.8V) or lower (1.05V) safety voltage limits without overheating or rupturing, although increased levels of swelling were seen after 20 cycles. The rate of irreversible capacity loss is increased in both cases and is more severe during overdischarge. This means that unbalanced cells in a series string age differently if some cells are allowed to exceed their normal operating voltage limits whilst others are kept within them. The BMS must keep all cells in a series string within the designated operating range so as to limit the effect of non-uniform aging. Because the overdischarged cells showed a much more severe capacity loss on cycling the EoD cut-off voltage may have a significant effect on the life of the cell. The EoD voltage should be optimised for the application for which the cell is intended. A higher EoD voltage would sacrifice cell capacity but might significantly extend the cycle life of the cell. A lower EoD voltage may be considered for applications of very low cycle life (e.g. launch vehicles) where more capacity is obtainable but degradation is more severe.

The string tests conclusively showed that cell-balancing is a vital function for a Li-S BMS. The tests also showed that there are several contributions to the imbalance of series cells, namely resistance, capacity and state of charge variations. The voltage differences caused by a resistance imbalance was significantly higher than the other contributions, which means that balancing the cells under load risks causing a greater imbalance than was originally there. This in turn affects the design of the cell-balancing electronics, discussed further in Section 7.3.3. The string tests also showed the need for designing a rigorous cell selection algorithm to limit discrepancies in cell characteristics in serially connected cells, and parameters to match were outlined in Section 7.1.3.

The swelling tests provided interesting and unexpected results that aid the design of the battery management system. The amount of physical swelling that occurred when the cells rested in the swelling voltage range appeared to be dependent on the age of the cell. Aged cells resting in the swelling range at 20°C showed no signs of physical swelling, even after a week of rest. This contrasts with evidence of new cells becoming swollen after around a day

in the swelling range. Physical swelling was also dependent on ambient temperature, where aged cells stored at 2.35V at 40°C swelled past the acceptable thickness after only 7-14 hours in storage. Despite aged cells showing less tendency to swell test results showed that the level of degradation was increased in these cells, whether they showed physical signs of swelling or not. This degradation appeared to be independent of the actual voltage at which the cell rested once in the swelling range. The design of the protection circuitry in the BMS should therefore be based on voltage and time measurements rather than relying on the detection of physical swelling as an indicator of danger.

These tests also give results on the Li-S cells' response to abusive conditions that could be expanded in future work to allow such conditions to be modelled. Should an emergency situation occur on a spacecraft or a delay occur on the launch pad, ground engineers need to know how to keep the battery within its safe operating limits, the best remedial action to take and the level of deterioration that may occur should remedial action be delayed.

It is clear that the BMS system must be designed with both the application and the cell chemistry in mind. A Li-S battery requires careful management so that it can operate safely under the given conditions. In the remainder of this chapter the functionality of a dedicated BMS is explored and the testing results from this chapter and Chapter 6 are used to select the appropriate methods of implementing this functionality. However, before this can be accomplished, an investigation into an appropriate battery topology and suitable applications for the cell must be made.

7.2 Battery Topologies

The voltage and current required by the power system governs the arrangement, or topology, of cells in a battery pack. It is important that the cells are arranged efficiently so that these requirements are met, but also that the battery can respond to any cell or string failures by maximising the available energy and limiting damage to the battery. Before the BMS functionality can be considered the various options for a Li-S battery topology are explored.

In Chapter 2 the s-p and p-s battery topologies were described. The advantage of the s-p topology is that if a series string fails then it is only the battery capacity and not the voltage that is affected. Additional strings can be incorporated into the battery design in anticipation of this loss. For s-p batteries that comprise of unmatched cells, each cell would require monitoring and balancing electronics. For cells of low voltage, such as with Li-S, the number of cells connected in series may be very large and so the balancing electronics would constitute a large proportion of the BMS. The additional circuitry and individual connections that this requires dramatically reduces the reliability of the battery, which is not ideal for space applications. Additionally, the current drain on the battery would almost certainly be unacceptably high. At worst this risks overdischarging the battery and at best the power available to the system is highly reduced. The s-p topology is almost exclusively used in batteries where the cells are extremely well matched and do not require balancing.

In a p-s topology battery it is easier to incorporate cell-balancing electronics because it only requires one circuit for each parallel string, rather than one for each cell. Current drain caused by cell monitoring circuits is much less than in s-p batteries, and is shared between parallel cells. Battery manufacturers who use large-scale cells that aren't as well matched as small cells therefore favour the p-s topology. However, the battery requires additional protection in the form of bypass circuitry. In the event of a cell failing open or short circuit, the whole parallel string to which it is connected will eventually be lost and the voltage of the battery is reduced by the value of one cell voltage (although the capacity is not affected). There must be bypass circuitry included, so as not to create an open circuit in the battery. This circuitry must be able to handle the load currents the battery will experience. In addition, if the charge management system is set to charge the battery to its original voltage then this may cause each cell to be overcharged, which reduces the life of the battery.

The Li-S cells tested in this work were not produced in high batch numbers and were therefore not as highly matched as it is possible to achieve with lithium-ion cells. In addition the voltage of a single Li-S cell is only 60% of that of Li-ion, whereas their capacity is

comparatively higher. A Li-S battery of equivalent voltage and capacity to a lithium-ion battery would generally have more cells in series and less parallel strings. If, in the future, lithium-sulphur cells are produced in the same batch numbers as Li-ion then it is possible that the requirement for cell-balancing is negated and the s-p topology could be adopted. The p-s topology appears to be a more suitable arrangement for the Li-S cell; a string failure would cause an average voltage drop of 2.15V with no reduction in capacity, but suitable bypass circuitry must be employed and the charge management electronics would need to adjust to the new battery voltage in order to avoid overcharging the battery.

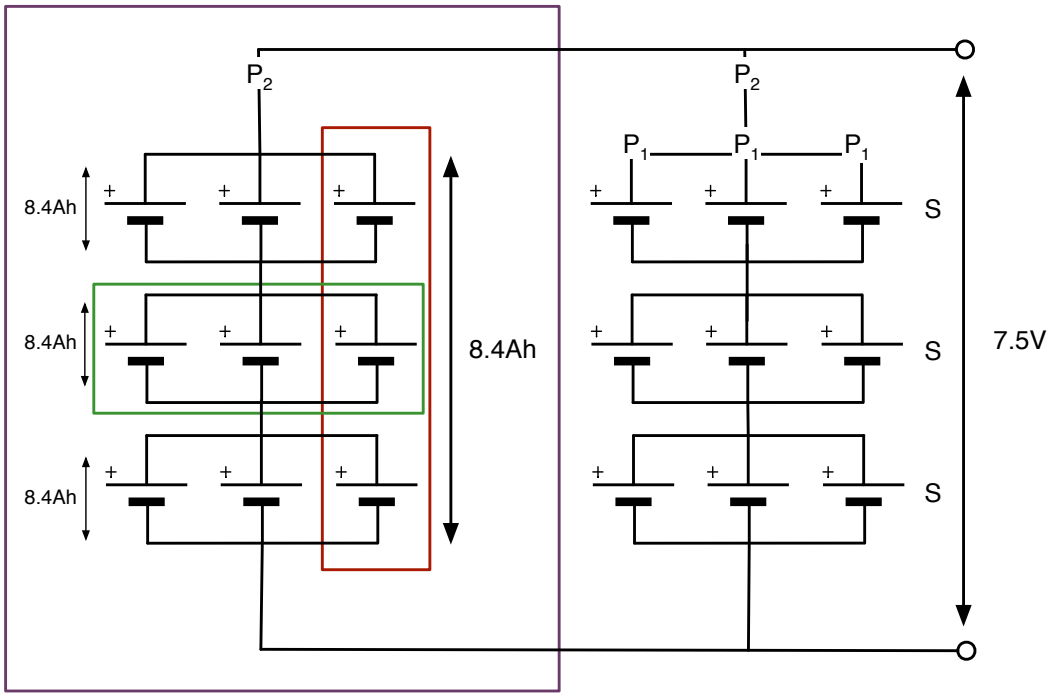

Figure 7.22: A $3p_1$-3s-$2p_2$ Li-S battery has a battery voltage of 7.5V and capacity of 16.8Ah

A compromise between these two battery arrangements would be to utilize a p_1-s-p_2 topology. An example of this topology can be seen in Figure 7.22, where the cell number and arrangement have been chosen for illustrative purposes only. In this battery topology the arrangement is similar to the s-p topology where 's' cells (circled red) are connected in series to form strings, which are then connected to each other in parallel 'p_2' strings (circled purple). The difference with the p_1-s-p_2 topology is that the 's' cells are in fact comprised of groups of cells (circled green) connected in parallel strings (p_1).

In this arrangement, the benefit of retaining full battery voltage in the case of a failure (as with the s-p topology) is preserved whilst reducing the number of cell-balancing circuits that would be required. However, a trade-off between number of balancing circuits and the amount of cell capacity the spacecraft designer is willing to lose in the case of a string failure must be made. Table 7.2 illustrates this trade-off for the p-s, s-p and p_1-s-p_2 equivalent battery to that in Figure 7.22.

Topology	Loss on string failure	Number of cell-balancing circuits
s-p	17% capacity, no voltage	18
p-s	No capacity, 30% voltage	3
$3p_1$-3s-$2p_2$	50% capacity, no voltage	6
$2p_1$-3s-$3p_2$	30% capacity, no voltage	9

Table 7.2: Comparison of battery topologies for a 7.5V, 16.8Ah Li-S battery.

If p_2 is maximised and p_1 has a value of 2, Table 7.2 shows that the employing the p_1-s-p_2 battery topology can halve the number of cell-balancing circuits if an increase in capacity loss can be tolerated in the event of a string failure. In the remainder of this chapter it is assumed that the s-p battery topology is unsuitable for a Li-S battery and that a battery designer would have to make an informed choice regarding the battery size and topology (using either the p_1-s-p_2 or the p-s topology) based on the power system and mission requirements.

7.3 BMS Specification for a Lithium-Sulphur Battery

Cell manufacturers remain optimistic about the future capabilities of the Li-S cell and improvements to cycle life and degradation are expected [8]. Li-ion cell technology started life in the same way until its chemistry and structure were optimised. It is not unreasonable to assume that at some point in the future the cell chemistry will be modified enough to improve the degradation and cycle life of Li-S to the point that they become a viable option for spaceflight. In preparation for this event the functionality of a battery management system designed to protect a Li-S battery should be considered.

The design of any BMS is highly dependent on the battery's application. An avionics launch vehicle battery for instance would require very little management as the battery is only discharged once and does not need to be recharged. A Li-S battery in LEO, however, would require more complex protection, the level of which depends on the mission. A small, short-duration CubeSat mission may not require life-extending management such as balancing circuitry, whereas an Earth observation satellite in LEO for 5 years would be required to balance cells, protect against abusive conditions and possibly implement life-extending charge algorithms. Therefore, the cell chemistry determines the functionality of the BMS, not its optimal design. The application, mission, budget (both cost and mass), power requirements and battery size and topology are the main influences on BMS design. Consequently, it is not possible to design an ideal, universal battery management system for a Li-S battery, without details of its application being known.

Nevertheless, assuming that at some point in the future, Li-S cells are adopted by the space industry (for the applications listed in Section 7.5), the BMS functionality that would be applicable to Li-S should be examined. The following subsections detail specific functions of the BMS and how they can be tailored to the Li-S cell. The functionality and influences on BMS design considered in this section are:

- Power system architecture: How the satellite or launch vehicle power system regulates the charge and discharge of the battery.
- Battery monitoring: Monitoring of current, voltage and temperature and keeping the battery within predetermined limits.
- Cell-balancing: Maintenance of SoC balance between serially connected cells.
- Swelling protection: Protection against extended rest in the swelling voltage range.
- SoC determination: Parameters that can be used to indicate battery SoC.
- In-cell protection: Additional protection circuitry may be required to replace the in-cell safety mechanism present in state of the art Li-ion cells.
- BMS topology: The BMS topology affects the operation of the battery.

As previously discussed, the design of the BMS also heavily depends on the mission it is intended for and this must be considered in conjunction with the above points.

7.3.1 Power system architecture

In Chapter 1 the solar array/battery combination of power generation in an Earth-orbiting satellite was described. When the satellite is in sunlight the satellite is powered by the solar array and the battery is charged. During periods of eclipse, the battery takes over as primary power source of the satellite. There are different methods of supplying the subsystems of the satellite with this power, which revolve around how the satellite's bus voltage is regulated [5], the choice of which is mission dependent. The choice of regulation affects the battery's sizing, as the correct voltage must be selected.

If Li-S cells were to be considered for an Earth-orbiting satellite battery, the same care would need to be taken in protecting it as when using a Li-ion battery. Flow of current to the battery and battery voltage should be regulated using a battery charge regulator (BCR). Preferably, the BCR should limit the charge current to C/5 (for the Sion cell in its present format) and the maximum battery voltage to 2.5V per series cell. In LEO satellites, however, there is a limit of around 1 hour of charge time while the solar arrays are in sunlight. The limited charge current means that the battery can only operate at a maximum of 20% DoD if the battery is to be fully recharged on each orbit. The consequences of this are discussed fully in Section 7.5.

A constant current constant voltage (CCCV) charge scheme would normally be employed. However, this may have to be adapted for cell-balancing or cycle life maximising purposes. The self-discharge current seen in the Li-S cells was also markedly higher than in Li-ion and so a trickle charge function may be needed if the battery is rested at full charge for long periods of time (in a GEO orbit for example). A battery discharge regulator (BDR) could also be employed to protect the battery from large discharge currents that could affect the temperature and the Li_2S distribution on the cathode, thereby reducing the risk of irreversible capacity loss.

7.3.2 Battery monitoring

The BCR and BDR take commands from the BMS to limit current or voltage based on readings taken from the battery. The BMS is required to monitor battery voltage, current and temperature and send this information to the BCR and BDR so that the correct charge and discharge current rate can be determined. As with a single Li-S cell, the maximum and minimum battery voltages (V_{max} and V_{min}) should be kept within specified limits, as in Equations 7.1 and 7.2 for the Sion Li-S cell.

$$V_{max} = 2.5 * s \quad [7.1]$$

$$V_{min} = 1.7 * s \quad [7.2]$$

Where s is the number of cells, or strings, connected in series. The temperature of the battery should also be monitored, and is usually accomplished by monitoring the hottest (the centre) and the coldest (a corner) parts of the battery using thermocouples. The BMS can use this information to determine whether the battery is in the correct temperature operating range (usually 0°C to 20°C) and implement remedial action if required. For instance, if a high rate discharge is causing the battery to overheat, the BMS may reduce or cut off the current. If the battery becomes too cold the BMS may request a heating element to be switched on. The temperature gradient across the cells can also be monitored, and this information may be used to predict cell degradation and discrepancies in cell-balance by the ground crew.

7.3.3 Cell-balancing

The charge regulator uses the battery voltage to know which charge mode to implement and so it is important that the cells in the battery are well balanced. The results of the string test, given in Section 7.1.3, show that the Li-S cells became unacceptably unbalanced if left to cycle without maximum voltage limits. It is clear that, Li-S cells require cell-balancing electronics, even for cells that appear to be well matched.

In Chapter 2 the various methods currently used to balance series cells were analysed. It is clear that care must be taken when attempting to balance cells because it would be easy to

unintentionally create more imbalance than would occur naturally if there is sufficient spread in cell resistance. Balancing circuits work by monitoring the individual cell voltages in a series string and by acting to bring those cell voltages to the same value, either by passively bleeding off excess charge or actively redistributing charge. In Li-ion cells internal resistance decreases as the state of charge increases, and at high states of charge the total resistance is very low, approximately 0.14Ω at 100% SoC [9]. It is for this reason that Li-ion cells are balanced at high states of charge; the resistance is at its lowest point so the voltage difference due to resistance variations between cells is minimised. The resistance profile of a Li-S cell is different to this. Figure 5.24 showed that charge resistance reduces to a minimum between 90-95% SoC and then rapidly increases as the cell approaches 100% SoC. A 3Ah Li-S cell is equivalent to two 1.5Ah Li-ion cells connected in parallel and so the resistance of the Li-S cell should be half the value of the Li-ion cell's resistance, ~0.07Ω. In fact, total internal resistance at 20°C and 100% SoC can exceed 0.3Ω in a Li-S cell, 4 times higher than the equivalent Li-ion cell. A 5% variation in charge resistance in the Li-S cell would, at the same charge rate, give a higher voltage variation than in Li-ion cells. If Li-S cells were to be balanced in the same way as Li-ion then the balancing electronics may inadvertently cause a greater imbalance than there was before. There are three approaches that can be made in this case.

1. Charge cells to a lower end voltage; resistance increases rapidly above 2.4V.
2. Reduce total charge current; this reduces the voltage difference due to resistance variations, but increases charge time.
3. Step down charge current; start charge at higher current and step down current at higher states of charge.

The maximum charge current of C/5 has been identified as a problem, as this limits the allowable DoD and the ability to fully recharge the battery, depending on the type of orbit. Assuming that the battery can be fully charged by the current available in points 2 and 3 of the above list, there still exists an additional problem. Using high charge currents over the whole SoC range is known to reduce cycle life. Tests have shown that optimal cycle life is

achieved by using low charge rates to charge up to around 80% SoC followed by a stepped increase in charge current to charge the final 20% [10]. This is certainly not an ideal charge scheme for cell-balancing and substantially increases the risk of causing further imbalance in the string. If, in the future, cycle life is markedly increased then this trade-off may become irrelevant and cell-balancing can be optimised at the end of charge by using lower currents.

There is little capacity input between 2.4V and 2.5V and so charging to the lower voltage of 2.4V may improve cell-balancing ability at little cost to cell capacity. However, this voltage is very close to the swelling voltage range and so the time the battery can spend at full charge before dropping into this range is greatly reduced.

As with power system architecture, the choice of cell-balancing method is influenced by factors other than cell chemistry. The amount of balancing current required and the time available to complete balancing are practical concerns that must be considered. For space applications, reliability and simplicity are also major factors. Complicated active balancing mechanisms, as previously described, may achieve a slightly higher level of balance than passive methods but this may come with the need for 10 times the number of electronic components and complex switching algorithms that inherently reduce the reliability of the whole system. Passive balancing may be the most effective method of cell-balancing for the Li-S cells. In active balancing systems, there would be so little time to shuttle charge around the battery that the increase in circuit components would not be worth the added efficiency. Additionally there would be a trade-off between charge time and efficiency at such low charge currents, which favours passive balancing methods. So, considering the points made above, a suitable cell-balancing mechanism for a string of *s* Sion Li-S cells connected in series is proposed as follows:

1. Maximum battery string voltage V_{max} should be limited to 2.4V**s*.
2. Apply charge current of C/5 to string.
3. Monitor individual *S* cell voltage.
4. When first cell reaches 2.3V reduce battery charge current (to C/20, for example).

5. When first cell reaches 2.4V that cell is bypassed by switching in a parallel resistor. Charge current must be known accurately in order to select the correct resistance value and to prevent discharge from the bypassed cell.
6. Continue for each series cell until all reach 2.4V.
7. Hold string voltage at 2.4V*s and allow current to taper off to pre-set limit.

It should be noted that this balancing scheme is not optimised for maximum cycle life. Further testing is required to determine the ideal final voltage limit optimised for balancing. As it stands, 2.4V is out of the swelling voltage range and cell resistance is at its lowest point so it would be an obvious starting place. It is also important that any cell-balancing circuitry be adaptable to any size or topology of battery and that it does not cause excessive current drain on the battery so as to risk overdischarge.

7.3.4 Swelling protection

The results of the swelling tests showed that it is necessary for the BMS to contain a function that keeps cells out of the swelling voltage range for extended periods of time and that the time in the swelling voltage range should be used as an indicator of potential damage rather than the detection of actual physical swelling.

In LEO the battery is cycled at low depths of discharge, typically 20-30%, which unfortunately coincides with the swelling voltage range. As long as the battery begins to charge immediately following the exit from eclipse the effect should be negligible, but a back up safety function should be considered for long duration missions. If the battery is required to supplement the power provided by the solar array at any point, or if the battery is used prior to the deployment of the solar array, this could be another cause for the battery to fall into the swelling range, providing a strong case for BMS protection.

GEO satellites are required to keep the battery fully charged until it is needed for various periods of time during 90 days of the year, as described in Section 1.2.2. Storage tests showed that the battery will self-discharge into the swelling range from 100% SoC after around 15

days. Care must be taken to counteract this by either keeping the battery above the swelling range by way of a continuous trickle charge current or regular time-limited top-up currents once a minimum voltage of say 2.39V is reached, or by storing the cells at a voltage below the swelling range until the use of the battery is anticipated.

A patent filed by Nexergy in 2010 contained circuitry to prevent the Li-S cell resting in the swelling voltage range was described. In this patent two swelling voltage ranges were identified, one at high states of charge and one at low states of charge. The warnings provided by Sion indicated a swelling voltage range of 2.35V ± 0.03V, which corresponds to the high SoC danger zone. However, no warnings were provided with regard to a low voltage range. The literature suggests that 1.9V could be an area of concern [11], although the EMF tests showed that cell voltage recovered to well above this voltage and so would not be able to spend any considerable amount of time in proximity to 1.9V. The algorithm described by the patent has been modified here to include the calendar age dependency of the swelling effects and to exclude the low voltage range and is depicted in Figure 7.23.

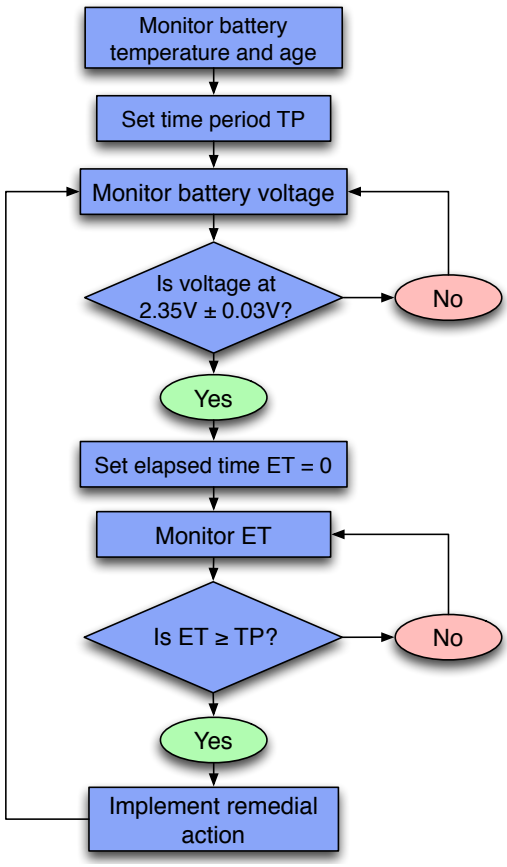

Figure 7.23: Swelling protection algorithm

Test results provide a temperature and age dependent look up table, which allows an acceptable rest time, TP, to be calculated. The current drain caused by the BMS must be accounted for in these timings. A simple version of this lookup table, which is not dependent on age or temperature, could allow a constant, short time (e.g. 2 hours) in the swelling voltage range just to err on the side of caution. The timings suggested in the patent are relatively long in comparison; 3 and 10 days are given as allowable rest times at high and low temperatures (not specified) respectively. This implies that the non-visual effects of resting a cell in the swelling range, whether it physically swells or not, were not taken into account for that study. For a satellite application, it is not only the danger of a swollen cell rupturing that is of concern but the effect on degradation of cycle life that needs to be considered.

7.3.5 State of charge determination

The need for state of charge determination in a space battery is, again, dependent on the application of that battery and is usually not a pivotal part of the BMS. In terrestrial applications SoC determination provides vital information to the user regarding how much charge is remaining in the battery or how much time it will last for at a given power consumption. In satellite and launch vehicle batteries the characteristics of the battery performance are modelled and tested ahead of time in order to make sure the battery SoC will stay in a designated range. They are also monitored during flight so that the cycle history and environmental conditions are well known.

It may be worth considering a state of charge indicator for a Li-S battery. Voltage monitoring in itself is a poor indicator for SoC due to the relatively flat charge and discharge profiles. Including a coulomb counting device will allow comparisons to be made between voltage and charge input or output which will help to monitor the degradation of the cell and to compare to the cell model on the ground. It is very important that cell degradation is known accurately because the satellite subsystems continue to require the same levels of power despite the fact the battery capacity is fading, and the battery usually does not have the opportunity to be fully cycled to determine the correct full capacity.

Because a maximum and minimum voltage defines the operating range of the battery it is relatively simple to determine end of charge conditions and so parameters such as pressure, temperature and resistance changes do not need to be used as indicators. Neither voltage, temperature or resistance change linearly with SoC and so continuous SoC monitoring is difficult. A dV/dt function could be used to estimate when the battery crosses from the first discharge region into the second, which could be used as a reference point. Monitoring charge in and out of the battery also allows the coulombic efficiency of the battery to be monitored.

7.3.6 In-cell protection

State of the art Li-ion space cells have internal safety mechanisms that can control or prevent a cell failure under certain conditions. There is some variation in the type and level of protection incorporated into cell casings. However there are, in general, three protection categories commonly in use, especially in the 18650-type cell. These are PTC polyswitches, current interrupt devices (CID) and cell vent control.

The positive temperature coefficient (PTC) polyswitch is a device made of a material whose resistance increases as its temperature increases. In the case where a cell becomes overheated, through the use of high current or through an abusive condition, the resistance of the switch increases rapidly, reducing the current flow into that cell. When the cell cools, so does the switch and current flow returns to normal. Li-ion cells that are overcharged generate a gas that increases the internal pressure of the cell, possibly causing an uncontrolled venting of the cell.

The CID is a disc shaped device that, when under pressure, bends to the point at which it breaks the circuit, interrupting the current flowing into the cell. This process rescues the cell from overcharging but is a permanent open circuit break that cannot be reversed. There is also a venting mechanism at the top of the cell, which enables the cell to vent in a controlled manner should pressure continue to rise after the activation of the CID. This reduces risk of the surrounding cells also venting.

The Li-S cell is currently manufactured as a pouch cell, which is not as robust as the cylindrical or prismatic space cells that are currently in use. It also makes the use of a CID impossible. Li-S cells currently have no internal mechanisms to protect against or control cell failure, therefore protection devices need to be incorporated into the protection circuitry. Abuse tests showed that cell temperature did not increase significantly up to 2.8V and below 1.7V, especially during overcharge, yet temperatures reached 40°C in the cells that ruptured. To protect against overheating, and possibly prevent rupturing, each cell could have a PTC protection switch connected to it in series and individual temperature monitoring to signal to the BMS to cut the current, if necessary. Although this provides a high level of protection, all of these extra connections and their redundant paths reduce its reliability. Connecting a PTC to a group of, rather than individual, cells and also having temperature monitoring for groups of closely situated cells reduces the number of required connections and improves reliability.

In addition to these protection devices it may also be worth considering some type of strain or pressure gauge to monitor the swelling of individual cells. This requires further investigation, however, a gauge of this type could prove vital to protecting cells in the battery from rupturing and causing extensive damage.

7.3.7 BMS topology

Due to Li-S having an intrinsically lower voltage compared to Li-ion, there will always be more cells connected in series in an equivalent battery. A BMS topology that seeks to minimise the effects of voltage imbalance must be selected. In Section 2.3.1 the various types of BMS topology were discussed. A centralised BMS topology increases the level of cell imbalance and so should be discounted for missions where cycle life is a major design factor. A distributed BMS minimises cell imbalance but would add significant weight and complexity to the subsystem, reducing its reliability. For the Li-S system a master-slave BMS topology should ideally be implemented. The system designer can collect series cells (or strings) into groups as small or as large as is necessary whilst having minimum impact on cell imbalances.

7.3.8 BMS functionality summary

It has been shown that a Li-S battery has specific protection requirements that must be met by the BMS. In summary these requirements are:

Battery monitoring	• Charge current regulated to maximum C/5. • Discharge current regulated to maximum 2C. • Battery voltage limits 1.7V*s – 2.5V*s. • Monitor battery temperature. • Keep battery within desired ranges by controlling heater and battery charge and discharge regulators.
Cell-balancing electronics	• Monitor individual cell (or parallel string) voltages. • Implement bespoke cell-balancing algorithm.
Swelling protection	• Use cell-balancing circuitry to monitor individual cell (or parallel string) voltages • Use battery temperature monitor to approximate cell temperature. • Monitor elapsed time since swelling voltage range entered. • Use lookup table to decide if remedial action is required. • Implement remedial action to prevent swelling.
Failure protection	• Individual cell (or group) temperature monitoring. • PTC device to reduce current in the event of overheating. • Possible use of a strain gauge to detect imminent failure.

7.4 A Note on Battery Pack Construction

As described in Chapter 1, the rigours of launch include extreme levels of vibration, acoustics and shock. The vacuum of space presents difficulties to pouch cells too, as their structure is not robust enough to survive without considerable mechanical support and constraint.

Ways to limit the temperature gradient across a battery pack must be considered, as this could create additional cell voltage imbalances. Also, with the cells predisposed to swelling, ways to either constrain or allow room for swelling must be investigated, whilst monitoring the effects on cell performance and safety. Results presented in [12] suggest that the cells can withstand certain levels of pressure, applied normal to the anode, and that this pressure aids cycle life by facilitating a more uniform lithium deposition.

7.5 Applications for Lithium-Sulphur Cells

The objective of this work has been to determine the suitability of the Li-S cell for use in space by way of cell characterisation, cell modelling and specification of battery management electronics. The results of the testing given in this work give an indication of the suitability of the Li-S cell for the applications described in Chapter 1. The suitability of Li-S cells for use on Earth-orbiting satellites, launch vehicles and interplanetary probes are discussed here.

Earth-orbiting satellites

Both LEO and GEO satellites require batteries that can undergo many thousands of cycles. Presently, the cycle life of Li-S cells is limited. Repetitive cycling at C/9 and a DOD of 100% saw the available capacity of the cell drop to 80% of its BoL capacity after 20 cycles, and cell failure at low current rate cycling. Li-ion cells, however, can attain 500-1000 cycles at 100% DoD before losing 20% capacity. Further testing is required to verify the capacity fade of Li-S cells at lower DoDs, which may improve cycle life, as Earth-orbiting satellites usually operate at 20-30% DoD. The overdischarge tests show that operating a Li-S cell at low voltages causes severe degradation and reduction of cycle life, supporting the hypothesis that increasing the lower operational cut-off voltage will improve cycle life.

The maximum charge current for the Li-S cell is presently limited to C/5. The 1-hour charge time available to LEO satellites means that the battery can only cycle at a maximum DoD of 20% and the battery sizing would have to compensate for this. This assumes the C/5 charge current can be used to fully charge the battery, which is not necessarily the case. Effective

cell-balancing requires low charge currents at the end of charge, which adds to the charge time and further reduces the DoD to which the cell can be discharged. The opposite charge scheme (low charge current followed by high current at EoC) has been shown to improve cycle life and so a trade-off must be performed.

A major drawback of using the Li-S cell, when compared to present state of the art, is the wait time that occurs before launch. It is common for launch windows to be missed and long delays to occur on the launch pad. The results of the storage tests showed that, after a full charge, there is a maximum of 15 days before the battery reaches the swelling voltage range and starts to become damaged. This time limit will be reduced as temperatures exceed 20°C. The spacecraft battery would therefore require special care on the launch pad. Charge could be maintained by allowing a trickle current to negate the effect of self-discharge, whilst clamping the battery at the maximum voltage to eliminate the risk of overcharge. A top-up current could also be applied if the battery voltage drops to a predetermined limit. Another consideration may be to charge the battery to a voltage below the swelling voltage range, although that would mean a reduction in capacity. There would need to be enough capacity remaining to power the satellite in the early operation phase, before the solar array has been deployed, and the battery must be able to be recharged. It is not uncommon for satellite batteries to need continued maintenance prior to launch. Nickel-hydrogen cells, for example, have special storage needs that require cells to be reconditioned every 7-14 days on the launch pad [12]. Lithium-ion cells, however, have negligible self-discharge and no dangerous voltage ranges, which is a distinct advantage over Li-S cells.

A Li-S battery would also require an increased level of management circuitry when compared to the Li-ion battery. Additional swelling protection, failure protection, cell-balancing circuitry, possible by-pass circuitry, and additional structural support would all contribute to the decrease in energy density of the battery. Future improvements to the cell format i.e. creating a prismatic or cylindrical cell that may have failure protection mechanisms already incorporated, would be of interest, but only if the energy density remained competitive.

Launch vehicles

Out of the numerous applications for launch vehicle batteries described in Section 1.2.2, a Li-S battery is most suited to the avionics system. This system requires a high energy density battery, which Li-S has in abundance. However, as detailed above, the wait time prior to launch and the maintenance required to keep the battery charged would be a serious hindrance to the adoption of this battery type. The savings made in weight and the possible advantages of having a "testable primary" battery would be negated by the management required to keep the battery charged and out of the swelling voltage range. Significant improvements to the prevention of parasitic reactions, decreasing levels of self-discharge, would need to be made if the Li-S cell were to be considered for launch vehicles.

Interplanetary missions

The level of degradation presently seen in Li-S cells means that their calendar lifetime is not long enough to be competitive for interplanetary missions, such as probes and rovers. However, high cycle life is not always a priority for interplanetary missions and so, if calendar life is improved in future Li-S cell modifications, it could be considered for such applications.

7.6 Conclusions

This chapter was split into two main parts. In the first part the OCV, abuse and string testing results were analysed with a view to understanding how the cells react to non-standard operating situations and how they perform in a series topology. This information was used, along with results from Chapter 6, to discuss options for an ideal battery topology, to describe the functionality of a dedicated Li-S BMS and to use this information to determine the suitability of Li-S cells for space applications. The results from the testing gave several insights into the Li-S system and were fully summarised in Section 7.1.5.

Possible battery topologies were discussed in Section 7.2. A battery arranged in the p_1-s-p_2 topology retains the inherent redundancy of the s-p topology whilst benefiting from fewer

balancing circuits, as with the p-s topology, but a trade-off between the reduction in circuitry and the increased capacity lost if a string should fail is key to finding the optimal solution.

The results of the tests presented in this and previous chapters were used to determine the functionality of a Li-S battery management system, not specific to any particular application or mission type. Several important functionalities were identified which should be used by the power system designer as a starting point from which to design the battery management electronics. This functionality was summarised in Section 7.3.8.

In addition to BMS functionality, the topology of the BMS itself and the design of the battery pack were considered. A master-slave topology would be the preferred option for Li-S cells as it would limit the cell imbalance caused by non-uniform current drain on the cells. A custom battery pack structure must be designed to protect the battery against the space environment and the rigours of launch. This structure may also serve the purpose of preventing (or accommodating) cell swelling, a feature that requires further investigation.

Recalling the design criteria specified in Section 1.7 the BMS must fully protect the battery and be constructed in such a way that is inherently redundant and reliable whilst also having the minimum effect on its energy density. For the Li-S battery, energy density is the biggest selling point and something that should be maintained. This chapter has shown that a threat to this high energy density is the additional weight of the swelling protection circuitry, not seen in Li-ion batteries, and the cell-balancing circuitry. The battery pack construction is also a major factor, as Li-S pouch cells require much more structural support than the equivalent Li-ion cells would.

In terms of the applications Li-S cells could be used for in their present form, several options were considered in Section 7.5. Vast improvements to cycle life need to be made before these cells can be considered for Earth orbit and so currently, Li-S is not a contender to replace Li-ion. Neither can these cells be considered for long duration interplanetary missions due to the severe aging. Launch vehicle batteries are the most promising application for Li-S although a battery would need specific care prior to launch until self-discharge is improved.

REFERENCES

[1] J. Jeevarajan and B. Duffield, "Performance and saftey studies on COTS Li-ion cells of cylindrical and pouch cell designs," in *NASA Battery Workshop*, Huntsville, AL, November 2011.

[2] J. Jeevarajan, Personal communication, December 2011.

[3] Aeroflex. (2012, May) Aeroflex. [Online]. http://www.aeroflex.com/ams/pagesproduct/prods-power-beu.cfm

[4] Y Barsukov. Texas Instruments Website. [Online]. http://focus.ti.com/download/trng/docs/seminar/Topic%202%20%20Battery%20Cell%20Balancing%20-%20What%20to%20Balance%20and%20How.pdf

[5] D. Loche and H. Barde, "Lithium-Ion Battery Cell Balancing in LEO," in *Space Power, Proceedings of the Sixth European Conference*, Porto, Portugal, 2002, p. 507.

[6] J. H. Lee, H. M. Lee, and S. Ahn, "Battery dimensional changes occurring during charge/discharge cycles—thin rectangular lithium ion and polymer cells ," *Journal of Power Sources*, vol. 119–121, pp. 833–837, 2003.

[7] X. He et al., "Expansion and shrinkage of the sulfur composite electrode in rechargeable lithium batteries," *Journal of Power Sources*, vol. 190, pp. 154-156, 2009.

[8] Y. V. Mikhaylik et al., "High Energy Rechargeable Li-S Cells for EV Application: Status, Remaining Problems and Solutions," *ECS Transactions*, vol. 25, no. 35, pp. 23-34, 2010.

[9] ABSL Space Products, Battery Electrical Analysis and Simulation Tool BEAST, V1.2 (2007).

[10] A.B. Gavrilov and Y.V. Mikhaylik, "Methods of Charging Lihtium Sulfur Batteries," US Patent 6,329,789, December 11, 2001.

[11] J-W Choi et al., "Rechargeable lithium/sulfur battery with liquid electrolytes containing toluene as additive," *Journal of Power Sources*, vol. 183, no. 1, pp. 441-445, 2008.

[12] NASA. Ni-H2 SPACECRAFT BATTERY HANDLING AND STORAGE. [Online]. http://engineer.jpl.nasa.gov/practices/1109.pdf

CHAPTER 8

DISCUSSION, CONCLUSIONS AND FURTHER WORK

In this final chapter, the main conclusions from the work presented are drawn together. This includes outlining the significant findings that contribute to the knowledge of the performance of Li-S cell technology and a critical analysis of the testing methodology, implementation of the battery model and specification of the BMS. From these conclusions further work to be undertaken in this field is proposed.

8.1 Discussion

8.1.1 Aims and objectives

The lithium-sulphur couple has such a high theoretical energy density that, in principle, it could contribute significant weight and cost savings for launching a spacecraft. It was for that reason that this research was undertaken, with an ultimate goal of determining the suitability of the cell for adoption by the space industry. In order to determine its suitability the objectives of the work were set to:

- Investigate the electrical, thermal and performance characteristics of the Sion Li-S cell using a range of empirical characterisation testing techniques;
- Use the results of the characterisation tests to create a novel, adaptable Li-S battery model, which could aid a power system designer in predicting the performance of the cell under a variety of power and temperature profiles;
- Use novel characterisation testing results to determine the protection requirements employed by a dedicated battery management system, for spacecraft applications;
- Determine the lithium-sulphur cells' suitability for specific space industry applications when cell performance, modelling, and electronic protection are accounted for.

In this thesis a novel, Li-S equivalent circuit battery model was proposed and successfully used to predict the capacity, temperature and electrical performance of the Li-S cell using data obtained from dedicated characterisation tests. The capacity contributions from each discharge region were dealt with individually to form a novel "split capacity" model. In addition, these characterisation results, previously not reported elsewhere in the literature, were used to determine the required functionality of a bespoke BMS and thus establish the cell's suitability for space industry applications. Before the main conclusions can be drawn, the significant results discovered during cell characterisation are described and a discussion is made on the findings of the work.

8.1.2 Significant test results

The large quantity of raw data, available from the characterisation testing, revealed important features of the Li-S cell chemistry. These findings, and their importance, are summarised below.

SCM measurement

A standard capacity measurement (SCM) cycle made 92% of the total cell capacity available. This result allows the capacity of each cell to be estimated accurately without having to complete a full capacity test. Defining an accurate measure of capacity is vital to the characterisation of Li-S cells and should be performed immediately prior to any characterisation test to prevent the consequences of degradation affecting results.

Degradation dependency on current rate

It was found that capacity degradation is higher when cells are cycled at low current rates, possibly because they reach a lower DoD, confirming results found in the literature for cells with lithium metal anodes. On analysis of life test data there was an apparent increase in degradation at very high current rates (2C), which could be evidence of increased cathode destruction occurring at high current rates.

Self-discharge

Investigations described in the literature have only described self-discharge behaviour at 100% SoC. This work extended on those findings to show that self-discharge reactions, of near-equal severity, also occur at 40% SoC. A capacity loss of 7.6% occurred in 1 month.

Peukert number

The Peukert number for a Sion Li-S cell was calculated to be 1.273, which has not been previously reported in the literature. This relatively high number, when compared to a value of around 1.02 for lithium-ion cells, means that the discharge capacity available at high current rates is much reduced. This number not only affects the operation of the cell but also is vital for accurate cell modelling and performance prediction.

Overcharge and overdischarge

Cells show a robustness to overcharge and overdischarge, for low cycle numbers (<20), but degradation is increased. The severity of degradation during overdischarge means that cycle life could be improved at lower DoDs. There was an increased level of swelling seen in these cells but, surprisingly, cell temperature was not affected when the operational voltage limits were exceeded. This limits the effectiveness of temperature based protection mechanisms.

Swelling

New cells show signs of swelling if left within the swelling voltage range 2.35V ± 0.03V for more than 24 hours. The level and rate of physical swelling seen increases with temperature and was also was found to have a link to the cell's age, something that had not previously been reported. More importantly, tests also revealed that levels of cell degradation, specifically resistance increase and capacity fade, were still increased whether physical swelling occurred or not. This was independent of the actual voltage the cells rested at (within the swelling range). It is therefore noted that aging of the Li-S cell could be seen as an advantage, in terms of swelling inhibition.

8.1.3 Discussion on the cell model

The final version of the Li-S equivalent circuit model presented in this thesis predicts the electrical and thermal response of the cell under varying temperatures and current loads in both the charge and discharge direction. An equivalent circuit model format of series/parallel combinations of resistors and capacitors was chosen for the following reasons:

- Ease of implementation into a power system model
- Ease of use by a power system designer
- Adaptability to future cell modifications
- Nature of testing facilities available
- Proprietary nature of cell chemical composition
- Testing restrictions imposed by manufacturer

The model is suitable for use by an engineer who does not need specific knowledge of the cell chemistry. In addition, it can be adapted to future cell modifications by way of repeating the characterisation tests and updating the lookup tables that form the basis of the model.

The results of the characterisation testing showed that there are improvements that could be made to the testing methodology, should this work be adapted to newer versions of the Li-S cell. Improvements to the testing methodology have the knock on effect of improving the accuracy of the cell model, especially at temperatures above and below 20°C and at high (>C/2) current rates and are discussed further in Section 8.3.

Parameter	**Dependencies**
EMF	Temperature, SoC
Ohmic Resistance	Temperature, SoC, Age
Diffusion Resistance	Temperature, SoC, Age, Current Rate
Capacitive Effects	Temperature, SoC, Age, Current Rate, Diffusion Resistance
Cell Capacity	Temperature, SoC, Age, Current Rate
Self-discharge	Temperature, SoC, Age, Rest Time
Swelling	Temperature, SoC, Age
Degradation	Temperature, SoC, Age, Cycle History

Table 8.1: Li-S cell model parameters and dependencies

A list of the battery model parameters and their dependencies are given in Table 8.1. This table shows the extent to which each model parameter is dependent on several different effects and illustrates the difficulty in separating out each independent variable. Every effort was made in this work to account for each dependency in the cell model, but it should be accepted that there may be considerable variation between cell batches and between different manufacturer's cells, and so the relationships determined in this work may be subject to revision. Two factors had a major effect on the model, not seen in Li-ion cells; the large amount of capacity that is recoverable during rest periods and the rate dependency of the capacity in the second discharge region. Both factors were incorporated into the equivalent circuit model using empirical data, although the foundations for these effects are heavily dependent on the cell's electrochemical interactions. As such, a full electrochemical analysis may be required if the model is to be improved for future cell formats. Such an analysis was impossible in this work due to the restrictions placed on the use of the cell.

Despite these many interdependencies and electrochemical effects, the equivalent circuit method and empirical test methodology gave a suitable solution to the objectives of this work. The model provides a basis on which to predict the performance of the Sion Li-S cell in a way that aids the design of a spacecraft or launch vehicle power system, but should not be seen as a qualification of the cell for use in space.

8.1.4 Battery management system functionality

The battery management system design will often depend critically on the mission or application for which the battery is to be used. The choice of cell chemistry dictates the functionality of the BMS, the details of which were fully discussed in Chapter 7.

The conclusions made from the analysis of test results showed that the Li-S battery requires levels of protection exceeding that of Li-ion for some applications and would, in all cases, also require a robust structure to protect the fragile pouch cells in the space environment. Each of these factors contributes to the reduction of energy density of the overall system. A full analysis of the effect on energy density would normally be made when a complete battery

pack is designed for a specific application. Only then can the full extent of the effect on energy density be appreciated and compared to an equivalent Li-ion battery pack.

8.2 Conclusions

The multitude of characterisation test data accumulated in this work was used to achieve the objectives stated in Section 8.1.1. The battery model described in Chapter 6 showed that it is indeed possible to model the Li-S cell using a "split capacity" equivalent circuit method, with limited knowledge of the specific electrochemical interactions in the cell, and that the model can provide results that closely predict real data. This should be seen as an important first step in accepting lithium-sulphur as a future contender for a satellite or launch vehicle battery into the space industry.

The analysis of the electronic protection requirements given in Chapter 7 showed that Li-S cells require special management, which differs from that of Li-ion. Depending on the topology chosen for the Li-S battery cell-bypass circuitry may or may not be necessary, but cell balancing and swelling protection circuitry will certainly be required as well as extra failure protection circuitry. In addition to this, the Li-S pouch cell would require a robust housing structure to protect it against the physical stress of launch and the space environment. These additional protection requirements all add to the mass of the battery pack and hence reduce the energy density of the battery system. The level that the energy density is reduced to is dependent on the battery size and topology, the design of the BMS and the mass of the battery casing and support structure.

The apparently advantageous energy density gap that Li-S technology has over Li-ion begins to close with these considerations and the negative aspects of Li-S become increasingly undesirable. Its low cell voltage, for example, is something that can never be improved upon. Low cycle life, high self-discharge, high levels of degradation and swelling within normal voltage limits are all aspects of the Li-S chemistry that can theoretically improve as the cell is developed, but as yet remain limiting factors to the adoption of Li-S into the space industry.

Advances in the manufacturing process (improving cell matching) and optimisation of cell chemistry may eventually reduce the requirements of the BMS and improve levels of degradation, making Li-S a more attractive option in the future.

8.3 Suggestions for Further Work

While the body of the work presented in this thesis has provided an overview of the wide range of cell characteristic testing needed to achieve a working cell model, more data is needed should the demand for a more specific battery model arise based on a new design, construction or cell chemistry. In this section modifications to certain testing procedures are suggested for further work, so as to aid in the characterisation of future Li-S cell formats. In addition, improvements to the battery model are suggested that could be undertaken if the amended characterisation procedure is implemented.

8.3.1 General improvements to testing methodology

In this work, there were a limited number of cells available for testing which ultimately meant that each test condition could not be applied to more than one or two cells. As such, tests using a single cell could not be wholly relied upon to provide an accurate picture of the average cell. In addition, due to the unknown nature of the cells prior to testing, the testing methodology was understandably changed and improved upon as results became available.

It is suggested that, should these tests be repeated on updated cell versions, no fewer than 5 cells should be used to characterise each parameter. This is vital to obtain information on cell-to-cell variations and improve the accuracy of average cell data. Ideally, the storage and degradation characteristics of the cell should be characterised prior to any other tests. The cells used in this work had high levels of degradation during both storage and cycling. These effects inevitably affected the results of other tests occurring concurrently. Once the general storage tests are completed for the new cell variation a new cell batch should then be used to characterise the electrical and thermal properties. A smaller set of storage tests can be run concurrently on the new batch, to act as a check on batch-to-batch variation.

New cells[1], of the same batch should be used for electrical and thermal characterisation and should be stored in a temperature-controlled environment of 20°C (or below) when not in use. It would take considerable cost and use of facilities to complete all of the required characterisation tests on cells of the exact same age, although that would be ideal. However, in the likely event that this is not possible, it should be kept in mind that performing tests on cells of the same age, but from different batches, would introduce the additional inaccuracy of variance between batches, which should be accounted for.

In tests that may occur after a period of rest, e.g. 1 week after the preceding cycle, the charge voltage profile and charge capacity is not representative for the current cell type. Therefore, a preconditioning SCM cycle should be performed prior to the start of each test, unless the storage tests on the new cell version suggest otherwise. If, in future cell modifications, the protection of the anode is improved and the SEI layer more stable, an SCM cycle preceding each test may not be necessary.

8.3.2 Improvements to test procedures

In addition to the general improvements described above there is room for optimisation to the individual tests that were performed on the cells in this work, and are given in this section. It should be noted that, although a value of 0.315A is used as the ideal operating current in these proposed tests, future cell modifications might require a different value, especially if the cell format is altered to a higher capacity cell, and should be provided by the manufacturer. Therefore, the values of temperature, time, voltage and capacity used in the following tests are based on the Sion Li-S cell used in this work, and may need to be revised in order to suit a new Li-S cell type or format.

EMF

An alternative test method to that used to define EMF in this work may improve the results found at low temperatures. Using an even lower current value, such as C/100, to perform

[1] Whilst the cell should be as new as possible, the acceptable age of the cell will vary, depending on

cycling without including any rests would improve the EMF value (because of the reduced effect of resistance) and remove the capacity variations caused by the rests. All test cells need to start in identical test conditions (SoC and temperature) before characterisation begins. This method changes the way in which the SCM and SoC are defined (as discussed below) and, as the length of the test is significantly increased, self-discharge should be accounted for.

Screening and capacity checks

Ideally the screening of all test cells should take place at the same time, should facilities allow. This gives an accurate description of the spread in capacities over the whole cell batch. To determine the SCM parameters accurately, the cells' discharge and charge capacities should be characterised separately, as described below.

Discharge SCM:

- Charge, discharge and charge cells using the current used to define EMF, stopping when the cell reaches 2.5V and define this point as 100% SoC. The total discharge capacity of the cell is known from the discharge in the initial cycle.
- Rest cells for 1 minute, allowing chemicals to adjust but also reducing the capacity loss that would occur from self-discharge if the rest was longer.
- Discharge cells at 0.315A until 1.7V (or desired cut-off voltage >1.7V) is reached.
- Calculate the difference between discharge capacities and the result gives the SoC to which the cell is discharged at 0.315A.
- Inaccuracies due to cycling degradation should be accounted for.

Charge SCM:

- Charge and discharge cells for 2 cycles using the current used to define EMF, stopping when the cell reaches 1.7V and define this point as 0% SoC. The total charge capacity of the cell is known from the charge in the second cycle.
- Rest cells for 1 minute.
- Taper charge cells to 2.5V using a current of 0.315A.

- Calculate the difference between charge capacities and the result gives the SoC to which the cell is charged to when taper charged at 0.315A to 2.5V.
- Inaccuracies due to cycling degradation should be accounted for.

Storage tests

It is important that more cells are used in each test condition than were used in the original tests. This is because the storage characteristics appeared to vary from cell to cell and it is imperative that this range is fully characterised, as it has implications for the battery management system. The number of tests should also be increased to include cells resting at different states of charge, in 10% increments for example, and at different temperatures in the range -20°C to 40°C. In addition, the long-term self-discharge effect should be characterised, even if the cell voltage is within, or has passed through, the swelling range. Tests completed in the first weeks of storage are likely to yield inaccurate results for self-discharge, especially at lower states of charge where capacity recovery masks the self-discharge effect.

A test to characterise the capacity recovery effect in more detail could be devised. Cells should first complete an SCM cycle before being discharged to a predetermined state of charge. After a certain number of hours (and possibly days) the cell should be discharged to its SCM voltage cut-off limit. Comparing the two discharge capacities for each cell shows how much capacity is recovered in the rest period (once cycling and aging capacity losses are accounted for) at that particular state of charge. An extensive study would need to be performed at different states of charge, temperatures, current rates and rest periods to fully characterise this effect. If cell numbers are limited this test can be incorporated into the resistance tests (see below).

Life tests

An extension to the life tests should include cycling to different DoDs to observe the effect on the cycle life of the cell. Additionally, the cells should be cycled at different temperatures and

using charge rates different to their ideal operating current. This would characterise the effect these parameters have on the cell's cycle life and determines an ideal charge algorithm.

Resistance tests

As the results in Chapter 5 showed, the resistance test methodology did not provide ideal results in extreme operating temperatures, or at high current rates. The close proximity of the rests that interrupted the cycling in these tests meant that the cells could not fully return to their equilibrium terminal voltage when current was flowing, nor to their true EMF value during rest. This heavily affected the resistance characterisation results at 0°C and introduced capacity variations caused by the SoC dependent capacity recovery effect. Consequently, the resistance testing methodology may benefit from changes that improve the accuracy of the model at low temperatures and high current rates.

The method for determining the Ohmic resistance of the Li-S cell can be described as follows:

1. Ensure that the EMF of the cell is known at each required test temperature.
2. Charge all test cells to the newly defined 100% SoC, or to the known percentage of SoC that the SCM charge allows, at 20°C.
3. Discharge one cell at 0.315A and at 20°C, performing 1 (or 2) second rests every 0.1Ah to determine Ohmic resistance (rate independent).
4. Discharge other test cells in the same way but having changed the temperature of the thermal chamber to the required test temperature (-20°C to 40°C) before discharge (in the previous step) begins.
5. Test could be repeated at intermittent values of SoC to increase lookup table data.

The method for determining the resistances and capacitances associated with diffusion can be determined using the methods described below. Method 1 describes the technique used to find these values for a simple 1^{st} order transient system (1 RC ladder). Method 2 expands the technique to an n^{th} order system (2 or more RC ladders).

Method 1:

1. Calculate the difference between the EMF and the voltage after the 1-second[2] rest has been applied using data from the Ohmic resistance tests.
2. Divide this voltage difference by the current rate to give the total resistance due to diffusion.
3. Pre-cycle a group of cells using the SCM cycle.
4. Charge these cells to 100% SoC at 20°C. Following this, set thermal chamber to required test temperature.
5. Discharge each cell at a rate of 0.315A by differing increments of 0.1Ah. If facilities and cell numbers allow this increment can be smaller. There should be multiple cells in each test condition.
6. Leave each cell to rest until $\frac{dV}{dt}$ is at a minimum, whilst continuously monitoring the voltage recovery curve.
7. The time constant of each curve can be found by fitting the curve (between 1 second rest and final resting value) to an equation of the form:

$$V_{term} = EMF - I_1R_1 - V_{Bmax}e^{-t/R_2C_2}$$

   Where the values of V_{Bmax} and R_2 are found in step 2 and R_1 is the Ohmic resistance.
8. The capacitance value of each curve is found by dividing the time constant by R_2.

Method 2:

1. Repeat steps 3-6 from Method 1 above.
2. Fit each curve to an equation of the form:

$$V_{term} = EMF - I_1R_1 - V_{2max}e^{-t/R_2C_2} \ \ldots \ V_{nmax}e^{-t/R_{n+1}C_{n+1}}$$

   Where *n* is the number of RC networks in the circuit.
3. The values for V_{nmax} are found from the curve fit, the associated R_{n+1} value can be found by dividing by the current, and the associated C_{n+1} are found by dividing the time constants by R_{n+1}.

[2] Assuming a 1 second rest is used to define Ohmic resistance.

Method 2 is not significantly different from the method used in this thesis. The key difference is that, instead of a single cell being used to characterise all resistances over all states of charge, many more cells are used so that each cell (or group of cells) characterises one recovery curve at one state of charge. This removes the step-cycling effect, as one cell is not required to perform more than one rest. If cell numbers are limited, the original test method could be used but with a longer period of current flow between rests (i.e. greater than 30 minutes). Rest time would also have to depend on when the voltage had recovered to the EMF value and not a pre-set time limit. By discharging the cells after the designated rest period the capacity recovery can also be characterised. This test should be repeated using a range of current rates in order to characterise the effect on the voltage and capacity recovery, and hence the rate-dependent resistance and capacitance values.

Hysteresis

The results of the hysteresis tests were affected by the level of degradation seen in the cell between screening and the commencement of the test. If the resistance of the cell was markedly different to that of the cells used to characterise resistance then the accuracy of the model could be reduced. The solution to this would be to characterise the hysteresis on a set of new cells, where cell capacity is known accurately, thereby reducing the effect of degradation. An Ohmic resistance test cycle may also be performed immediately prior to the hysteresis test so as to accurately determine the effect that resistance has on hysteresis.

In addition, the current rate used to characterise the hysteresis curves could be lowered in order that the voltage follow the EMF more closely. In the model presented in this work a second order exponential was used to characterise the hysteresis voltage transfer, as this provided the best fit to the data. This may be modified to a lower or higher order should future testing establish the need to, without having significant effect on the mathematics. In repeating these tests, engineers should use cells of the same batch and age and, should facilities and cell numbers allow, multiple cells should be used to characterise each test condition, including at different temperatures.

EMF dependency on temperature

The apparent worsening of the hysteresis effect during a slower thermal cycle was likely to be due to the cells not being at an equilibrium voltage when the test began, rather than the speed of the thermal cycle. On repeating these tests care must be taken to ensure that the cells have returned to their EMF value before thermal cycling can begin. Monitoring the change in voltage with time $\left(\frac{dV}{dt}\right)$ would tell the test engineer the time at which equilibrium had been reached and hence at which point thermal cycling could commence. This will take longer for cells at lower states of charge, as the voltage recovery has been shown to take longer in the second discharge region. Care must also be taken with cells at high states of charge as self-discharge may affect results, although this was not the case with the cells tested in this work and future cell variations should only improve self-discharge reactions. As with all other tests, the results would benefit from multiple cells tested in the same condition.

8.3.3 Additional testing for model expansion

Some aspects of the Li-S cell's electrical response were not deemed fundamental to the operation of the model in this work. For example, the first charge of a cell after a period of rest was shown to have a higher voltage profile than the standard model. The charge capacity is much higher than subsequent charges and the resistance is also significantly higher. An investigation of this effect may provide an accurate prediction of the required charge time if the storage time is known.

The literature implies that the Peukert number is temperature dependent and analysis of the life tests suggest that it also degrades, or gets larger, as cycle number and possibly age increases. A full characterisation of the Peukert effect in the second discharge region would aid in the prediction of the life of the battery under varying current loads and temperatures.

The cell model would also benefit from an improvement to the thermal model. Additional shock cooling tests would improve the estimation of the thermal conductance. Also, dedicated battery calorimeter equipment would be required to determine an accurate thermal capacity.

Further tests, on a block of cells in a battery pack, would give a better indication of the temperature response of an average cell, taking cell-to-cell interactions into account.

8.3.4 Improvements to the BMS specification

The functionality of the BMS described in this work was based on the results of the testing presented in Chapter 7. If testing facilities should allow, it would be beneficial to the design of the BMS to complete an investigation into the cell's response to severely abusive conditions. This would aid in the design of failure prevention circuitry or in-built protection mechanisms.

It may also be of benefit to test, and perhaps model, the various cell topologies discussed in this work. This would give an improved view of battery level dynamics, both thermal and electrical. The additional cycling fade seen in the string test, as opposed to a single cell, shows that the behaviour of a battery can be different to a scalable version of a single cell.

A more detailed investigation into the dependency that physical swelling and degradation in the swelling range has on age and temperature would improve the specification of the BMS functionality and aid in the mechanical design of the battery pack.

~:~

The Li-S cell has proved to be an interesting contender for the future of batteries intended for spaceflight. Its electrochemistry is far more complex than the Li-ion cell and therefore considerably more difficult to model, it has a higher level of degradation and a shorter cycle and calendar life than Li-ion cells, and the swelling that occurs in the normal operating voltage range may limit its applications. However, let it not be forgotten that Li-ion technology started life just as humbly, with a similar battle against nickel-based cells to become the world's most superior battery type to date. The Li-S cell is yet to be optimised and, having a theoretical energy density far exceeding that of any other useable electrochemical couple, it still holds promise to be of use in the space industry in the future. Lithium-sulphur's battle against Li-ion is not over yet.

APPENDIX A

DERIVATION OF PRINCIPAL EQUATIONS

A.1 Derivation of theoretical capacity

The value for theoretical capacity is derived from Faraday's Law of Electrolysis and is given in Equation A.1.

$$Q = \frac{nF}{M_r} \quad [A.1]$$

Where Q is the theoretical capacity of the battery, n is the number of electrons transferred per mole of reaction, M_r is the atomic weight of sulphur (g/mol) and F is Faraday's constant, which is equal to 96,485 C/mol.

The overall reaction that occurs at the cathode of a Li-S cell can be represented by the simple reduction reaction, shown in Equation A.2, during discharge. Though, in reality, there are intermittent stages to this reaction that are more complex:

$$S + 2e^- \leftrightarrows S^{2-} \quad [A.2]$$

Equation A.2 shows that there are 2 electrons transferred per mole of reaction so *n* is equal to 2 in Equation A.1 and the atomic weight of sulphur is known to be 32.064 g/mol. From these values the theoretical capacity of the sulphur electrode can be calculated:

$$Q = \frac{nF}{M_r}$$

$$Q = \frac{2 \times 96485 \text{ C/mol}}{32.064 \text{ g/mol}}$$

$$Q = 6018.28 \text{ C/g}$$

There are 3600 Coulombs (C) in 1 Amp-hour and so this capacity can be converted to the more familiar milliamp hours per gram:

$$Q = \frac{6018.28\ \mathrm{C\,g^{-1}}}{3.6\ \mathrm{C\ mAh^{-1}}}$$

$$Q = 1672\ \mathrm{mAh/g}$$

This value is the accepted value of the theoretical capacity of the lithium sulphur couple.

A.2 Derivation of specific energy and energy density

For a spontaneous electrochemical reaction, the Gibbs free energy equation relates the equilibrium cell potential to the energy available from that reaction and is given by Equation A.3.

$$\Delta G = nFE \qquad [A.3]$$

Where ΔG is the Gibbs Energy, or available energy, n is the number of electrons per mole of product, F is Faraday's constant and E is the electrode potential of the reaction. By using the two electrode reactions given in Chapter 3 (Equations 3.1 and 3.2) the total cell reaction can be given as in Equation A.4.

$$S + 2Li \leftrightarrows Li_2S \qquad [A.4]$$

The final discharge product is lithium sulphide (Li_2S) whose atomic weight is the sum of double the atomic weight of lithium and the atomic weight of sulphur:

$$W_{Li_2S} = 2 \times 6.941\ \mathrm{g\ mol^{-1}} + 32.064\ \mathrm{g\ mol^{-1}}$$

$$W_{Li_2S} = 0.045946\ \mathrm{kg\ mol^{-1}}$$

In order to find the theoretical energy density of the cell these calculations must now be substituted into the Gibbs free energy equation (Equation A.3) using an average cell potential value of 2.23V:

$$\Delta G = nFE$$

$$\Delta G = 2 \times 96485 \text{ C mol}^{-1} \times 2.23V$$

$$\Delta G = 430323.1 \text{ J mol}^{-1}$$

Using 3600 Joules in 1 Watt hour (Wh) this value can be converted into $Wh\ mol^{-1}$ as follows:

$$\Delta G = \frac{430323.1 \text{ J mol}^{-1}}{3600 \text{ J Wh}^{-1}}$$

$$\Delta G = 119.5 \text{ Wh mol}^{-1}$$

As it is known that the final discharge product of the reaction is lithium sulphide and its atomic weight is 0.045946 kg mol^{-1} then the value for energy can be further converted into Watt-hours per kilogram of lithium sulphide.

$$\Delta G = \frac{119.5 \text{ Wh mol}^{-1}}{0.045946 \text{ kg mol}^{-1}}$$

$$\Delta G = 2600 \text{ Wh kg}^{-1}$$

So the theoretical specific energy of a lithium sulphur cell is 2600 Wh kg^{-1}. Similarly, to calculate the energy density of the cell the atomic volume of lithium sulphide must be used instead of its atomic weight. It is the sum of double the atomic volume of lithium and the atomic volume of sulphur:

$$V_{Li_2S} = 2 \times 0.0131 \text{ l mol}^{-1} + 0.0155 \text{ l mol}^{-1}$$

$$V_{Li_2S} = 0.0417 \text{ l mol}^{-1}$$

The Gibbs free energy can then be converted into Watt-hours per litre as shown below:

$$\Delta G = 119.5 \text{ Wh mol}^{-1}$$

$$\Delta G = \frac{119.5 \text{ Wh mol}^{-1}}{0.0417 \text{ l mol}^{-1}}$$

$$\Delta G = 2860 \text{ Wh l}^{-1}$$

So the theoretical energy density of a lithium sulphur cell is 2860 Wh l^{-1} when using an average cell voltage of 2.23V.

A.3 Derivation of power dissipation

This theory, acquired from work done by N. A. Godshall and J. R. Driscoll [1], shows how characterisation testing of the variation of open circuit voltage (EMF) with temperature can give a data set from which the battery temperature can be calculated.

The total heat generated in an electrochemical cell, q_t, is given by the sum of the heat due to cell polarization q_p, the heat due to entropy effects q_s and the heat due to other losses such as self-discharge:

$$q_t = q_s + q_p + q_{other} \quad [A.5]$$

The Gibbs free energy ΔG of the reaction is given by:

$$\Delta G = \Delta H - T\Delta S \quad [A.6]$$

Where H is enthalpy, S is entropy and T is temperature. Then, combining the first and second laws of thermodynamics results in Equation A.7:

$$\partial \Delta G = \Delta V \partial P - \Delta S \partial T \quad [A.7]$$

Where V is volume and P is pressure. At constant pressure:

$$\partial \Delta G = -\Delta S \partial T \quad [A.8]$$

$$\frac{\partial \Delta G}{\partial T} = -\Delta S \quad [A.9]$$

Substituting in the alternative form of the Gibbs free energy equation [A.3]:

$$\Delta S = nF \frac{\partial E}{\partial T} \quad [A.10]$$

Therefore, the entropy change of an electrochemical reaction at equilibrium may be derived from knowing the way that the EMF of the cell varies with temperature. The enthalpy change ΔH can then be found as follows:

$$-nFE = \Delta H - T\Delta S \quad [A.11]$$

$$E = -\frac{\Delta H}{nF} + \frac{T\Delta S}{nF} \quad [A.12]$$

Substituting in Equation A.10:

$$E = -\frac{\Delta H}{nF} + T\frac{\partial E}{\partial T} \quad [A.13]$$

$$E_H = -\frac{\Delta H}{nF} = E - T\frac{\partial E}{\partial T} \quad [A.14]$$

Where E_H is the thermoneutral potential and represents the part of the cell voltage that is due to the enthalpy term. The thermoneutral potential is the potential that corresponds to an isothermal reaction, where the cell does not produce or gain any heat. It is also the theoretical open circuit voltage at absolute zero.

Going back to Equation A.5 the heat due to the entropy effect (q_s) is given by:

$$q_s = T\Delta S = T.nF\frac{\partial E}{\partial T} \quad [A.15]$$

The heat due to polarization (or internal resistance) effects is given by:

$$q_p = -nF(E - V_{term}) \quad [A.16]$$

This shows the dependency of the heat output on the voltage drop between the EMF (E) and the voltage seen at the terminals, V_{term}. Summing these q terms gives the total heat generated by the cell q_t. Self-discharge and other effects have been neglected in this result.

$$q_t = q_s + q_p = T.nF\frac{\partial E}{\partial T} - nF(E - V_{term}) \quad [A.17]$$

$$q_t = -nF\left(E - V_{term} - \frac{\partial E}{\partial T}\right) \quad [A.18]$$

Where:

$$E - V_{term} = -I.R \quad [A.19]$$

Therefore:

$$q_t = -nF\left(-I.R - T\frac{\partial E}{\partial T}\right) \quad [A.20]$$

Differentiating q_t with respect to time gives the rate of change of heat, or power dissipated P_{diss}, in Watts. The rate of change of nF over time gives the rate of change of charge which is equal to the current, so:

$$P_{diss} = \frac{dq_t}{dt} = \frac{-nF\left(-I.R - T\frac{dE}{dT}\right)}{dt} \quad [A.21]$$

$$P_{diss} = -I\left(-I.R - T\frac{dE}{dT}\right) \quad [A.22]$$

$$P_{diss} = I^2R + I.T\frac{dE}{dT} \quad [A.23]$$

This value of power dissipation is used in the standard heat transfer equation to determine the temperature of the cells and walls of a battery pack.

REFERENCES

[1] N. A. Godshall and J. R. Driscoll, "Determination of the Thermoneutral Potential of Li / $SOCl_2$ Cells" *J. Electrochem. Soc*. 1984 vol.131, no.10, pp. 2221-2226

APPENDIX B

CELL DATA SHEETS

In Chapter 3 the Sion Li-S cell was compared to the current state-of-the-art lithium-ion batteries used in the space industry for various applications. The data sheets of these batteries are reproduced here as follows:

B.1 Sion lithium-sulphur cell

B.2 ABSL 18650HC lithium-ion cell

B.3 SAFT VL 34P lithium-ion cell

B.4 SAFT VES 180 lithium-ion cell

B.1 Sion Li-S Cell

Lithium Sulfur Rechargeable Battery Data Sheet

Lithium sulfur has the highest theoretical specific and volumetric energy densities of any rechargeable battery chemistry (2550 Wh/kg and 2862 Wh/l theoretically). SION Power has learned how to unlock this potential and has created a unique rechargeable battery system. This patented technology is enabling new applications for rechargeable batteries and replacing existing primary and rechargeable batteries in applications where weight is a critical factor.

Typical applications include:

- Unmanned Vehicle Systems
- Weight sensitive electronic applications
- Military communication systems
- Sensors

Electrical Specifications:

Nominal Voltage:	2.15V
Maximum Charge Voltage:	2.5V
Minimum Voltage on Discharge:	1.7V
Nominal Capacity @ 25°C:	2.5 Ah @ C/5
Maximum continuous discharge rate:	2C
Maximum charge rate:	C/5
Specific Energy:	350 Wh/kg
Energy Density:	320 Wh/l
Cell Impedance:	25 mΩ

Mechanical Specifications:

Configuration:	Prismatic
Length:	55 mm (top flanged folded)
Width:	37 mm
Thickness:	11.5 mm
Weight:	~16 g

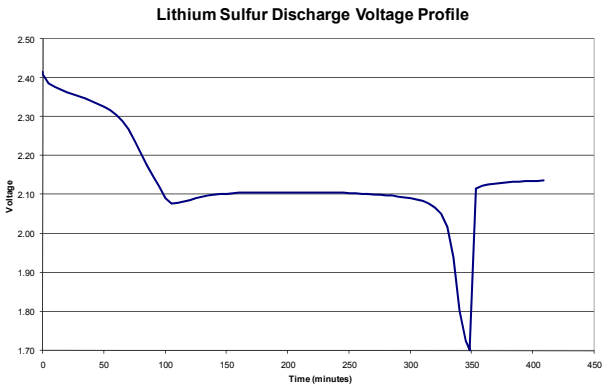

Environmental Specifications:

Discharge Temperature:	-20°C to +45°C
Charge Temperature:	-20°C to +45°C
Storage Temperature:	-40°C to +50°C

SION Power Inc., 2900E. Elvira Rd., Tucson, AZ 85756 Tel: +1.520.799.7500 Fax: 1.520.799.7501
www.sionpower.com

Date: 10/3/08 - Supersedes: 09/28/05

B.2 ABSL 18650HC Cell

ABSL HC Data Sheets UK A4 use 7/8/06 10:56 am Page 1

ABSL 18650HC Cell

ABSL SPACE PRODUCTS

Space Qualified High-Endurance Lithium-ion Secondary Cell

The ABSL 18650HC has more space heritage than any other Lithium-ion cell. It has extensive in-orbit heritage, and tens of millions of hours of characterisation under simulated life testing. Many flight proven battery designs are available for GEO, LEO and interplanetary missions where long-life and high energy density are the key requirements.

Physical
Diameter: 18.0 mm
Height: 65.0 mm
Mass: 40.5 g

Electrical
Voltage Range: 4.2 V – 2.5 V
Nominal Voltage: 3.6 V
Capacity: 1.5 Ah

Performance
Max Charge Current: 1.5 A
Max Discharge Current: 1.5 A
Short Pulse Discharge: 4.5 A for durations up to 1 second

Thermal
Storage Limits
–40°C to +70°C
Operating Limits
–30°C to +60C

Mechanical
Shock: 2,000 g @ 10,000 Hz
Max Quasi-Static Load Limit: 20 g
Random Vibration Limit: 30.4 g_{RMS}

Additional Benefits
Low risk – proven calendar and cycle life
Excellent safety – built-in protection devices
Simple system interfaces – individual cell monitoring not required

The ABSL 18650HC is employed within a number of space qualified batteries such as PROBA, in orbit since Oct 2001

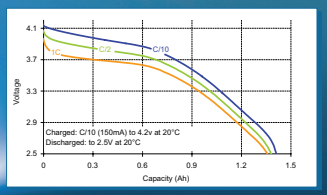

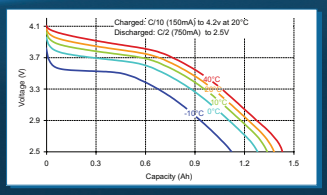

FOR MORE INFORMATION PLEASE CONTACT:

North America
Chris Pearson
TEL: (+1) 303 241 1229
EMAIL: chris.pearson@abslpower.com

Rest of the world
Nick Russel
TEL: +44 (0)1865 408 724
EMAIL: nick.russel@abslpower.com

B.3 SAFT VL 34P

Rechargeable lithium-ion battery
VL 34P - High power cell

Saft's VL 34P cell is ideally suited for applications requiring high discharge, continuous or pulse power; fast re-charge; low temperature performance; long cycle and calendar life; and/or low heat generation.

Saft always supplies cells as complete energy storage systems customized as needed to meet customer specifications.

Saft's battery systems

Individual lithium-ion cells need to be mechanically and electrically integrated into battery systems to operate properly. The battery system includes electronic devices for performance, thermal and safety management specific to each application.

Benefits

- Excellent power density combined with good energy storage
- Hermetically sealed cells
- Maintenance free battery
- Operates in any orientation
- No memory effect
- State of charge identifiable by voltage
- U.S. Department of Transportation approved

Features

- High discharge, pulse and continuous power combined with high energy
- Fast re-charge
- Excellent low temperature performance
- Long cycle and calendar life
- Low heat generation
- Exceptionally high efficiency
- Pre-engineered solutions available (see Power Module & HEMV battery data sheets)

Applications

- Military hybrid electric vehicles
- High pulse power
- Directed energy weapons
- Silent watch
- Portable power

Optimized for 1 C to 15 C continuous discharge or up to 70 C pulse power

Cell electrical characteristics	
Nominal capacity at C rate at 4.1 V/2.5 V & 25°C	33 Ah
Nominal voltage	3.65 V
Energy	120 Wh/432 kJ
Recommended maximum discharge current at 25°C	
Continuous	500+ A
2 s pulse	1,900 A
200 ms pulse	3,000+ A
Power (25°C/100% SoC)	
Continuous	1250 W
2 s pulse	3600 W
200 ms pulse	5700 W
Impedance (25°C/50% SoC at 100 A)	
2 s pulse	< 1 mΩ
200 ms pulse	~ 0.8 mΩ
Low temperature performance*	See chart on p. 2
Cell mechanical characteristics	
Diameter	54 mm
Height**	195 mm
Mass	0.94 kg
Volume**	0.41 L
Cell operating conditions	
Lower voltage limit for discharge*** (- 60°C to + 60°C)	
Continuous	2.0 V
Pulse	1.9 V
Charging method	Constant current/constant voltage (CCCV)
Charging voltage	4.1 ± 0.04 V
Recommended continuous charge current at 25°C	C/2
Fast charging is acceptable, depending on conditions of use	~ 15 minutes (at 120 A rate)****
Operating temperature	
Discharge	- 60°C to + 60°C
Charge****	
Storage and transportation temperature	- 60°C to + 65°C

**Consult Saft for system performance*

***Includes terminals*

****Voltage limits serve as recommendations only - contact Saft for specific use*

*****Fast charging may impact life - contact Saft for higher current or temperature*

July 2009

VL 34P

Battery-level features

- Saft provides complete battery system design
- Incorporation of several levels of redundant safety features to prevent abuse conditions such as overcharge, over-discharge, and short circuit
- Incorporating electronics for performance efficiency:
  - Charge/floating/discharge management
  - Cell balancing
- Battery protection controller at system level
- CanProbe® at module level

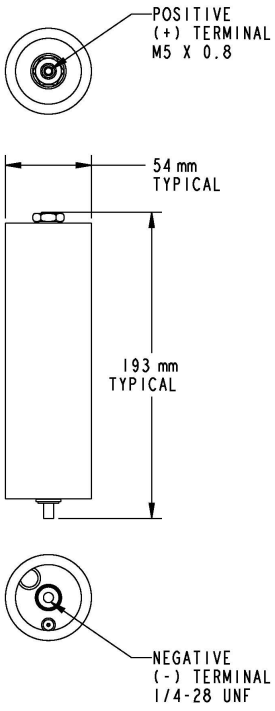

Rate performance at 25° C

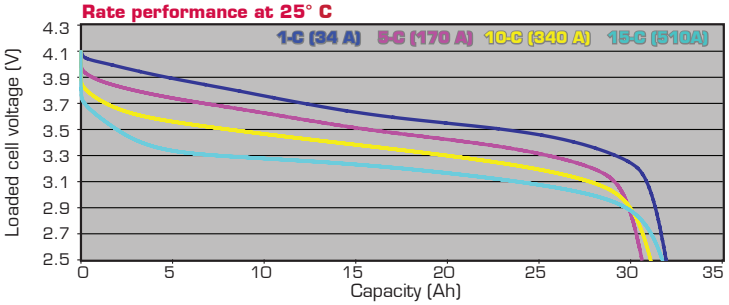

Rate capability at - 30°C

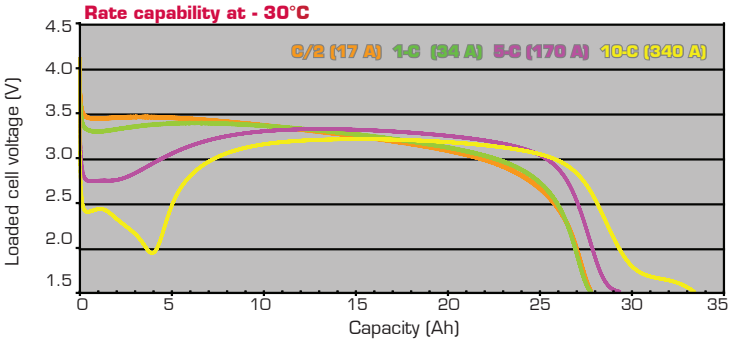

2 sec discharge impedance at 100 A

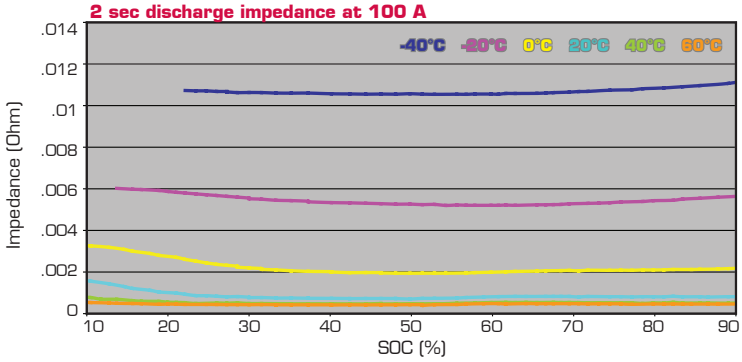

18 sec 2650 W discharge from 4.1 V at 25°C

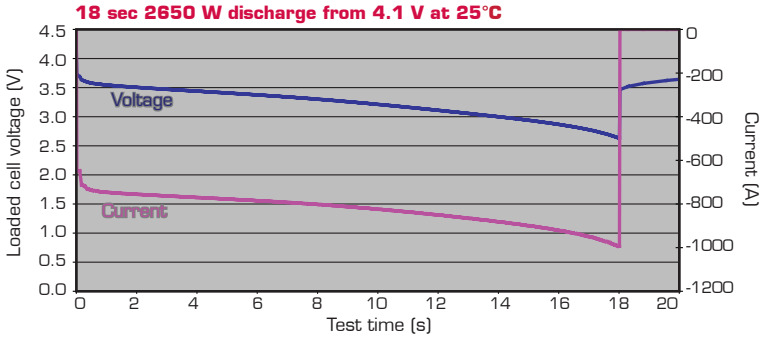

Saft America, Inc.
Space & Defense Division
107 Beaver Court
Cockeysville, MD 21030 - USA
Tel +1 410 771 3200
Fax +1 410 771 1144
SaftDefenseUS@saftbatteries.com

www.saftbatteries.com

Doc N° 54072-2-0709
Edition: July 2009

B.4 SAFT VES 180

Rechargeable lithium battery

VES 180 – Very high specific energy space cell

Characteristics

- Very high specific energy
- Specific space cell design and processes
- Modular and flexible battery range

Benefits

- Excellent energy density and specific energy
- Hermetically-sealed cells
- Long cycle life:
  18 year GEO at 80 % DOD
  60,000 LEO cycles at 20 % DOD
- Qualified in 2007

Main applications

- GEO, MEO space applications
- LEO satellites *(Radar, Optical…)*
- High energy applications

Selected program

- VES 180 Li-ion cell has been selected for Galileo IOV *(in-orbit validation)*, Optus D3, Alphabus etc…

Cell electrical characteristics

Nominal voltage	3.6 V
Nominal capacity at C/1.5 rate at 4.1 V/3 V & 20°C	50 Ah
Maximum discharge current at 25°C	100 A (Continuous ~2 s pulse)
Specific energy (minimum)	175 Wh/Kg
Energy density	180 Wh/l

Cell mechanical characteristics

Diameter	53 mm
Height (max)	250 mm
Mass (max)	1.11 kg

Cell operating conditions

Lower voltage limit for discharge	Continuous (0°C to + 45°C) 2.57 V
Charging method	Constant current/constant voltage (CCCV)
Charging voltage (max)	4.1 V
Recommended continuous charge current	GEO/MEO C/10 LEO (20 % DOD) C/5
Operating temperature	Charge + 10°C to + 35°C Discharge 0°C to + 40°C
Storage and transportation temperature	- 40°C to + 65°C

NB: VES 180 are sold only in modules or batteries.

June 2008

VES 180

Key features

- Graphite-based anode
- Nickel alloy oxide-based cathode
- Specific space terminal and feed-through
- Specific individual stack to cylinder diameter matching
- Leak before burst compliant to ESA Procedures and Specifications Standards (PSS)
- Completely maintenance free
- Operates in any orientation

Capacity versus discharge current
- EOCV (End Of Charge Voltage) = 4.1 V @ 20°C

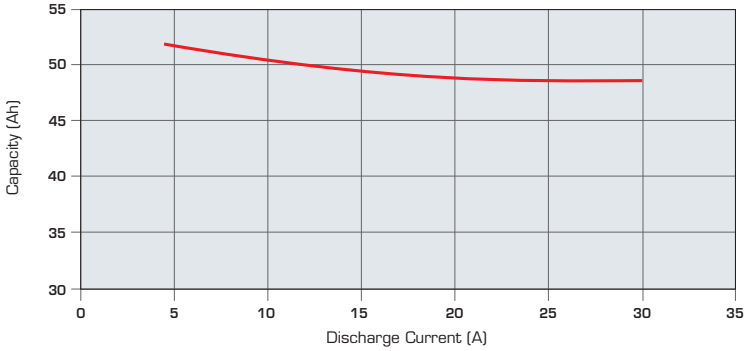

Energy versus Temperature
- EOCV (End Of Charge Voltage) = 4.1 V @ C/2 discharge rate

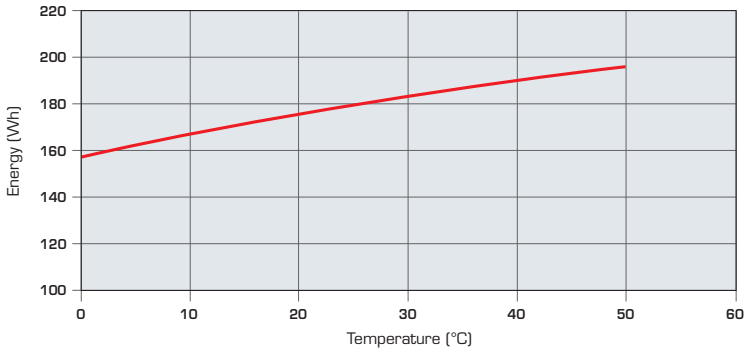

Saft
Specialty Battery Group
12, rue Sadi Carnot
93170 Bagnolet - France
Tel.: +33 (0)1 49 93 19 18
Fax: +33 (0)1 49 93 19 69

www.saftbatteries.com

Doc. Nº 33019-2-0608

Published by the Communications Department.

Photo credit: Saft

Société anonyme au capital de 31 944 000 €
RCS Bobigny B 383 703 873

Produced by Arthur Associates Limited.

APPENDIX C

DETAILS OF TEST EQUIPMENT

C.1 Thermal chambers

Chamber 1

Manufacturer: Design Environmental, UK

Temperature Range: -40°C to 60°C

Calibration: ±1°C

Chamber 3

Manufacturer: Vötsch, Germany

Model No.: VT4010

Temperature Range: -40°C to 180°C

Calibration: ±0.5°C to ±1°C

Chamber 2 (not pictured)

Manufacturer: Vötsch, Germany

Model No.: VT7010

Temperature Range: -70°C to 180°C

Calibration: ±0.5°C to ±1°C

Chamber 25

Manufacturer: Vötsch, Germany

Model No.: VT4020

Temperature Range: -40°C to 180°C

Calibration: ±0.5°C to ±1.5°C

More information on Vötsch VT chambers:

http://www.v-it.com/sixcms/media.php/2335/VIT_Laboratory%20Temperature%20test%20chambers%5B1%5D.pdf

Chamber 8

Manufacturer: TAS, UK

Model No.: ECO MT 900

Temperature Range: -40°C to 100°C

Calibration: ±1°C

More information on TAS chambers:

http://www.tasltd.co.uk/ecospec.html

C.2 Maccor battery tester

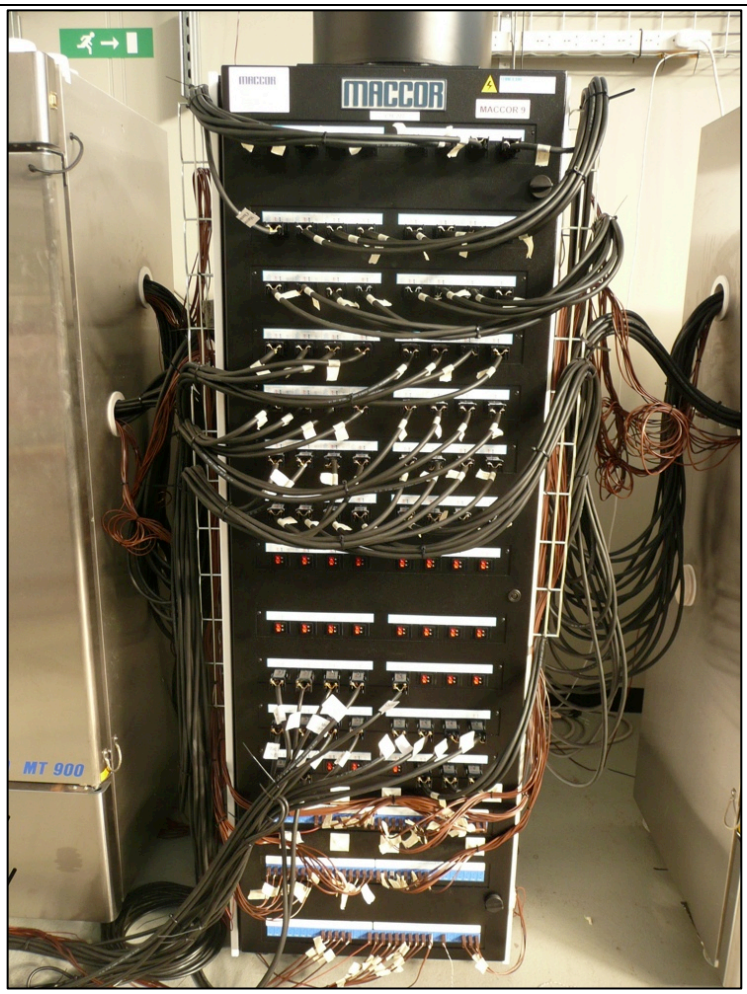

Custom Battery Tester

Manufacturer: Maccor, USA

Voltage range: ±5V or 0-10V channels

Voltage accuracy: 0.02% full scale

Current range: 0-5A and 0-10A channels

Current accuracy: 0.02% full scale

More Information:

http://www.maccor.com/ProductDocs/Data%20Sheet%20for%20Series%204000%20Test%20System.pdf

C.3 Miscellaneous equipment

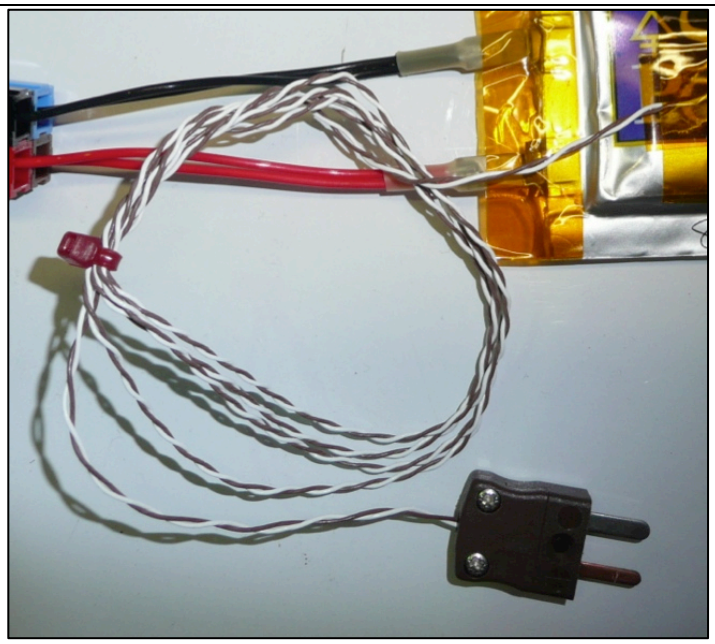

T-Type Thermocouple

Rated: –75oC to +250oC

RS Code: 363-0266

Data Sheet:

http://docs-europe.electrocomponents.com/webdocs/0bce/0900766b80bceddb.pdf

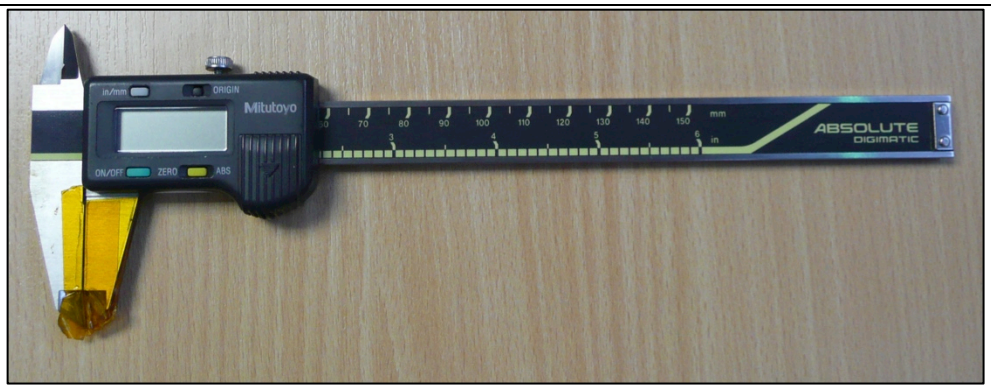

Callipers

Make/Model: Mitutoyo Absolute Digimatic Calliper 500-196-20

Range: 150mm (6in)

Resolution: 0.01mm (0.0005in)

Accuracy: 0.02mm

Harness Cable

Specification: 4 core H07RNF cable, 1.5sq.mm 50m

RS Code: 660-3567

Data Sheet:

http://docs-europe.electrocomponents.com/webdocs/0da7/0900766b80da7070.pdf

Power/Sense Line Cable

Specification: Single Core 20 AWG 19/0.2mm Red/Black

Current rating: 11A

Voltage rating: 600V

Number of strands: 19

Size of strands: 0.2mm

APPENDIX D

EXAMPLE MACCOR PROGRAM

D.1 Hysteresis test; charge to discharge

Step	Type	Mode	Value	Limit	Value	End Type	Op	Value	Go To	Report Type	Value	Options
1	Rest					Step Time	=	00:05:00	2	Step Time	00:01:00	ANNN
2	Charge	Current	0.315	Voltage	2.55	Voltage	>=	2.5	3	Step Time	00:05:00	ANNN
						Voltage	>=	2.54	67			
						Voltage	<=	1.66	67			
3	Charge	Current	0.315	Voltage	2.5	Current	<=	0.05	4	Step Time	00:00:05	ANYN
						Voltage	>=	2.54	67			
						Voltage	<=	1.66	67			
4	Rest					Step Time	=	02:00:00	5	Step Time	00:05:00	ANNN
5	Discharge	Current	0.315	Voltage	1.7	Current	<=	0.05	6	Step Time	00:10:00	ANNY
						Voltage	>=	2.54	67			
						Voltage	<=	1.66	67			
6	Rest					Step Time	=	02:00:00	7	Step Time	00:05:00	ANNN
7	Charge	Current	0.315	Voltage	2.5	Step Time	=	00:30:00	8	Step Time	00:05:00	ANNN
						Current	<=	0.05	8			
						Voltage	>=	2.54	67			
						Voltage	<=	1.66	67			
8	Discharge	Current	0.315	Voltage	1.7	Step Time	=	00:30:00	9	Step Time	00:00:10	ANNY
						Current	<=	0.05	10			
						Voltage	>=	2.54	67			
						Voltage	<=	1.66	67			
9	Discharge	Current	0.315	Voltage	1.7	Current	<=	0.05	10	Step Time	00:05:00	ANYY
						Voltage	>=	2.54	67			
						Voltage	<=	1.66	67			

10	Rest					Step Time	=	02:00:00	11	Step Time	00:05:00	ANNN
11	Charge	Current	0.315	Voltage	2.5	Step Time	=	01:00:00	12	Step Time	00:05:00	ANNN
						Current	<=	0.05	12			
						Voltage	>=	2.54	67			
						Voltage	<=	1.66	67			
12	Discharge	Current	0.315	Voltage	1.7	Step Time	=	00:30:00	13	Step Time	00:00:10	ANNY
						Current	<=	0.05	14			
						Voltage	>=	2.54	67			
						Voltage	<=	1.66	67			
13	Discharge	Current	0.315	Voltage	1.7	Current	<=	0.05	14	Step Time	00:05:00	ANYY
						Voltage	>=	2.54	67			
						Voltage	<=	1.66	67			
14	Rest					Step Time	=	02:00:00	15	Step Time	00:05:00	ANNN
15	Charge	Current	0.315	Voltage	2.5	Step Time	=	01:30:00	16	Step Time	00:05:00	ANNN
						Current	<=	0.05	16			
						Voltage	>=	2.54	67			
						Voltage	<=	1.66	67			
16	Discharge	Current	0.315	Voltage	1.7	Step Time	=	00:30:00	17	Step Time	00:00:10	ANNY
						Current	<=	0.05	18			
						Voltage	>=	2.54	67			
						Voltage	<=	1.66	67			
17	Discharge	Current	0.315	Voltage	1.7	Current	<=	0.05	18	Step Time	00:05:00	ANYY
						Voltage	>=	2.54	67			
						Voltage	<=	1.66	67			
18	Rest					Step Time	=	02:00:00	19	Step Time	00:05:00	ANNN
19	Charge	Current	0.315	Voltage	2.5	Step Time	=	02:00:00	20	Step Time	00:05:00	ANNN
						Current	<=	0.05	20			
						Voltage	>=	2.54	67			
						Voltage	<=	1.66	67			
20	Discharge	Current	0.315	Voltage	1.7	Step Time	=	00:30:00	21	Step Time	00:00:10	ANNY

						Current	<=	0.05	22			
						Voltage	>=	2.54	67			
						Voltage	<=	1.66	67			
21	Discharge	Current	0.315	Voltage	1.7	Current	<=	0.05	22	Step Time	00:05:00	ANYY
						Voltage	>=	2.54	67			
						Voltage	<=	1.66	67			
22	Rest					Step Time	=	02:00:00	23	Step Time	00:05:00	ANNN
23	Charge	Current	0.315	Voltage	2.5	Step Time	=	02:30:00	24	Step Time	00:05:00	ANNN
						Current	<=	0.05	24			
						Voltage	>=	2.54	67			
						Voltage	<=	1.66	67			
24	Discharge	Current	0.315	Voltage	1.7	Step Time	=	00:30:00	25	Step Time	00:00:10	ANNY
						Current	<=	0.05	26			
						Voltage	>=	2.54	67			
						Voltage	<=	1.66	67			
25	Discharge	Current	0.315	Voltage	1.7	Current	<=	0.05	26	Step Time	00:05:00	ANYY
						Voltage	>=	2.54	67			
						Voltage	<=	1.66	67			
26	Rest					Step Time	=	02:00:00	27	Step Time	00:05:00	ANNN
27	Charge	Current	0.315	Voltage	2.5	Step Time	=	03:00:00	28	Step Time	00:05:00	ANNN
						Current	<=	0.05	29			
						Voltage	>=	2.54	67			
						Voltage	<=	1.66	67			
28	Discharge	Current	0.315	Voltage	1.7	Step Time	=	00:30:00	29	Step Time	00:00:10	ANNY
						Current	<=	0.05	29			
						Voltage	>=	2.54	67			
						Voltage	<=	1.66	67			
29	Discharge	Current	0.315	Voltage	1.7	Current	<=	0.05	30	Step Time	00:05:00	ANYY
						Voltage	>=	2.54	67			
						Voltage	<=	1.66	67			
30	Rest					Step Time	=	02:00:00	31	Step Time	00:05:00	ANNN

31	Charge	Current	0.315	Voltage	2.5	Step Time	=	03:30:00	32	Step Time	00:05:00	ANNN
						Current	<=	0.05	32			
						Voltage	>=	2.54	67			
						Voltage	<=	1.66	67			
32	Discharge	Current	0.315	Voltage	1.7	Step Time	=	00:30:00	33	Step Time	00:00:10	ANNY
						Current	<=	0.05	34			
						Voltage	>=	2.54	67			
						Voltage	<=	1.66	67			
33	Discharge	Current	0.315	Voltage	1.7	Current	<=	0.05	34	Step Time	00:05:00	ANYY
						Voltage	>=	2.54	67			
						Voltage	<=	1.66	67			
34	Rest					Step Time	=	02:00:00	35	Step Time	00:05:00	ANNN
35	Charge	Current	0.315	Voltage	2.5	Step Time	=	04:00:00	36	Step Time	00:05:00	ANNN
						Current	<=	0.05	36			
						Voltage	>=	2.54	67			
						Voltage	<=	1.66	67			
36	Discharge	Current	0.315	Voltage	1.7	Step Time	=	00:30:00	37	Step Time	00:00:10	ANNY
						Current	<=	0.05	38			
						Voltage	>=	2.54	67			
						Voltage	<=	1.66	67			
37	Discharge	Current	0.315	Voltage	1.7	Current	<=	0.05	38	Step Time	00:05:00	ANYY
						Voltage	>=	2.54	67			
						Voltage	<=	1.66	67			
38	Rest					Step Time	=	02:00:00	39	Step Time	00:05:00	ANNN
39	Charge	Current	0.315	Voltage	2.5	Step Time	=	04:30:00	40	Step Time	00:05:00	ANNN
						Current	<=	0.05	40			
						Voltage	>=	2.54	67			
						Voltage	<=	1.66	67			
40	Discharge	Current	0.315	Voltage	1.7	Step Time	=	00:30:00	41	Step Time	00:00:10	ANNY
						Current	<=	0.05	42			
						Voltage	>=	2.54	67			

						Voltage	<=	1.66	67			
41	Discharge	Current	0.315	Voltage	1.7	Current	<=	0.05	42	Step Time	00:05:00	ANYY
						Voltage	>=	2.54	67			
						Voltage	<=	1.66	67			
42	Rest					Step Time	=	02:00:00	43	Step Time	00:05:00	ANNN
43	Charge	Current	0.315	Voltage	2.5	Step Time	=	05:00:00	44	Step Time	00:05:00	ANNN
						Current	<=	0.05	44			
						Voltage	>=	2.54	67			
						Voltage	<=	1.66	67			
44	Discharge	Current	0.315	Voltage	1.7	Step Time	=	00:30:00	45	Step Time	00:00:10	ANNY
						Current	<=	0.05	46			
						Voltage	>=	2.54	67			
						Voltage	<=	1.66	67			
45	Discharge	Current	0.315	Voltage	1.7	Current	<=	0.05	46	Step Time	00:05:00	ANYY
						Voltage	>=	2.54	67			
						Voltage	<=	1.66	67			
46	Rest					Step Time	=	02:00:00	47	Step Time	00:05:00	ANNN
47	Charge	Current	0.315	Voltage	2.5	Step Time	=	05:30:00	48	Step Time	00:05:00	ANNN
						Current	<=	0.05	48			
						Voltage	>=	2.54	67			
						Voltage	<=	1.66	67			
48	Discharge	Current	0.315	Voltage	1.7	Step Time	=	00:30:00	49	Step Time	00:00:10	ANNY
						Current	<=	0.05	50			
						Voltage	>=	2.54	67			
						Voltage	<=	1.66	67			
49	Discharge	Current	0.315	Voltage	1.7	Current	<=	0.05	50	Step Time	00:05:00	ANYY
						Voltage	>=	2.54	67			
						Voltage	<=	1.66	67			
50	Rest					Step Time	=	02:00:00	51	Step Time	00:05:00	ANNN
51	Charge	Current	0.315	Voltage	2.5	Step Time	=	06:00:00	52	Step Time	00:05:00	ANNN

						Current	<=	0.05	52			
						Voltage	>=	2.54	67			
						Voltage	<=	1.66	67			
52	Discharge	Current	0.315	Voltage	1.7	Step Time	=	00:30:00	53	Step Time	00:00:10	ANNY
						Current	<=	0.05	54			
						Voltage	>=	2.54	67			
						Voltage	<=	1.66	67			
53	Discharge	Current	0.315	Voltage	1.7	Current	<=	0.05	54	Step Time	00:05:00	ANYY
						Voltage	>=	2.54	67			
						Voltage	<=	1.66	67			
54	Rest					Step Time	=	02:00:00	55	Step Time	00:05:00	ANNN
55	Charge	Current	0.315	Voltage	2.5	Step Time	=	06:30:00	56	Step Time	00:05:00	ANNN
						Current	<=	0.05	56			
						Voltage	>=	2.54	67			
						Voltage	<=	1.66	67			
56	Discharge	Current	0.315	Voltage	1.7	Step Time	=	00:30:00	57	Step Time	00:00:10	ANNY
						Current	<=	0.05	58			
						Voltage	>=	2.54	67			
						Voltage	<=	1.66	67			
57	Discharge	Current	0.315	Voltage	1.7	Current	<=	0.05	58	Step Time	00:05:00	ANYY
						Voltage	>=	2.54	67			
						Voltage	<=	1.66	67			
58	Rest					Step Time	=	02:00:00	59	Step Time	00:05:00	ANNN
59	Charge	Current	0.315	Voltage	2.5	Step Time	=	07:00:00	60	Step Time	00:05:00	ANNN
						Current	<=	0.05	60			
						Voltage	>=	2.54	67			
						Voltage	<=	1.66	67			
60	Discharge	Current	0.315	Voltage	1.7	Step Time	=	00:30:00	61	Step Time	00:00:10	ANNY
						Current	<=	0.05	62			
						Voltage	>=	2.54	67			
						Voltage	<=	1.66	67			
61	Discharge	Current	0.315	Voltage	1.7	Current	<=	0.05	62	Step	00:05:00	ANYY

										Time		
						Voltage	>=	2.54	67			
						Voltage	<=	1.66	67			
62	Rest					Step Time	=	02:00:00	63	Step Time	00:05:00	ANNN
63	Charge	Current	0.315	Voltage	2.5	Step Time	=	07:30:00	64	Step Time	00:05:00	ANNN
						Current	<=	0.05	64			
						Voltage	>=	2.54	67			
						Voltage	<=	1.66	67			
64	Discharge	Current	0.315	Voltage	1.7	Step Time	=	00:30:00	65	Step Time	00:00:10	ANNY
						Current	<=	0.05	66			
						Voltage	>=	2.54	67			
						Voltage	<=	1.66	67			
65	Discharge	Current	0.315	Voltage	1.7	Current	<=	0.05	66	Step Time	00:05:00	ANYY
						Voltage	>=	2.54	67			
						Voltage	<=	1.66	67			
66	Rest					Step Time	=	02:00:00	67	Step Time	00:05:00	ANNN
67	Rest					Step Time	=	500:00:00	68	Step Time	00:10:00	ANNN
68	End											

The entire set of Maccor test programs used in this work are too extensive to include here but are provided for reference on the CD that accompanies this thesis.

APPENDIX E

MODEL LOOKUP DATA TABLES

The raw data used in the Li-S equivalent circuit model is reproduced here in the following sections:

E.1 Cell data

E.2 EMF data

E.3 EMF dependence on temperature

E.4 Discharge resistances

E.5 Charge resistances

E.6 Discharge capacitances

E.7 Charge capacitances

E.8 Hysteresis factors

E.1 Cell data

Thermal conductance from cell to environment = 0.07 (WK^{-1})

Thermal radiance from cell to environment = 3.86×10^{-11}(WK^{-4})

Cell Heat Capacity: 26.4(JK^{-1})

Age Constant = 0.0017 ($hr^{-0.5}$)

Cycling Constant, A_{cyc} = 0.9 (Ah);

Cycing Time Constant, k_{cyc} = 0.7(A^{-1});

Efficiency Degradation Factor = 0.003

Recovery Factor = $0.02hr^{-1}$

E.2 EMF data

	Discharge EMF			Charge EMF		
SoC	**0**℃	**20**℃	**40**℃	**0**℃	**20**℃	**40**℃
0	2.103	2.098	2.094	2.103	2.098	2.094
1	2.102	2.098	2.094	2.117	2.113	2.109
2	2.103	2.099	2.096	2.127	2.124	2.120
3	2.105	2.102	2.098	2.135	2.131	2.128
4	2.107	2.104	2.101	2.141	2.138	2.134
5	2.110	2.107	2.104	2.146	2.143	2.140
6	2.112	2.110	2.108	2.150	2.147	2.145
7	2.115	2.113	2.111	2.153	2.151	2.149
8	2.117	2.116	2.114	2.156	2.155	2.153
9	2.120	2.118	2.117	2.159	2.158	2.156
10	2.122	2.120	2.119	2.162	2.160	2.159
11	2.123	2.123	2.122	2.164	2.163	2.162
12	2.125	2.125	2.124	2.166	2.165	2.165
13	2.127	2.126	2.126	2.168	2.168	2.168
14	2.128	2.128	2.128	2.170	2.170	2.170
15	2.129	2.130	2.130	2.172	2.172	2.172
16	2.131	2.131	2.131	2.174	2.174	2.174
17	2.133	2.133	2.132	2.176	2.175	2.175
18	2.135	2.134	2.133	2.177	2.177	2.176
19	2.136	2.135	2.135	2.179	2.178	2.177
20	2.138	2.137	2.136	2.180	2.179	2.178
21	2.139	2.138	2.137	2.182	2.180	2.179
22	2.140	2.138	2.137	2.183	2.182	2.181
23	2.140	2.139	2.137	2.185	2.183	2.182
24	2.141	2.139	2.138	2.186	2.185	2.183
25	2.141	2.139	2.138	2.188	2.186	2.185
26	2.141	2.140	2.138	2.190	2.188	2.186
27	2.141	2.140	2.138	2.191	2.190	2.188
28	2.142	2.140	2.138	2.193	2.191	2.190
29	2.142	2.140	2.138	2.195	2.193	2.191
30	2.143	2.141	2.138	2.197	2.195	2.192
31	2.144	2.141	2.138	2.199	2.196	2.193
32	2.146	2.142	2.138	2.201	2.197	2.193
33	2.146	2.142	2.138	2.203	2.199	2.195
34	2.147	2.143	2.138	2.205	2.200	2.196
35	2.148	2.143	2.139	2.206	2.202	2.197
36	2.148	2.144	2.139	2.208	2.203	2.199
37	2.148	2.143	2.139	2.210	2.205	2.201
38	2.148	2.143	2.138	2.213	2.208	2.203
39	2.148	2.143	2.138	2.215	2.210	2.204
40	2.148	2.143	2.137	2.217	2.212	2.206
41	2.148	2.143	2.137	2.219	2.214	2.208
42	2.148	2.143	2.137	2.221	2.216	2.210
43	2.149	2.143	2.137	2.224	2.218	2.212
44	2.149	2.143	2.137	2.226	2.220	2.214
45	2.149	2.143	2.137	2.228	2.222	2.216
46	2.150	2.144	2.138	2.230	2.224	2.218
47	2.150	2.144	2.138	2.233	2.227	2.221
48	2.150	2.144	2.138	2.235	2.229	2.223
49	2.151	2.145	2.139	2.238	2.232	2.226

50	2.151	2.145	2.139	2.241	2.235	2.229
51	2.150	2.144	2.138	2.243	2.237	2.231
52	2.150	2.144	2.138	2.246	2.240	2.234
53	2.149	2.143	2.137	2.249	2.243	2.237
54	2.149	2.143	2.137	2.252	2.246	2.240
55	2.148	2.142	2.136	2.255	2.249	2.243
56	2.148	2.142	2.136	2.258	2.252	2.246
57	2.149	2.143	2.137	2.260	2.254	2.248
58	2.149	2.143	2.137	2.263	2.257	2.251
59	2.150	2.144	2.138	2.266	2.260	2.254
60	2.151	2.145	2.139	2.268	2.262	2.256
61	2.152	2.146	2.140	2.272	2.266	2.260
62	2.153	2.147	2.141	2.275	2.269	2.263
63	2.154	2.148	2.142	2.278	2.272	2.266
64	2.154	2.148	2.142	2.281	2.275	2.269
65	2.154	2.148	2.142	2.283	2.277	2.271
66	2.153	2.147	2.141	2.286	2.280	2.274
67	2.153	2.147	2.141	2.289	2.283	2.277
68	2.152	2.146	2.140	2.291	2.285	2.279
69	2.151	2.145	2.139	2.294	2.288	2.282
70	2.149	2.143	2.137	2.296	2.290	2.284
71	2.147	2.141	2.135	2.299	2.293	2.287
72	2.147	2.141	2.134	2.303	2.296	2.290
73	2.151	2.145	2.138	2.306	2.299	2.293
74	2.162	2.155	2.148	2.310	2.303	2.296
75	2.179	2.172	2.164	2.313	2.306	2.299
76	2.196	2.189	2.181	2.317	2.309	2.301
77	2.214	2.206	2.198	2.321	2.313	2.305
78	2.233	2.225	2.216	2.325	2.316	2.308
79	2.253	2.244	2.235	2.330	2.320	2.311
80	2.274	2.264	2.254	2.334	2.324	2.314
81	2.292	2.281	2.271	2.339	2.328	2.318
82	2.309	2.298	2.286	2.344	2.333	2.321
83	2.323	2.311	2.299	2.350	2.338	2.326
84	2.335	2.323	2.310	2.355	2.343	2.330
85	2.346	2.333	2.320	2.361	2.347	2.334
86	2.353	2.339	2.325	2.365	2.351	2.337
87	2.359	2.345	2.331	2.368	2.354	2.340
88	2.364	2.350	2.336	2.371	2.357	2.343
89	2.368	2.354	2.340	2.374	2.360	2.346
90	2.372	2.358	2.344	2.378	2.364	2.350
91	2.377	2.363	2.349	2.382	2.368	2.354
92	2.381	2.367	2.353	2.386	2.372	2.358
93	2.385	2.371	2.357	2.389	2.375	2.361
94	2.390	2.375	2.361	2.394	2.379	2.365
95	2.395	2.379	2.364	2.398	2.383	2.368
96	2.400	2.384	2.368	2.403	2.388	2.372
97	2.405	2.389	2.373	2.410	2.393	2.377
98	2.412	2.395	2.378	2.418	2.401	2.384
99	2.427	2.409	2.392	2.431	2.413	2.396
100	2.445	2.427	2.409	2.473	2.455	2.437

E.3 EMF dependence on temperature

SoC	dE/dT	SoC	dE/dT
0	-0.00022	51	-0.00030
1	-0.00020	52	-0.00030
2	-0.00018	53	-0.00030
3	-0.00017	54	-0.00030
4	-0.00015	55	-0.00030
5	-0.00014	56	-0.00030
6	-0.00012	57	-0.00030
7	-0.00011	58	-0.00030
8	-0.00009	59	-0.00030
9	-0.00007	60	-0.00030
10	-0.00006	61	-0.00030
11	-0.00004	62	-0.00030
12	-0.00003	63	-0.00030
13	-0.00001	64	-0.00030
14	0.00000	65	-0.00030
15	0.00002	66	-0.00030
16	0.00000	67	-0.00030
17	-0.00002	68	-0.00030
18	-0.00004	69	-0.00030
19	-0.00005	70	-0.00030
20	-0.00005	71	-0.00030
21	-0.00006	72	-0.00032
22	-0.00006	73	-0.00033
23	-0.00007	74	-0.00035
24	-0.00007	75	-0.00037
25	-0.00008	76	-0.00038
26	-0.00008	77	-0.00040
27	-0.00009	78	-0.00043
28	-0.00009	79	-0.00047
29	-0.00010	80	-0.00050
30	-0.00013	81	-0.00053
31	-0.00017	82	-0.00057
32	-0.00020	83	-0.00060
33	-0.00021	84	-0.00063
34	-0.00022	85	-0.00067
35	-0.00023	86	-0.00070
36	-0.00024	87	-0.00070
37	-0.00025	88	-0.00070
38	-0.00025	89	-0.00070
39	-0.00026	90	-0.00070
40	-0.00027	91	-0.00070
41	-0.00028	92	-0.00070
42	-0.00029	93	-0.00070
43	-0.00030	94	-0.00073
44	-0.00030	95	-0.00076
45	-0.00030	96	-0.00079
46	-0.00030	97	-0.00081
47	-0.00030	98	-0.00084
48	-0.00030	99	-0.00087
49	-0.00030	100	-0.00090
50	-0.00030		

E.4 Discharge resistances

	R1 Discharge			R2 Discharge			R3 Discharge		
SoC	**0**℃	**20**℃	**40**℃	**0**℃	**20**℃	**40**℃	**0**℃	**20**℃	**40**℃
0	3.274	0.680	0.146	4.638	3.381	1.074	3.667	3.081	0.354
1	3.192	0.639	0.139	4.556	3.029	0.995	3.584	2.856	0.311
2	3.110	0.597	0.132	4.474	2.676	0.915	3.501	2.631	0.269
3	3.028	0.556	0.126	4.393	2.323	0.835	3.418	2.407	0.229
4	2.946	0.514	0.119	4.311	1.971	0.741	3.335	2.182	0.187
5	2.864	0.473	0.112	4.229	1.618	0.645	3.251	1.958	0.147
6	2.782	0.432	0.106	4.147	1.266	0.545	3.168	1.733	0.110
7	2.700	0.390	0.099	4.066	0.913	0.459	3.085	1.509	0.079
8	2.618	0.349	0.092	3.984	0.561	0.370	3.002	1.284	0.052
9	2.536	0.307	0.086	3.902	0.208	0.315	2.918	1.060	0.033
10	2.454	0.266	0.079	3.821	0.097	0.244	2.835	0.835	0.028
11	2.372	0.224	0.072	3.739	0.111	0.192	2.752	0.611	0.035
12	2.290	0.183	0.066	3.657	0.112	0.128	2.669	0.287	0.045
13	2.208	0.141	0.059	3.575	0.105	0.072	2.585	0.089	0.061
14	2.126	0.100	0.052	3.494	0.085	0.065	2.502	0.064	0.048
15	2.044	0.059	0.046	3.412	0.079	0.062	2.419	0.057	0.045
16	1.962	0.049	0.039	3.330	0.073	0.060	2.336	0.054	0.043
17	1.880	0.045	0.034	3.248	0.071	0.056	2.253	0.050	0.039
18	1.798	0.042	0.031	3.167	0.070	0.054	2.169	0.048	0.037
19	1.716	0.040	0.029	3.085	0.070	0.052	2.086	0.048	0.035
20	1.634	0.038	0.028	3.003	0.070	0.051	2.003	0.047	0.034
21	1.554	0.037	0.026	2.918	0.069	0.050	1.921	0.046	0.033
22	1.476	0.036	0.025	2.827	0.069	0.048	1.843	0.045	0.031
23	1.398	0.035	0.024	2.750	0.069	0.047	1.750	0.044	0.030
24	1.322	0.034	0.023	2.675	0.069	0.046	1.655	0.043	0.029
25	1.259	0.034	0.022	2.565	0.069	0.045	1.581	0.042	0.028
26	1.199	0.033	0.021	2.463	0.069	0.044	1.495	0.042	0.027
27	1.143	0.033	0.021	2.369	0.069	0.043	1.399	0.041	0.025
28	1.074	0.033	0.020	2.275	0.069	0.042	1.314	0.040	0.024
29	1.008	0.032	0.019	2.176	0.070	0.041	1.233	0.039	0.023
30	0.956	0.032	0.019	2.061	0.069	0.040	1.153	0.039	0.023
31	0.901	0.032	0.018	1.949	0.070	0.039	1.073	0.038	0.022
32	0.842	0.032	0.018	1.840	0.070	0.038	0.994	0.038	0.021
33	0.779	0.032	0.017	1.723	0.070	0.039	0.926	0.038	0.021
34	0.721	0.031	0.017	1.604	0.070	0.039	0.856	0.037	0.021
35	0.670	0.031	0.018	1.482	0.070	0.039	0.783	0.037	0.021
36	0.620	0.032	0.017	1.358	0.069	0.038	0.710	0.036	0.020
37	0.569	0.032	0.017	1.233	0.069	0.037	0.638	0.036	0.019
38	0.514	0.032	0.017	1.105	0.069	0.036	0.575	0.036	0.019
39	0.459	0.032	0.016	0.978	0.068	0.035	0.510	0.036	0.018
40	0.404	0.032	0.016	0.851	0.068	0.034	0.445	0.035	0.018
41	0.347	0.032	0.016	0.729	0.068	0.033	0.377	0.035	0.017
42	0.323	0.033	0.016	0.677	0.069	0.033	0.348	0.035	0.017
43	0.299	0.033	0.016	0.622	0.068	0.033	0.321	0.035	0.017
44	0.277	0.033	0.016	0.568	0.068	0.033	0.293	0.035	0.017
45	0.255	0.033	0.016	0.517	0.068	0.033	0.267	0.035	0.017
46	0.236	0.034	0.017	0.469	0.068	0.033	0.246	0.035	0.017
47	0.217	0.035	0.017	0.425	0.068	0.033	0.225	0.036	0.018
48	0.202	0.035	0.017	0.388	0.067	0.034	0.209	0.036	0.018
49	0.187	0.036	0.018	0.354	0.067	0.034	0.193	0.037	0.019

50	0.177	0.036	0.018	0.326	0.067	0.034	0.181	0.037	0.019
51	0.167	0.037	0.018	0.301	0.067	0.033	0.169	0.038	0.019
52	0.159	0.038	0.018	0.279	0.067	0.032	0.160	0.038	0.019
53	0.151	0.039	0.018	0.259	0.067	0.032	0.152	0.039	0.019
54	0.145	0.040	0.018	0.242	0.067	0.031	0.145	0.040	0.018
55	0.139	0.041	0.018	0.227	0.067	0.030	0.139	0.041	0.018
56	0.135	0.042	0.019	0.215	0.067	0.030	0.134	0.042	0.019
57	0.132	0.044	0.020	0.204	0.067	0.030	0.129	0.043	0.019
58	0.131	0.045	0.021	0.196	0.067	0.031	0.126	0.043	0.020
59	0.129	0.047	0.022	0.190	0.069	0.033	0.122	0.044	0.021
60	0.129	0.049	0.024	0.184	0.070	0.034	0.119	0.045	0.022
61	0.129	0.051	0.026	0.178	0.071	0.035	0.116	0.046	0.023
62	0.130	0.054	0.027	0.174	0.072	0.037	0.114	0.047	0.024
63	0.131	0.056	0.028	0.170	0.073	0.037	0.112	0.048	0.024
64	0.129	0.058	0.029	0.164	0.074	0.037	0.108	0.049	0.024
65	0.128	0.061	0.030	0.157	0.075	0.037	0.103	0.050	0.024
66	0.133	0.065	0.031	0.157	0.077	0.037	0.104	0.051	0.024
67	0.139	0.069	0.033	0.157	0.078	0.038	0.104	0.052	0.025
68	0.141	0.073	0.035	0.152	0.079	0.038	0.102	0.053	0.026
69	0.141	0.078	0.037	0.146	0.081	0.039	0.099	0.055	0.026
70	0.147	0.084	0.041	0.144	0.082	0.040	0.102	0.058	0.029
71	0.157	0.090	0.045	0.143	0.082	0.041	0.106	0.060	0.031
72	0.172	0.094	0.036	0.138	0.075	0.029	0.104	0.057	0.022
73	0.195	0.095	0.025	0.126	0.061	0.016	0.102	0.050	0.013
74	0.231	0.092	0.018	0.102	0.040	0.008	0.099	0.038	0.008
75	0.240	0.089	0.017	0.101	0.036	0.007	0.098	0.035	0.007
76	0.236	0.085	0.015	0.100	0.034	0.006	0.096	0.033	0.006
77	0.227	0.082	0.012	0.095	0.034	0.005	0.094	0.032	0.005
78	0.218	0.079	0.010	0.092	0.034	0.004	0.092	0.030	0.004
79	0.208	0.075	0.010	0.090	0.033	0.004	0.089	0.029	0.004
80	0.203	0.073	0.011	0.085	0.030	0.005	0.082	0.028	0.004
81	0.200	0.070	0.015	0.079	0.027	0.006	0.073	0.025	0.005
82	0.199	0.067	0.019	0.071	0.023	0.007	0.062	0.020	0.006
83	0.192	0.064	0.023	0.060	0.020	0.007	0.053	0.017	0.007
84	0.182	0.061	0.028	0.051	0.017	0.008	0.046	0.015	0.007
85	0.165	0.057	0.031	0.048	0.016	0.009	0.041	0.014	0.008
86	0.152	0.054	0.031	0.041	0.013	0.008	0.034	0.012	0.007
87	0.141	0.051	0.031	0.031	0.009	0.007	0.027	0.009	0.006
88	0.128	0.049	0.031	0.026	0.008	0.006	0.020	0.009	0.005
89	0.116	0.047	0.031	0.021	0.006	0.006	0.014	0.008	0.004
90	0.104	0.046	0.033	0.017	0.005	0.005	0.012	0.005	0.004
91	0.094	0.044	0.035	0.014	0.005	0.005	0.010	0.005	0.004
92	0.085	0.043	0.037	0.012	0.005	0.005	0.009	0.006	0.004
93	0.077	0.042	0.039	0.011	0.005	0.005	0.009	0.006	0.005
94	0.070	0.042	0.040	0.009	0.005	0.005	0.008	0.006	0.005
95	0.066	0.042	0.042	0.009	0.005	0.006	0.008	0.005	0.005
96	0.063	0.042	0.044	0.008	0.005	0.006	0.008	0.005	0.006
97	0.061	0.042	0.050	0.008	0.005	0.007	0.008	0.005	0.006
98	0.058	0.043	0.054	0.009	0.006	0.008	0.008	0.006	0.007
99	0.051	0.043	0.027	0.009	0.008	0.005	0.007	0.006	0.004
100	0.013	0.043	0.022	0.002	0.009	0.004	0.002	0.007	0.003

E.5 Charge resistances

	R1 Charge			R2 Charge			R3 Charge		
SoC	**0**℃	**20**℃	**40**℃	**0**℃	**20**℃	**40**℃	**0**℃	**20**℃	**40**℃
0	0.058	0.058	0.069	0.037	0.037	0.040	0.034	0.034	0.045
1	0.056	0.056	0.067	0.036	0.036	0.040	0.033	0.033	0.043
2	0.053	0.053	0.064	0.035	0.035	0.040	0.033	0.033	0.042
3	0.051	0.051	0.061	0.034	0.034	0.039	0.033	0.033	0.041
4	0.048	0.048	0.058	0.033	0.033	0.039	0.033	0.033	0.040
5	0.046	0.046	0.055	0.032	0.032	0.039	0.032	0.032	0.038
6	0.044	0.044	0.052	0.031	0.031	0.038	0.032	0.032	0.037
7	0.041	0.041	0.049	0.030	0.030	0.038	0.032	0.032	0.036
8	0.039	0.039	0.047	0.029	0.029	0.038	0.032	0.032	0.035
9	0.036	0.036	0.044	0.028	0.028	0.038	0.031	0.031	0.033
10	0.034	0.034	0.041	0.027	0.027	0.037	0.031	0.031	0.032
11	0.032	0.032	0.038	0.026	0.026	0.037	0.031	0.031	0.031
12	0.029	0.029	0.035	0.025	0.025	0.037	0.031	0.031	0.030
13	0.027	0.027	0.032	0.024	0.024	0.036	0.030	0.030	0.028
14	0.025	0.025	0.029	0.023	0.023	0.036	0.030	0.030	0.027
15	0.022	0.022	0.026	0.022	0.022	0.036	0.030	0.030	0.026
16	0.019	0.019	0.024	0.021	0.021	0.037	0.030	0.030	0.026
17	0.018	0.018	0.023	0.020	0.020	0.037	0.029	0.029	0.026
18	0.017	0.017	0.022	0.020	0.020	0.038	0.029	0.029	0.026
19	0.016	0.016	0.022	0.019	0.019	0.039	0.028	0.028	0.026
20	0.015	0.015	0.021	0.018	0.018	0.039	0.027	0.027	0.026
21	0.014	0.014	0.021	0.017	0.017	0.040	0.027	0.027	0.026
22	0.014	0.014	0.021	0.017	0.017	0.040	0.026	0.026	0.026
23	0.013	0.013	0.021	0.016	0.016	0.041	0.026	0.026	0.026
24	0.013	0.013	0.021	0.016	0.016	0.042	0.026	0.026	0.026
25	0.012	0.012	0.021	0.016	0.016	0.042	0.025	0.025	0.026
26	0.012	0.012	0.021	0.015	0.015	0.043	0.025	0.025	0.026
27	0.012	0.012	0.021	0.014	0.014	0.043	0.024	0.024	0.026
28	0.011	0.011	0.021	0.014	0.014	0.044	0.024	0.024	0.026
29	0.011	0.011	0.021	0.014	0.014	0.045	0.024	0.024	0.025
30	0.011	0.011	0.022	0.014	0.014	0.047	0.024	0.024	0.026
31	0.012	0.012	0.023	0.014	0.014	0.049	0.025	0.025	0.027
32	0.012	0.012	0.024	0.014	0.014	0.052	0.026	0.026	0.028
33	0.012	0.012	0.024	0.015	0.015	0.054	0.027	0.027	0.029
34	0.013	0.013	0.025	0.015	0.015	0.055	0.028	0.028	0.030
35	0.013	0.013	0.026	0.015	0.015	0.057	0.029	0.029	0.030
36	0.014	0.014	0.026	0.016	0.016	0.058	0.030	0.030	0.030
37	0.014	0.014	0.027	0.016	0.016	0.059	0.030	0.030	0.030
38	0.014	0.014	0.028	0.016	0.016	0.059	0.031	0.031	0.031
39	0.015	0.015	0.028	0.016	0.016	0.060	0.031	0.031	0.031
40	0.015	0.015	0.029	0.017	0.017	0.061	0.032	0.032	0.032
41	0.016	0.016	0.030	0.017	0.017	0.063	0.033	0.033	0.032
42	0.016	0.016	0.031	0.017	0.017	0.064	0.034	0.034	0.033
43	0.017	0.017	0.031	0.018	0.018	0.065	0.035	0.035	0.034
44	0.017	0.017	0.032	0.018	0.018	0.066	0.036	0.036	0.034
45	0.018	0.018	0.033	0.019	0.019	0.067	0.037	0.037	0.034
46	0.019	0.019	0.034	0.020	0.020	0.067	0.037	0.037	0.035
47	0.020	0.020	0.034	0.020	0.020	0.067	0.039	0.039	0.036
48	0.021	0.021	0.035	0.021	0.021	0.068	0.040	0.040	0.036
49	0.021	0.021	0.036	0.022	0.022	0.067	0.041	0.041	0.037

50	0.022	0.022	0.036	0.023	0.023	0.067	0.041	0.041	0.037
51	0.023	0.023	0.037	0.024	0.024	0.066	0.042	0.042	0.037
52	0.025	0.025	0.037	0.025	0.025	0.065	0.043	0.043	0.038
53	0.026	0.026	0.038	0.026	0.026	0.065	0.044	0.044	0.038
54	0.026	0.026	0.038	0.027	0.027	0.064	0.044	0.044	0.038
55	0.028	0.028	0.038	0.028	0.028	0.063	0.045	0.045	0.038
56	0.029	0.029	0.039	0.029	0.029	0.061	0.046	0.046	0.038
57	0.031	0.031	0.039	0.030	0.030	0.060	0.048	0.048	0.038
58	0.033	0.033	0.040	0.032	0.032	0.059	0.049	0.049	0.038
59	0.034	0.034	0.040	0.033	0.033	0.058	0.051	0.051	0.038
60	0.036	0.036	0.040	0.034	0.034	0.057	0.052	0.052	0.037
61	0.038	0.038	0.040	0.034	0.034	0.055	0.052	0.052	0.036
62	0.039	0.039	0.040	0.034	0.034	0.053	0.052	0.052	0.035
63	0.041	0.041	0.039	0.035	0.035	0.051	0.053	0.053	0.034
64	0.042	0.042	0.039	0.035	0.035	0.049	0.053	0.053	0.033
65	0.044	0.044	0.039	0.035	0.035	0.048	0.054	0.054	0.031
66	0.045	0.045	0.039	0.035	0.035	0.046	0.054	0.054	0.030
67	0.047	0.047	0.039	0.035	0.035	0.044	0.053	0.053	0.029
68	0.049	0.049	0.040	0.036	0.036	0.043	0.053	0.053	0.029
69	0.051	0.051	0.040	0.036	0.036	0.042	0.053	0.053	0.028
70	0.053	0.053	0.041	0.036	0.036	0.040	0.051	0.051	0.028
71	0.054	0.054	0.041	0.036	0.036	0.037	0.049	0.049	0.028
72	0.058	0.058	0.043	0.035	0.035	0.035	0.046	0.046	0.026
73	0.063	0.063	0.047	0.033	0.033	0.030	0.041	0.041	0.025
74	0.072	0.072	0.054	0.031	0.031	0.024	0.032	0.032	0.023
75	0.072	0.072	0.054	0.030	0.030	0.023	0.031	0.031	0.022
76	0.071	0.071	0.053	0.029	0.029	0.022	0.030	0.030	0.022
77	0.070	0.070	0.052	0.029	0.029	0.022	0.029	0.029	0.022
78	0.068	0.068	0.051	0.028	0.028	0.022	0.029	0.029	0.022
79	0.065	0.065	0.050	0.028	0.028	0.022	0.028	0.028	0.022
80	0.065	0.065	0.051	0.026	0.026	0.021	0.027	0.027	0.020
81	0.064	0.064	0.052	0.023	0.023	0.020	0.025	0.025	0.019
82	0.064	0.064	0.054	0.020	0.020	0.019	0.023	0.023	0.017
83	0.061	0.061	0.054	0.017	0.017	0.017	0.019	0.019	0.015
84	0.057	0.057	0.055	0.015	0.015	0.015	0.016	0.016	0.014
85	0.051	0.051	0.053	0.013	0.013	0.015	0.015	0.015	0.013
86	0.047	0.047	0.052	0.011	0.011	0.014	0.013	0.013	0.012
87	0.050	0.050	0.054	0.010	0.010	0.012	0.011	0.011	0.010
88	0.051	0.051	0.055	0.008	0.008	0.011	0.010	0.010	0.009
89	0.051	0.051	0.056	0.006	0.006	0.010	0.009	0.009	0.007
90	0.051	0.051	0.056	0.006	0.006	0.009	0.008	0.008	0.006
91	0.050	0.050	0.055	0.005	0.005	0.008	0.007	0.007	0.006
92	0.050	0.050	0.057	0.006	0.006	0.008	0.007	0.007	0.006
93	0.050	0.050	0.059	0.006	0.006	0.008	0.007	0.007	0.007
94	0.050	0.050	0.065	0.006	0.006	0.009	0.007	0.007	0.008
95	0.052	0.052	0.075	0.006	0.006	0.010	0.007	0.007	0.009
96	0.053	0.053	0.085	0.007	0.007	0.011	0.007	0.007	0.011
97	0.060	0.060	0.114	0.008	0.008	0.015	0.008	0.008	0.015
98	0.065	0.065	0.140	0.009	0.009	0.021	0.010	0.010	0.019
99	0.136	0.136	0.226	0.020	0.020	0.039	0.023	0.023	0.033
100	0.203	0.203	0.308	0.031	0.031	0.058	0.038	0.038	0.048

E.6 Discharge capacitances

	C2 Discharge			C3 Discharge		
SoC	**0**℃	**20**℃	**40**℃	**0**℃	**20**℃	**40**℃
0	2000	2000	4263	50	1000	1258
1	2000	2000	4510	50	1000	1258
2	2000	2000	4756	50	1000	1258
3	2000	2000	5003	50	1000	1258
4	2000	2000	5250	50	1000	1258
5	2000	2000	5497	50	1000	1258
6	2000	2000	5743	50	1000	1258
7	2000	2000	5990	50	1000	1258
8	2000	2000	6237	50	1000	1258
9	2000	2000	6483	64	1000	1258
10	2000	2432	6730	51	1000	1258
11	2000	5809	6977	20	1000	1258
12	2000	4695	7223	42	1000	1258
13	2000	4684	7470	200	1000	1258
14	2000	6180	7717	547	1000	1258
15	2000	7259	7964	722	1000	1258
16	2000	8128	8210	842	1000	1258
17	2000	8517	8457	897	1000	1258
18	2000	8888	8704	957	1000	1258
19	2000	9246	8950	1018	1018	1258
20	2000	9609	9197	1078	1078	1258
21	2000	9972	9444	1143	1143	1258
22	2000	10333	9690	1215	1215	1258
23	2000	10317	9937	1243	1243	1258
24	2000	10184	10184	1258	1258	1258
25	2000	10431	10431	1337	1337	1337
26	10657	10657	10657	1400	1400	1400
27	10861	10861	10861	1445	1445	1445
28	11102	11102	11102	1477	1477	1477
29	11310	11310	11310	1515	1515	1515
30	11393	11393	11393	1575	1575	1575
31	11501	11501	11501	1610	1610	1610
32	11623	11623	11623	1628	1628	1628
33	11790	11790	11790	1630	1630	1630
34	12150	12150	12150	1679	1679	1679
35	12509	12509	12509	1728	1728	1728
36	12781	12781	12781	1753	1753	1753
37	13073	13073	13073	1778	1778	1778
38	13657	13657	13657	1841	1841	1841
39	13933	13933	13933	1874	1874	1874
40	13926	13926	13926	1880	1880	1880
41	14082	14082	14082	1878	1878	1878
42	14269	14269	14269	1877	1877	1877
43	14486	14486	14486	1878	1878	1878
44	14528	14528	14528	1876	1876	1876
45	14498	14498	14498	1873	1873	1873
46	14813	14813	14813	1891	1891	1891
47	14978	14978	14978	1895	1895	1895
48	14939	14939	14939	1878	1878	1878
49	14952	14952	14952	1882	1882	1882

50	14975	14975	14975	1887	1887	1887
51	14983	14983	14983	1873	1873	1873
52	14981	14981	14981	1873	1873	1873
53	14973	14973	14973	1883	1883	1883
54	14647	14647	14647	1854	1854	1854
55	14385	14385	14385	1832	1832	1832
56	14285	14285	14285	1826	1826	1826
57	14093	14093	14093	1814	1814	1814
58	13883	13883	13883	1800	1800	1800
59	13857	13857	13857	1788	1788	1788
60	13635	13635	13635	1777	1777	1777
61	13197	13197	13197	1767	1767	1767
62	12845	12845	12845	1769	1769	1769
63	12607	12607	12607	1772	1772	1772
64	12696	12696	12696	1777	1777	1777
65	12636	12636	12636	1782	1782	1782
66	12482	12482	12482	1788	1788	1788
67	12079	12079	12079	1779	1779	1779
68	11657	11657	11657	1768	1768	1768
69	11204	11204	11204	1757	1757	1757
70	10909	10909	10909	1723	1723	1723
71	10824	10824	10824	1702	1702	1702
72	11724	11724	11724	1809	1809	1809
73	13801	13801	13801	1998	1998	1998
74	16956	16956	16956	2261	2261	2261
75	18494	18494	18494	2356	2356	2356
76	19643	19643	19643	2420	2420	2420
77	20253	20253	20253	2453	2453	2453
78	19801	19801	19801	2429	2429	2429
79	18929	18929	18929	2382	2382	2382
80	20454	20454	20454	2430	2430	2430
81	21653	21653	21653	2477	2477	2477
82	22413	22413	22413	2524	2524	2524
83	23126	23126	23126	2569	2569	2569
84	24507	24507	24507	2616	2616	2616
85	28801	28801	28801	2677	2677	2677
86	30493	30493	30493	5000	5000	5000
87	30222	30222	30222	5000	5000	5000
88	39713	39713	39713	5000	5000	5000
89	51259	51259	51259	5000	5000	5000
90	65927	65927	65927	5000	5000	5000
91	74508	74508	74508	5000	5000	5000
92	80611	80611	80611	5000	5000	5000
93	86404	86404	86404	5000	5000	5000
94	83191	83191	83191	5000	5000	5000
95	70046	70046	70046	5000	5000	5000
96	61691	61691	61691	5000	5000	5000
97	52569	52569	52569	5000	5000	5000
98	38408	38408	38408	5000	5000	5000
99	24247	24247	24247	5000	5000	5000
100	10086	10086	10086	5000	5000	5000

E.7 Charge capacitances

	C2 Charge			C3 Charge		
SoC	**0**℃	**20**℃	**40**℃	**0**℃	**20**℃	**40**℃
0	10333	10333	10333	1215	1215	1215
1	10333	10333	10333	1215	1215	1215
2	10333	10333	10333	1215	1215	1215
3	10333	10333	10333	1215	1215	1215
4	10333	10333	10333	1215	1215	1215
5	10333	10333	10333	1215	1215	1215
6	10333	10333	10333	1215	1215	1215
7	10333	10333	10333	1215	1215	1215
8	10333	10333	10333	1215	1215	1215
9	10333	10333	10333	1215	1215	1215
10	10333	10333	10333	1215	1215	1215
11	10333	10333	10333	1215	1215	1215
12	10333	10333	10333	1215	1215	1215
13	10333	10333	10333	1215	1215	1215
14	10333	10333	10333	1215	1215	1215
15	10333	10333	10333	1215	1215	1215
16	10333	10333	10333	1215	1215	1215
17	10333	10333	10333	1215	1215	1215
18	10333	10333	10333	1215	1215	1215
19	10333	10333	10333	1215	1215	1215
20	10333	10333	10333	1215	1215	1215
21	10333	10333	10333	1215	1215	1215
22	10333	10333	10333	1215	1215	1215
23	10317	10317	10317	1243	1243	1243
24	10184	10184	10184	1258	1258	1258
25	10431	10431	10431	1337	1337	1337
26	10657	10657	10657	1400	1400	1400
27	10861	10861	10861	1445	1445	1445
28	11102	11102	11102	1477	1477	1477
29	11310	11310	11310	1515	1515	1515
30	11393	11393	11393	1575	1575	1575
31	11501	11501	11501	1610	1610	1610
32	11623	11623	11623	1628	1628	1628
33	11790	11790	11790	1630	1630	1630
34	12150	12150	12150	1679	1679	1679
35	12509	12509	12509	1728	1728	1728
36	12781	12781	12781	1753	1753	1753
37	13073	13073	13073	1778	1778	1778
38	13657	13657	13657	1841	1841	1841
39	13933	13933	13933	1874	1874	1874
40	13926	13926	13926	1880	1880	1880
41	14082	14082	14082	1878	1878	1878
42	14269	14269	14269	1877	1877	1877
43	14486	14486	14486	1878	1878	1878
44	14528	14528	14528	1876	1876	1876
45	14498	14498	14498	1873	1873	1873
46	14813	14813	14813	1891	1891	1891
47	14978	14978	14978	1895	1895	1895
48	14939	14939	14939	1878	1878	1878
49	14952	14952	14952	1882	1882	1882

50	14975	14975	14975	1887	1887	1887
51	14983	14983	14983	1873	1873	1873
52	14981	14981	14981	1873	1873	1873
53	14973	14973	14973	1883	1883	1883
54	14647	14647	14647	1854	1854	1854
55	14385	14385	14385	1832	1832	1832
56	14285	14285	14285	1826	1826	1826
57	14093	14093	14093	1814	1814	1814
58	13883	13883	13883	1800	1800	1800
59	13857	13857	13857	1788	1788	1788
60	13635	13635	13635	1777	1777	1777
61	13197	13197	13197	1767	1767	1767
62	12845	12845	12845	1769	1769	1769
63	12607	12607	12607	1772	1772	1772
64	12696	12696	12696	1777	1777	1777
65	12636	12636	12636	1782	1782	1782
66	12482	12482	12482	1788	1788	1788
67	12079	12079	12079	1779	1779	1779
68	11657	11657	11657	1768	1768	1768
69	11204	11204	11204	1757	1757	1757
70	10909	10909	10909	1723	1723	1723
71	10824	10824	10824	1702	1702	1702
72	11724	11724	11724	1809	1809	1809
73	13801	13801	13801	1998	1998	1998
74	16956	16956	16956	2261	2261	2261
75	18494	18494	18494	2356	2356	2356
76	19643	19643	19643	2420	2420	2420
77	20253	20253	20253	2453	2453	2453
78	19801	19801	19801	2429	2429	2429
79	18929	18929	18929	2382	2382	2382
80	20454	20454	20454	2430	2430	2430
81	21653	21653	21653	2477	2477	2477
82	22413	22413	22413	2524	2524	2524
83	23126	23126	23126	2569	2569	2569
84	24507	24507	24507	2616	2616	2616
85	28801	28801	28801	2677	2677	2677
86	30493	30493	30493	5000	5000	5000
87	30222	30222	30222	5000	5000	5000
88	39713	39713	39713	5000	5000	5000
89	51259	51259	51259	5000	5000	5000
90	65927	65927	65927	5000	5000	5000
91	74508	74508	74508	5000	5000	5000
92	80611	80611	80611	5000	5000	5000
93	86404	86404	86404	5000	5000	5000
94	83191	83191	83191	5000	5000	5000
95	70046	70046	70046	5000	5000	5000
96	61691	61691	61691	5000	5000	5000
97	52569	52569	52569	5000	5000	5000
98	38408	38408	38408	5000	5000	5000
99	24247	24247	24247	5000	5000	5000
100	10086	10086	10086	5000	5000	5000

E.8 Hysteresis factors

	Hysteresis Discharge				Hysteresis Charge			
SoC	Cons1	Cons2	Tau1	Tau2	Cons1	Cons2	Tau1	Tau2
0	0.500	0.500	0.001	0.001	0.508	0.492	31.500	31.500
1	0.500	0.500	0.001	0.001	0.507	0.493	29.925	29.925
2	0.500	0.500	0.001	0.001	0.505	0.495	28.350	28.350
3	0.500	0.500	0.001	0.001	0.503	0.497	26.775	26.775
4	0.500	0.500	0.001	0.001	0.502	0.498	25.200	25.200
5	0.500	0.500	0.001	0.001	0.500	0.500	23.625	23.625
6	0.500	0.500	0.001	0.001	0.498	0.502	22.050	22.050
7	0.500	0.500	0.001	0.001	0.497	0.503	20.475	20.475
8	0.409	0.591	0.069	0.001	0.495	0.505	18.900	18.900
9	0.318	0.682	0.138	0.001	0.493	0.507	17.325	17.325
10	0.227	0.773	0.207	0.001	0.492	0.508	15.750	15.750
11	0.136	0.864	0.275	0.001	0.490	0.510	14.175	14.175
12	0.215	0.785	0.344	0.001	0.488	0.512	12.600	12.600
13	0.294	0.706	0.413	0.001	0.487	0.513	11.025	11.025
14	0.373	0.627	0.481	0.001	0.485	0.515	9.450	9.450
15	0.452	0.548	0.416	0.242	0.483	0.517	7.875	7.875
16	0.453	0.547	0.350	0.484	0.400	0.600	7.560	6.314
17	0.454	0.546	0.285	0.726	0.317	0.683	7.245	4.754
18	0.455	0.545	0.219	0.967	0.234	0.766	6.930	3.193
19	0.456	0.544	0.153	1.209	0.151	0.849	6.615	1.633
20	0.457	0.543	0.088	1.451	0.067	0.933	6.300	0.072
21	0.447	0.553	0.022	1.692	0.072	0.928	5.061	1.108
22	0.436	0.564	0.024	2.400	0.077	0.923	3.823	2.143
23	0.425	0.575	0.026	3.108	0.081	0.919	2.584	3.179
24	0.415	0.585	0.029	3.815	0.086	0.914	1.346	4.214
25	0.404	0.596	0.031	4.523	0.091	0.909	0.107	5.250
26	0.393	0.607	0.033	5.231	0.095	0.905	0.104	5.100
27	0.381	0.619	0.035	5.938	0.099	0.901	0.102	4.950
28	0.370	0.630	0.038	6.646	0.103	0.897	0.099	4.800
29	0.358	0.642	0.047	7.312	0.107	0.893	0.096	4.650
30	0.351	0.649	0.056	7.977	0.111	0.889	0.094	4.500
31	0.335	0.665	0.065	8.643	0.114	0.886	0.093	4.300
32	0.324	0.676	0.074	9.308	0.118	0.882	0.092	4.100
33	0.321	0.679	0.084	9.974	0.122	0.878	0.091	3.900
34	0.318	0.682	0.093	10.639	0.125	0.875	0.090	3.700
35	0.315	0.685	0.102	11.305	0.129	0.871	0.089	3.500
36	0.313	0.687	0.111	11.971	0.133	0.867	0.090	3.430
37	0.310	0.690	0.138	14.824	0.137	0.863	0.090	3.360
38	0.307	0.693	0.166	17.677	0.145	0.855	0.091	3.220
39	0.305	0.695	0.193	20.531	0.145	0.855	0.091	3.220
40	0.302	0.698	0.220	23.384	0.149	0.851	0.091	3.150
41	0.305	0.695	0.247	26.238	0.155	0.845	0.093	3.093
42	0.308	0.692	0.275	29.091	0.161	0.839	0.095	3.035
43	0.311	0.689	0.302	31.944	0.166	0.834	0.097	2.978
44	0.314	0.686	0.277	28.547	0.172	0.828	0.100	2.921
45	0.318	0.682	0.252	25.149	0.178	0.822	0.102	2.864
46	0.321	0.679	0.227	21.752	0.185	0.815	0.106	2.816
47	0.324	0.676	0.202	18.354	0.191	0.809	0.110	2.768
48	0.327	0.673	0.176	14.956	0.198	0.802	0.114	2.720
49	0.330	0.670	0.151	11.559	0.205	0.795	0.118	2.673
50	0.303	0.697	0.126	8.161	0.211	0.789	0.123	2.625

51	0.277	0.723	0.101	4.764	0.217	0.783	0.116	2.520
52	0.250	0.750	0.120	5.149	0.224	0.776	0.110	2.415
53	0.224	0.776	0.139	5.534	0.230	0.770	0.104	2.310
54	0.197	0.803	0.158	5.919	0.236	0.764	0.098	2.205
55	0.171	0.829	0.177	6.304	0.242	0.758	0.091	2.100
56	0.144	0.856	0.196	6.689	0.251	0.749	0.093	2.074
57	0.117	0.883	0.215	7.074	0.260	0.740	0.095	2.048
58	0.126	0.874	0.234	7.459	0.268	0.732	0.097	2.021
59	0.135	0.865	0.253	7.844	0.277	0.723	0.099	1.995
60	0.143	0.857	0.272	8.230	0.286	0.714	0.101	1.969
61	0.152	0.848	0.284	8.394	0.300	0.700	0.103	1.946
62	0.161	0.839	0.296	8.558	0.314	0.686	0.104	1.922
63	0.170	0.830	0.307	8.723	0.328	0.672	0.105	1.899
64	0.178	0.822	0.319	8.887	0.342	0.658	0.106	1.876
65	0.181	0.819	0.331	9.052	0.357	0.643	0.108	1.853
66	0.184	0.816	0.343	9.216	0.371	0.629	0.109	1.830
67	0.187	0.813	0.355	9.381	0.385	0.615	0.110	1.807
68	0.190	0.810	0.366	9.545	0.399	0.601	0.111	1.783
69	0.193	0.807	0.327	8.615	0.413	0.587	0.112	1.760
70	0.196	0.804	0.097	3.326	0.427	0.573	0.114	1.737
71	0.199	0.801	0.247	6.753	0.441	0.559	0.115	1.714
72	0.202	0.798	0.207	5.823	0.469	0.531	0.117	1.668
73	0.224	0.776	0.167	4.892	0.469	0.531	0.117	1.668
74	0.247	0.753	0.127	3.962	0.484	0.516	0.119	1.644
75	0.269	0.731	0.088	3.031	0.498	0.502	0.120	1.621
76	0.292	0.708	0.086	2.972	0.512	0.488	0.121	1.598
77	0.314	0.686	0.084	2.913	0.526	0.474	0.122	1.575
78	0.336	0.664	0.082	2.854	0.540	0.460	0.124	1.552
79	0.359	0.641	0.080	2.795	0.554	0.446	0.125	1.529
80	0.351	0.649	0.078	2.736	0.568	0.432	0.126	1.506
81	0.344	0.656	0.514	2.200	0.582	0.418	0.127	1.482
82	0.336	0.664	0.951	1.664	0.596	0.404	0.129	1.459
83	0.329	0.671	1.387	1.128	0.611	0.389	0.130	1.436
84	0.321	0.679	1.823	0.592	0.625	0.375	0.131	1.413
85	0.314	0.686	2.259	0.056	0.639	0.361	0.132	1.390
86	0.306	0.694	2.073	0.043	0.653	0.347	0.134	1.367
87	0.334	0.666	1.887	0.029	0.667	0.333	0.135	1.343
88	0.362	0.638	1.701	0.016	0.681	0.319	0.136	1.320
89	0.389	0.611	1.515	0.003	0.695	0.305	0.137	1.297
90	0.417	0.583	1.144	0.010	0.709	0.291	0.139	1.274
91	0.445	0.555	0.774	0.018	0.723	0.277	0.140	1.251
92	0.472	0.528	0.403	0.025	0.737	0.263	0.141	1.228
93	0.500	0.500	0.033	0.033	0.752	0.248	0.142	1.204
94	0.528	0.472	0.033	0.040	0.766	0.234	0.144	1.181
95	0.555	0.445	0.033	0.047	0.780	0.220	0.145	1.158
96	0.583	0.417	0.033	0.055	0.794	0.206	0.146	1.135
97	0.611	0.389	0.033	0.062	0.808	0.192	0.147	1.112
98	0.638	0.362	0.033	0.070	0.822	0.178	0.149	1.089
99	0.666	0.334	0.033	0.077	0.836	0.164	0.150	1.065
100	0.694	0.306	0.033	0.084	0.850	0.150	0.151	1.042

APPENDIX F

CORE MODEL CODE

INITIALISE MODEL

```
%%Data Import and Setup

hStep = 40; % solve step time

InitialTemp = 20; % set by user
CellTemp1 = InitialTemp; %Cell Temp
AmbientTemp = InitialTemp; % Environmental Temp
InitialSoC = 100; % set by user
SoC = InitialSoC;

start_mode = -1; %0=rest, 1=charge,-1=discharge, set by user.
mode = start_mode;
previous_mode = start_mode;
mode_flag = 0; % to determine mode change

SC = 1; %SeriesCells
PS1 = 1;%ParallelStrings1;
PS2 = 1;%ParallelStrings2;
StringFailure = 0;
ActiveStrings = PS2 - StringFailure; %strings remaining after failure

MaxVoltage = 2.5;
MinVoltage = 1.7;
MaxSoC = 100;
MinSoC = 0;

Qc1env = 0.07; % conductive heat transfer coefficient
Qr1env = 3.86*10^-11;% radiative heat transfer coefficient
mCp1 = 26.4;% heat capacity.

%% Initial Capacity and Fade
% User inputs history of cell, previous cycle number and at what rate,
age of cell in days, otherwise model assumes cell is brand new.
History = 0;
if History == 1 %user sets History to 1 if cell has a history.
    CellAge = 180; %age of cell in days since manufacture
    CycNo = 1;
    AvgI = 0.315; %Average current rate that the cell has been used at
else
    CellAge = 0;
    CycNo = 0;
    AvgI = 0;
end
SCMCap = 2.68; % Ah, nominal dchg capacity found during SCM, set by user.
DchgCap = SCMCap/0.92; % Ah, full dchg capacity.
AgeConst = 0.0017; % Constant to determine calendar aging degradation
CycConst = 0.94; % Constant to determine cycling degradation
CycTimeConst = 0.7; % Time constant to determine cycling degradation
```

```
EffDeg = 0.003; %efficiency degradation 0.3% per cycle
Qcyc = (CycConst * exp(-CycTimeConst*AvgI)*CycNo)*DchgCap/100;
Qage = (AgeConst* CellAge^0.5)*DchgCap/100; %irreversible capcity lost
due to age of cell
I1 = 0.315;
RateCap = (SCMCap) - ((SCMCap)*0.315^0.273)*(I1^-0.273); %Ah Rate
capacity adjustment for Q2
TotDchgCap = (DchgCap - Qage - Qcyc);
TotChgCap = (TotDchgCap)/(0.967 - (EffDeg*CycNo));
Q1 = TotDchgCap*0.28;
Q2 = TotDchgCap*0.72 - RateCap;
if mode == 1
    CellCap = TotChgCap;
elseif mode == -1 && SoC >= 72
    split = 1;
    CellCap = TotDchgCap;
elseif mode == -1 && SoC < 72
    split = 2;
    CellCap = Q1 + Q2;
end
TotDchgCap = (DchgCap - CapAdj - Qage - Qcyc);
TotChgCap = (TotDchgCap)/(0.967 - (EffDeg*CycNo));

%% Initialise Recoverable Capacity

RestTime = 0; %Time since current stopped

Qmax = (17-0.17*SoC)*CellCap/100; %Maximum recoverable capacity
RecFact = 0.02;%0.46; %Recovery factor k found from linear regression,
SoC, rate, temperature dependent.
Ir = 0;

%% Import current and power user defined profiles

[ProfileNum, ProfileText, ProfileVals] = xlsread
('Model_Data.xlsx','Profile');

% Find number of rows
ProfileEndRowCalc = strcmp('End', ProfileText);
ProfileEndRow = 1;
while ProfileEndRowCalc (ProfileEndRow, 1) ~= 1;
    ProfileEndRow = ProfileEndRow + 1;
end

Duration = ProfileNum (ProfileEndRow-2, 1); % minutes
StartTime = (ProfileNum (1,1))*60; %seconds

%% Import cell data

A = xlsread ('Model_Data.xlsx'); %Contains EMF, dV/dT, Self-Discharge
B = xlsread ('Model_Data.xlsx', 'DchgResistances');
C = xlsread ('Model_Data.xlsx', 'ChgResistances');
D = xlsread ('Model_Data.xlsx', 'Capacitances');
E = xlsread ('Model_Data.xlsx', 'Hysteresis');
```

```
%% Import Current/Power/Temperature Profiles
%Current look up data
Current_Time = ProfileNum (1:ProfileEndRow-2,1);
Current_Values = ProfileNum (1:ProfileEndRow-2,2);
%Power look up data
Power_Time = ProfileNum (1:ProfileEndRow-2,1);
Power_Values = ProfileNum (1:ProfileEndRow-2,3);
%EnvTemp look up data
EnvTemp_Time = ProfileNum (1:ProfileEndRow-2,1);
EnvTemp_Values = ProfileNum (1:ProfileEndRow-2,4);

%% Import Cell Data Look Up Tables
%dVdT look up data
dVdT_SoC = A(4:104, 5);
dVdT_Values = A(4:104,15);

% R1 Discharge lookup table
R1Dchg_Temp = B (3,2:4);
R1Dchg_SoC = B (4:104,1);
R1Dchg_Values = B(4:104, 2:4);

% R1 Charge lookup table
R1Chg_Temp = C (3,2:4);
R1Chg_SoC = C (4:104,1);
R1Chg_Values = C(4:104, 2:4);

% R2 Discharge lookup table
R2Dchg_Temp = B (3,6:8);
R2Dchg_SoC = B (4:104,1);
R2Dchg_Values = B(4:104, 6:8);

% R2 Charge lookup table
R2Chg_Temp = C (3,6:8);
R2Chg_SoC = C (4:104,1);
R2Chg_Values = C(4:104, 6:8);

% R3 Discharge lookup table
R3Dchg_Temp = B (3,10:12);
R3Dchg_SoC = B (4:104,1);
R3Dchg_Values = B(4:104, 10:12);

% R3 Charge lookup table
R3Chg_Temp = C (3,10:12);
R3Chg_SoC = C (4:104,1);
R3Chg_Values = C(4:104, 10:12);

% Capacitance C2 lookup table DISCHARGE
C2_Temp = D (3,2:4);
C2_SoC = D (4:104,1);
C2_Values = D(4:104, 2:4);

% Capacitance C3 lookup table DISCHARGE
C3_Temp = D (3,6:8);
C3_SoC = D (4:104,1);
C3_Values = D(4:104, 6:8);

% Capacitance C2 lookup table CHARGE
C2Chg_Temp = D (3,14:16);
C2Chg_SoC = D (4:104,1);
C2Chg_Values = D(4:104,14:16);
```

```
% Capacitance C3 lookup table CHARGE
C3Chg_Temp = D (3,10:12);
C3Chg_SoC = D (4:104,1);
C3Chg_Values = D(4:104,10:12);

% Self Discharge Current Isd lookup table
Isd_Temp = A (3,17:19);
Isd_SoC = A (4:104,5);
Isd_Values = A(4:104,17:19);

% SoC vs EMF Lookup Table Charge (Known initial SoC - corresponding EMF
value found)

ChEMF_TEMP1 = A (3,11:13);
ChEMF_SoC1 = A (4:104,5);
ChEMF_Values1 = A(4:104,11:13); % Look up data

% SoC vs EMF Lookup Table Discharge (Known initial SoC - corresponding
EMF value found)

DChEMF_TEMP1 = A (3,7:9);
DChEMF_SoC1 = A(4:104,5);
DChEMF_Values1 = A (4:104,7:9); % Look up data

%Hysteresis Look Up DISCHARGE
DChCons1_Val = E (4:104,2);
DChCons1_SoC = E(4:104,1);
DChCons2_Val = E (4:104,3);
DChCons2_SoC = E(4:104,1);
DChTau1_Val = E (4:104,4);
DChTau1_SoC = E(4:104,1);
DChTau2_Val = E (4:104,5);
DChTau2_SoC = E(4:104,1);

%Hysteresis Look Up CHARGE
ChCons1_Val = E (4:104,7);
ChCons1_SoC = E(4:104,1);
ChCons2_Val = E (4:104,8);
ChCons2_SoC = E(4:104,1);
ChTau2_Val = E (4:104,9);
ChTau2_SoC = E(4:104,1);
ChTau1_Val = E (4:104,10);
ChTau1_SoC = E(4:104,1);

%% Set initial EMF Factor depending on mode

if mode  == 1;
    EMFFac = 1; % chg curve
elseif mode == -1;
    EMFFac =  0;% dchg curve
end

%% Set initial TransSoC to zero

TransSoC = 0; % capacity transferred since last mode change
```

```
%% Find Initial EMF Value from given SoC and Temp using EMF Callback
Function

[EMF,EMFCh,EMFDCh]    =    EMFFunct    (mode,previous_mode,    DChEMF_TEMP1,
DChEMF_SoC1, DChEMF_Values1,ChEMF_TEMP1, ChEMF_SoC1, ChEMF_Values1,...

DChCons1_SoC,DChCons1_Val,DChCons2_SoC,DChCons2_Val,DChTau1_SoC,DChTau1_V
al,...

DChTau2_SoC,DChTau2_Val,ChCons1_SoC,ChCons1_Val,ChCons2_SoC,ChCons2_Val,.
..

ChTau1_SoC,ChTau1_Val,ChTau2_SoC,ChTau2_Val,TransSoC,EMFFac,CellTemp1,
SoC);

%% Determine user defined power/temperature profile
Current = interp1(Current_Time,Current_Values,StartTime);
Power = interp1(Power_Time,Power_Values,StartTime);
EnvTemp = interp1(EnvTemp_Time,EnvTemp_Values,StartTime);

%%  Find  intial  current  (I1)  value  so  that  intial  rate  dependent
resistance can be calculated
if Power ~=0
    I1 = Power/EMF;
else
    I1 = Current;
end

if I1 == 0;
    RateDep = 1;
else
    RateDep = (1.5*(((I1)^2)^0.5)^0.36);
end

%% Determine initial resistance, capacitance and dV/dT values

R1Chg    =    (interp2(R1Chg_Temp,    R1Chg_SoC,    R1Chg_Values,CellTemp1,
SoC)+(0.00001*CellAge)) / RateDep;
R1Dchg   =   (interp2(R1Dchg_Temp,   R1Dchg_SoC,   R1Dchg_Values,   CellTemp1,
SoC)+(0.00001*CellAge))/ RateDep;

R2Chg    =    (interp2(R2Chg_Temp,    R2Chg_SoC,    R2Chg_Values,CellTemp1,
SoC)+(0.00001*CellAge))/ RateDep;
R2Dchg   =   (interp2(R2Dchg_Temp,   R2Dchg_SoC,   R2Dchg_Values,   CellTemp1,
SoC)+(0.00001*CellAge))/ RateDep;

R3Chg    =    (interp2(R3Chg_Temp,    R3Chg_SoC,    R3Chg_Values,CellTemp1,
SoC)+(0.00001*CellAge))/ RateDep;
R3Dchg   =   (interp2(R3Dchg_Temp,   R3Dchg_SoC,   R3Dchg_Values,   CellTemp1,
SoC)+(0.00001*CellAge))/ RateDep;

dVdT = interp1(dVdT_SoC,dVdT_Values,SoC);
C3D = interp2(C3_Temp, C3_SoC, C3_Values, CellTemp1, SoC);
C2D = interp2(C2_Temp, C2_SoC, C2_Values, CellTemp1, SoC);

C3C = interp2(C3Chg_Temp, C3Chg_SoC, C3Chg_Values, CellTemp1, SoC);
C2C = interp2(C2Chg_Temp, C2Chg_SoC, C2Chg_Values, CellTemp1, SoC);
```

```
%% Determine reversible capacity changes from Irev Callback Function

[Qmax,Isd,Ir] = IrevFunct (I1, CellCap, RecFact, RestTime, Isd_Temp,
Isd_SoC, Isd_Values, CellTemp1, SoC);

%% Determine equivalent circuit parameters from determined intial values
% Initial voltage values
V1 = EMF;
V2 = EMF;

% Determine I1 and Power depending on whether current or power is
defined.

if mode == 1 || (mode == 0 && previous_mode == 1)
   if Power > 0 %for charge - power known
       P = Power;
       I1 = (-V1 + ((V1)^2 + 4*R1Chg*P)^0.5)/(2*R1Chg);
   elseif Power == 0 %for charge - current known
       I1 = Current;
       P = (I1^2)*R1Chg + I1*V1;
   end
elseif mode == -1 || (mode == 0 && previous_mode == -1)
   if  Power < 0 %for discharge - power known
       P= Power;
       I1 = (-V1 + ((V1)^2 + 4*R1Dchg*P)^0.5)/(2*R1Dchg);
   elseif  Power == 0 %for discharge - power known
       I1 = Current;
       P = (I1^2)*R1Dchg + I1*V1;
   end
end

% determine initial I2, I3, I4 and Vterm
if mode == -1 || (mode == 0 && previous_mode == -1)%dchg
   I2 = (V1-V2)/R2Dchg;
   I3 = (V2 - EMF)/R3Dchg;
   I4 = I1+Isd+Ir;
   Vterm = V1 + I1*R1Dchg;
elseif mode == 1 || (mode == 0 && previous_mode == -1)%chg
   I2 = (V1-V2)/R2Chg;
   I3 = (V2 - EMF)/R3Chg;
   I4 = I1+Isd+Ir;
   Vterm = V1 + I1*R1Chg;
end

%% Limit terminal voltage if it hits its maximum or minimum
if Vterm > MaxVoltage
    Vterm = MaxVoltage;
    I1 = ((Vterm - V1)/R1Chg);
    I2 = (V1-V2)/R2Chg;
    I3 = (V2 - EMF)/R3Chg;
    I4 = I1+Isd+Ir;
    P = I1*Vterm;
elseif Vterm < MinVoltage
    Vterm = MinVoltage;
    I1 = ((Vterm - V1)/R1Dchg);
    I2 = (V1-V2)/R2Dchg;
    I3 = (V2 - EMF)/R3Dchg;
    I4 = I1+Isd+Ir;
    P = I1*Vterm;
end
```

RUN MODEL SOLVER ROUTINE

```
%% Initialise Runge Kutta

CurrentTime = datestr(now);

KFactor(1) = 0.5;
KFactor(2) = 0.5;
KFactor(3) = 1;
KFactor(4) = 0;

limit = 0;
counter=1;
Time = StartTime*60; % Time given in seconds

while Time <= Duration*60 - hStep; %Time given in seconds

    TempCellTemp1 = CellTemp1;

    for K=1:4

        %Estimate delta change for 1 timestep
        if mode == -1 || (mode == 0 && previous_mode == -1)
            DeltaSoC(K) = (I4 * hStep)/(36*CellCap);
            DeltaCellTemp1(K) = hStep*((I1^2)*R1Dchg + (I2^2)*R2Dchg +
            (I3^2)*R3Dchg + I1*(TempCellTemp1+273.15)*dVdT - Qc1env*
            (TempCellTemp1 - AmbientTemp) - Qr1env*((TempCellTemp1^4)-
            (AmbientTemp^4)))/mCp1;
        elseif mode == 1 || (mode == 0 && previous_mode == 1)
            DeltaSoC(K) = (I4 * hStep)/(36*CellCap);
            DeltaCellTemp1(K) = hStep*((I1^2)*R1Chg + (I2^2)*R2Chg +
            (I3^2)*R3Chg + I1*(TempCellTemp1+273.15)*dVdT - Qc1env*
            (TempCellTemp1 - AmbientTemp) - Qr1env*((TempCellTemp1^4)-
            (AmbientTemp^4)))/mCp1;
        end

        %Determine temporary values for next iteration
        TempSoC = SoC + KFactor(K) * DeltaSoC(K);
        if TempSoC > MaxSoC
            limit = 1;
        elseif TempSoC < MinSoC
            limit = -1;
        end
        TempCellTemp1 = CellTemp1 + KFactor(K) * DeltaCellTemp1(K);
        TempTime = Time + KFactor(K) * hStep;
        TempTransSoC = TransSoC + KFactor(K) * DeltaSoC(K);

        %Update interpolated parameters with new temporary estimates
        %TempEMF
        Prev_EMF=EMF;
        [EMF,EMFCh, EMFDCh] = EMFFunct (mode,previous_mode,DChEMF_TEMP1,
        DChEMF_SoC1,        DChEMF_Values1,ChEMF_TEMP1,        ChEMF_SoC1,
        ChEMF_Values1,DChCons1_SoC,DChCons1_Val,DChCons2_SoC,DChCons2_Va
        l,
        DChTau1_SoC,DChTau1_Val,DChTau2_SoC,DChTau2_Val,ChCons1_SoC,ChCo
        ns1_Val,
        ChCons2_SoC,ChCons2_Val,ChTau1_SoC,ChTau1_Val,ChTau2_SoC,ChTau2_
        Val,TransSoC,EMFFac,TempCellTemp1, TempSoC);
```

```
if mode == 1 || (mode == 0 && previous_mode == 1);
    DeltaEMF(K) =EMF-Prev_EMF ;
    DeltaV2(K) =  DeltaEMF(K) + (I1-I3)*hStep/C3C;
    DeltaV1(K) = DeltaV2(K) + (I1-I2)*hStep/C2C;
elseif mode == -1 || (mode == 0 && previous_mode == -1);
    DeltaEMF(K) = Prev_EMF-EMF;
    DeltaV2(K) = DeltaEMF(K) + (I1-I3)*hStep/C3D;
    DeltaV1(K) = DeltaV2(K) + (I1-I2)*hStep/C2D;
end

TempEMF = EMF + KFactor(K) * DeltaEMF(K);
TempV1 = V1 + KFactor(K) * DeltaV1(K);
TempV2 = V2 + KFactor(K) * DeltaV2(K);

if I1 == 0;
    RateDep = 1;
else
    RateDep = (1.5*(((I1)^2)^0.5)^0.36);
end

R1Chg = (interp2(R1Chg_Temp, R1Chg_SoC,
R1Chg_Values,TempCellTemp1, TempSoC)+(0.00001*CellAge))/RateDep;
R1Dchg = (interp2(R1Dchg_Temp, R1Dchg_SoC, R1Dchg_Values,
TempCellTemp1, TempSoC)+(0.00001*CellAge))/ RateDep;

R2Chg = (interp2(R2Chg_Temp, R2Chg_SoC,
R2Chg_Values,TempCellTemp1, TempSoC)+(0.00001*CellAge))/RateDep;
R2Dchg = (interp2(R2Dchg_Temp, R2Dchg_SoC, R2Dchg_Values,
TempCellTemp1, TempSoC)+(0.00001*CellAge))/ RateDep;

R3Chg = (interp2(R3Chg_Temp, R3Chg_SoC,
R3Chg_Values,TempCellTemp1, TempSoC)+(0.00001*CellAge))/RateDep;
R3Dchg = (interp2(R3Dchg_Temp, R3Dchg_SoC, R3Dchg_Values,
TempCellTemp1, TempSoC)+(0.00001*CellAge))/ RateDep;

dVdT = interp1(dVdT_SoC,dVdT_Values,TempSoC);

C3D   =   interp2(C3_Temp,   C3_SoC,   C3_Values,   TempCellTemp1,
TempSoC);
C2D   =   interp2(C2_Temp,   C2_SoC,   C2_Values,   TempCellTemp1,
TempSoC);

C3C = interp2(C3Chg_Temp, C3Chg_SoC, C3Chg_Values, TempCellTemp1,
TempSoC);
C2C = interp2(C2Chg_Temp, C2Chg_SoC, C2Chg_Values, TempCellTemp1,
TempSoC);

[Qmax,Isd,Ir]   =   IrevFunct   (I1,CellCap,   RecFact,   RestTime,
Isd_Temp, Isd_SoC, Isd_Values, TempCellTemp1, TempSoC);


%user input profiles

Current = interp1(Current_Time,Current_Values,TempTime/60
Power = interp1(Power_Time,Power_Values,TempTime/60);
EnvTemp = interp1(EnvTemp_Time,EnvTemp_Values,TempTime/60);
```

```
%update parameters for next K iteration

    if mode == -1 || (mode == 0 && previous_mode == -1)%Discharge
       if ((TempV1)^2 + 4*R1Dchg*P) > 0
           if Power < 0
               P = Power;
               I1 = (-(TempV1)+((TempV1)^2+4*R1Dchg*P)^0.5)/(2*R1Dchg);
           elseif Power == 0
               I1 = Current;
               P = (I1^2)*R1Dchg + I1*TempV1;
           end
       elseif ((TempV1)^2 + 4*R1Dchg*P) <~ 0
           if Power < 0
               P = Power;
               I1 = -(TempV1)/(2*R1Dchg);
           elseif Power == 0
               I1 = Current;
               P = -((TempV1)^2/(4*R1Dchg)); %V1^2 + 4RP = 0
           end
       end
    elseif mode ==1 || (mode == 0 && previous_mode == 1)% charge
        if Power > 0
               P = Power;
               I1=(-(TempV1) + ((TempV1 )^2 + 4*R1Chg*P)^0.5)/(2*R1Chg);
         elseif Power == 0
               I1 = Current;
               P = (I1^2)*R1Chg +I1*TempV1;
         end
    end
    end

      % determine I2, I3, I4 and Vterm
       if mode == -1 || (mode == 0 && previous_mode == -1)%dchg
          I2 = (TempV1-TempV2)/R2Dchg;
          I3 = (TempV2 - TempEMF)/R3Dchg;
          I4 = I1+Isd+Ir;
          Vterm = TempV1 + I1*R1Dchg;
       elseif mode == 1 || (mode == 0 && previous_mode == 1)%chg
          I2 = (TempV1-TempV2)/R2Chg;
          I3 = (TempV2 - TempEMF)/R3Chg;
          I4 = I1+Isd+Ir;
          Vterm = TempV1 + I1*R1Chg;
       end

       %Protection for over and under voltage
         if Vterm > MaxVoltage
           Vterm = MaxVoltage;
           I1 = ((Vterm - TempV1)/R1Chg);
           I2 = (TempV1-TempV2)/R2Chg;
           I3 = (TempV2 - TempEMF)/R3Chg;
           I4 = I1+Isd+Ir;
           P = I1*Vterm;
           DeltaEMF(K) = EMF - EMFCh;
           DeltaSoC(K) = (I4 * hStep)/(36*CellCap);
           DeltaCellTemp1(K)=hStep*(I1^2*R1Chg+I2^2*R2Chg+ I3^2*R3Chg
           + I1*(TempCellTemp1+273.15)*dVdT - Qc1env* (TempCellTemp1 -
           AmbientTemp)-Qr1env*((TempCellTemp1^4)-
           (AmbientTemp^4)))/mCp1;

           DeltaV2(K) = DeltaEMF(K) + (I1-I3)*hStep/C3D;
           DeltaV1(K) = DeltaV2(K) + (I1-I2)*hStep/C2D;
```

```
        elseif Vterm < MinVoltage
            Vterm = MinVoltage;
            I1 = ((Vterm - TempV1)/R1Dchg);
            I2 = (TempV1-TempV2)/R2Dchg;
            I3 = (TempV2 - TempEMF)/R3Dchg;
            I4 = I1+Isd+Ir;
            P = I1*Vterm;
            DeltaEMF(K) =  EMF - EMFDCh;
            DeltaSoC(K) = (I4 * hStep)/(36*CellCap);

            DeltaCellTemp1(K)=hStep*(I1^2*R1Dchg+I2^2*R2Dchg+I3^2*R3Dchg
            + I1*(TempCellTemp1+273.15)*dVdT - Qc1env* (TempCellTemp1 -
            AmbientTemp)-Qr1env*((TempCellTemp1^4)-
            (AmbientTemp^4)))/mCp1;
            DeltaV2(K) = DeltaEMF(K) + (I1-I3)*hStep/C3D;
            DeltaV1(K) = DeltaV2(K) + (I1-I2)*hStep/C2D;
          end

    %Weighted Summation of Runge Kutta estimates

    SoC = SoC + (DeltaSoC(1) + 2*DeltaSoC(2) + 2*DeltaSoC(3) +
    DeltaSoC(4))/6;

    TransSoC = TransSoC + (DeltaSoC(1) + 2*DeltaSoC(2) + 2*DeltaSoC(3) +
    DeltaSoC(4))/6;

    CellTemp1 = CellTemp1 + (DeltaCellTemp1(1) + 2*DeltaCellTemp1(2) +
    2*DeltaCellTemp1(3) + DeltaCellTemp1(4))/6;

    V1 = V1 + (DeltaV1(1) + 2*DeltaV1(2) + 2*DeltaV1(3) + DeltaV1(4))/6;
    V2 = V2 + (DeltaV2(1) + 2*DeltaV2(2) + 2*DeltaV2(3) + DeltaV2(4))/6;

    Time = Time + hStep;
    RestTime = RestTime +(hStep/3600);%time since current stopped (hours)

% Update interpolated parameters for next time step

   [EMF,EMFCh,  EMFDCh]  =  EMFFunct  (mode,previous_mode,  DChEMF_TEMP1,
    DChEMF_SoC1,  DChEMF_Values1,ChEMF_TEMP1,  ChEMF_SoC1,  ChEMF_Values1,
    DChCons1_SoC,DChCons1_Val,DChCons2_SoC,DChCons2_Val,DChTau1_SoC,DChTa
    u1_Val,DChTau2_SoC,DChTau2_Val,ChCons1_SoC,ChCons1_Val,ChCons2_SoC,Ch
    Cons2_Val,ChTau1_SoC,ChTau1_Val,ChTau2_SoC,ChTau2_Val,TransSoC,EMFFac
    ,CellTemp1, SoC);

    if I1 == 0;
        RateDep = 1;
    else
        RateDep = (1.5*(((I1)^2)^0.5)^0.36);
    end

    R1Chg   =   (interp2(R1Chg_Temp,   R1Chg_SoC,   R1Chg_Values,CellTemp1,
    SoC)+(0.00001*CellAge)) / RateDep;
    R1Dchg = (interp2(R1Dchg_Temp, R1Dchg_SoC, R1Dchg_Values, CellTemp1,
    SoC)+(0.00001*CellAge))/ RateDep;

    R2Chg   =   (interp2(R2Chg_Temp,   R2Chg_SoC,   R2Chg_Values,CellTemp1,
    SoC)+(0.00001*CellAge))/ RateDep;
    R2Dchg = (interp2(R2Dchg_Temp, R2Dchg_SoC, R2Dchg_Values, CellTemp1,
    SoC)+(0.00001*CellAge))/ RateDep;
```

```
    R3Chg   =   (interp2(R3Chg_Temp,   R3Chg_SoC,   R3Chg_Values,CellTemp1,
    SoC)+(0.00001*CellAge))/ RateDep;
    R3Dchg  =  (interp2(R3Dchg_Temp,  R3Dchg_SoC,  R3Dchg_Values,  CellTemp1,
    SoC)+(0.00001*CellAge))/ RateDep;

    dVdT = interp1(dVdT_SoC,dVdT_Values,SoC);

    C3D = interp2(C3_Temp, C3_SoC, C3_Values, CellTemp1, SoC);
    C2D = interp2(C2_Temp, C2_SoC, C2_Values, CellTemp1, SoC);

    C3C = interp2(C3Chg_Temp, C3Chg_SoC, C3Chg_Values, CellTemp1, SoC);
    C2C = interp2(C2Chg_Temp, C2Chg_SoC, C2Chg_Values, CellTemp1, SoC);

    [Qmax,Isd,Ir] = IrevFunct (I1,CellCap, RecFact, RestTime, Isd_Temp,
    Isd_SoC, Isd_Values, CellTemp1, SoC);

    Current = interp1(Current_Time,Current_Values,Time/60);
    P = interp1(Power_Time,Power_Values,Time/60);
    EnvTemp = interp1(EnvTemp_Time,EnvTemp_Values,Time/60);

   % Calculate Updated Values
   %calculate new values of I1 and Power
     if mode == -1 || (mode == 0 && previous_mode == -1) % discharge
        if ((V1)^2 + 4*R1Dchg*P) > 0
            if  Power < 0
                P = Power;
                I1 = (-V1 + ((V1)^2 + 4*R1Dchg*Power)^0.5)/(2*R1Dchg);
            elseif Power == 0
                I1 = Current;
                P = (I1^2)*R1Dchg +I1*V1;
            end
        elseif ((V1)^2 + 4*R1Dchg*P) <~ 0
            if  Power < 0
                P = Power;
                I1 = -(V1)/(2*R1Dchg);
            elseif Power == 0
                I1 = Current;
                P = (-(V1)^2/(4*R1Dchg));
            end
        end
     elseif mode ==1 || (mode == 0 && previous_mode == 1) % power is
never negative in charge
         if Power > 0
                P = Power;
                I1=(-(TempV1) + ((TempV1 )^2 + 4*R1Chg*P)^0.5)/(2*R1Chg);
         elseif Power == 0
                I1 = Current;
                P = (I1^2)*R1Chg +I1*TempV1;
         end
     end
```

```
      % determine I2, I3, I4 and Vterm
       if mode == -1 || (mode == 0 && previous_mode == -1)%dchg
           I2 = (V1-V2)/R2Dchg;
           I3 = (V2 - EMF)/R3Dchg;
           I4 = I1+Isd+Ir;
           Vterm = V1 + I1*R1Dchg;
        elseif mode == 1 || (mode == 0 && previous_mode == 1)%chg
           I2 = (V1-V2)/R2Chg;
           I3 = (V2 - EMF)/R3Chg;
           I4 = I1+Isd+Ir;
           Vterm = V1 + I1*R1Chg;
        end

    %Protection for over and under voltage
    if Vterm >= MaxVoltage
        Vterm = MaxVoltage;
        I1 = ((Vterm - V1)/R1Chg);
        I2 = (V1-V2)/R2Chg;
        I3 = (V2 - EMF)/R3Chg;
        I4 = I1+Isd+Ir;
        P = I1*Vterm;
    elseif Vterm <= MinVoltage
        Vterm = MinVoltage;
        I1 = ((Vterm - V1)/R1Dchg);
        I2 = (V1-V2)/R2Dchg;
        I3 = (V2 - EMF)/R3Dchg;
        I4 = I1+Isd+Ir;
        P = I1*Vterm;
    end

    % mode change detection

 if I1 < 0; %change to current in order to include Power?
     if mode == 1;
        TransSoC = 0;
        %EMFFac = 1;
        EMFFac = (EMF - EMFDCh)/(EMFCh - EMFDCh);
     end
     if mode ~= -1
        previous_mode = mode;
        mode = -1;
     end
 elseif I1 > 0;
     if mode == -1;
        TransSoC = 0;
        EMFFac = (EMF - EMFDCh)/(EMFCh - EMFDCh);
        %EMFFac = 1;
     end
     if mode ~= 1
      previous_mode = mode;
      mode = 1;
   end
elseif I1 == 0;
   if mode ~= 0;
      RestTime = 0; %resets RestTime to 0 %rest time in Hours
      previous_mode = mode;
      mode = 0;
   end
end
```

```
% Correct capacity depending on region

    if mode == 1
      CellCap = TotChgCap;
    elseif mode == -1 && SoC >= 72
      CellCap = TotDchgCap;
    elseif mode == -1 && SoC < 72
      CellCap = Q1 + Q2;
    End

 % Cycle count

if start_mode == 0 % Allows the start mode to equal 0
    start_mode = mode;%changes start_mode to first mode other than 0
elseif previous_mode ~= mode % signals mode change
    if mode == start_mode && mode_flag==1 %increment cycle number when
returning to start mode
        CycNo = CycNo+1;
        mode_flag = 0;
    elseif mode == - start_mode
        mode_flag = 1;
    end
end
    CellTemp1_track(counter)=CellTemp1;

    SoC_track(counter)=SoC;
    Vterm_track(counter)=Vterm;
    EMF_track(counter)=EMF;
    P_track(counter)=P;
    R1_track(counter)=R1;
    R2_track(counter)=R2;
    C2D_track(counter)=C2;
    C3D_track(counter)=C3;
    I1_track(counter)=I1;
    I2_track(counter)=I2;
    I2_track(counter)=I2;
    I4_track(counter)=I4;
    Isd_track(counter)=Isd;
    Ir_track(counter)=Ir;
    Time_track(counter)=Time;
    mode_track(counter)=mode;
    CycNo_track(counter) = CycNo;
    RestTime_track(counter)=RestTime;
```

OUTPUT RESULTS

```
Rtot_Chg = ((R1Chg+R2Chg+R3Chg)*SC)/(PS1*PS2)

Rtot_Dchg = ((R1Dchg+R2Dchg+R3Dchg)*SC)/(PS1*PS2)


EMF = EMF*SC
Vterm = Vterm*SC
BattCap = CellCap*PS1*PS2

plot(Time_track,Vterm_track,'b');
    axis([0 40000 1.7 2.5]);
    xlabel('Time'); ylabel('Vterm');
    hold on
    getframe;

    counter=counter+1;
end
hold on
```

EMF CALLBACK

```
function [EMF, EMFCh, EMFDCh] = EMFFunct
(mode,previous_mode,DChEMF_TEMP1, DChEMF_SoC1,
DChEMF_Values1,ChEMF_TEMP1, ChEMF_SoC1, ChEMF_Values1,...


DChCons1_SoC,DChCons1_Val,DChCons2_SoC,DChCons2_Val,DChTau1_SoC,DChTau1_V
al,...


DChTau2_SoC,DChTau2_Val,ChCons1_SoC,ChCons1_Val,ChCons2_SoC,ChCons2_Val,.
..


ChTau1_SoC,ChTau1_Val,ChTau2_SoC,ChTau2_Val,TransSoC,EMFFac,CellTemp1,
SoC)



%Lookup EMF for both chg and dchg

EMFDCh = interp2(DChEMF_TEMP1, DChEMF_SoC1, DChEMF_Values1, CellTemp1,
SoC);

EMFCh = interp2(ChEMF_TEMP1, ChEMF_SoC1, ChEMF_Values1, CellTemp1, SoC);



%Interpolate Hysteresis Values

DchgCons1 = interp1(DChCons1_SoC,DChCons1_Val ,SoC);

DchgCons2 = interp1(DChCons2_SoC,DChCons2_Val ,SoC);

DchgTau1 = interp1(DChTau1_SoC,DChTau1_Val ,SoC);
```

```
DchgTau2 = interp1(DChTau2_SoC,DChTau2_Val ,SoC);

ChgCons1 = interp1(ChCons1_SoC,ChCons1_Val ,SoC);

ChgCons2 = interp1(ChCons2_SoC,ChCons2_Val ,SoC);

ChgTau1 = interp1(ChTau1_SoC,ChTau1_Val ,SoC);

ChgTau2 = interp1(ChTau2_SoC,ChTau2_Val ,SoC);


%Find actual EMF based on mode and hysteresis

if mode == 1

    TransFrac1 = exp(-TransSoC/DchgTau1);

    TransFrac2 = exp(-TransSoC/DchgTau2);

    EMF    =    EMFCh    -    DchgCons1*TransFrac1*(EMFCh-EMFDCh)*(1-EMFFac)-
DchgCons2*TransFrac2*(EMFCh-EMFDCh)*(1-EMFFac);

elseif mode == -1

    TransFrac1 = exp(TransSoC/ChgTau1);

    TransFrac2 = exp(TransSoC/ChgTau2);

    EMF    =    EMFDCh    +    ChgCons1*TransFrac1*(EMFCh-EMFDCh)*(EMFFac)+
ChgCons2*TransFrac2*(EMFCh-EMFDCh)*(EMFFac);

elseif mode == 0

    if previous_mode == -1

        EMF = EMFDCh;

    elseif previous_mode == 1

        EMF = EMFCh;

    end

end

end
```

Reversible Capacity Callback Function

```
Function [Qmax,Isd,Ir] = IrevFunct (I1, CellCap, RecFact, RestTime,
Isd_Temp, Isd_SoC, Isd_Values, CellTemp1, SoC)


    if I1 == 0 && RestTime > 0.0001
      Isd = interp2(Isd_Temp, Isd_SoC, Isd_Values, CellTemp1,...
         ...SoC)*(RestTime^-0.5); %Self discharge current
        Qmax = (17-0.17*SoC)*CellCap/100;
        Ir = RecFact*Qmax*exp(-RecFact*RestTime);
    else
        Isd = 0;
        Qmax = 0;
        Ir = 0;
    end
end
```